Modelling, Design and Analysis of Electric Vehicle ChargingStation with Integrated Renewable Energy

A Thesis Submitted to the
Delhi Technological University
For the Award of Doctor of Philosophy
In
Electrical Engineering

Submitted By:

MOHD BILAL

(2K17/PhD/EE/05)

Under the Supervision of

Dr. M. Rizwan

Professor

DEPARTMENT OF ELECTRICAL ENGINEERING

DELHI TECHNOLOGICAL UNIVERSITY

(Formerly Delhi College of Engineering)

DELHI-110042, INDIA

2022

Table of Contents

DECLARATION

I Mohd Bilal a student of Ph.D. hereby declare that the thesis titled **Modelling, Design and Analysis of Electric Vehicle Charging Station with Integrated Renewable Energy** which is submitted by me to the Department of Electrical Engineering, Delhi Technological University, Delhi in partial fulfillment of the requirement for the award of the degree of Doctor of Philosophy has not previously formed the basis for the award of any Degree, Diploma Associate ship, fellowship or other similar title or recognition.

M. Bilal

Place: Delhi **(Mohd Bilal)**

Date: 29/07/2022

CERTIFICATE

On the basis of the declaration submitted by Mr. Mohd Bilal, student of Ph.D., I hereby certify that the thesis titled **Modelling, Design and Analysis of Electric Vehicle Charging Station with Integrated Renewable Energy** which is submitted to the Department of Electrical Engineering, Delhi Technological University, Delhi in partial fulfillment of the requirement for the award of the degree of Doctor of Philosophy is an original contribution with existing knowledge and faithful record of research carried out by him under my guidance and supervision.

To the best of my knowledge this work has not been submitted in part or full for any Degree or Diploma to this University or elsewhere.

Date: 29/07/2022

(Prof. M. Rizwan)
Supervisor
Department of Electrical Engineering
Delhi Technological University
Delhi, India

ACKNOWLEDGEMENT

First and foremost, I sincerely acknowledge my most sincere gratitude to my supervisors Prof. M. Rizwan for their valuable guidance, support, and motivation throughout this research work. They have been outstanding mentors and working with them has been a remarkable experience. The valuable hours of discussion that I had with them undoubtedly helped in supplementing my thoughts in the right direction for attaining the desired objectives. I consider it my proud privilege to have worked with them, ever ready to lend a helping hand. I am forever thankful to them for all their wise words and inspiring thoughts.

I am also thankful to all faculty members of the Department of Electrical Engineering, Delhi Technological University, Delhi, for their encouragement and moral support for the completion of this thesis.

I would like to extend my special thanks to SRC members mainly Prof. T. S. Bhatti, Professor, Department of Energy Science and Engineering, IIT Delhi who have given me valuable guidance and advice to improve the quality of my research work.

I extend my thanks to my friends and colleagues especially, Dr. Astitva Kumar, Dr. Saket Gupta, Dr. Aakash Seth, Ganesh Jaiswal, Isaka J. Mwakitalima, Issak Abdow Hassan for their constant motivation and for reminding me to complete my work at the earliest.

The assistance of the valuable staff in the Renewable Energy Research Facility of Delhi Technological University is gratefully acknowledged. I am especially thankful to Mr. Vickey Kumar Prasad, Mr. Ankit Kumar, and Mr. Manoj Kumar for their substantial assistance during my research.

I want to take this opportunity to thank my parents, from the bottom of my heart for everything that they have done and continues to do for me. They never lost their faith in me and sacrificed a great lot in her life to help me come this far. I also want to thank my brothers, Irfan Alam, Arshad Mohammad, and Riyaz Hussain for being a constant source of support.

This acknowledgment would not be complete without mentioning my wife. She has been the steady wind under my wings. She is my core support system and words cannot articulate my admiration for her. She gave me unconditional support and continues to be a source of inspiration during my research.

I am wholly indebted to ALMIGHTY who is omnipotent and superpower of the universe.

M. Bilal

Place: Delhi **(Mohd Bilal)**

Date: 29/07/2022

LIST OF FIGURES

LIST OF TABLES

LIST OF SYMBOLS AND ABBREVIATION

List of Symbols

P_{gi}	Active power generation at i^{th} bus
P_{di}	Active power demand at i^{th} bus
Q_{gi}	Reactive power generation of i^{th} bus
Q_{di}	Reactive power demand of i^{th} bus
V_i	Voltage magnitude at i^{th} bus
V_j	Voltage magnitude at j^{th} bus
Y_{ij}	Admittance of $(i,j)^{th}$ term of bus admittance matrix
δ_i	Phase angle of voltage at i^{th} bus
δ_j	Phase angle of voltage at j^{th} bus
θ_{ij}	Angle of Y_{ij}
P_{CS}^{i}	Electricity demand of i^{th}CS
P^i	Capacity of i^{th} CS
p_{best}	Personal best
g_{best}	Global best
$v_i(t+1)$	Velocities of the i^{th} particle at instances t+1
$v_i(t)$	Velocities of the i^{th} particle at instance t
$x_i(t+1)$	Position of the i^{th} particle at instances t+1
$x_i(t)$	Position of the i^{th} particle at instance t
$w(t)$	Weight of particle at iteration t
w_{min}	Minimum value of weight
w_{max}	Maximum value of weight
$\overrightarrow{A}, \overrightarrow{C}$	Coefficient vectors
$\overrightarrow{X_p}$	Position vector of prey
$\overrightarrow{X}$	Position vector of wolf
$C_{initial}$	Initial fixed cost of charging station
C_{land}	Rental cost of land

B	Area requirement per connector
N_{CS}	Number of charging station
N_{EV}	Number of electric vehicles
i	Charging station index
j	Electric vehicle index
NC_i	Number of charging connectors at i^{th}CS
CP	Rated power of connectors
$CS_C(i)$	Capacity of i^{th}CS
w	Area of cross section of transmission line
CT_i	Transmission cost of i^{th}CS
S_j	Trajectory length to the charging station
$s_{i,j}$	Trajectory length of j^{th} EV to i^{th}CS
D	Distance between i^{th}CS and nearest electric substation
P_{EVL}	EV energy loss
DE	Maximum number of EVs that can be charged by a connector
$C_{EV/Km}$	Cost of traveling of EV per Km
ES	Electric substation
N_{ES}	Number of electric substations
x_{CS}	Abscissae of charging station
y_{CS}	Ordinate of charging station
x_{EV}	Abscissae of electric vehicle
y_{EV}	Ordinate of electric vehicle
x_{ES}	Abscissae of electric substation
y_{ES}	Ordinate of electric substation
ξ	Availability of electric supply
χ	Failure rate
Ψ	Repair rate
r	Repair time
$\rho(i)$	Average operating hours of i^{th}CS
η_i	Unavailability of electric supply at i^{th}CS

T	Average charging time of an EV
ξ_{fi}	Station feeder availability of feeder fi
ξ_{D4x}	Availability of electric supply on bus $D4x$.
ξ_T	Availability of power transformer in substation
ξ_{D6x}	Availability of electric supply on bus $D6x$
P_{loss}	Active power loss
Q_{loss}	Reactive power loss
N_{br}	Number of branches (line)
N_{bus}	Number of buses
T_{load}	Total load in the system
$P_{avail,bs}$	Already available load at bs^{th}bus
P_{EVCS}^{bs}	EVCS load connected to bs^{th} bus.
C_R	Charging rate
DC_R	Discharging rate
$Q_{cap}(bs)$	Reactive power injected at bs^{th} bus
$P_{T,loss}^{cap}$	Total reactive power loss after integrating capacitor
Q_N^{inj}	Net injected reactive power
K_{ep}	Cost of energy paid per kWh
T	Time period in hours
β	Depreciation factor
C_i^{cap}	Installation cost of capacitor per location
C_i^{EVCS}	Installation cost of EVCS per location
N_{cap}	Number of capacitors
K_{cp}	Cost of purchase of capacitor per kVAr
C_O^{cap}	Operating cost of capacitors and EVCS
C_o^{EVCS}	Operating cost of EVCS
$Q_{cap}(bs)$	Amount of reactive power injected at bs^{th} bus
$E^d(h)$	Average demand of energy at hour h
F_h	Rate of failure at hour h

R_h	Outage time at hour h
PC_t	Penalty cost incurred for unsupplied energy at day t in $/kWh
$P_{D,k}$	Active power demand at k^{th} bus
$Q_{D,k}$	Reactive power demand at k^{th} bus
$P^{DG}(k)$	Total real power injected by DGs at k^{th} bus
$Q^{DG}(k)$	Total reactive power injected by DGs at k^{th} bus
$P_{SPV-out}(t)$	Solar photovoltaic power output
η_{SPV}	Efficiency of solar panel
A_{SPV}	Surface area of the solar panel
$G_h(t)$	Hourly solar irradiance falling on the surface of solar panel
T_{cell}	Temperature of cell
T_a	Ambient temperature
P_{max}	Maximum power output of solar panel
V_{max}	Maximum value of voltage
I_{max}	Maximum value of current
N_{SPV}	Number of installed solar PV panel
$u(t)$	Fuel consumption in litres per hour
$P_{DG}(t)$	Power output of diesel generator in kW
$P_{rated-DG}$	Rated power of diesel generator
a	Constant value (0.246)
b	Constant value (0.08415)
$\eta_{overall}$	Overall efficiency of DG
$\eta_{brake\ thermal}$	Brake thermal efficiency of DG
$SOC_{bat}(t+1)$	State of charge of battery at time instant $(t+1)$
$SOC_{bat}(t)$	State of charge of battery at time instant (t)
$P_S^{grid}(t)$	Extra energy to be sold to the grid in kWh
$SOC_{bat}^{min}(t)$	Minimum SOC of battery
$SOC_{bat}^{max}(t)$	Maximum SOC of battery
D_{Km}	Number of kilometers travelled
$E_{req/km}$	Energy needed per kilometer

T	Duration of charging
Q_{bat}^{EV}	Capacity of EV battery
N_{SPV}	Number of solar panels
V_{bus}	Voltage level of bus
V_{bat}	Voltage level of single battery
P_{bat}^{max}	Maximum input/output power of battery.
$P_{P}^{grid}(t)$	Energy to be borrowed from the grid in kWh
$P_{D}^{EV}(t)$	Energy demand of EV
$P_{EVCS-dem}(t)$	Power demand of EVCS
NPC_{SPV}	Net present cost of solar panel
C_{SPV}^{CAP}	Capital cost of solar panel
C_{SPV}^{REP}	Replacement cost of solar panel
C_{SPV}^{OM}	Operation and maintenance cost of solar panel
C_{SPV}^{SAL}	Salvage cost of solar panel
σ	Self-discharge rate of battery
η_{bdinv}	Efficiency of bi-directional inverter
η_{bat}	Round trip efficiency of the battery
η_{bat}^{charge}	Charging efficiency of battery
$\eta_{bat}^{discharge}$	Discharging efficiency of battery
C_{total}	Total capacity of battery bank
N_{bat}	Total number of batteries
N_{bat}^{series}	Number of batteries connected in series
C_{sbat}	Capacity of a single battery
NPC_{bat}	Net present cost of battery
C_{bat}^{CAP}	Capital cost of battery
C_{bat}^{REP}	Replacement cost of battery
C_{bat}^{OM}	Operation and maintenance cost of battery
C_{bat}^{SAL}	Salvage cost of battery
ψ_{bat}	Cost of one battery in $.

ω_{bat}	OM cost of battery
μ_{bat}	Escalation rate of battery
ε_{bat}	Resale value of one battery in $
ζ_{bat}^{rep}	Replacement cost of battery
NPC_{bdinv}	Net present cost of battery
C_{bdinv}^{CAP}	Capital cost of bidirectional inverter
ψ_{SPV}	Initial cost and of each SPV panel
P_{SPV}	Power rating of each SPV panel
ζ_{SPV}^{rep}	Cost of replacing the SPV panel
R	Rate of interest
Ω	Life span of project in years
ω_{SPV}	OM cost of each panel
μ_{SPV}	Escalation rate
ε_{SPV}	Resale price solar panel after completing their life
∂	Inflation rate
ε_{bdinv}	Resale value of bidirectional inverter in $
ζ_{bdinv}^{rep}	Replacement cost of bidirectional inverter
ξ_S^{grid}	Cost for unit sale of electricity to the utility grid
ξ_P^{grid}	Cost for unit purchase of electricity from the utility grid
C_P^{grid}	Cost of purchasing electricity from the grid
C_S^{grid}	Cost of selling electricity to the grid
$P_{gen}(t)$	Total power generated by energy components
E_{bat}^{min}	Minimum energy of battery bank
E_{bat}^{max}	Maximum energy of battery bank
P_{def}	Deferrable load

List of Abbreviations

ACO	Ant Colony Optimization
AER	All Electric Range
AENS	Average Energy Not Supplied
APL	Active Power Loss
ASAI	Average Service Availability Index
ASUI	Average Service Unavailability Index
BCBV	Branch Current to Bus Voltage
BESS	Battery Energy Storage System
BIBC	Bus Injection to Branch Current
BLSA	Binary Lightning Search Algorithm
CAIDI	Customer Average Interruption Duration Index
CCL	Charging Cost Loss
CFRLM	Capacitated Flow Refueling Location Model
COR	Competition Over Resources
CPP	Critical Peak Pricing
CRF	Capital Recovery Factor
CSO	Chicken Swarm Optimization
CSEC	Charging Station Electrification Cost
DE	Differential Evolution
DG	Distributed Generation
DLC	Direct Load Control
DLF	Direct Load Flow
DOD	Depth of Discharge
DRPs	Demand Response Programs

DSM	Demand Side Management
EDRP	Emergency Demand Response Programs
EA	Evolutionary Algorithm
EENS	Expected Energy Not Supplied
EEI	Edison Electric Institute
ER-ACO	Energy Routing-Ant Colony Optimization
ESU	Energy Storage Unit
EV	Electric Vehicle
EVLC	Electric Vehicle Energy Loss Cost
EVCS	Electric Vehicle Charging Station
GA	Genetic Algorithm
GHG	Greenhouse Gases
GPL	Grid Power Loss
GWO	Grey Wolf Optimization
HHO	Harris Hawk Optimization
HS	Harmony Search
HGWOPSO	Hybrid Grey Wolf Optimizer Particle Swarm Optimization
HOMER	Hybrid Optimization of Multiple Energy Resources
IC	Investment Cost
ICC	Uninterrupted Charging Cost
IEI	Institute for Electric Innovation
LCOE	Levelized Cost of Energy
LFS	Load Flow Strategy
LIP	Linear Integer Programming
LPSP	Lack of Power Supply Probability

MAS	Multi Agent System
MFO	Moth Flame Optimization
MIP	Mixed Integer Programming
NBR	Number of Battery Replacements
NOCT	Nominal Operating Cell Temperature
NPC	Net Present Cost
PHEVs	Plug-in Hybrid Electric Vehicles
PE	Electricity Price
PSO	Particle Swarm Optimization
RE	Renewable Energy
RF	Renewable Fraction
RTP	Real Time Pricing
SAIDI	System Average Interruption Duration Index
SAIFI	System Average Interruption Frequency Index
SEC	Specific Electricity Consumption
SNN	Shared Nearest Neighbor
SOC	State of Charge
SPV	Solar Photovoltaic
RES	Renewable Energy Sources
TD	Total Number of Days in 5 Years
TL	Transportation Loss
TLBO	Teaching Learning-based Optimization
TNPC	Total Net Present Cost
TOU	Time of Use
TTC	Travel Time Cost

V2G	Vehicle to Grid
VDI	Voltage Deviation Index
VSF	Voltage Sensitivity Factor
VSI	Voltage Stability Index
WT	Wind Turbine

ABSTRACT

The major concern of metropolitan cities is reducing greenhouse gas emissions due to conventional engine-based vehicles. Excessive usage of such vehicles leads to health issues not only in humans but also worsens the ecological system of the earth. The release of various toxic oxides like CO_2, NO_2, SO_2, etc. is one of the significant factors for global warming and change in climate. Researchers and policymakers worldwide advocate the implementation of an alternative mode of transport in the form of electric vehicles (EVs) to minimize the content of greenhouse gases. The technological advancement from conventional engine-based vehicles to EVs has numerous environmental and economic advantages, which include flexibility in fuels, easy charging, decent performance, and less reliance on fossil fuels. For the broad adoption of EVs, electric vehicle charging stations (EVCS) are inevitable. Inappropriate locations of EVCS impose negative impact on the efficiency of the electric grid. Therefore, this thesis focused on improving the grid's efficiency by increasing its reliability, optimizing the benefits of EV users, and lowering the station development cost. These objectives can be realized by investigating the optimum locations and sizing of EVCS in the electrical grid network.

This thesis comprehensively examines the impact of EV charging stations on distribution network operating parameters such as power loss, voltage stability index, voltage profile and reliability.

Further, the single-objective formulation of EV charging stations, distributed generation sources and capacitors placement with power loss minimization as the objective function is illustrated in different chapters of this thesis. Distributed generation sources and

capacitors are incorporated into the distribution network to minimize the power losses, maintaining the voltage profile and keeping the reliability of system within limits.

The control and power management of EVs in grid-connected systems are the primary focus of researchers. However, one of the important aspects that must be addressed is an economic analysis that takes into account the power exchange with the grid. The fast adoption of EVs poses both constraints and opportunities for the current electricity system. A small grid-connected SPV and DG-based hybrid system with EVs is presented in this thesis for a charging station in North west region of Delhi, India. The main objective is to formulate a statistical model of a solar and diesel generator-based hybrid system with EVs and a backup grid. Furthermore, the purpose of this work is to reduce power interchange with the grid and utilize renewable energy sources to meet the load demand of EV load.

The charging station placement problem's objective functions are highly non-linear in nature. The conventional optimization algorithms have limitations when it comes to solving this problem. As a result, the current work employs meta-heuristics to solve the charging station, distributed generation, and capacitor placement problems. A novel hybrid algorithm based on the combination of particle swarm optimization (PSO) and grey wolf optimization (GWO) is developed and used to solve the charging station, distributed generation, and capacitor placement problems. It is expected that combining PSO and GWO will improve solution quality and promote rapid convergence to the best solution. The proposed HGWOPSO is first tested on standard benchmark functions before being applied to the charging station placement problem in standard IEEE 33–bus and IEEE 69–bus distribution networks.

CHAPTER 1

INTRODUCTION

1.1 GENERAL

Communities around the world are suffering from the consequence of global warming due to greenhouse gases (GHGs) emissions. The transportation sector of any country produces considerable amount of GHGs which has detrimental effect on the climate of the earth. Fig. 1.1 shows the typical data of GHGs emissions in different countries of the world. The total annual GHGs emission in Delhi city is found to be 37.9 million tCO_2e. The per capita emission of Delhi city is estimated to be 2.26 tons per year which is lower when compared with other cities emitting GHGs. Fig 1.2. shows that the amount of GHGs emission in Delhi city is 37.9 million tCO_2e which is about five times lesser than the Beijing city, having a similar population as that of Delhi city. Pollution due to conventional vehicles creates health issues and the life of living beings is deteriorating day by day. Approximately 89% of people in Delhi are feeling sick or not in their comfort zone because of the poor quality of air and it is believed that conventional vehicles which are based on fossil fuels are the major cause of pollution. The use of conventional vehicles is one of the causes of the deterioration of air quality.

Electric transportation is growing rapidly. The updated sales of electric vehicles (EVs) till 2030 have been developed by Edison Electric Institute (EEI) and Institute for Electric Innovation (IEI) [1]. It is approximated that by 2030, the number of electric cars that will drive on the roads will be 18.7 million, and to help 18.7 million EVs in 2030 will

require about 9.6 million charging points [1]. It requires significant expense for developing EV charging infrastructure. Fig. 1.3. shows the EEI/IEI Forecast of EV in 2030.

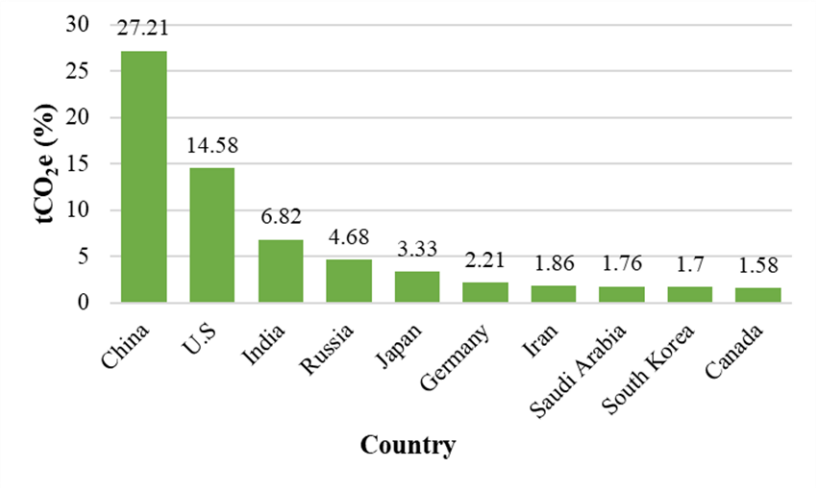

Fig. 1. 1. Typical data of GHG emission in different countries [2]

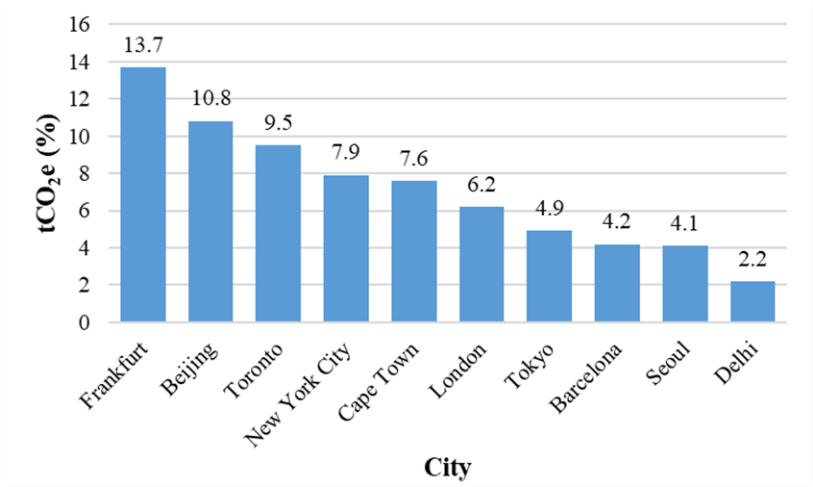

Fig. 1. 2. Annual per capita tCO_2e emission in different cities of the world [3]

Transitioning to EVs from conventional vehicles reduces the emission of gases up to some extent to solve the global warming problem. EVs neither harm the environment in a nefarious way nor do they lead to an increase in the prices of oil. EV is a future technology with numerous environmental advantages in various sectors. Although having these large-

scale advantages, there are challenges for power engineers to optimally place the charging stations (CS).

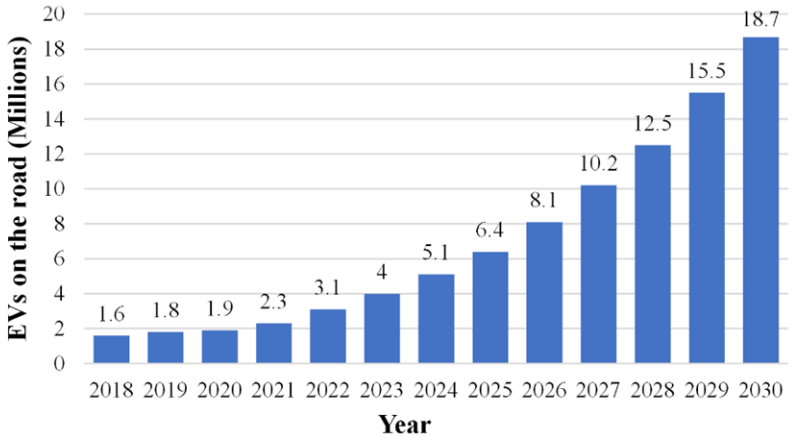

Fig. 1. 3. EEI/IEI Forecast of EV in 2030 [1]

Also, the random placement of electric vehicle charging stations (EVCS) affects adversely the acceptance of charging stations, the traffic network layout, and EV driver's convenience. If the placement of the EVCS is not proper, then fluctuation in voltages and power problems arises. The placing of the EVCS causes increases in demand for the load on the power grid, which increases peak demand and decreases in reserve margin. The placement of EVCS in the distribution network should be done in such a way that it has the least impact on the distribution network's operating parameters. The abovementioned factors motivated us to investigate the proper planning of EV charging infrastructure.

1.2 CHARGING INFRASTRUCTURE PLANNING SCENARIO IN INDIA

Changing the approach to EVs from traditional vehicles is still at an initial stage, as EVs make up a few percent of all the vehicles currently operating in the country (the list of countries per vehicle per capita in 2017), as shown in Fig. 1.4. However, a large

number of electric rickshaws can be witnessed running in not only some small towns and villages but also in many cities of India.

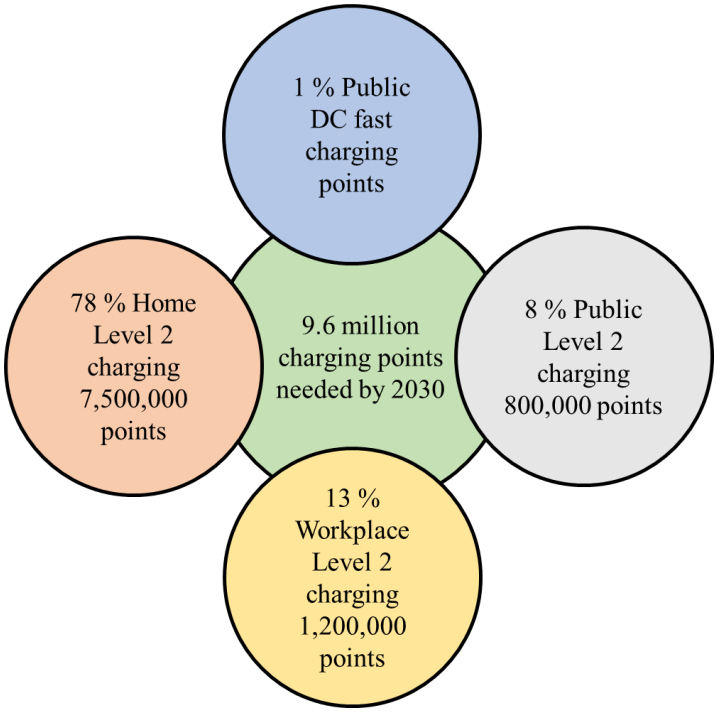

Fig. 1. 4. EV charging infrastructure in 2030 based on EEI/IEI Forecast [1]

The current population of EVs in India is very low. However, EVs (Electric rickshaws) are being operated in many Indian towns and villages. EVs are suitable for short-distance traveling and can be changed easily by a normal household socket. Despite a very low EV market, many companies are investing in the development of CS because of the reasons listed below:

(i) The Government of India promulgated in 2013 the progressive 'National Mission Movement for Electric Mobility Plan (NEMMP) until 2020' to focus on national energy security, pollution caused by vehicles, and the expansion of domestic production capacity. Taking into account the Paris Agreement, the government plans to introduce EVs into widespread use by 2030 [4].

(ii) An insufficient amount of CSs is the main reason for the smaller number of used EVs. It is, therefore, necessary to develop a sustainable charging infrastructure to make more and more use of EVs.

Thus, the growth of infrastructure for CSs is on the verge of beginning in India. The main landmarks in the development of the charging framework (The Times of India) in India are: (a) It is being planned by the Indian Government to set up 206 CSs [4]. (b) TATA Power Delhi has planned to invest 100 crore rupees for establishing 1000 CSs in Delhi [4].

Some factors inhibit the establishment of charging infrastructure. A few of them are listed below:

(a) Bleak in the EV market.

(b) The power grid's a complicated structure.

The EV Industries in India are constantly growing but the lack of CSs and policies made by the Indian government poses difficulty in the growth of the EV industry. The number of EVs sold in the years 2017 and 2018 is 56,000 units as against 25,000 units in the years 2016 and 2017. According to the view held by the Society of Manufacturers of Electric Vehicles (SMEV), in 2017 and 2018, the sales of electric cars decreased to 1200 units from 2000 units in 2016 and 2017, a slump of 40% is recorded. However, the number of electric two-wheelers for the years 2017 and 2018 is increased to 54,800 units, as shown in Table 1.1. Electric two-wheelers showed rapid growth of 138% as 54,800 units sold in 2017 and 2018 as compared to 23,000 units in the years 2016 and 2017. The reason for the

rapid growth of electric two-wheelers is its affordability and its use for short distances, which reduces the problem of range anxiety.

Table 1. 1 Typical data of electric two-wheelers and electric cars in the year 2016-21 [5]

Category	2016-17	2017-18	2018-19	2019-20	2020-21
Two-Wheelers	23000	54800	126000	152000	233971
Cars	2000	1200	2670	3400	5905
Total EVs	25000	56000	128670	155400	239876

1.3 TYPES OF CHARGING SYSTEM FOR EVs

Charging stations are the spots for providing fuels to the EVs. The main components of the charging station comprise cords, connectors, and an interface with the power grid. Availability of effective charging infrastructure is indispensable for EV deployment on large scale. EVs require additional charging when they run out of power. The electricity from the grid is alternating current (AC), whereas the vehicles' batteries are direct current (DC). As a result, the charger must be capable of converting AC to DC. According to Electric Power Research Institute, charging levels are characterized in three ways: AC level 1, AC level 2, and DC fast charging. In AC level 1 charging, the standard charger has a power of 1.4 kW and is less commonly used due to its slowness. It typically takes 8 to 17 hours to fully charge the battery using this technology. The most prevalent chargers i.e., AC level 2, have a power output of 3.8 kW. As a result, normal charging takes four hours to fully charge the EV battery.

Before charging, AC is rectified to DC. This technology operates at a higher voltage range of 200 V–450 V. Depending on whether the charger provides 80A or 200A, it can deliver between 20 kW and 90 kW. This means that it will take between 20 minutes and

80 minutes to fully charge the battery. In the literature, DC fast charging is assumed to be 45 kW supplying 200A current, resulting in a charging time of 30 minutes.

1.4 IMPACT OF EV INTEGRATION ON DISTRIBUTION SYSTEM

On a national scale, there is currently enough generating potential to charge EVs. This, however, varies depending on the region. The distribution system has the most influence in determining whether the power can handle the CS demand.

It is critical to use smart charging to manage the widespread adoption of EVs. The developed algorithms with vehicle-to-grid technology will allow for a smooth load while also managing the increased penetration of EVs. As smart grids with distributed energy resources become more common, they will become more prevalent. It will enable EVs to connect in a plug-and-forget manner, with the vehicles identifying and providing the information required for an energy transaction.

The energy stored in an EV can be used in a variety of ways, including:

1) Peak shaving

2) Load smoothing

3) Backup source

4) Ancillary services

Using distributed energy resources in EV energy management has many advantages. This is especially useful when making energy management decisions locally without consulting the system operator. The distribution loss increases as the load

increases. As a result, the use of distributed resources is beneficial in minimizing system loss. Using EVs can also help to relieve congestion on transmission lines. These factors, when combined, create opportunities for utilities to invest in transmission and generation.

1.5 SERVICE INCENTIVES

The primary function of an EV is to serve as a convenient means of transportation for its operator. As a result, it is critical to provide incentives for consumers who want to take part in the vehicle-to-grid power transfer scenario. Economic payback to offset the initial purchase cost of an EV is one of the possible incentives. The implications of vehicle lifetime and battery degradation could be reduced with better management. However, with a high penetration of EVs, vehicle-to-grid makes more sense. Incentives should be provided for the use of EV idle state in the charging station for ancillary services.

1.6 GENERAL OVERVIEW FOR PLANNING OF CHARGING INFRASTRUCTURE

The optimal siting and sizing of charging stations in the distribution network are involved in the charging station placement problem. The location of charging stations is determined by a variety of factors, including economics, operational parameters, and the convenience of EV users. Fig. 1.5 depicts a simplified layout for charging station placement.

The first step, as shown in Fig. 1.5, is to choose the test networks where the charging station will be located. Following that, the input parameters required to evaluate the optimal location and number of charging stations are set. Then, objective functions and constraints

are defined, and finally, an optimization algorithm is run to provide the optimal locations as well as the capacity of each charging station based on the number of EVs that arrive for charging.

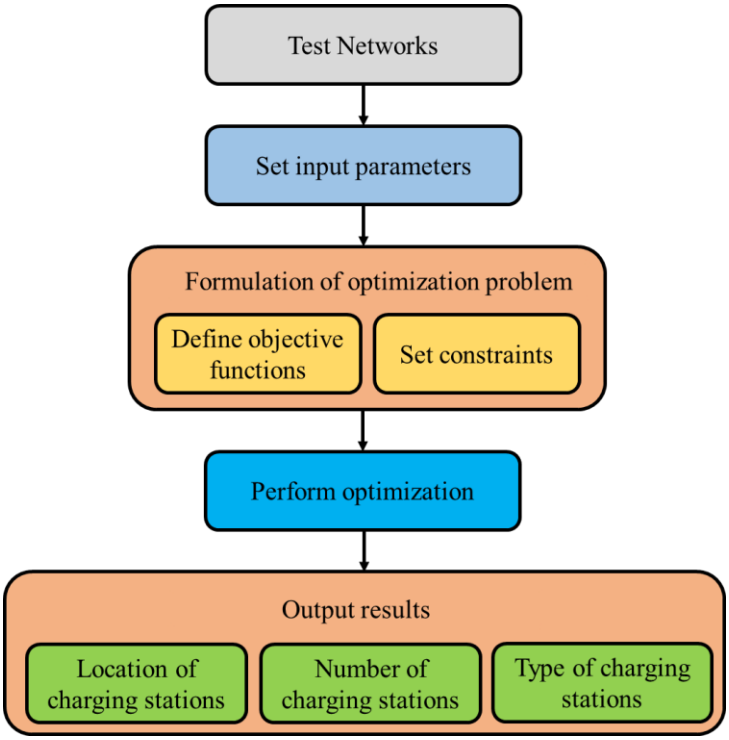

Fig. 1. 5. Overview of charging station placement

1.7 OUTLINE OF THESIS

This thesis covers eight chapters including introduction, literature review, study and analysis of load flow method, test systems, and optimization algorithms, the feasibility analysis of EVCS: a case study of metropolitan city of India, single-objective formulation of charging station and distributed generation placement problem, single-objective formulation of charging station and capacitor placement problem, techno-economic and environmental analysis of grid-connected EVCS, conclusions and future scope followed by references.

Chapter 1: This chapter provides insights into scenario of charging infrastructure planning in India. Various levels of EV charging and their impact on the distribution network is presented in detail. In addition, a brief layout for planning the charging infrastructure is discussed.

Chapter 2: A comprehensive literature survey is presented in this chapter. The literature review comprises modeling of EV load, the impact of renewable integration into the distribution network, simultaneous allocation of capacitor and EVCS in the distribution network. Moreover, techno-economic and environmental analysis of grid-connected EVCS is thoroughly performed. In addition to this, the application of intelligent techniques for the sizing and siting of EV load and other components is carried out. Based on this, the final section of the chapter introduces a knowledge gap analysis.

Chapter 3: This chapter describes the mathematical modeling of the radial distribution systems. The load flow technique has been discussed using the bus injection to branch current (BIBC) and branch current to bus voltage (BCBV) matrices. Moreover, this chapter provides a high-level overview of population-based optimization techniques such as particle swarm optimization and grey wolf optimization. HGWOPSO, a hybrid metaheuristic technique based on GWO and PSO, has been designed and its implementation of various benchmark functions is discussed in detail.

Chapter 4: This chapter emphasizes the planning of EVCS in the most populated areas of South Delhi, India. Allocation of EVCS is based on minimizing the overall cost which includes investment cost, CS electrification cost, EV energy loss cost, and travel time cost. Various intelligent algorithms have been employed to deal with this planning problem.

Chapter 5: In this chapter, a hybrid optimization strategy is suggested for the optimal planning of EVCS. DGs units are utilized to reduce the charging impact of EVs. Distributed generation (DG) sources are used in the suggested technique to preserve voltage profile, reduce active power loss and improve reliability. The joint impact of EVs and DG integration is presented for two standard test systems. The efficacy of the suggested method is tested in MATLAB, and the results are equated with present techniques which are shown in the last section of the chapter followed by the conclusion.

Chapter 6: This chapter presents the addition of EVCS and capacitors in radial distribution network with different percentages of EVs participating in the vehicle to grid mode. Also, the operating cost and installation cost of EVCS, as well as capacitors, have been included for the estimation of net profit. Reliability improvement benefits have been determined with and without EVs penetration in V2G. Moreover, a new technique entitled modified grey wolf particle swarm optimization (HGWOPSO) is proposed.

Chapter 7: The mathematical modeling and design of various energy sources are carried out in this chapter. The optimal number of components of the energy system and their sizing is thoroughly discussed. Moreover, techno-economic and environmental analysis of various configurations is comprehensively illustrated in this chapter.

Chapter 8: This chapter of the thesis presents the research work's findings. Furthermore, the future scope of the research work is briefly discussed.

CHAPTER 2

LITERATURE REVIEW

2.1 INTRODUCTION

This chapter presents the available literature on different aspects of EV charging infrastructures such as the impact of EV charging load on the distribution system, charging station placement problem formulation, and application of different optimization techniques for exploring the optimal location of the charging station. Further, this chapter describes the integration of distributed generation and capacitor along with the charging station to the distribution network. Based on the literature survey, research gaps are identified and problem formulation is carried out accordingly.

2.2 IMPACT OF EVCS LOAD ON DISTRIBUTION NETWORK

Though electrification of the transport industry has many positive effects, such as reduced CO_2 emissions, pollution, and global warming, the adverse impact of EV chargers on the utility grid cannot be overlooked. Fig. 2.1. shows how the location of the charging station affects the system parameters.

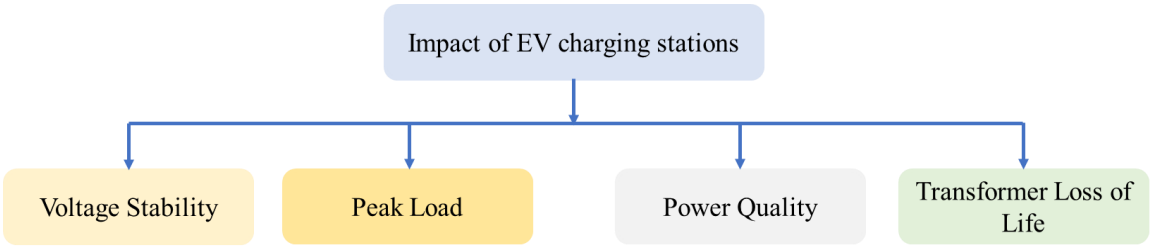

Fig. 2. 1. Impact of EV charging station on distribution network

Higher market penetration of electric vehicles leads to increased power requirements for charging, which could have negative consequences for the power system. This section discusses the negative effects of EV charging on several electric grid factors.

2.2.1 Impact of EVCS on Voltage Stability

One of the most serious negative consequences of EV charging stations is the challenge to voltage stability. The capability of an electrical ability to sustain stable voltages at all buses after disturbances have been removed from a given starting operating condition is known as voltage stability. One of the main causes of voltage instability is a sudden rise in load. The abrupt increase in load caused by charging electric vehicles causes voltage instability. A simulation model of EV penetration at the Otto-von-Guericke University Magdeburg's power system distribution network is developed in [6]. The various scenarios for EV penetration were created using real-time vehicle arrival and departure data. They evaluated voltage stability at all nodes in the distribution network and found that the simulated scenarios did not induce voltage instability. Based on a positive sequence voltage ranking index, the weakest bus in a 13-bus network is determined in the presence of EV charging stations [7]. A new framework for analyzing the dynamic stability of electrical network is introduced in the existence of EV charging loads [8]. In [9], authors investigated the fluctuation of a 16-bus commercial distribution network's voltage sensitivity index in the presence EVCS and they also presented a strategy for EVCS installation based on the voltage sensitivity index. In [10], authors observed the influence of EV load on the voltage stability of a two-bus distribution network. They also demonstrated a novel approach for representing EV load. The consequences of placing EV charging load on nodal voltage deviation is studied in [11]. The authors used an IEEE 30

test network to conduct their research and found that nodal voltage variation is directly related to EV penetration level. In [12], authors explored the effects of charging stations load on voltage profile in an IEEE-33 bus network, taking into account several EV charging load models such as constant power load, constant current load, and constant impedance load. According to the authors in [13], the negative impact of EVs on voltage stability can be mitigated to some extent by controlled charging.

2.2.2 Influence of EVCS on Peak Load Demand

The increasing load requirement for charging stations causes the grid's peak load demand to rise, resulting in a reduction in reserve margin. Authors in [14] investigated the impact of EV load on Australia's Metropolitan distribution network. They found that with uncontrolled charging and 100 percent PEV penetration, peak load shifting of 43 percent is necessary. Authors studied the fluctuation in network peak load demand due to the installation of EV fast charging stations on roads [15]. The impact of EV charging load on peak load requirements considering different possible cases of EV penetration is analyzed in [16]. It is commented by the authors that the rise in afternoon peak load induced by industrial charging of EVs is less than the rise in load produced by home charging of private EVs, according to the authors. Authors in [17] claimed that unplanned EV charging raises load requirements, and a charging discharging model has been recommended to limit peak load demand.

2.2.3 Effect of EVCS on Power Quality

Power quality is defined as a distribution network's ability to provide a consistent and disturbance-free output that is within voltage and frequency limitations [18]. The EV charging load's nonlinear behavior poses a danger to power quality. Some of the most

prevalent power quality issues are harmonics [19], and voltage sag [20]–[21]. Harmonics are current or voltage waveform sub-components whose frequency is an integral multiple of the reference signal [22]. Total harmonic distortion (THD) is a measurement of the difference between the actual obtained and reference frequency [23]. In [24], authors used statistical analysis to examine the impact of EV charger load on distribution system harmonic voltages. They categorized the chargers based on the amount of THD they generated. They also found that during the summer, even with 45 percent EV penetration, voltage distortion is minimal. Authors in [25] investigated the impact of a highly nonlinear EV load on the residential distribution network. They came to the conclusion that EV penetration levels of more than 25% will have an impact on power quality. The influence of EV charging load on voltage profile and harmonics of an urban low voltage electricity distribution network was studied in [26]. The authors of [27] compared how THD can be decreased by using a coordinated charging method that is planned ahead of time.

2.2.4 Assessment of EVCS on Transformer Performance

The increased stress placed on distribution transformers by large-scale EV deployment contributes to the transformer's life cycle being shortened. According to [28], an increase in load produces an increase in the transformer's hot spot temperature. The charging of electric vehicles results in an increase in load, which leads to an increase in hot spot temperature. The authors of [29] looked at the influence of coordinated charging, tariff-based charging, and unplanned charging on transformer loss of life and came to the conclusion that uncontrolled charging is bad for transformer efficiency. Researchers in [30] conducted a similar study and determined that uncontrolled charging promotes transformer ageing.

2.3 OPTIMAL PLACEMENT AND SIZING OF EVCS

In the literature, the placement of EVCS is based on different approaches, i.e., objective functions, solution techniques, geographical conditions and demand side management (DSM).

2.3.1 Objective Functions

Different objective functions have been considered for the optimal placement of EVCS. Costs, power loss and voltage sensitivity factors are some of the objectives considered for placement of CS. A brief outline of various objective functions has been taken into consideration while defining the problem of CS placement.

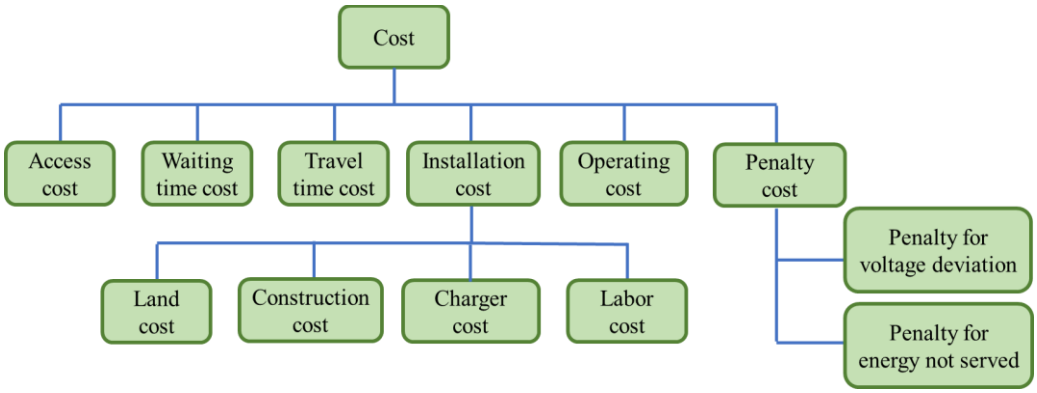

Fig. 2. 2. Subdivisions of cost function

A) Cost

Cost is treated as one of the objectives of the literature. The different types of costs associated with the CS location are indicated in Fig. 2. 2. Installation cost is the cost of installing CSs, which can be divided into charger cost, labor cost, construction cost and land cost, as shown in Fig. 2. 2. [31], [32]. Operating cost deals with the electricity cost required for providing charging services [33]. It includes billing transaction costs, repairing cost and so on. Access Cost refers to the additional cost acquired by EV users to arrive at

the CS where the EVs could be charged from the place where the need for charging the EVs arises [34]. Penalty Cost is the cost given by the utility for deviation in voltage [35]. Waiting Time cost refers to the cost earned by the EV users for staying at the CS because of the inaccessibility of charging points [36]. Land cost refers to the cost of land per unit area at the potential site for the CS. The cost of land would include all expenses associated with the acquisition of the property, as well as those needed to get it ready for use by the company [37]. Construction cost refers to all the expenses or costs incurred by a builder or a contractor for material, equipment, services, labor, utilities and so on as well as all the overhead costs [37].

B) Power loss

Power loss is also the objective function that has been considered in the literature for the optimum placing of the CS. In managing the distribution system with the addition of new units, it is essential that the location selected results in minimum increments in power loss [38]. CS is a heavy load that, when placed on a particular bus in the distribution network, results in increment in power loss [12]. The main goal is to select the optimal location in the distribution system at which the increment in power loss is as low as possible.

C) Voltage sensitivity factor (VSF)

VSF is one of the measures for choosing the optimum location of CS. It is an important factor for measuring system strength or reliability. In general, the sensitivity factor (SF) of a system can be represented as F (Z, μ), defined in (2.1) [9]

$$\text{Sensitivity factor} = \left\|\frac{dZ}{d\mu}\right\| \tag{2.1}$$

SF's large value ensures that the system is dangerous and ultimately collapsible. In VSF, the voltage of the system is measured by the change in loading as defined in (2.2) [9]

$$\text{Voltage sensitivity factor} = \left\|\frac{dV}{dP}\right\| \tag{2.2}$$

Even modest changes in the loading can result in a major change in the magnitude of voltage. High sensitivity can be defined as a large change in voltage, even due to a small change in load. This is an indicator of bus strength.

D) Constraints

The planning of charging infrastructure considers various constraints in transportation and distribution network as shown in Fig. 2.3. The power flow equation as defined by Eqns. (2.3) and (2.4) and demand balance equation as in Eqn. (2.5), are considered as equality constraints and should be satisfied for charging infrastructure planning [4]. The mathematical representation of the power flow equation is as follows:

$$P_{gi} = P_{di} + V_i \sum V_j Y_{ij} \cos(\delta_i - \delta_j - \theta_{ij}) \tag{2.3}$$

$$Q_{gi} = Q_{di} + V_i \sum V_j Y_{ij} \sin(\delta_i - \delta_j - \theta_{ij}) \tag{2.4}$$

where P_{gi} and Q_{gi} are the active power generation and reactive power generation of i^{th} bus respectively. $P_{di}\ and\ Q_{di}$ are the active power demand and reactive power demand of i^{th} bus respectively. V_i and V_j represents the voltage magnitude of starting and ending bus. $\delta_i\ and\ \delta_j$ are the phase angle of voltage at bus i and j respectively. θ_{ij} is the

angle of Y_{ij}. Y_{ij} is the magnitude of admittance of $(i,j)^{th}$ term of bus admittance matrix. The demand balance equation is defined as in Eqn. (2.5).

$$P_{CS}^{i} - P^{i} = 0 \tag{2.5}$$

where P_{CS}^{i} is the electricity demand of i^{th}CS and P^{i} is the capacity of i^{th} CS. It is essential that limits such as voltage limit, current limit or thermal limit are met after the CS is placed in the distribution network. The number of CSs required to charge the batteries of the EV shall be appropriately assigned. Also, there must be a considerable separation between each pair of CSs. The separation between the two CSs is also considered with the distance is treated as a constraint [4]. In [39], a new model is designed considering set coverage and vehicle refueling logic. A multipurpose issue was considered to minimize costs and maximize coverage. Authors presented a charge location model combined with a P-dispersion approach for the locations of CS [40]. This approach aims at lowering the trip energy and the location cost incurred while satisfying the mobility energy demand. The graph theory concepts for the modelling of the transportation network to determine the shortest route between the point where they need for charging arises and the allocated CS [32]. Based on charging demand, optimization of station size at each location is done. The single objective function of the overall cost is considered in this paper. Authors in [41] have discussed the 'queue' theory for the location of CS. Due to the limited size of CS, the vehicle should wait in queues in the case if the whole space is engaged. CS capacity, waiting time and charging time are the factors considered by the author in this paper. A new model is suggested for the CS location in [42]. The cost of travel, which is carried by

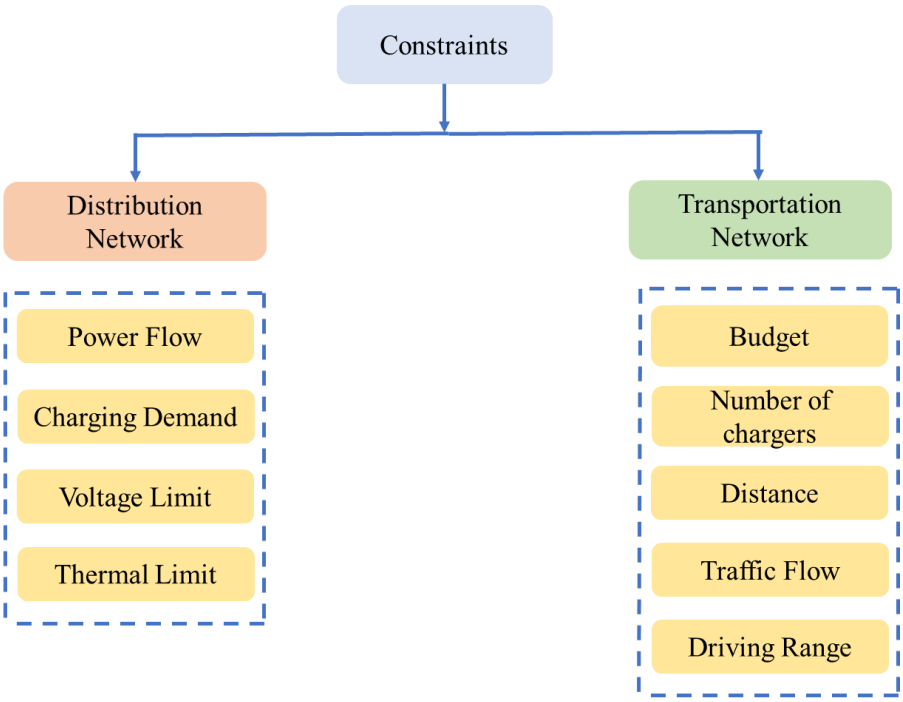

Fig. 2. 3. Various constraints considered in charging infrastructure location problem

users of EV, is considered as one of the goals that need to be minimized, and at the same time solves the problem of the place where the CS should be located and the number of chargers that will be used in each CS. Authors in [35] discussed the optimal planning of EVCS. Mathematical modelling of the EVCS is performed and the objective functions are considered: investment costs, operating costs, maintenance costs, network losses to minimize. A complicated, non-linear and combinatorial optimization problem is proposed for optimal EVCS planning and the distribution system, objectives considered are EVCS investment cost and energy and power loss [43]. Authors in [44] effectively determined the optimal location of the CS and its size in order to obtain maximum benefit, which includes increased reliability, reduced power loss and peak power.

2.3.2 Solution Techniques

The objectives used for CS placement problems are having more than one variable and are complicated in nature. Studies are conducted based on both an analytical and a

nature-oriented algorithm to solve the problem of locating CS. A brief analysis of several optimization techniques that are utilized by the various researchers to find the best positioning of the CS was searched in this part of this paper.

A) Classical Optimization Algorithm

Classical or analytical methods of optimization under the influence of differential calculus can be used to determine the optimized value of continuous and differentiable functions [4]. Some of the classic optimization methods commonly used to determine the location of a CS are integer programming (IP), linear integer programming (LIP), game-theoretic approach and a primal-dual method.

B) Evolutionary Algorithm (EA)

EA are the algorithms derived from nature and based on the principle of 'survival of the fittest'. Most of the EA has some central idea. The search process begins with a randomly generated set of population. An increase in the number of iterations leads to the best solution in the consequent generation.

Some of the benefits of an EA are

(i) Simple computation and concept.

(ii) It can be hybridized with a classical technique.

(iii) Fast convergence.

C) Particle Swarm Optimization (PSO)

PSO deals with the social behavior of the number of particles in a swarm, and each particle is presented as a solution to the problem. The PSO is capable to determine high-

efficiency solutions in comparison to other techniques. PSO can be implemented easily and has fast convergence when compared with a genetic algorithm (GA) because of the absence of evolution parameters, i.e., mutation and crossover. In [45], authors analyzed various factors affecting the CS planning and then the model is developed. Global search capabilities of PSO and Voronoi diagrams are combined for optimal planning of EVCS. First, the weighted Voronoi diagram is used to divide the defined area, and then PSO is applied to find the best location. In the above case, the author did not discuss the sizing of CS. In [46], authors established a mathematical model with optimal siting as well as the sizing of EVCS. The objectives considered in this paper are land cost, construction cost, operation cost, traffic flow, service range and serviceability. The author is aimed at minimizing the total comprehensive cost and charging ability and distance is taken as a constraint. In this paper, the slight modifications are made in the inertia weight and utilize a modified PSO approach, i.e., chaotic quantum PSO to solve the mathematical model discussed in this paper. The randomness of the chaotic operator increases the accuracy of the algorithm and has good convergence speed. In [47], authors used the PSO technique in which coefficients are varying in time for vehicle-to-grid (V2G) CS placement and sizing at a peak period in the grid. From the results of the simulation, it is examined that the V2G CS placement maximizing the net benefits, reduces the loss of energy, the saving of peak power and the improvement in reliability.

D) Genetic Algorithm (GA)

GA is a nature-inspired optimization technique motivated by the process of natural selection. GA can determine the globally optimized solution in a given search space. Authors in [31] utilized GA for minimizing transportation costs based on the grid partition

method. This paper is aiming at the placement methods of EVCS in city traffic networks. Traffic density and capacity of CS are taken as constraints. However, land cost, fixed cost, cost of operation has not been considered for optimization of the system. Thus, a global solution is not obtained. In [48], authors determined the optimal location of EVCS. The location of CS is based on economics, coverage, size and ease. Modified GA is introduced to reduce the cost of investment and the cost of transportation to locate the CS optimally. Authors presented a multi-objective problem, minimizing investment cost and feeder energy loss. The presented approach is tested on the IEEE-33 distribution system and a comparison of hierarchical HGA and traditional GA is done. The hierarchical HGA approach is found to be more successful in terms of solving the blind search difficulty [43].

E) Ant Colony Optimization (ACO)

It is also one of the well-known optimization techniques used in the literature to find the optimum placing of EVCS. Authors in [49] utilized ACO to optimize the total cost, which consists of travelling cost, operating cost, cost of power line loss for finding the CS optimal location in a distribution system while preserving the security of the power system and traffic flow are taken as a constraint. The test is conducted on the IEEE-69 bus to check the results. Authors developed an energy-efficient routing approach for EVs [50]. ACO is employed for maximizing energy efficiency. Simulation of Energy Routing-ACO (ER-ACO) is compared with other ACO techniques and it is found that the proposed techniques enhance energy efficiency. In [51], authors formulated the CS placement problem in the city of Guwahati, India. The optimal allocation of CS is based on a multi-objective function, which considers several factors such as voltage stability, power loss, reliability, variable road traffic and other economic factors. This optimization problem is

solved using a hybrid optimization algorithm, i.e., chicken swarm optimization (CSO) and teaching– learning-based optimization (TLBO). The test is conducted on the IEEE-10 bus system to verify the technique. The ACO limitation is that it has a slower speed compared to other optimization methods.

F) Integer Programming

An IP problem is a technique in which few or every variable is treated as an integer. A LIP is a word in which the objective function and constraints are defined linearly [52]. On the other hand, in the case of mixed-IP (MIP), only some variables are defined as an integer [53]. Authors in [54] developed an IP model to identify the best sets of routes and CS locations. The goals minimized with the IP approach are transportation costs, the cost of charging and the cost of placing CS. In [55], authors build up the Game theory model to solve the problem of EVCS placement and the same was transformed into the LIP problem and later on, the primal dual-path algorithm was used to deal with the problem to make the process easy and viable. However, factors such as network of the road, structure, traffic condition and constraints related to the capacity of the distribution network are not being considered. Authors suggested a mathematical approach in this paper to tackle the problem of distribution network expansion as well as the siting and sizing of EVCS [33]. A MIP approach is used to solve the problem with voltage limit is treated as a constraint and a requirement of radial network topology. In [56], the siting of fast CS for PHEVs based on the coordination between the power and transportation networks is discussed. Capacitated flow refueling location model (CFRLM) is introduced for the estimation of the charging demand of PHEVs with the incorporation of driving range and flow of traffic. MILP is employed for CS planning in coupled transportation and power grid network. This paper

deals with the minimization of investment cost while satisfying the charging demand for PHEVs. The disadvantage of IP is that it is unable to deal with stochastic issues associated with EVCS.

G) Other Techniques

Other techniques are also considered in the literature for finding the ideal site and the size of EVCS. Authors in [57] developed a cost model in which investment cost and operation cost are taken as objectives to be optimized. The model involves traffic conditions, geographic conditions and accessibility for siting of EVCS. MATLAB Programming is done to find out the cost and optimum combination of CS. In [46], authors presented a new modelling approach for the layout of EVCS. Different factors that have been considered which have effects on the layout of EVCS are charging demand, the performance of the battery, the time required to charge the battery, manner of energy supply and the location of CS. In [58], authors considered transportation loss (TL) grid power loss (GPL) and build-up costs as the objectives for the optimal location of fast CS. Battery SOC, GPL, Google Map API are taken as constraints in the recommended method. A latest and effective optimization technique, i.e., binary lightning search algorithm (BLSA) is employed for the optimization purpose. Authors in [59] described a new intelligent control plan for load management based on peak demand, the improvement in voltage profile and minimization of power loss to synchronize several chargers, taking into account the daily residential load pattern. A new approach is proposed in which transportation costs, construction costs and substation energy costs are considered as a target function for optimal planning of a fast CS (RCS) [60]. BLSA, a novel optimization technique, is utilizing for solving the objective function. The same optimization technique is applied to

traditional RCS. The test is conducted on the IEEE-34 bus system to validate the results. Authors in [61] presented fast CS planning on coupled power and transportation networks. A closed-form modelling is done for fast CS considering charging demand and driving range of PHEVs. A modified CFRLM based on sub-paths is utilized for capturing charging demand that is varying in nature and the driving range is treated as a constraint. Then, a new approach, i.e., mixed-integer second-order cone programming model, is proposed for the planning of fast CS.

Table 2. 1. Analysis of various optimization methods applied in EVCS sizing and siting problems [4]

S. No	Algorithm	Advantages	Disadvantages
1	GA	Implementation is easy, more appropriate for placement problems	Computational time is large to solve the problem
2	PSO	Computation is simple and able to determine sub-optimal solution	Early convergence
3	ACO	Has ability to discover good solutions	Convergence time is not certain
4	Greedy Algorithm	Produce feasible solution in small time	Near-optimal solutions are obtained
5	Linear Integer Programming	Solves distinct combination of problems	Not suitable for stochastic problems

It is observed that, various optimization techniques have been adopted for determining the optimal solution for sizing and siting of EVCS. In this context, Table 2.1 provides a comparison analysis between various optimization methods that are applied in EVCS siting and sizing problems.

2.3.3 Geographic Conditions

The location of CS should be chosen such that the charging service can be provided to as many EVs as possible. Thus, the flow of EVs must be maximized while planning EVCS. The objective function which describes EV flow is given as

$$Max\ f = \sum_{x \epsilon X} f_x y_x \tag{2.6}$$

where X is the set of the non-zero flow path and f_x is the traffic flow rate. And, y_x = 1 if at least one facility is provided on path x = 0 otherwise. In many studies, the flow of EV is assigned as population coverage. In [62], authors presented an optimized recharge planning strategy for the road network. The developed optimization model of the system generates the equilibrium of traffic flow and based on that; the queuing theory is introduced to find the CS capacity with the consideration of waiting time. Finally, for the economic analysis, cost functions are made for the selection of cost-effective schemes. Authors in [63] modelled the optimization structure to determine the objective design of the CS in order to reduce the total energy consumption and travel distance to the nearby CS from the point where charging is necessary. GA is utilized to solve the problem. The spatial and temporal transportation behaviors for the placement of fast EVCS on a round freeway is considered [64]. The above approach gives an idea of charging points along the highway and takes into account the uncertainties in battery performance and transport behavior. The shared nearest neighbor (SNN) clustering algorithm is used to determine the EVCS locations on a round freeway. Finally, The Queuing Theory has developed the capacity determination model, which determines the number of chargers required in each CS, which reduces the total cost, i.e., the sum of the cost of the charger and the waiting cost. Authors

in [65] overcame the problem of locating the CS in such a way that the proposed approach should benefit the EV owner, CS owner and the operator of the network. A Logit Nested Model is used to inspect the load sequence of the owner of EV and judge the total demand at the CS. Competition among CS as a Bayesian Game has been formulated. A bi-level programming model is proposed for determining the optimal location of CS with EV, All Electric Range (AER) is taken into consideration [66]. With this approach, the location of the CS is optimized for minimizing traffic flow. While in the lower level, EV driving range constraint is defined. Later, the bi-level problem is formulated as a single-level program and later on, the problem is made of linear nature for designing the meta-heuristic algorithm.

2.3.4 Demand Side Management (DSM)

The goal of DSM is to inform consumers that consumers should use less energy during peak times and make the most of it during off-peak hours, i.e., at night and on weekends. DSM programs comprise planning, executing and controlling activities of electric utilities, which are made to motivate energy users to batter their level and electricity usage pattern. Demand response programs (DRPs) motivate the electricity user to cut or reduce electricity use during peak hours at the cost of low electricity bills. The DRPs are categorized into time-based programs and incentive-based programs. In time-based programs, the price of electricity changes at different times, depending on the cost of the energy supplied. These programs can further be subdivided into Time of Use (ToU), Real-Time Pricing (RTP) and Critical Peak Pricing Programs (CPP).

Incentive programs are designed to encourage energy users to leverage energy efficiency. Incentive-based programs can be categorized as Direct Load Control (DLC),

Emergency DRP (EDRP), Capacity Market Program, Interruptible/curtailable service, Demand Bidding and Ancillary service programs. Fig. 2.4 shows the classification of DRPs. In the current scenario, it is essential to consider DSM to find the optimal location of EVCS. Control schemes of battery capacity are essential while considering the DSM for the determination of the optimal location of EVCS. The studies reported in the literature mainly focus on the economic aspect and transportation sector. Authors in [67] considered DRPs to find the optimal site as well as the size of EVCS. The DRPs are categorized into incentive-based programs and a time-based program. In this paper, investment cost, the cost required for making the connection, cost incurred in losses and DR cost are considered as the objectives which are solved using PSO. In [68], authors proposed the optimal sizing of CS considering power loss and voltage drop as objectives. The authors came up with the new approach, i.e., demand response (DR), for improving power loss and maintaining the voltage profile. Time of use (TOU), Critical peak pricing (CPP) and Real time pricing (RTP) are incorporated into the problem. GA is utilized to tackle the problem.

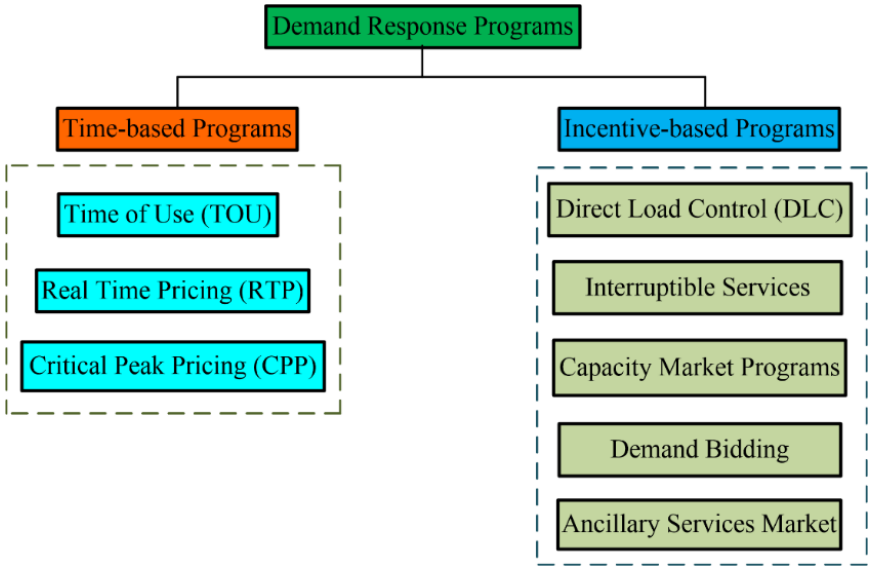

Fig. 2. 4. Classification of demand response programs

Different researchers have considered the different approaches for the optimal location of CS. These approaches are based on the selection of objective functions, solution techniques utilized, consideration of geographic conditions and inclusion of DRPs.

The chart given in Fig. 2.5(a) shows that the available literature predominantly states that the optimal location of CS based on four different approaches. The approaches are (a) objective functions, (b) solution techniques, (c) geographic conditions and (d) DSM.

The literature survey depicts that ~21% of research is based on objective function considered for placing the CS. The literature surveyed also shows that 57% of the research was based on the solution technique for the placement of CS. Similarly, the research based on DSM is 7% and research based on the geographic condition has a proportion of 15% in the literature survey.

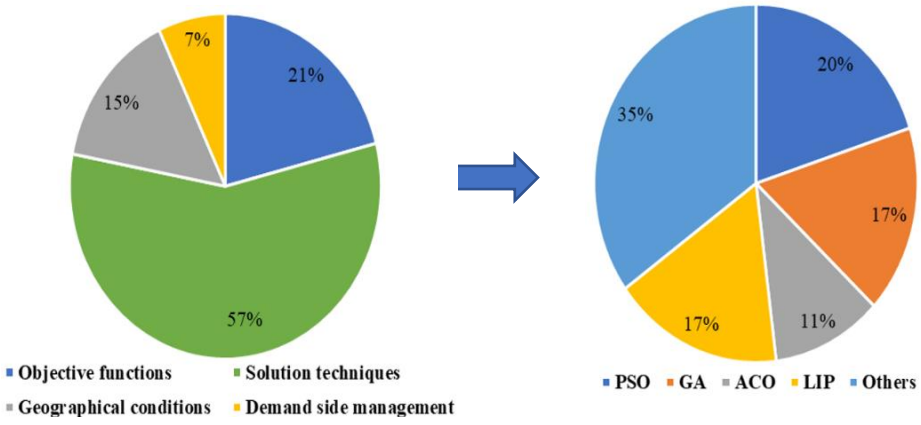

(a) (b)

Fig. 2. 5. Survey of different approaches considered in literature for optimal siting and sizing of EVCS

As far as the solution techniques are concerned, there are many techniques that are utilized by the researchers. Approximately 20% of the researchers utilized the PSO technique in their research as surveyed. Similarly, 17% of researchers have used GA, 11%

used the ACO technique and 17% utilized LIP technique for the CS placement. It can also be said that 35% of the researchers utilized other techniques like queuing theory, BLSA etc.

2.4 REVIEW ON INTEGRATION OF EVCS AND CAPACITORS IN DISTRIBUTION SYSTEMS

Many research studies in the domain of EVs allocation, operation management in the distribution network along with capacitors are summarized as follows:

EVCS allocation in electric distribution networks causes challenges for grid operators if proper planning procedure is not considered [69]. Researchers and academicians are looking for the appropriate planning of EVCS in power systems [70]. Various researches have been conducted on integrating EVCS into the electric power network. In this context, the influence of integrating EVCS to the electric power networks in terms of system's power loss and voltage profile is addressed in [71]. The EVCS has been optimally planned for the 30-bus system [72]. Also, fluctuations in voltage have been considered and EV Load is assumed to be voltage dependent. In [73], allocation of distributed generations (DGs) and EVCS have been performed for IEEE 30-bus and IEEE 69-bus system. A hybrid algorithm-based optimal scheduling of EV parking lot has been carried out in electric power network of Allahabad city (India) by minimizing the installation cost and improving the power quality [74]. A new approach i.e., demand side management is introduced for the allocation of EVCS in electric power networks. Optimal planning of EVCS infrastructure has been performed by decreasing the cost of installation, cost of operation, and maintenance cost by taking care of system reliability [75]. The

constraints include the reliability checking of electric power network, ensuring reliability of EV charging and the service quality of charging infrastructure. A battery capacity-constrained EV flow capturing location model is suggested for maximizing the EV traffic flow. The proposed technique is executed on 33-bus distribution system and 25-node road network. In [76], authors have planned the EVCS placement in superimposed distribution network and road network. The 2 m point estimation approach is used to consider EV uncertainties. Also, differential evolution (DE) and Harris Hawks optimization (HHO) methods are used for optimization purposes. A new methodology has been adopted for the optimal location and sizing of parking lots by enhancing network reliability and minimizing the cost [77]. Several cost functions are taken into consideration, including the cost for improving reliability, cost of improving power loss, etc. competition over resources (COR), have been utilized for optimization purposes.

The number of heuristic methods has been modeled for the optimal placement of capacitors. In [78], DE approach-based siting and sizing of shunt capacitors along with distributed generation is discussed with the goal of lessening the power loss of the system. Authors proposed the two-step procedure for investigating the appropriate location and sizes of capacitors in distribution network. The power loss is optimized by employing the ant colony optimization [79]. The suggested approach is implemented on 34-bus and 85-bus radial distribution system. In [80], optimal power flow is carried out using hybrid of DE and harmony search (HS) algorithm. The optimization problem is aimed at minimizing the fuel cost and transmission loss as objectives. In [81], a new strategy is introduced for the proper positioning of the EVCS, which focuses on congestion management and the compensation for reactive power to allocate parking lots and capacitors. Biogeography-

based optimization approach was considered for the optimum size of the parking lot. Authors presented the grasshopper optimization algorithm based on two stage fuzzy multi-objective approach for optimum sizing and placement of EVCS, distributed generations and capacitors in the electrical distribution network [82]. The objectives considered in this paper are cost of generation, power losses and voltage stability factor. A new comprehensive strategy for the parking lots and capacitor allocation is presented with the consideration of congestion management [83]. Quantum-Behaved and Gaussian Mutational Dragonfly Algorithm is utilized to optimize real and reactive power loss. An efficient optimization technique for the optimum location and sizing of static VAR compensator in hybrid electric network is discussed.

2.5 REVIEW ON INTEGRATION OF EVCS AND DG IN DISTRIBUTION SYSTEMS

Some research works are concentrated on mitigating the severity of EVs on the power system. In [84] , the authors present a sustainable, intelligent load balancing control approach for lowering electrical losses and improving system voltage. Reactive power regulation is utilized in EVCS to enhance the voltage profile [85]. The reliability and techno-economic benefits of DG integration have been demonstrated [86]. Therefore, DGs integration has been proposed as a viable approach for mitigating the charging consequences of EVs [87]. The author utilized particle swarm optimization for the EVCS and DGs allocation in an unbalanced radial distribution network [88]. The author suggested a hybrid grey wolf optimizer for 33-bus, 69-bus, and Indian 85-bus distribution networks to reduce power loss [89]. Authors in [90] created optimization models to collectively

manage the locations and sizes of EVCS, solar photovoltaic power plants, and energy storage systems in power systems while considering future power strategic management. The author employed modified single and multi-objective Harris Hawks Optimization algorithms for obtaining the nodes to optimally locate the DGs in the radial power network. Finding ideal nodes is done with the goals of minimizing power loss, preserving voltage levels, and improving the voltage stability index [91]. The authors of [92] proposed an indicator for determining the best location for DGs in electrical networks. This indicator is used to address a variety of issues, such as total electrical loss minimization, energy not supplied, and voltage variation. By system reconfiguration and the integration of solar/wind-based DGs, another endpoint, namely annual energy reduction loss, is seen [93]. Additionally, an innovative two-stage stochastic programming method is presented, and the uncertainty issues, as well as load fluctuation, are investigated, particularly for wind and solar energy production [94]. The overall cost is decreased in this technique by including battery storage systems into the distribution network and planning for demand response programs. Simultaneously, due to the appropriate size of battery energy storage and optimal position, the improved reliability of power system reliability is obtained. A multi-objective optimization model is presented with the objective of reducing power loss, improving voltage deviation, and cost in order to assign EVCS and capacitors in candidate buses optimally [95]. In an unbalanced distribution system, solar PV units are used to adjust for EV charging demand [96]. Cost, dependability, power losses, and voltage profile are all taken into account when synchronizing charging stations and DGs [68]. Capacity reinforcement with DGs is recommended to offset the growing penetration of EVs, with reliability improvement as one of the objectives [97]. The authors in [98] discuss the

development of a charging station that incorporates wind production and storage. The best DG penetration level for a specific EV energy consumption is evaluated [99].

2.6 REVIEW ON SOLAR PHOTOVOLTAIC-BASED EVCS

A serious threat is encountered by transport sector throughout the world due to increasing concentration of particulate matter (PM) in the atmosphere. The polluting agents like carbon monoxide, nitrogen dioxide, sulfur dioxide, etc., have deteriorating effects on human health. Keeping in view, the government of countries all over the world are trying to provide a sustainable and eco-friendly nature of environment. The combustion engines based on non-renewable sources of energy produce green-house gases in large quantities which have negative impact on environment. Also, the optimal location of EVCS is of utmost importance for charging EVs [100]. EVs do not produce any harmful end product. Thus, there is an increasing demand of EVs in transportation industry. However, the power required for recharging the batteries of EVs directly from the power grid will create an additional load, especially during peak hours, i.e., during day time [101]. For the sake of minimizing the overload on grid network due to charging of EVs, many alternative solutions have been developed. One of the solutions is to employ solar photovoltaic (SPV) for charging EVs. Due to recent developments in the area of PV modules, they are becoming cost-effective and gained popularity in EV charging application [102]. Application of PV modules in EV charging has many advantageous such as low maintenance cost and no fuel wastage [103]. The PV application for charging EV can be upgraded by new developments in conversion technologies, battery management system (BMS), and their installation practices [104]. During day time, EV can be charged directly using solar power, and this method of charging is popularly known as “charging while

parking" [105]. EVs can be charged conveniently by parking them below the PV-based parking lot as shown in Fig. 2.6.

This approach of PV-based charging of EVs proves to be eco-friendly and cost-effective in nature, which is generally employed at workplaces, such as near big malls and offices, and parking firms [106]. This method of overhead PV-based charging system protects EVs from direct sun and rain, which is common in hot and humid climatic conditions. Over the past few years, many methods have been proposed related to PV–EV charging. The most feasible method is the PV–grid combination to charge EVs. In PV–EV charging, initially, SPV is utilized for charging EVs and shifts to grid system when power from SPV is unavailable or insufficient. Whereas in standalone type, charging process is

Fig. 2. 6. PV–based parking lot for EV charging [105]

carried out using solar PV only [107]. This approach of charging EV is predominant in areas where power grid is unavailable. There are certain modifications for standalone approach, such as the inclusion of fuel cell and battery bank as power source. During last few years, many review and research papers have been published on recent trends and developments in the area of solar PV–based EV charging. In this paper, techno-economic feasibilities of charging EV using the combination of PV and grid as well as PV–standalone

are discussed and compared with grid only system. This paper presented the feasibility analysis and some of the important aspects of different modes of operation of PV–based EVs charging. Several PV–based approaches for charging EV such as PV–grid charging and PV–standalone is described in this paper. Furthermore, the inclusion of energy storage unit (ESU) for storing the energy obtained from solar PV and grid, especially when there are no EVs required for charging is mentioned which is rarely available in the literature.

2.6.1 PV–EV Charging Approaches

EV takes a large amount of current from utility system during charging, which imposes an extra load on the system [108]. Moreover, if charging of EV is carried out during peak hours, i.e., day time, the EV owner has to pay a high tariff.

Renewable energy system (RES) should be used for EV charging for reducing the overload on grid and to enhance its stability [109]. At present, the most common charging approaches which involve PV are PV-grid charging and PV-standalone. In former case, it is possible to charge EV even during inadequate irradiance level by taking power utility grid [110].

It is also more advantageous because the power obtained from SPV can be supplied to the grid when EV is not available for charging. While in latter one, i.e., PV-standalone is well suited in those areas where the availability of utility grid either very low or it is quite expensive [111]. Its setup is simpler due to fewer conversion stages are required.

1) PV-Grid Charging

A specific configuration of PV-grid charging mechanism is shown in Fig. 2. 7. It comprises three major sections (1) DC-DC converter with MPPT capability, (2) bi-

directional inverter, and (3) bi-directional DC charger. For the stabilization of the voltage of DC bus, the ESU has also been recommended. It also provides compensation for the fluctuating behavior of RES [112]. Regardless of these advantages, the initial cost, operating cost, and maintenance cost of ESU are high. However, the reduction in initial investment can be made using lead-acid battery. Furthermore, for safety issues, BMS is introduced which also maintains the battery life of EV and ESU. All main components are integrated

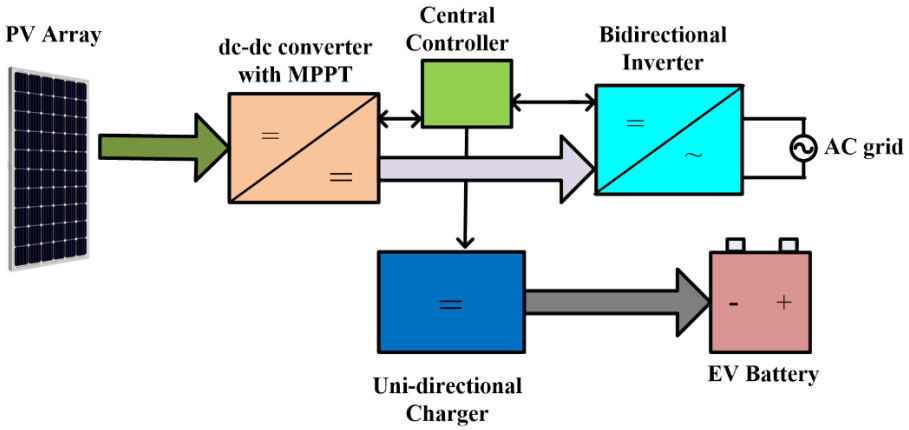

Fig. 2. 7. Typical block diagram of PV-grid for EV charging mechanism [113][114]

conveniently at the DC common bus. The voltage of DC bus is variable in nature, but typically its value ranges between 200 V and 400 V. The DC bus acts as a medium for signaling, i.e., transfer the signal within the system [114]. A central controller is introduced which decides the flow of power and activates the converter. It operates on the basis of some decision-making algorithm. It is mainly designed based on some objectives, i.e., charging cost minimization, maximizing profit, etc.

a) DC-DC Converter with Capability of MPPT

The primary goal of MPPT-based DC-DC converter is to take out large amount of power from the PV panel. Usually, this converter is operated either in boost or buck-boost

mode. In Fig. 2. 8, the working of MPPT has been described. At a specific sampling cycle, sensors are employed for sensing the voltage and current obtained from the solar panel [115]. Magnitude of both voltage and current is injected into MPPT which determines MPP. Once determined, it generates the reference value of current I_{PV}^{*} and voltage V_{PV}^{*}. These values should be comparable to the DC-DC converter. After this, measured value of power is compared with MPP value. If there is mismatch between the two values, duty cycle is adjusted to decrease the difference. PI controller or hysteresis controller are used for adjustment process. When the two power values, i.e., measured power and reference power becomes equal, the array will deliver the maximum power.

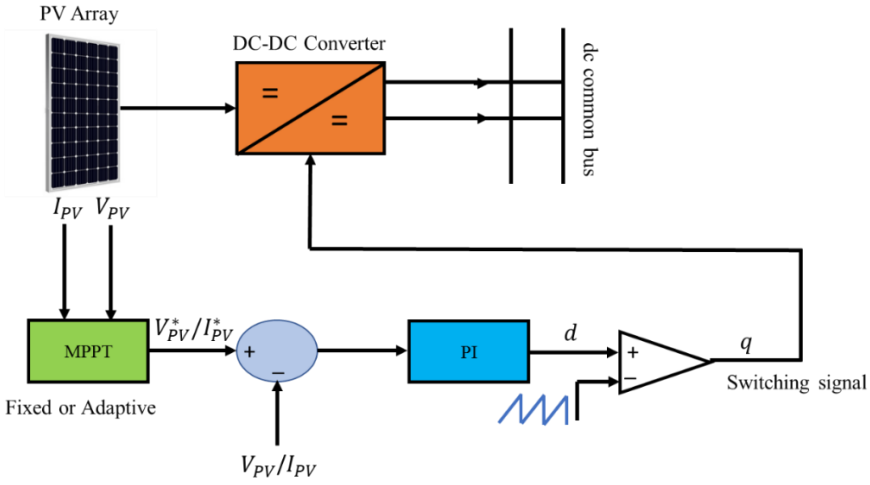

Fig. 2. 8. MPPT-based DC-DC converter

b) DC-AC Bi-Directional Inverter

The bi-directional DC-AC inverter operates in the entire four portions of current/voltage regime [116]. Therefore, it either work as an inverter, i.e., DC bus power is injected into the grid or as a rectifier, i.e., power can be taken out from the grid for the charging of DC bus. It acts as boost converter in rectification mode and as buck converter

in inversion mode. Moreover, it must operate at controllable power factor during inversion process.

c) Bi-directional DC-DC Charger

The DC charger is employed for controlling the current and voltage to a level such that it matches with EV which is being charged. It needs to be directional, i.e., power flows in both directions for full power control. In discharging, it acts as a boost converter, while in charging, it acts as a buck converter. It can be assumed as current controlled source which supplies current to the battery, estimated by the variation between the battery voltage and set reference value.

d) Charging Operation

Initially, when EV connected with the grid battery has a state of charge (SOC) lesser than 100%. In PV-grid network without incorporating ESU, vehicle to grid (V2G), and vehicle to vehicle (V2V) operations, the charging process sequence is as stated [110].

Case 1: If power supplied by solar PV is higher than what EV requires, than in this case additional power is generally provided to the grid and grid energy does not play any role in EV charging.

Case 2: In this case, charging of EV takes place only due to the grid power because of unavailability of PV power either due to bad climatic condition or during night hours.

Case 3: In this case, EV is initially charged by PV power. But due to low irradiance, the remaining charging is carried out by grid power.

Case 4: If there is no requirement of charging EV, power delivered by solar PV is injected into the utility grid directly; providing financial benefit to the owner.

Mode 1: EV connected to PV only

If power delivered by solar PV is enough for charging EV, then EV charging is done completely by solar PV. Schematics of charger and converter used for charging process are shown in Fig. 2.9 (a) [117]. System is connected partially to the grid in this particular mode and alone PV perform the charging activity. The charger is employed for regulating the DC voltage so that it matches with the EV.

Mode 2: EV connected to grid only

On the other hand, if PV is not capable of providing power to EV, the EV charging takes place using grid power only. Bi-directional inverter is used to convert AC grid power to DC and the obtained DC voltage is conditioned using charger as shown in Fig. 2.9 (b) [117].

Mode 3: PV and grid-based charging of EV

In certain special cases, where PV generated power is not enough to charge vehicle than grid connected PV could be utilized. Schematic for grid connected PV is as shown in Fig. 2.9 (c) [117]. The quantity of power output delivered by solar PV decides the energy to be taken from grid. The remaining energy is provided by the grid. Because of irregular irradiance condition, the power taken from the solar PV must be continuously monitored and accordingly make some adjustment for taking grid power for maintaining the EV charging profile.

Mode 4: Grid inversion mode

In this mode, there is no EV need to be recharged and solar PV is continuously producing power, all the power will be supplied to the grid by means of DC-DC converter and bi-directional inverter as shown in Fig. 2.9 (d) [117].

Mode 5: Vehicle to grid (V2G) mode

In this mode of operation [118], power flow takes place from vehicle to grid. The tariff is high during some specific hours of a day. Thus, additional energy stored in EV parked in a lot is fed to the grid. Such type of charging is performed via bi-directional inverter and bi-directional DC-DC charger as illustrated in Fig. 2.9 (e).

Mode 6: Vehicle to Vehicle (V2V) mode

This mode deals with the flow of power/energy between the two vehicles as illustrated in Fig. 2.9 (f) [118]. In some hours of the day, energy is transferred from the EV which has surplus energy to the vehicle which is assumed to depart from the parking lot earlier or does not have enough SOC. This process also affects the life of battery. That is why it is practically uncommon in practice.

Mode 7: Power transfer from PV to ESU

In some cases, when no EV need to be charged either due to unavailability of EV or they are fully charged then ESU are employed to store the power taken form solar PV to meet the future requirement. This charging mode minimizes the dependence on grid because energy stored in ESU will be utilized.

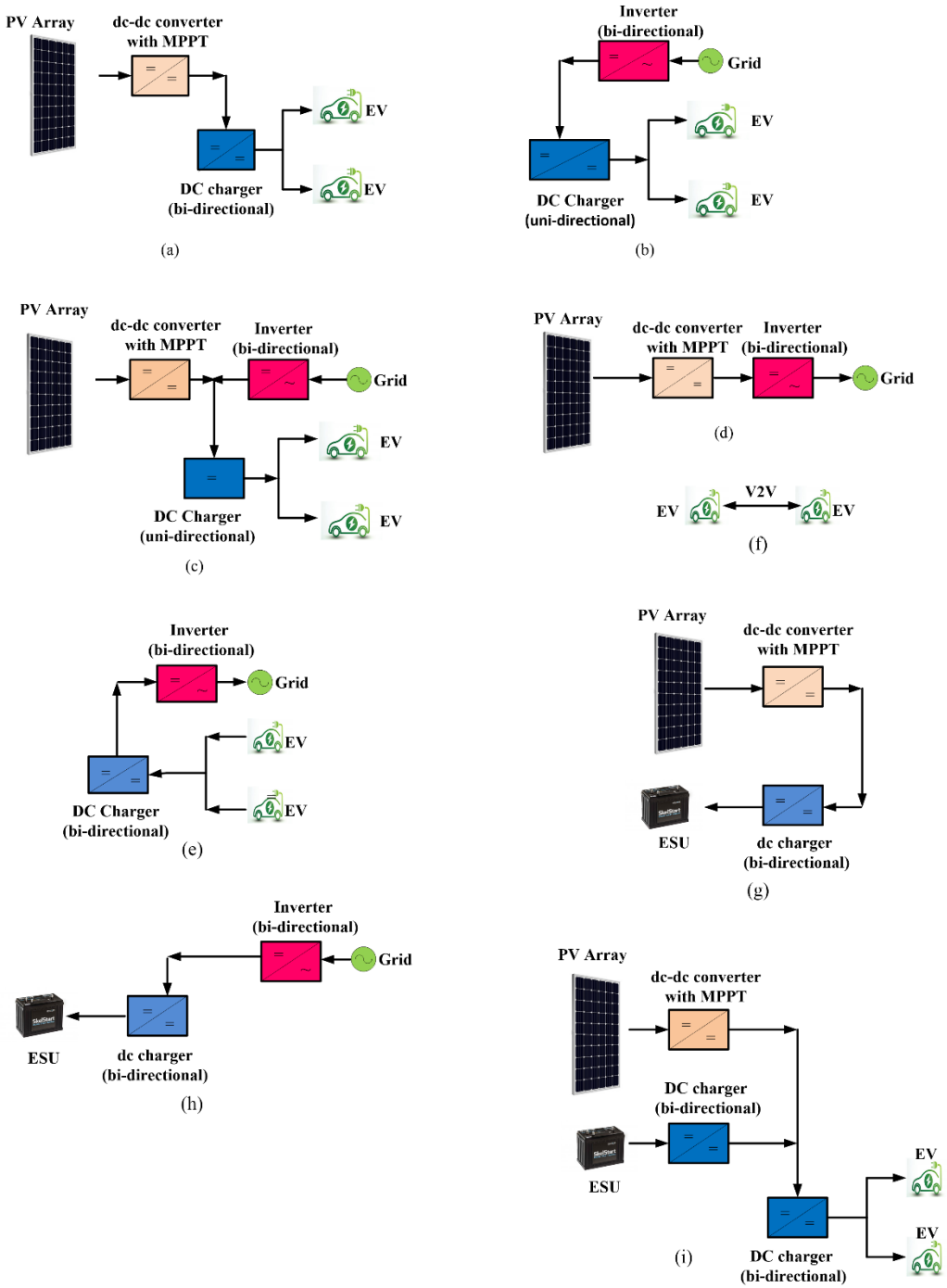

Fig. 2. 9. Possible modes of operation. a) Mode 1: charging of EV by PV only; b) Mode 2: charging from grid only; c) Mode 3: combination of energy from PV as well as grid; d) Mode 4: EV is not available and solar power is fed to the grid; e) Mode 5: V2G mode; f) Mode 6: V2V mode; g) Mode 7: PV power is fed to the ESU when EV is not available; h) Mode 8: EV and PV not available and grid is charging ESU in case of low SOC; i) Mode 9: PV is not available and ESU is supplying energy to EV

Mode 8: Power transfer from grid to ESU

When grid is lightly loaded and electricity prices are low, i.e., night time and there is a need to charge ESU, then energy can be transferred from grid to ESU in order to maintain its charging profile as shown in Fig. 2.9 (h) [117]. This mode has the advantage of low grid tariff to be utilized for CS benefit.

Mode 9: Power transfer from PV and ESU to EV

PV power and ESU are combined to charge EV as shown in Fig. 2.9 (i) [117]. This mode becomes active when PV power is insufficient to charge EV and ESU has enough SOC. This operation mode reduces the burden on grid for EV charging.

2) PV-Standalone Charging

In PV-standalone, charging of EV takes place completely by solar PV without involving grid as illustrated in Fig. 2. 10 [119]. This approach of EV charging is more reliable as the less power conversion steps are required. The PV modules should be sized such that the charging demand of specified number of EVs must be met. Due to the fluctuations in irradiance level, this method is unpopular in comparison with former charging approach.

Two charging approaches are existed on PV-standalone system (a) EV are directly connected to PV as illustrated in Fig. 2.10 (a), (b) EV and PV are connected via intermediate ESU, i.e., battery bank as shown in Fig. 2.10 (b), (c) [120]. In addition to this, there are various methods which involve hybrid solution. However, the limitation of direct charging of EV is inadequate and fluctuating nature of solar power. While ESU stores extra

energy and to be used during the non-availability of PV power [121]. Also, ESU flatten the sudden changes in output power form solar PV [121]. The EV charger controller has a significant effect on this process. DC-DC converter has the capability of tracking MPP. It is employed for regulating the PV voltage in a way such that the charging current must be an optimized value.

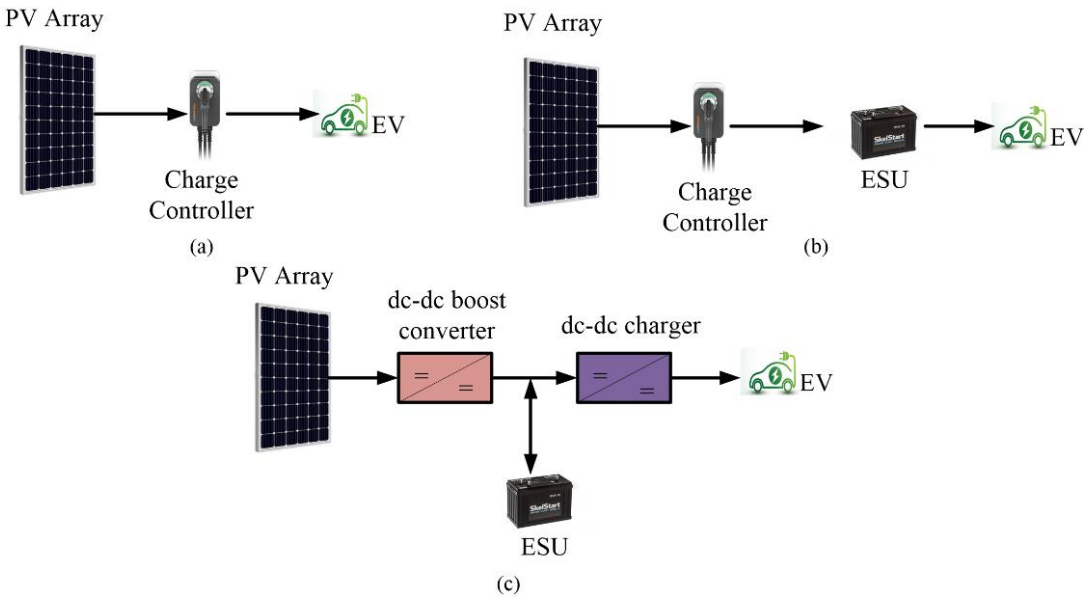

Fig. 2. 10. PV-standalone charging mechanism: (a) without a battery, (b) with battery, (c) with battery

2.7 KNOWLEDGE GAP ANALYSIS

The following are the key research areas where some gaps are identified. These gaps are as follows:

- To the best of author's knowledge, numerous studies have been conducted so far for the siting and sizing of EVCS in distribution and transportation network. But few of them addressed the aforementioned problem by taking the realistic data of EVs into account. Also, impact on reliability of grid in terms of charging

cost loss is rarely performed in past studies. Reliability evaluation is an important factor to be taken into account for the optimal planning of EVCS. Furthermore, application of intelligent meta-heuristic technique for the particular case study has not been performed in prior works. This research work is focused on optimal planning of EVCS in different well-known areas of South Delhi considering land cost, coordinates i.e., latitude and longitude, elevation and population density of charging station location. Moreover, reliability analysis is carried out to investigate the impact on grid. Therefore, this work will be carried out by utilizing GWO for the planning of CS in the proposed site.

- A lot of studies have been carried out for integrating the EVCS and capacitors into the distribution networks but in a separate manner. Also, vehicle to grid (V2G) facility of EVs along with the placement of capacitors for improving the reliability of grid network is discussed in few research works only. The benefits of capacitor allocation for reducing power loss and enhancing the voltage profile on incorporating EVCS into distribution networks have not been adequately reported in aforementioned planning studies. The joint placement of capacitor and EVCS can reduce power loss, enhancing power factor correction, and many more. Therefore, modeling and application of hybrid intelligent algorithm can be investigated for the allocation of capacitors in presence of EVCS in radial distribution network. The hybrid algorithms combine the desirable attributes of the two algorithms and leads to better results.

- The majority of related literature and studies are focused on the impact of EVs on voltage level and system losses, with little emphasis on reliability. EVs are another category of load that enters the grid network, and the reliability of these EV loads is largely overlooked. Despite the abundance of research on DG siting and sizing in the literature, its impact on the reliability of grid networks is a growing subject of research that has received little attention in previous studies. Therefore, the use of a hybrid intelligent methodology can be investigated for DGs allocation in the presence of EVCS in a radial distribution network.
- The control and power management of EVs in grid-connected systems are the primary focus of researchers. However, one of the important aspects that must be addressed is an economic analysis that takes into account the power exchange with the grid. The fast adoption of EVs poses both constraints and opportunities for the current electricity system. A small grid-connected SPV and DG-based hybrid system with EVs are presented in this article for a charging station in the northwest region of Delhi, India. The main objective is to formulate a statistical model of a solar and diesel generator-based hybrid system with EVs and a backup grid. Furthermore, the purpose of this research is to reduce power interchange with the grid. The application of hybrid algorithm has never been introduced before for satisfying the EV load requirement using hybrid SPV and DG with utility grid as a backup. To our knowledge, no previous study has compared the performance of so many different sizing methodologies on a single energy system. Hence, the employment of hybrid intelligent algorithm can be studied for the optimal

designing of different components of hybrid energy system to satisfy the load demand of EV load.

2.8 PROBLEM FORMULATION

Based on the research gaps, the following main objectives are proposed:

- ✓ To perform the feasibility analysis of EV charging station
- ✓ To perform the optimal planning of EV charging station integrated with capacitors
- ✓ To perform the coordinated allocation of EV charging station and distributed generation
- ✓ To perform the techno-economic and environmental analysis of EV charging station

CHAPTER 3

STUDY AND ANALYSIS OF LOAD FLOW METHOD, TEST SYSTEMS, AND OPTIMIZATION ALGORITHMS

3.1 INTRODUCTION

As illustrated in Chapter 2, the computational time required to perform load flow for optimal placement of EVCS and DGs in different distribution systems using optimization algorithms is essential to determine the convergence rate. The characteristics of EVCS load and various types of DG and their integration into distribution systems have a considerable effect on the system's technical quality, financial procedure, and emission reduction.

In the power transmission system, load flow techniques such as Gauss-Seidel [122], Newton–Raphson [123], and the Fast Decoupled method [124] are particularly well suited. These traditional techniques encounter convergence challenges because of their large resistance to reactance ratio, un-transposed lines, imbalance loading, and also their distinct topological configuration and features. Some modified conventional load flow techniques, such as the Gauss implicit Z-matrix method [125], are extensively utilized, but they fail to converge for radial and weakly meshed networks. Following that, a compensation-based technique [126] is anticipated in place of the forward and backward sweep technique. Though, this strategy necessitates a new datatype and searching mechanism. Some other technique [127] uses a feeder lateral-based model for load flow, which requires data arranged in accordance with the layer-lateral. Authors in [128] proposed a topographically based load flow technique in which admittance and Jacobian matrix are no longer

mandatory, as in traditional load flow approaches. Hence, the proposed method for load flow is reported to be more reliable and requires less computing effort. The topographical-based load flow method is first described in this chapter, which is relatively simple and requires less computing effort [128]. Also, several test networks that have been used to validate the proposed method are included in this chapter. Moreover, this chapter concentrates on optimization algorithms and their mathematical modeling. Optimization techniques aid in the finding of optimal solutions, as well as unconstrained maxima and minima, for a wide range of applications. The chapter focuses primarily on swarm-based optimization techniques such as particle swarm optimization (PSO) and the grey wolf optimizer (GWO). Finally, the chapter explains the modeling and development of a hybrid technique referred to as Hybrid Grey Wolf Optimizer Particle Swarm Optimization (HGWOPSO). It integrates the exploitation and exploration characteristics of GWO and PSO. The hybrid methodology outperforms both the GWO and PSO techniques. The hybrid approach is compared to other standalone approaches in terms of computational time, convergence rate, an optimum solution.

3.2 LOAD FLOW TECHNIQUE

One of the most common ways to conduct load flow analysis of the radial distribution system is to use a direct approach algorithm. Robust convergence, simplicity, decent speed, and low memory usage are the characteristics feature of this algorithm. In this method, two matrices are made with the assistance of line data and load data. The desired matrices i.e., bus injection to branch current matrix (BIBC) and branch current to bus voltage matrix (BCBV) are developed. Fig. 3.1 shows the simple line diagram of the

6-bus radial distribution network. The direct approach method involves the following steps to perform the load flow.

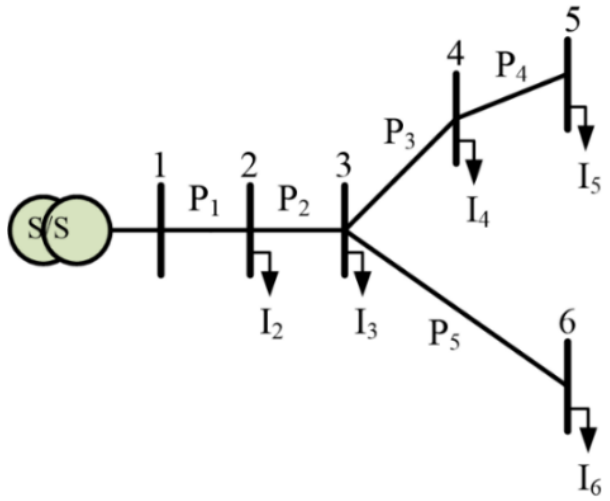

Fig. 3. 1. Connection diagram of the 6-bus distribution system

Step 1: Initialization

Initialize the following parameters:

- Line and load data of distribution network.
- The base voltage and base MVA.
- Evaluate the base impedance.
- Convert the actual values of line and load data in per unit.
- Assume voltage at each node is 1 p.u.
- Set tolerance Є =0.0001 and $\Delta V_{max} = 0$.

Step 2: Initialization of iteration count k=1

Step 3: Compute load current at each node

$$I_{bs}^{(k)} = \left(\frac{P_{bs}+iQ_{bs}}{V_{bs}^{(k-1)}}\right)^{*} \quad bs = 1, 2, 3 \ldots N_{bus} \tag{3.1}$$

$$I_{bs}^{(k)} = \begin{bmatrix} I_2^{(k)} \\ I_3^{(k)} \\ I_4^{(k)} \\ I_5^{(k)} \\ I_6^{(k)} \end{bmatrix} \tag{3.2}$$

Step 4: Creation of BIBC matrix

In BIBC matrix formation, bus injections are converted into branch currents. For a simple 6-bus distribution system shown in Fig. 3.1. The equations converting the bus injection to branch currents are as follows.

$$P_1 = I_2 + I_3 + I_4 + I_5 + I_6 \tag{3.3}$$

$$P_2 = I_3 + I_4 + I_5 + I_6 \tag{3.4}$$

$$P_3 = I_4 + I_5 \tag{3.5}$$

$$P_4 = I_5 \tag{3.6}$$

$$P_5 = I_6 \tag{3.7}$$

The above equations can be represented in matrix form as:

$$\begin{bmatrix} P_1 \\ P_2 \\ P_3 \\ P_4 \\ P_5 \end{bmatrix} = \begin{bmatrix} 1 & 1 & 1 & 1 & 1 \\ 0 & 0 & 0 & 0 & 0 \\ 0 & 0 & 0 & 0 & 0 \\ 0 & 0 & 0 & 0 & 0 \\ 0 & 0 & 0 & 0 & 0 \end{bmatrix} \begin{bmatrix} I_1 \\ I_2 \\ I_3 \\ I_4 \\ I_5 \end{bmatrix} \tag{3.8}$$

The above equation can be expressed in compact form as:

$$[P] = [BIBC][I_{bs}] \tag{3.9}$$

Step 5: Creation of BCBV matrix

In BCBV matrix formation, branch currents are converted into bus voltages. The conversion matrix for branch currents into bus voltages is shown below.

$$\begin{bmatrix} V_1 \\ V_2 \\ V_3 \\ V_4 \\ V_5 \end{bmatrix} - \begin{bmatrix} V_2 \\ V_3 \\ V_4 \\ V_5 \\ V_6 \end{bmatrix} = \begin{bmatrix} Z_{12} & 0 & 0 & 0 & 0 \\ Z_{12} & Z_{23} & 0 & 0 & 0 \\ Z_{12} & Z_{23} & Z_{34} & 0 & 0 \\ Z_{12} & Z_{23} & Z_{34} & Z_{45} & 0 \\ Z_{12} & Z_{23} & 0 & 0 & Z_{36} \end{bmatrix} \begin{bmatrix} P_1 \\ P_2 \\ P_3 \\ P_4 \\ P_5 \end{bmatrix} \tag{3.10}$$

The above equation can be written in condensed form as:

$$[\Delta V] = [BCBV][P] \tag{3.11}$$

Step 6: Creation of direct load flow (DLF) matrix

DLF matrix is prepared by multiplying BIBC and BCBV matrix.

$$[DLF] = [BIBC][BCBV] \tag{3.12}$$

Step 7: Compute voltage of each node with respect to substation node voltage.

$$\left[\Delta V^{(k)}\right] = [DLF]\left[I_{bs}{}^{(k)}\right] \tag{3.13}$$

$$\text{where, } \left[\Delta V^{(k)}\right] = \begin{bmatrix} \Delta V_2{}^{(k)} \\ \Delta V_3{}^{(k)} \\ \Delta V_4{}^{(k)} \\ \Delta V_5{}^{(k)} \\ \Delta V_6{}^{(k)} \end{bmatrix} = \begin{bmatrix} V_1 - V_2 \\ V_1 - V_3 \\ V_1 - V_4 \\ V_1 - V_5 \\ V_1 - V_6 \end{bmatrix} \tag{3.14}$$

Step 8: Increase iteration counter by 1.

$$k = k + 1 \tag{3.15}$$

Step 9: Update bus voltage

$$V_{bs}^{(k)} = V_1 - \Delta V_{bs}^{(k)} \qquad bs = 2, 3 \ldots N_{bus} \tag{3.16}$$

Step 10: Compute error in voltage

The error in voltage at each bus can be determined by Eqn. (3.17).

$$\Delta V_{bs}^{(k)} = V_{bs}^{(k)} - V_{bs}^{(k-1)} \quad (3.17)$$

The maximum error can be checked by

$$\Delta V_{max}^{k} = \max\left(\Delta V_{2}^{k}, \Delta V_{3}^{k}, \Delta V_{4}^{k} \ldots\ldots \Delta V_{N_{bus}}^{k}\right) \quad (3.18)$$

After calculating the error in voltage at each bus, convergence of voltage can be checked as:

If $\Delta V_{max}^{k} \leq \epsilon(0.0001)$, go to step 12, otherwise update the iteration number and go to step 3.

Fig. 3.2. shows the flow chart of direct approach method for load flow analysis in distribution system

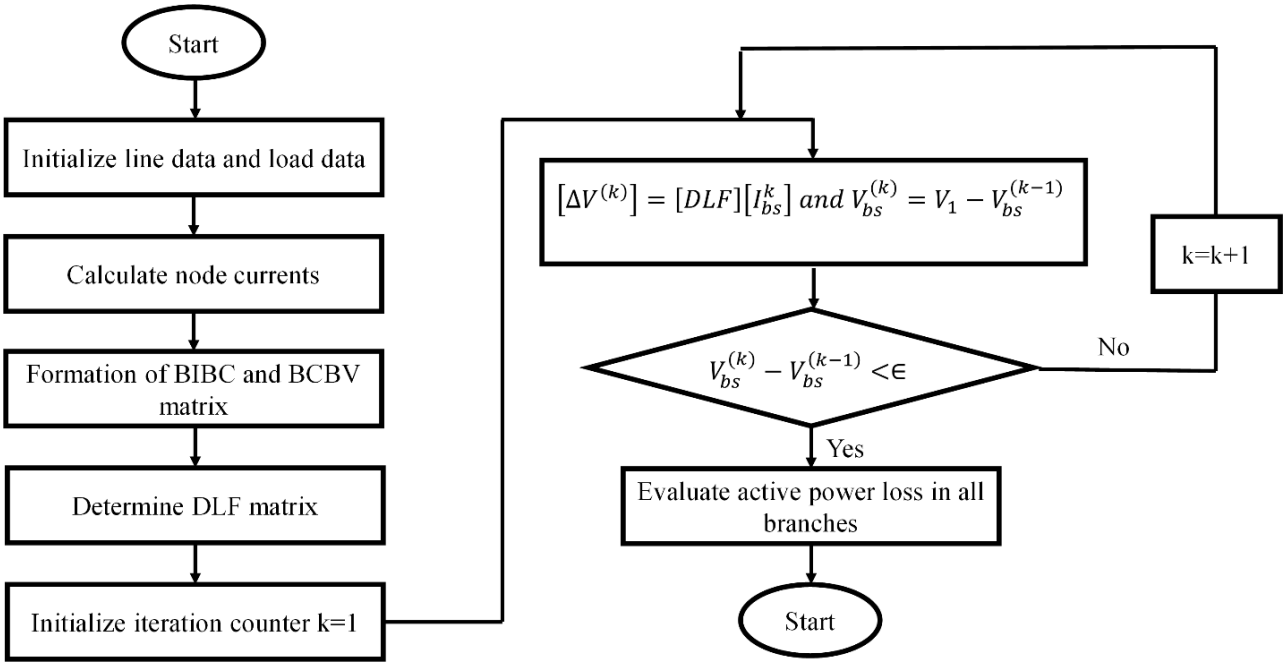

Fig. 3. 2. Flow chart of direct approach-based load flow method

3.3 TEST SYSTEMS

This thesis comprises of different methodological approaches and optimization techniques used for the optimal integration of EV charging load, DG and capacitor in electrical power network. The direct approach-based load flow and suggested intelligent algorithms are executed in MATLAB R2016a on an Intel i7, 3.2 GHz, 4 GB RAM, desktop PC. The proposed algorithms are validated on standard test system such as IEEE 33-bus and IEEE 34-bus system for EVCS and capacitor placement while IEEE 33-bus and IEEE 69-bus system for EVCS and DG integration. This chapter includes a brief description of each system, with line and load data provided in the appendix.

3.3.1 IEEE 33-bus System

The detailed diagram of IEEE 33 bus radial distribution system is shown in Fig. 3.3. The IEEE-33 bus distribution network has 33 nodes and 32 branches. The system is allowed to operate at 100 MVA and 12.66 kV. It has total real power loads of 3715 kW and total reactive power loads of 2300 kVAr. The base value of active and reactive power is observed to be 201.9 kW and 134.7 kVAr, respectively. The line parameters and existing load demand of IEEE 33-bus network is mentioned in appendix Table A.1.

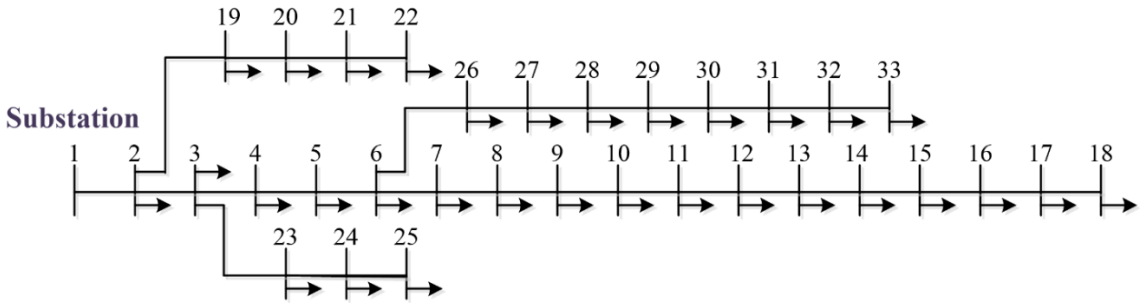

Fig. 3. 3. Single line diagram of IEEE 33-bus system

3.3.2 IEEE 34-bus System

The detailed diagram of IEEE 34-bus radial distribution system is shown in Fig. 3.4. The 34-bus distribution network has 34 nodes and 33 branches. The system is allowed to operate at 100 MVA and 12.66 kV. It has total real power loads of 4636.5 kW and total reactive power loads of 2873.5 kVAr. The base value of active and reactive power is observed to be 163.45 kW and 48.01 kVAr, respectively. The line parameters and existing load demand of IEEE 34-bus network is mentioned in appendix Table A.2.

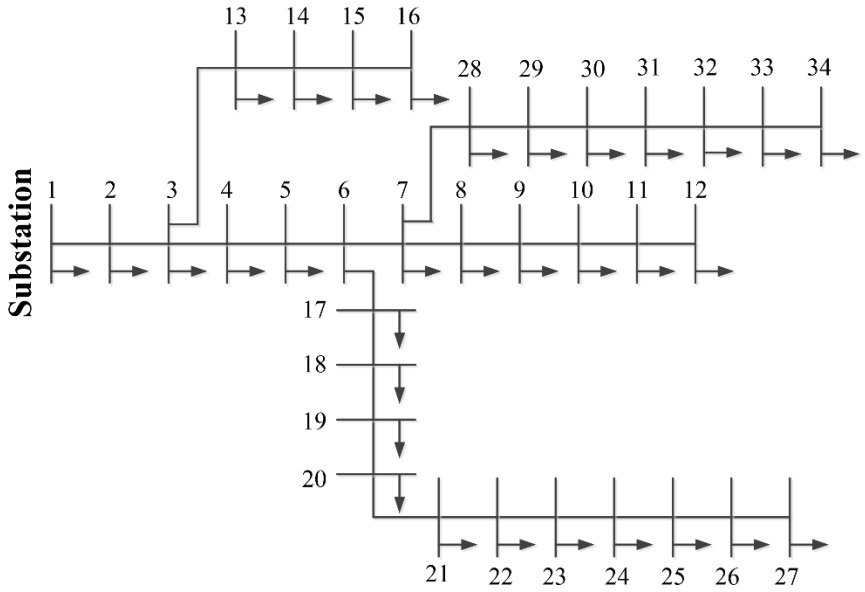

Fig. 3. 4. Single line diagram of IEEE 34-bus system

3.3.3 IEEE 69-bus System

The detailed diagram of IEEE 69-bus radial distribution system is shown in Fig. 3.5. The 69-bus distribution network has 69 nodes and 68 branches. The system is allowed to operate at 100 MVA and 12.66 kV. It has total real power loads of 3801.4 kW and total reactive power loads of 2693.6 kVAr. The base value of active and reactive power is observed to be 224.9 kW and 102.1 kVAr, respectively. The line parameters and existing load demand of IEEE 69-bus network is mentioned in appendix Table A.3.

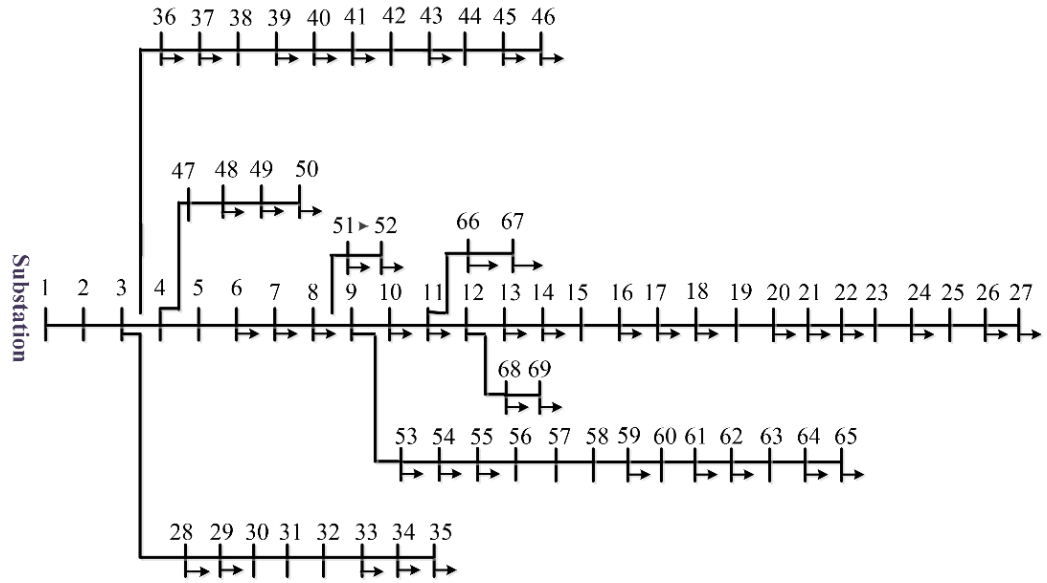

Fig. 3. 5. Single line diagram of IEEE 69-bus system

3.4 BRIEF DESCRIPTION OF OPTIMIZATION ALGORITHMS

The idea behind optimization is to implement solutions iteratively until a satisfied or optimal solution is found. The significant application of optimization methods is to reduce costs, losses, and improved efficiency. These methods are classified into two major categories:

a) Deterministic algorithm

These algorithms are based on a certain set of rules for getting from one solution to the other. These are conventional techniques also referred to as classic optimization techniques. They employ differential calculus to find the best solution:

b) Stochastic Algorithm

As the name implies, these algorithms have stochastic interpretation rules deduced from surroundings. These have restrictions that are determined by random variables.

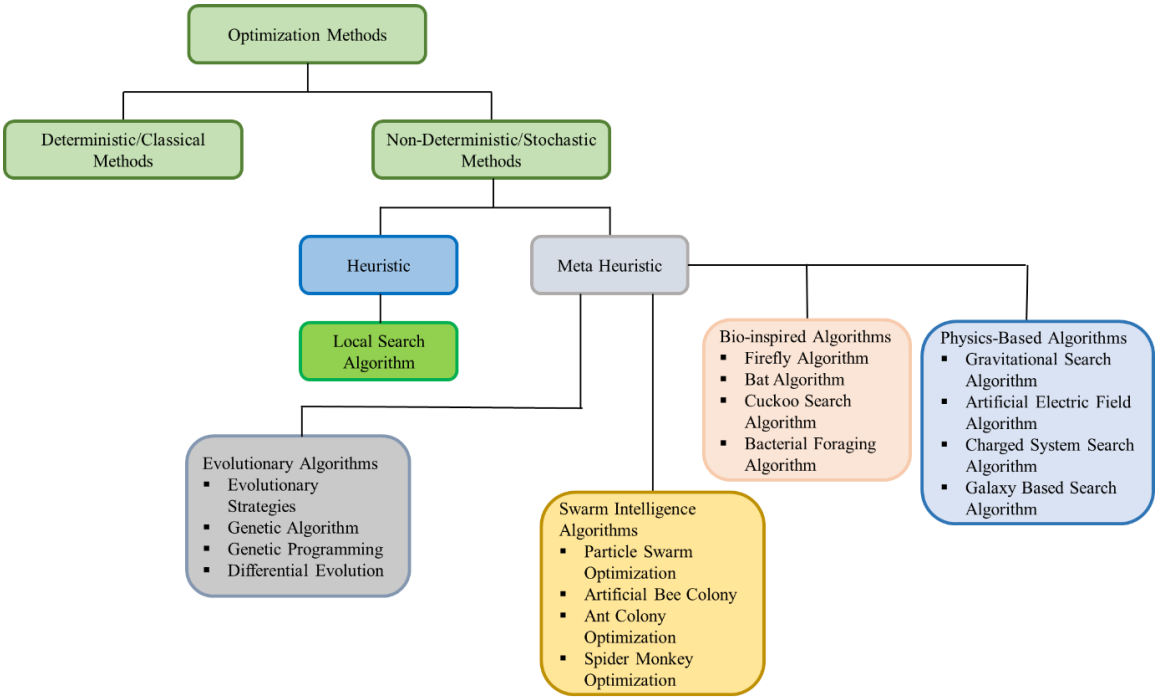

Fig. 3. 6. Categorization of optimization methods

Fig. 3.6 depicts the differentiation of various optimization methods. An optimized design problem is solved by correlating various solutions obtained through previous understanding. Thus, the viability of every design is evaluated first, followed by a review of the result found using the estimated objective function of each iteration, and the optimum outcome is taken into account for adoption. Further to that, it is difficult to follow a single procedure for the formulation of all electrical engineering design problems. Fig. 3.7 depicts the steps needed to solve an optimal design problem.

3.4.1 Design Variables

An optimized design problem includes multiple design parameters, some of which are extremely important to the proper operation of the design. These parameters are referred to as design variables. These variables remain constant or change in response to the more important design variables.

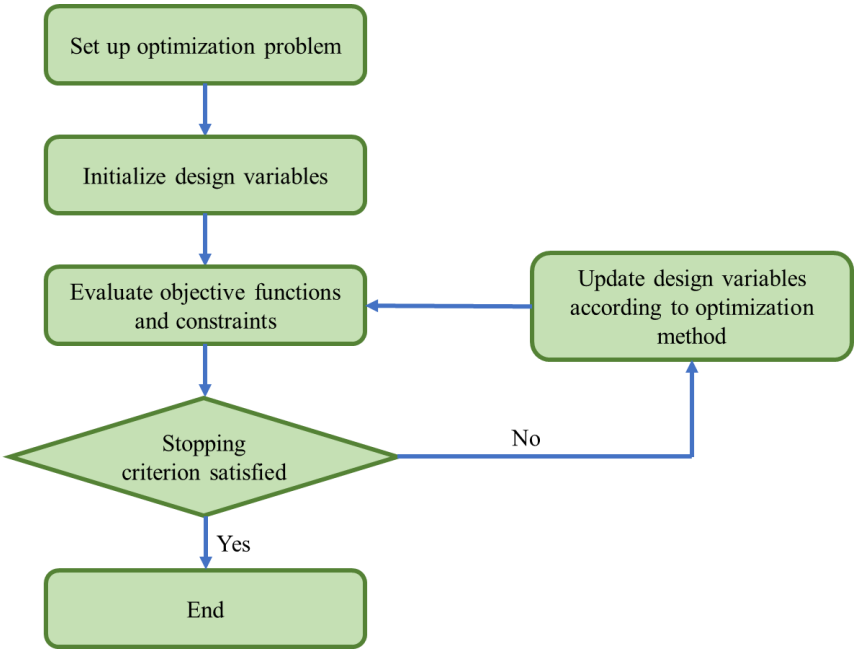

Fig. 3. 7. A flowchart for optimum design procedure

3.4.2 Constraints

The constraints describe functional relationships between design variables and other design parameters that specify physical phenomena and resource constraints. The type and nature of these are determined by the users. There are primarily two kinds of constraints:

a) Inequality constraints

b) Equality constraints

3.4.3 Objective Functions

The formulation of the objective function is critical in designing an optimized problem. Although these objective functions are mathematical quantities, some of them may be impossible to formulate mathematically. To solve such problems, these functions can be maximized or minimized.

3.4.4 Variable Bounds

Bounds are the variables that define the maximum and minimum limits of each design variable. Some optimization methods do not require these, whereas in others, they must be defined for an optimum solution.

3.5 SWARM BASED OPTIMIZATION

There are three important parameters that determine the best solution in swarm-based optimization methods.

- *Inertia Factor*: This factor is responsible for compelling the swarm or population in the same path.
- *Cognitive Factor*: This factor compels the swarm or population to relocate in a local search region based on its own experience of life, which is referred to as exploration.
- *Social Learning Term*: This term pushes the population or swarm to keep moving to the ideal previous position of its neighbors, which is referred to as exploitation.

3.5.1 Particle Swarm Optimization

Kennedy and Eberhart, in 1995, devised the PSO as a nature-inspired optimization method [129]. PSO uses a swarm-based exploration method to find the global optimal. Its motivation is derived from the behavior of birds. The particles are taken and moved across the exploration area to search for the optimal population that solves the challenge. Particles are formed in a multidimensional exploration field, and each particle alters its location based on past knowledge and that of its neighbors. Also, particles are directed by the optimal location that they and their neighbors have reached. It has a large search ability in

terms of candidate resolution spaces. The advantages of this optimization algorithm include its better precision, easy operation, fertility, and ability to generate a group of particles in the exploration space with random velocities. PSO is an approach that falls somewhere between a genetic algorithm and evolutionary algorithms. In order to determine the function with new waypoints at a given iteration, the position and velocity of an individual particle are altered. The performance of PSO method relies on four parameters which are as follows: personal best (p_{best}), global best (g_{best}), c_1 and c_2. A single PSO particle leaves trails in the exploration space for its coordinates that are related to the best result it has achieved up to this point, and this fitness value is known as p_{best}. If a particle achieves the overall superior value, it is referred to as the global best, g_{best}. The searching and exploitation capabilities of PSO depends on initializing the parameters. The following equations can be used to update the position and velocity of each particle in a swarm at each iteration.

$$v_i(t+1) = w(t) * v_i(t) + c_1 * r_1 * \left(p_{best} - x_i(t)\right) + c_2 * r_2 * \left(g_{best} - x_i(t)\right) \quad (3.19)$$

$$x_i(t+1) = x_i(t) + v_i(t+1) \quad (3.20)$$

$v_i(t+1)$ and $v_i(t)$ are the velocities of the i^{th} particles at instances (t+1) and t respectively,

$x_i(t+1)$ and $x_i(t)$ are the position of the i^{th} particles at instances (t+1) and t respectively,

$c_1$and c_2 are the acceleration coefficients which is taken into account for the variation of particle's velocity in the directions of p_{best} and g_{best}.

$r_1$and r_2 are the random variables which varies in the range of 0 and 1.

p_{best} and g_{best} represents the personal and global best values.

The position and velocities of every particle is modified using the current position, current velocity, distance of each particle's current position from p_{best} and g_{best}.

$w(t)$ is the weight of particle at iteration t and can be computed using Eqn. (3.21)

$$w(t) = w_{max} - \frac{(w_{max} - w_{min})}{T} * t \tag{3.21}$$

The values of w_{max} and w_{min} are assumed to be 0.9 and 0.4 respectively, t denotes the current iteration and T indicates the total number of iterations.

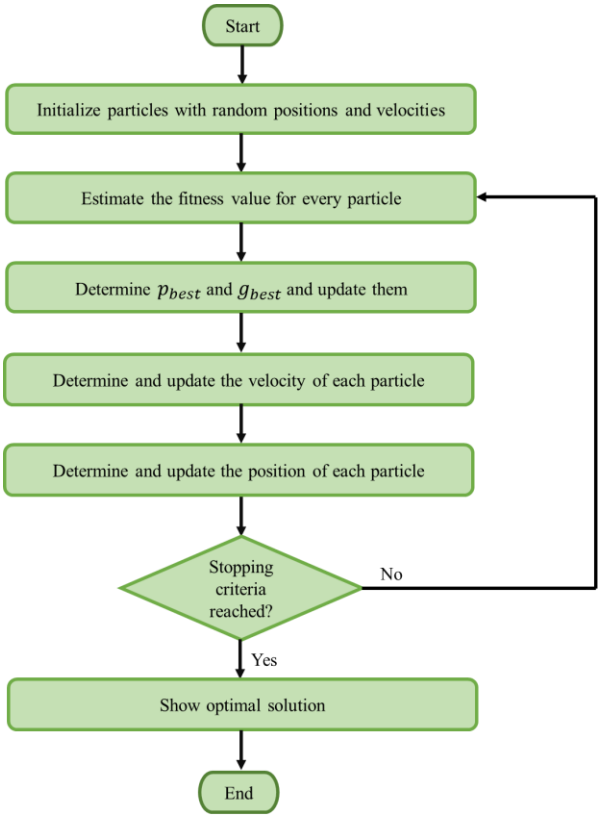

Fig. 3. 8. The flowchart of PSO method

The inertia weight has a substantial impact on the PSO algorithm's convergence. A large value of inertia weight i.e., w makes it easier to conduct a global search, whereas a small value of inertia weight makes it easier to conduct a local search. When compared to

fixed inertia weight settings, linearly decreasing the inertia weight from a relatively large value to a small value over the course of the iteration, PSO yields the best performance.

3.5.2 Grey Wolf Optimization

Mirjalili et al. are the ones who first introduced GWO in the year 2014 [130]. It takes its cues from the natural behavior and chasing method of grey wolves. They follow a strict leadership system in a pack. The group's leaders are known as alpha (α) wolves. Grey wolves are divided into two categories. The alpha comes under the first category, while the rest of the pack members are considered in the second category. They assist the alphas. The beta (β) wolves are their name. Furthermore, delta (δ) wolves have a lower priority than those of the previous two categories of wolves. Their goal is to surrender to alpha and beta wolves while maintaining influence over omega wolves. The omegas (ω) are the wolves with the lowest priority, as they must obey the foremost grey wolves. The social hierarchy of grey wolves is portrayed in Fig. 3.9.

3.5.2.1 Mathematical Modeling of GWO

The major steps involved in the mathematical modeling of GWO include social hierarchy of GWO, encircling prey and hunting prey.

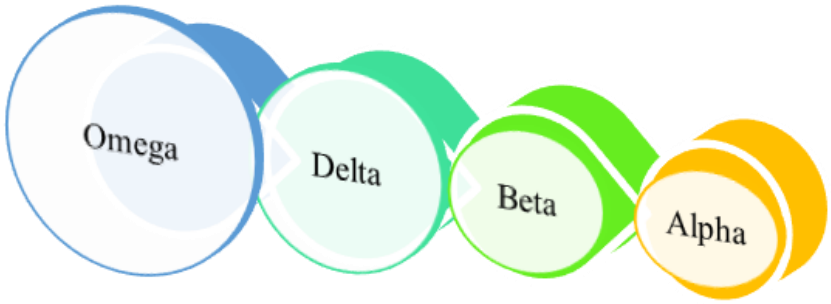

Fig. 3. 9. Social hierarchy in grey wolves

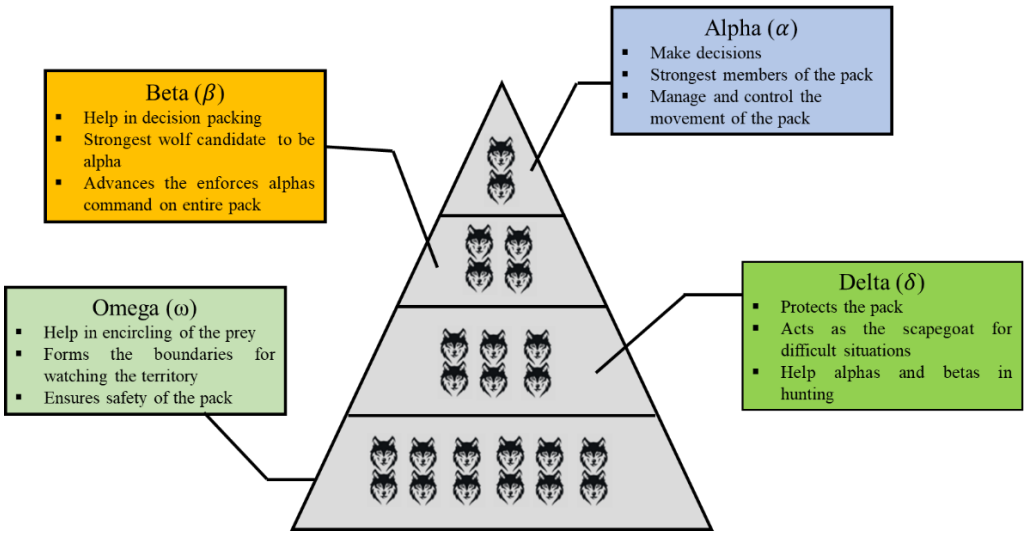

Fig. 3. 10. Social hierarchy of grey wolves and their functions

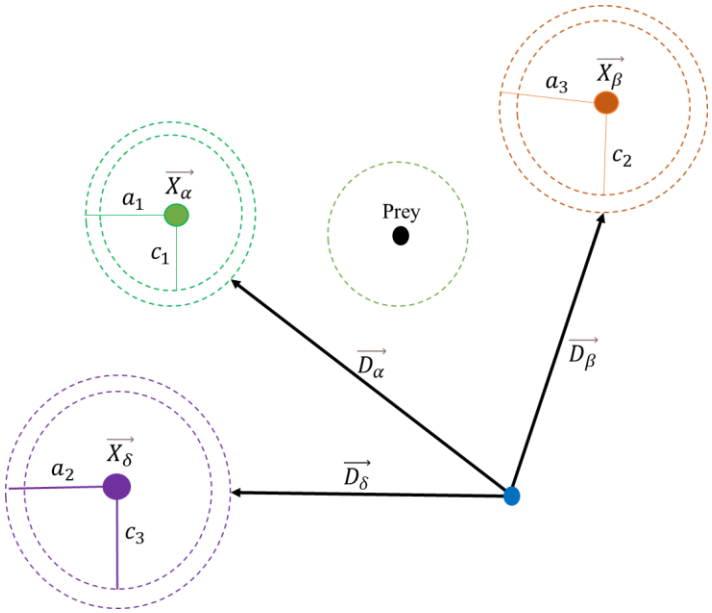

Fig. 3. 11. Position update of wolves

1) Social Hierarchy of Grey Wolves

Alpha wolf is known as the best suitable solution in the mathematical description of the grey wolf hierarchy. As a result, beta wolf is the second most acceptable solution, while delta is the third most suitable alternative. The omegas represent the farthest solutions. The hunting process is guided by alpha, beta, and delta in the GWO approach. The omegas should only follow the same steps as the wolves with higher priorities and obey them.

2) Encircling the Prey

The grey wolves enclosing the prey while hunting. The encircling of grey wolves can be modeled using Eqns. (3.22) and (3.23).

$$\overrightarrow{D} = \left|\overrightarrow{C} . \overrightarrow{X_p}(t) - \overrightarrow{X}(t)\right| \tag{3.22}$$

$$\overrightarrow{X}(t+1) = \overrightarrow{X_p}(t) - \overrightarrow{A} . \overrightarrow{D} \tag{3.23}$$

where t indicates the iteration, $\overrightarrow{A}$ and $\overrightarrow{C}$ represents the constant (coefficient) vectors, position vector of prey and wolf are represented by $\overrightarrow{X_p}$ and $\overrightarrow{X}$ respectively.

$\overrightarrow{A}$ and $\overrightarrow{C}$ can be formulated as follows:

$$\overrightarrow{A} = 2\overrightarrow{a} . \overrightarrow{r_1} - \overrightarrow{a} \tag{3.24}$$

$$\overrightarrow{C} = 2 . \overrightarrow{r_2} \tag{3.25}$$

The value of $\overrightarrow{a}$ declines proportionally from two to zero over the entire iterations. $\overrightarrow{r_1}$ and $\overrightarrow{r_2}$ are the arbitrary random vectors taken between 0 and 1.

3) Hunting Mechanism of Grey Wolves

The alphas, betas, and deltas often drive the hunting process as they have more knowledge in predicting the location of the prey. The rest of the exploration mediators must follow the location of the optimal mediator and make adjustments as needed [131].

$$\overrightarrow{D_\alpha} = \left|\overrightarrow{C} . \overrightarrow{X_\alpha} - \overrightarrow{X}\right| \tag{3.26}$$

$$\overrightarrow{D_\beta} = \left|\overrightarrow{C} . \overrightarrow{X_\beta} - \overrightarrow{X}\right| \tag{3.27}$$

$$\overrightarrow{D_\delta} = \left|\overrightarrow{C} . \overrightarrow{X_\delta} - \overrightarrow{X}\right| \tag{3.28}$$

$$\overrightarrow{X_1} = \overrightarrow{X_\alpha} - \overrightarrow{A_1} . \overrightarrow{D_\alpha} \tag{3.29}$$

$$\overrightarrow{Z_2} = \overrightarrow{X_\beta} - \overrightarrow{A_2}.\overrightarrow{D_\beta} \quad (3.30)$$

$$\overrightarrow{X_3} = \overrightarrow{X_\delta} - \overrightarrow{A_3}.\overrightarrow{D_\delta} \quad (3.31)$$

$$\overrightarrow{X}(t+1) = \frac{\overrightarrow{X_1} + \overrightarrow{X_2} + \overrightarrow{X_3}}{3} \quad (3.32)$$

4) Attacking Process of Grey Wolves

A is a number that falls between [-2a, 2a]. If |A| is greater than one, the wolves will attack their prey. Exploitation refers to the ability to attack the prey, while exploration is the skill of determining a prey. The population is led away from the prey by the erratic values of A. If |A| is greater than 1, the wolves will depart from their prey.

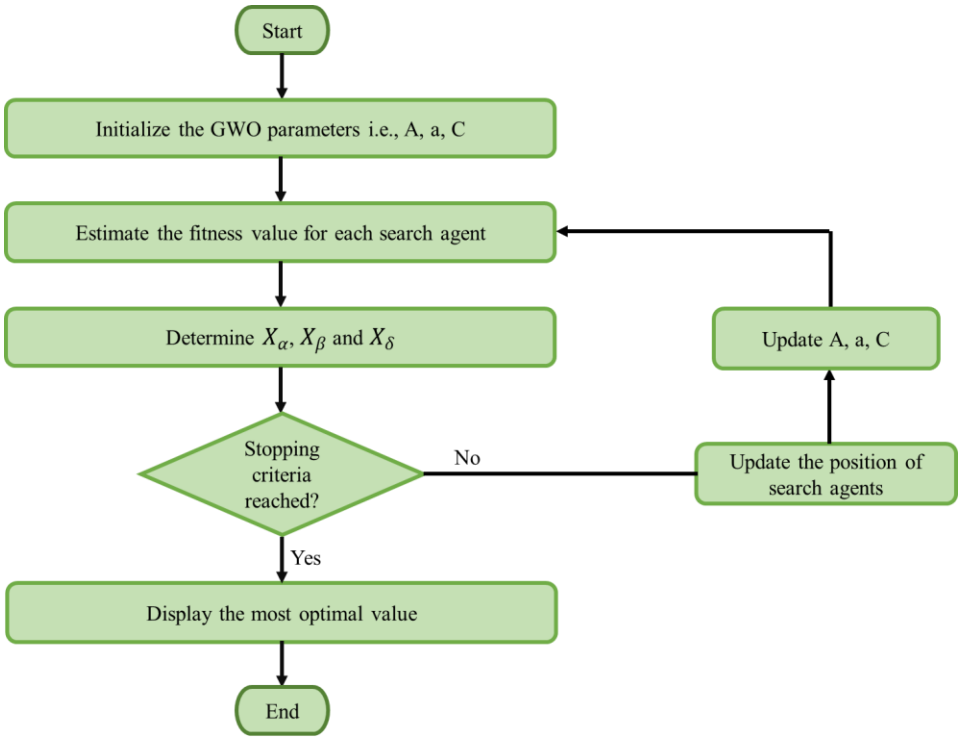

Fig. 3. 12. The flowchart of GWO method

The process for updating the position of wolves is displayed in Fig. 3.11. The flowchart in Fig. 3.12 describes the steps for GWO algorithm development. In GWO algorithm, maximum number of iteration and tolerance error is used for stopping criteria.

3.6 HYBRID GREY WOLF OPTIMIZER PARTICLE SWARM OPTIMIZATION

The presented technique is the hybrid technique that is inspired by the attacking movement of grey wolves to capture their prey and swarming action of group of birds to achieve the target i.e., food. In GWO, the pack is categorized into four main groups of different hierarchical levels such as alpha, beta, delta and omega. Alpha holds the highest positions in hierarchy and believed to be the key decision-makers and the rest follows the decision made by alpha. The process of surrounding, searching and attacking the prey is managed by optimization techniques using mathematical equations [132]. The position of grey wolves is updated according to GWO algorithm and can be stated as follows:

$$\overrightarrow{x_{1,2,3}} = \overrightarrow{x_{\alpha,\beta,\delta}} - \vec{a}.\overrightarrow{d_{\alpha,\beta,\delta}} \tag{3.33}$$

$$\overrightarrow{d_{\alpha,\beta,\delta,}} = \left|\vec{c}\,.\overrightarrow{x_{\alpha,\beta,\delta}} - w_{PSO} * \vec{x}(t)\right| \tag{3.34}$$

$$\vec{x}(t+1) = \frac{\overrightarrow{x_1} + \overrightarrow{x_2} + \overrightarrow{x_3}}{3} \tag{3.35}$$

The hybrid approach is presented with the amalgamation of GWO and PSO. The shortcoming of PSO is that it could not explore for the optimal solution in a wide search range and gets stuck in local optima. Whereas, GWO suffers with the disadvantage of poor exploitation. Therefore, hybrid of GWO and PSO is employed to mitigate the drawbacks of individual algorithm. The major concern is to enhance the PSO's exploitation capabilities with GWO's exploration capabilities to maintain a good balance between the exploration and exploitation in order to escape out from local optima and leads to optimal solution with easy convergence. In this study, HGWOPSO is proposed in which the initial population is updated by GWO and then PSO again updates the updated solutions [132].

Furthermore, the proposed hybrid approach is selected to solve the optimization problem because of its high rate of convergence and capability of handling discrete as well as integer variable problem involving a smaller number of control parameters. The improved equations for alpha, beta and delta wolves are updated using Eqn. (3.33)- (3.35). The velocity and updated equation of PSO is improved to Eqn. (3.36)- (3.38).

$$x_i(t+1) = x_i(t) + v_i(t+1) \tag{3.36}$$

$$w_{PSO}(t) = w_{max} - \frac{(w_{max} - w_{min})}{T} * t \tag{3.37}$$

$$v_i(t+1) = w_{PSO}(t) * v_i(t) + c_1 r_{PSO}^1 \left(x_1 - x_i(t)\right) + c_2 r_{PSO}^2 \left(x_2 - x_i(t)\right) + c_3 r_{PSO}^3 \left(x_3 - x_i(t)\right) \tag{3.38}$$

3.7 RESULTS AND DISCUSSIONS

The proposed HGWOPSO is first applied to seven standard mathematical benchmark functions for validation. The complete details of these functions and their outcomes are provided in Table 3.1 and Table 3.2, respectively. Comparative results in terms of maximum iterations and optimal solution of seven mathematical benchmark functions for 30 independent runs validate that the proposed optimization technique is superior to GWO. HGWOPSO converges to a global optimum without getting stuck in local optimal solution, resulting in faster convergence.

The performance of hybrid method is shown in Table 3.2 in terms of optimum solution and maximum iterations required for convergence. The hybrid method outperforms standalone GWO method particularly when the functions are operated on high dimensions.

Table 3. 1. List of standard mathematical benchmark functions

S. No	Function Name	Mathematical Formulation	Dimension (D)	Search Range
1.	Sphere	$f(x) = \sum_{p=1}^{D} x_p^2$	30	[-100,100]
2.	Rosenbrock	$f(x) = \sum_{p=1}^{D} \left[100 * \left(x_p^2 - x_{p+1}\right)^2 + \left(1 - x_p\right)^2\right]$	30	[-2.048,2.048]
3.	Rastragin	$f(x) = \sum_{p=1}^{D} \left[x_p^2 - 10\cos\left(2\pi x_p\right) + 10\right]$	30	[-5.12,5.12]
4.	Greiwank	$f(x) = \frac{1}{4000}\sum_{p=1}^{D} x_p^2 - \prod_{p=1}^{D} \cos\left(\frac{x_p}{\sqrt{p}}\right) + 1$	30	[-600,600]
5.	Schewefel	$f(x) = \sum_{p=1}^{D}\left(\sum_{q=1}^{p} x_q\right)^2$	30	[-100,100]
6.	Ackley	$f(x) = -20e^{\left(-0.2\sqrt{\frac{1}{D}\sum_{p=1}^{D} x_p^2}\right)} - e^{\left(\frac{1}{D}\sum_{p=1}^{D}\cos\left(2\pi x_p\right)\right)} + 20 + e^1$	30	[-32.76,32.76]
7.	Alpine	$f(x) = \sum_{p=1}^{D-1}\left\lvert x_p \sin x_p + 0.1x_p\right\rvert$	30	[-10, 10]

Table 3. 2. Comparison of results obtained from HGWOPSO and GWO applied on standard benchmark functions

Function Name	HGWOPSO		GWO	
	Maximum Iterations	Optimal Solution	Maximum Iterations	Optimal Solution
Sphere	1000	$1.55*10^{-22}$	897	$5.89*10^{-20}$
Rosenbrock	425	$2.72*10^{-2}$	515	$5.81*10^{1}$
Rastragin	343	$7.57*10^{-13}$	419	$5.53*10^{-9}$
Greiwank	1000	$4.25*10^{-2}$	1000	$3.45*10^{-2}$
Schewefel	1000	8592.7	1000	7956.4
Ackley	1000	$7.74*10^{-9}$	785	$9.14*10^{-5}$
Alpine	1000	-192.55	1000	-192.45

3.8 SUMMARY

In this chapter, the implementation of direct approach-based load flow technique is thoroughly described. This technique is implemented before the placement of EVCS, distributed generation and capacitor. It is easy to implement and possess fast computation procedure. Further, the basic information of three test networks i.e., IEEE 33-bus, IEEE 34-bus and IEEE 69-bus that have been used is described in this chapter. This chapter also describes the use of various optimization techniques for attaining optimum solution. The important factors utilized for the tuning of swarm based meta-heuristic have been presented. In addition to this, the comparison analysis of implementation of HGWOPSO and GWO algorithms on standard mathematical benchmark functions have been discussed in this chapter. The designed technique i.e., HGWOPSO is found to be faster in terms of computational speed and convergence. The hybrid method outperforms standalone GWO method particularly when the functions are operated on high dimensions. Also, HGWOPSO can effectively handle the nonlinearities and probabilistic nature of renewable energy sources when properly modeled.

CHAPTER 4

FEASIBILITY ANALYSIS OF EVCS CONSIDERING COST-BASED FUNCTIONS

4.1 INTRODUCTION

Nowadays, Electric vehicles (EVs) are gaining popularity because of the reduction in consumption of fossil fuels and high demand in the power sector. The cost-effective and eco-friendly natures of EVs are the major concerns that lead to the deployment of EVs on a large scale. EVs can be categorized into battery EVs and hybrid EVs. Electric vehicle charging stations (EVCS) are installed to supply electricity for charging EVs. The capacity of EV battery ranges between 20 kWh to 60 kWh. Several charging levels are available for EV charging. Out of which, three standard charging levels which are predominantly used have been developed. Charging level 1 is based on a single-phase AC system in which 20 kWh battery is charged in 7 hours, whereas charging level 2 utilizes a three-phase AC system in which 20 kWh battery is fully charged in 1 hour only. Moreover, charging level 3 also known as the fast-charging level, the battery gets fully charged in 20 min-30 min. It is based on a direct-current (DC) system. It is necessary to have a fast-charging station for the wide adoption of EVs. The easy availability of fast CS is the key to the commercial deployment of EVs. Various issues concerning the development of fast CS have been discussed in the literature, more prominent of them being charging time, battery life, accessibility of public CS, and integration to the energy supply grid.

This chapter is focused on optimal planning of EVCS in different well-known areas of South Delhi considering land cost, coordinates i.e., latitude and longitude, elevation, and

population density of CS location. Moreover, reliability analysis is carried out to investigate the impact on the grid. Therefore, this work will be carried out by utilizing grey wolf optimization (GWO) for the planning of CS in the proposed site. GWO is simple to execute because of its simple structure, low storage and computational requirements, good convergence due to continuous search space reduction and fewer decision variables, and its ability to avoid local minima and search for global minima over a large search range.

4.2 COMPONENTS AND MODELS OF EVCS

The interaction among CSs, EVs and electric substations is shown in Fig. 4.1. which depicts that CS is connected to an electric substation and EV takes power from CS.

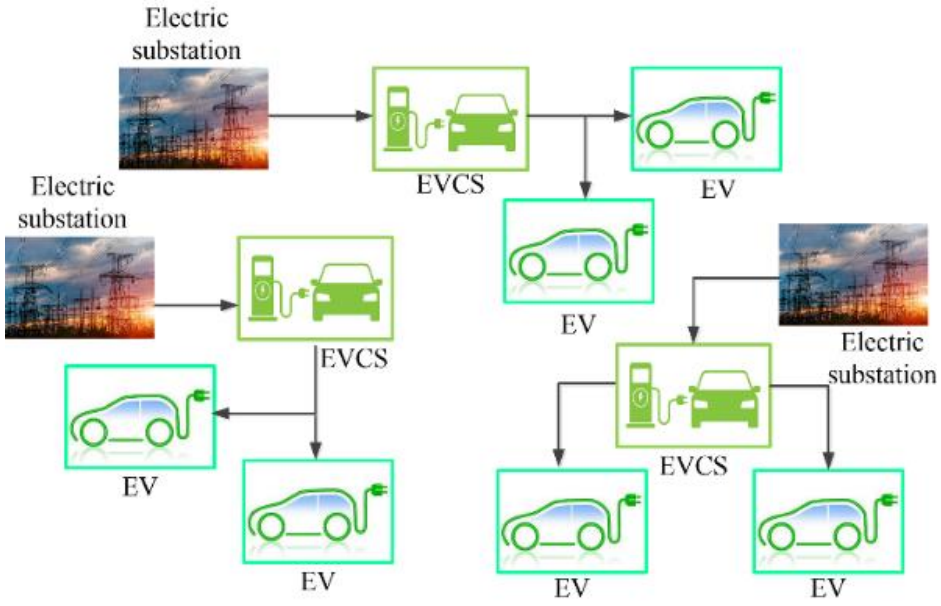

Fig. 4. 1. Interaction among CSs, EVs, and electric substation

Fig. 4.2. shows the single line diagram of the interconnection of charging station (m) and substation (x) via feeder (F_m). High voltage and low voltage bus bars of the electric substation are denoted by D6x and D4x respectively. Two transformers are assumed to be

connected in parallel in the electric substation. D4i indicates the incoming bus bar of the CS.

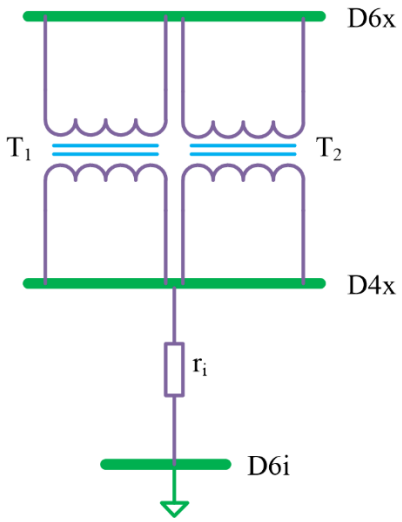

Fig. 4. 2. Single line diagram for station connected to the electric grid [133]

4.2.1 Investment Cost (IC)

The investment cost can be divided into three parts. The first part is the cost incurred for establishing the equipment and facilities for CS. The second part is associated with the rental cost of land and the third part is the cost required for developing the connectors. Investment cost can be formulated mathematically as follows [67]

$$IC = \sum_{i=1}^{N_{CS}} (C_{initial} + B.C_{land}.NC_i + C_{con}.CP.(NC_i - 1)) \quad (4.1)$$

In the current work, it is assumed that the land is taken on rent for 5 years and hence, the operational and maintenance cost has been ignored. Also, the area requirement per connector is considered to be 25 m^2 [67].

The cost of equipment depends on the capacity of CS. The rental cost of land depends on the quality of land and varies in different city locations. In the proposed methodology, charging stations are installed at locations with different land costs. Since

the development cost of the charging connectors will decrease in the future by improving the technology, a considerable portion of the investment cost depends on it. The typical layout of EVCS per connector is shown in Fig. 4.3. For a connector, it is required to have a minimum width of 2.74 m and length of 5.28 m as shown in Figure 3. 0.92 Minimum clearance of 0.92 m is needed between the two connectors if there is a use of more than one connector.

Moreover, the charging station capacity is a function of the number of charging connectors (NC_i) and rated power of connector (CP).

Thus, the capacity of i^{th}CS can be determined as [134]:

$$CS_C(i) = CP \times NC_i \tag{4.2}$$

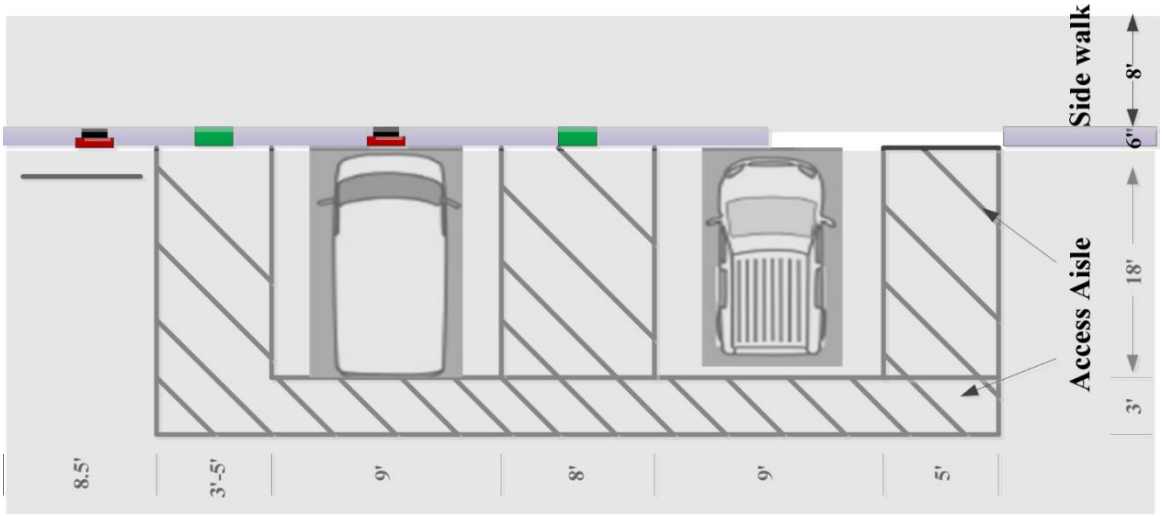

Fig. 4. 3. General CS station layout per connector [134]

4.2.2 CS Electrification Cost (CSEC)

The overall connection cost strongly depends on the separation between the charging station and nearest electric substation as well as the connection technology. The charging station and electric substation are assumed to be connected directly through

dedicated overhead lines. Some conductors which are easily available and frequently used for overhead lines are listed in Table 4. 1. The area of cross-section rated current for different types of conductors used for overhead lines is also given in Table 4. 1.

The transmission cost of the overhead line depends on the area of cross-section of the line and can be evaluated as follows [133]:

$$CT_i = 8000 + 65.7w \tag{4.3}$$

Table 4. 1 Conductor used for dedicated overhead line [133]

Name	Cross-section area in mm^2	Rated current in ampere
FOX	42.77	192
MINK	73.6	288
DOG	118.5	380
PARTRIDGE	156.9	460

The overall connection cost of i^{th} CS can be determined as [67]

$$CSEC = \sum_{i=1}^{N_{CS}} (CT_i * D_i) \tag{4.4}$$

4.2.3 EV Energy Loss Cost (EVLC)

For charging the batteries of EV, the definite path must be followed by EV to reach the nearest charging station. For j^{th} EV, charging loss can be determined as follows [67]

$$P_{EVL} = \sum_{j=1}^{N_{EV}} (SEC * S_j) \tag{4.5}$$

Thus, the EV energy loss cost can be calculated as follows:

$$EVLC = P_{EVL} * PE * TD \tag{4.6}$$

In this article, S_j is the distance traveled between EV and CS and it should be evaluated assuming the urban roads. The values of S_j are calculated using geographic information.

4.2.4 Travel Time Cost (TTC)

The travel time cost is the cost required for reaching the nearest charging station from the point where the need for charging arises or the point of charging demand. It depends on the distance between the EV position and nearest CS and the cost of traveling per Km of EV. According to [135], it can mathematically be written as :

$$\mathrm{TTC} = S_j * C_{EV/km} \tag{4.7}$$

4.3 OPTIMIZATION PROBLEM

This section describes the optimization model based on minimizing the aforementioned objective functions, associated constraints, and methodology for assigning the EVs to the nearest charging station.

4.3.1 Objective of the Optimization

The aim of the optimization problem is the minimization of the total cost related to the charging demand of the electric vehicle.

$$\text{Min } F=\sum_{i=1}^{N_{CS}}(IC_i + CSEC_i) + \sum_{j=1}^{N_{EV}} EVLC_j + \sum_{j=1}^{N_{EV}} TTC_j \tag{4.8}$$

4.3.2 Constraints

The optimization problem for optimal sizing and placement of CS is subjected to some existing constraints associated with CS and EVs which are as follows:

a) Each CS must have at least one charging connector.

$$NC_i \geq 1 \qquad i=1, 2, 3\ldots\ldots N_{CS} \tag{4.9}$$

b) The connector must be able to charge all EVs.

$$\sum_{i=1}^{N_{CS}}(NC_i \times DE) > N_{EV} \tag{4.10}$$

c) The trajectory length of each EV to the CS can be determined as:

$$S_j = \min\,(s_{i,j}) \tag{4.11}$$

d) The maximum number of EVs that can be charged in one CS is limited by

$$NC_i \times DE > N_{EV_i} \tag{4.12}$$

e) The number of EVs which are charged by each CS is given as follow:

$$N_{EV_i} = \sum_{j=1}^{N_{EV}} (1 + \mathrm{sgn}(S_j - s_{i,j}))/2 \tag{4.13}$$

4.3.3 Assumptions

Various assumptions have been taken in this work which is as follows:

- The positions of EVCS and EV are considered to be distributed normally.
- The number of EVs in a given area decides the number of EVCS in that area.
- EV owner charges their EVs in a fixed CS.

4.3.4 Methodology

1) Determination of S and D matrices

Two matrices that represent the distance between substation, charging station, and EV position and CS need to be modeled. D matrix indicates the distance of each CS from every substation whereas the S matrix denotes the distance of each EV from every CS.

Matrix D describes the distance between i^{th} CS and n^{th} electric substation. Hence the order of matrix D would be (i×n).

$$D= [d_{i,n}]_{N_{CS} \times N_{ES}} \tag{4.14}$$

$$\text{where, } d_{i,n} = \sqrt{\left(x_{CS_i} - x_{ES_n}\right)^2 + \left(y_{CS_i} - y_{ES_n}\right)^2} \tag{4.15}$$

$$i= 1, 2, 3\ldots\ldots\ldots N_{CS}$$

$$n= 1, 2, 3\ldots\ldots\ldots N_{ES}$$

Matrix S represents the distance between j^{th} EV and i^{th} CS. Thus, the order of matrix L is (j×i).

$$S= [s_{i,j}]_{N_{EV} \times N_{CS}} \tag{4.16}$$

$$\text{where, } s_{i,j} = \sqrt{\left(x_{CS_i} - x_{EV_j}\right)^2 + \left(y_{CS_i} - y_{EV_j}\right)^2} \tag{4.17}$$

$$j= 1, 2, 3\ldots\ldots\ldots\ldots N_{EV}$$

The values of x and y are computed based on geographical information in an area under study.

2) Implementation of the proposed approach

The main goal of optimal siting and sizing of EVCS is to determine where the CS should be installed to minimize the investment cost and electrification cost for CS and minimize energy loss cost and travel time cost for EVs. The flow chart of the proposed approach is shown in Fig. 4.4 and it is based on the following steps.

Step 1: The input data such as fixed cost, connector development cost, and other parameters should be defined.

Step 2: The EVCSs are positioned along the main urban roads in South Delhi and EVs locations are generated randomly based on normal distribution functions.

Step 3: Select each charging station and assign EV to each CS based on the criteria of minimum distance.

Step 4: Calculate various objective functions i.e., investment cost, CS electrification cost, EV energy loss cost and travel time cost.

Step 5: Check the subjected constraints using Equation (4.9) – (4.13), if satisfied, print the results for each cost function, else go to step 2.

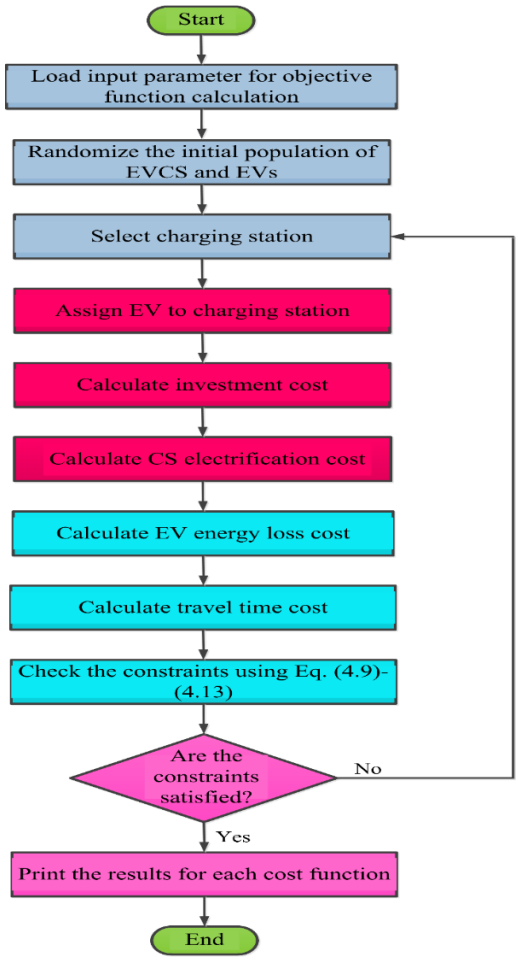

Fig. 4. 4. Flow chart of the proposed approach

4.4 APPLICATION OF GWO ALGORITHM FOR OPTIMAL SITING AND SIZING OF EVCS

A Series of steps has been adopted for implementing GWO for minimizing the multi-objective cost-based functions. The procedure is explained with the help of the flowchart shown in Fig. 4.5. The initially chosen number of iterations, problem dimension, and the number of search agents (NSA) are applied.

Step 1: Initialization

The driving source of the algorithm i.e., NSA, max iteration, dimension, and boundaries of the problem are initialized. In this study, NSA is assumed to be 30 while the maximum number of iterations is taken as 100.

Step 2: Grey wolf positions generation

The population of all search agents is randomly generated using GWO and the first three positions are initialized as alpha, beta, and delta. After this, objective function values for each search agent are calculated.

Step 3: Quality solution

The constraints are checked for determining the quality solution. If the constraints are satisfied, then the objective function is calculated and if the constraints are violated, the results are discarded.

Step 4: Selecting best positions of search agent

The positions of alpha, beta, and delta wolves are updated not including the omega wolf. Eqns. (3.26) – (3.32) in chapter 3 are utilized for selecting the best solution so far.

Step 5: Determining the new positions of search agents

The new positions of all search agents are determined and the whole process is repeated.

Step 6: Termination criteria

The termination criteria are set as the maximum number of iterations in the proposed work. When the number of iterations exceeds the assigned number of iterations, the simulation will be stopped and the optimized value of objective functions will be displayed.

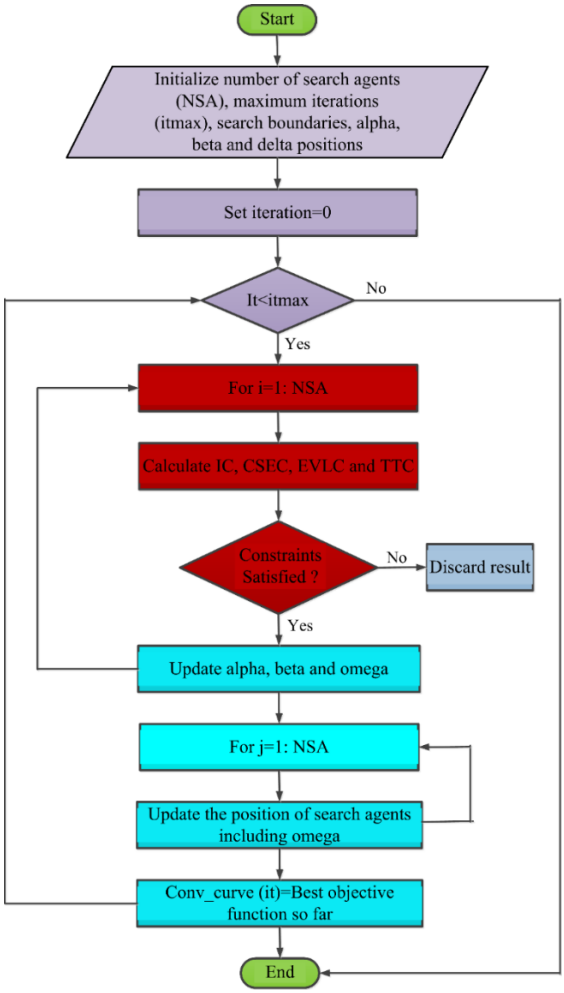

Fig. 4. 5. Flowchart of GWO algorithm for the proposed approach

4.5 RESULT AND DISCUSSION

This section describes the explanation of planning region, reliability analysis, simulation results, and main findings.

4.5.1 Description of the System Under Study

The approach has been applied to an area of 218.5 Km^2 in the South Delhi area of New Delhi, India. The coordinates, elevation, and population density of different CS locations are provided in Table 4.2.

There are 15000 vehicles assumed to be EVs in the study zone. Out of which, only three percent of the total EVs are considered for daily charging. Around 500 EVs have been assumed to be charged every day. EVs positions have been generated randomly based on the Cartesian geographic system as indicated in Fig. 4.6. 11 substations are located nearby 20 CS and provide electric supply to the nearby CS. In Fig. 4.6, green circles, red stars and blue diamonds represent the EVs, CSs, and electric substations considered in this work respectively.

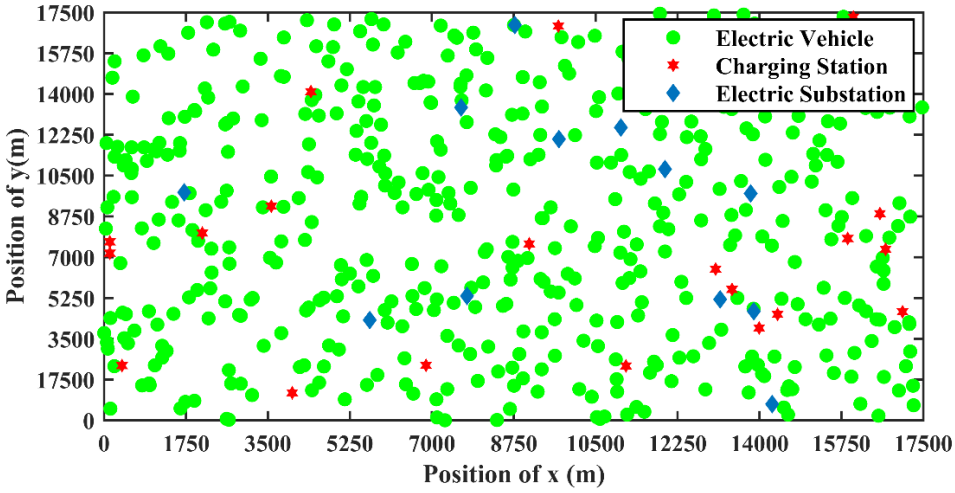

Fig. 4. 6. Positions of EVs, charging stations and electric substations

20 CS have been placed in different well-known areas of South Delhi and located on Google Map as shown in Fig. 4.7. In addition to this, the input parameters required for solving the objective functions are listed in Table 4.3.

Table 4. 2. Charging station information [136]

Charging Station Location	Coordinates		Elevation (m)	Population density (people per km^2)
	Latitude	Longitude		
Saket	28.5221	77.2012	240	20110
Shivalik	28.5340	77.2053	227	23414
Greater Kailash	28.5555	77.2337	224	26450
Lajpat Nagar	28.5649	77.2403	211	34599
New Friends Colony	28.5675	77.2691	208	8956
Kalkaji	28.5400	77.2592	239	24803
Hauz Khas	28.5479	77.2031	223	7974
Safdarjung	28.5647	77.1949	221	29682
Vasant Vihar	28.5603	77.1617	240	17475
Green Park	28.5584	77.2029	218	35903
Panchsheel	28.5415	77.2161	224	11576
Defence Colony	28.5734	77.2326	212	16837
Nehru Place	28.5503	77.2502	231	24036
Chanakyapuri	28.5972	77.1904	220	7498
Chirag Delhi	28.5376	77.2283	225	22552
Vasant Kunj	28.5293	77.1484	264	10536
Chhatarpur	28.4959	77.1848	261	13101
RK puram	28.5660	77.1767	229	14620
Golf Links	28.5973	77.2323	209	5919
Malviya Nagar	28.5342	77.2094	226	29945

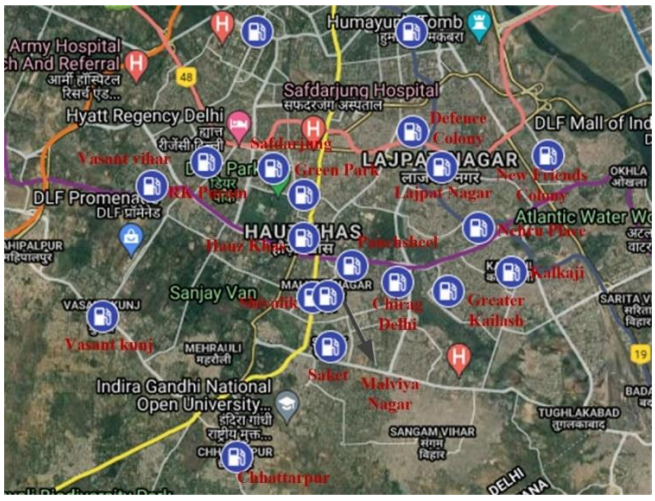

Fig. 4. 7. Location of CS in South Delhi areas in Google Map [137]

Table 4. 3. Input parameter required for objective function calculation [134]

Parameter	Value	Unit
N_{EV}	500	–
N_{CS}	20	–
N_S	11	–
SEC	7	km/kWh
PE	90.48	$
$\mathbf{C_{initial}}$	72204.52	$
$\mathbf{C_{con}}$	214.89	$/kW
CP	96	kW
DE	30	–
TD	1825	Days
w	156.9	mm^2
T	0.5	hour
$C_{EV/Km}$	0.34	$/Km

4.5.2 Impact on the Reliability of Utility Grid

The reliability impact of the electric grid is an important factor that must be taken into account for the optimal planning of EVCS [138] . Deterioration of electric substation components such as substation transformer and line cause disruption in providing electric supply to CS. EV charging loss creates issues for CS operators and EV owners in terms of economy. Several models and reliability indices are needed to address the reliability issue of the utility grid for optimal planning of EVCS.

Availability (ξ) of a basic element can be described in terms of the rate of failure, rate of repair of the basic component of substation i.e., transformer and lines [139]. Thus, the availability (ξ) can be given as:

$$\xi = \frac{\Psi}{\Psi+\chi} \tag{4.18}$$

Table 4.4 presents the failure rate and repair rate of substation transformers and lines. One of the important indexes which measure the reliability impact of the utility grid

Table 4. 4. Data required for determining the reliability [139]

		Value	Unit
Line	Failure rate	0.1	Failure/km/year
	Repair time	4	hour
Transformer	Failure rate	0.1	Failure/year
	Repair time	100	hour
ICC		0.90	$/kWh

is charging loss cost (CCL). CCL refers to the cost of EVs which remain uncharged due to collapse in the utility grid. CCL may be defined in terms of operating hours of each CS, CS capacity, unavailability of electric supply for i^{th} CS and uninterrupted charging cost. CCL can be given as follows:

$$\mathrm{CCL(i)} = 1825 * \rho(\mathrm{i}) * \mathrm{C(i)} * \eta_{\mathrm{i}} * \mathrm{ICC} \tag{4.19}$$

Average operating hours i.e., $\rho(i)$ of each CS can be determined as follows:

$$\rho(\mathrm{i}) = \frac{\mathrm{N_{EV_i}}}{\mathrm{NC_i}} * \mathrm{T} \text{ in hours} \tag{4.20}$$

ICC refers to the cost paid by CS operator and EV owner due to disruption in EV charging because of collapse in the grid.

Unavailability of electric supply for i^{th} CS can be calculated as:

$$\eta_{\mathrm{i}} = 1 - \xi_{\mathrm{i}} \tag{4.21}$$

$$\xi_{\mathrm{i}} = \xi_{\mathrm{fi}} * \xi_{\mathrm{D4x}} \tag{4.22}$$

ξ_{fi} denote the station feeder availability of feeder fi and ξ_{D4x} is the availability of electric supply on bus D4x.

Availability of electric supply on bus $D4x$ can be calculated as:

$$\xi_{4\mathrm{x}} = \xi_{6\mathrm{x}}\,(1 - (1 - \xi_{\mathrm{T}})\text{^}2)) \tag{4.23}$$

Calculation of ξ_{D6x} depends on the nature of the substation i.e., whether it is a PQ bus or not.

$$\xi_{6x} = (1 - (1 - \xi_T)\text{^}2)) \tag{4.24}$$

4.5.3 Simulation Results and Main Achievements

The optimized value of the objective function has a strong dependence on CS capacity, the number of EVs charged at each CS and the number of charging connectors utilized to recharge the EVs. For charging, EV will follow the path of minimum distance to reach the CS. The number of EVs charged at each CS can be approximately determined by Eq. (4.13). Fig. 4.8. shows the number of EVs assigned at each CS.

Thus, the number of charging connectors installed at each CS can be obtained as follows:

$$NC_i = \frac{N_{EV_i} \times NC(max)}{N_{EV}} \tag{4.25}$$

Thus, the number of charging connectors utilized at each charging station for feeding the assigned number of EVs are displayed in Table 4.5.

Based on this, different cost functions considered in this paper can be evaluated.

Investment cost mainly depends on land cost and the number of charging connectors. Areas in Delhi are divided from category A to category H based on land cost. In the considered study zone, different areas come under different categories. Land costs of different considered areas are indicated in Table 4.6.

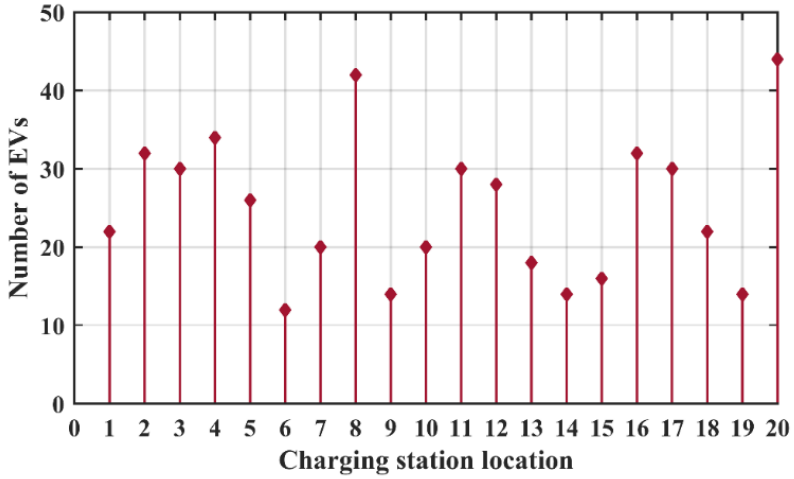

Fig. 4. 8. Number of EVs charged at each CS

Table 4. 5. Optimized number of charging connectors required at different CS installed in South Delhi areas

Charging Station Location	Number of charging connectors utilized
Saket	3
Shivalik	4
Greater Kailash	3
Lajpat Nagar	4
New Friends Colony	3
Kalkaji	2
Hauz Khas	2
Safdarjung	5
Vasant Vihar	2
Green Park	2
Panchsheel	3
Defence Colony	3
Nehru Place	2
Chanakyapuri	2
Chirag Delhi	2
Vasant Kunj	4
Chhatarpur	3
RK puram	3
Golf Links	2
Malviya Nagar	5

Table 4. 6. Land cost of areas in South Delhi [140]

Charging Station Location	Land Cost ($/m^2)
Saket	2178.77
Shivalik	3349.87
Greater Kailash	3349.87
Lajpat Nagar	2178.77
New Friends Colony	10539.82
Kalkaji	2178.77
Hauz Khas	3349.87
Safdarjung	3349.87
Vasant Vihar	10539.82
Green Park	3349.87
Panchsheel	3349.87
Defence Colony	3349.87
Nehru Place	10539.82
Chanakyapuri	10539.82
Chirag Delhi	3349.87
Vasant Kunj	2178.77
Chhatarpur	3349.87
RK puram	3349.87
Golf Links	10539.82
Malviya Nagar	2178.77

The investment cost for different CS sites has been evaluated using the proposed GWO. The overall investment cost incurred by utilizing GWO comes out to be $ 8657600. The effectiveness of the proposed GWO is confirmed by comparing the results with other intelligent techniques such as PSO ($ 9143400). It is revealed that the investment cost calculated using GWO is 5.3% less than that of PSO. This comparison shows the preeminence of GWO over PSO. In this regard, the comparative analysis of investment cost investigated using different intelligent algorithms is shown in Fig. 4.9. It should also be remembered that investment costs are high in areas with high land costs and that use a large number of charging connectors. Charging stations that need a greater number of connectors to have a higher set-up cost, which leads to a substantial increase in investment costs because connector set-up costs account for a significant portion of the total

cost. That's why areas such as New Friends Colony, Vasant Vihar, Chanakyapuri, and Golf Links have a high investment cost because of their high land cost and ample quantity of connectors required to serve EVs in these regions. On the other hand, Saket, Hauz Khas and Kalkaji etc., have lower investment costs due to lower land costs and a limited number of charging connectors. A comparison of the investment cost of each CS site obtained using GWO and PSO is presented in Table 4.7. Further improvement in investment cost can be made when the government and public sector unit contributes to the development of the charging station and utilizes available public lands for its installation.

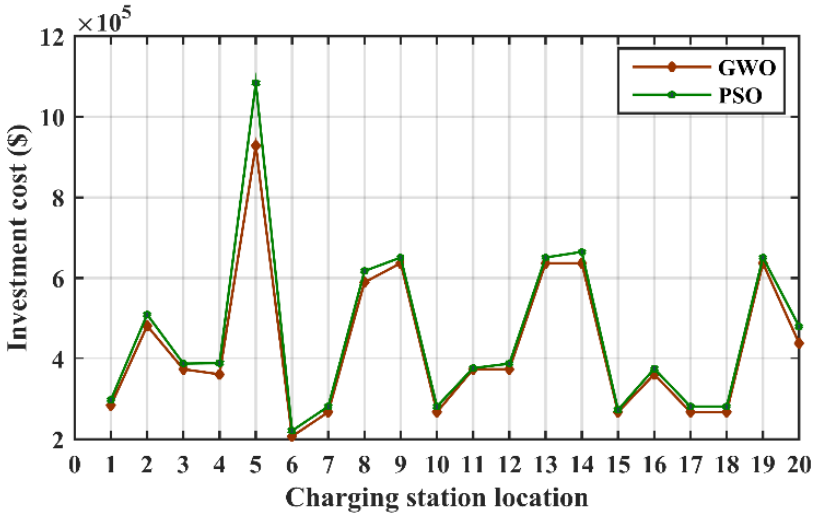

Fig. 4. 9. Investment Cost for different CS in South Delhi areas

In addition, CS electrification cost is highly influenced by the separation between the CS and electric substation. However, the distance of each CS from every substation has been evaluated based on Cartesian geographic information. Based on this, the electrification cost of each CS site is determined by using the proposed GWO. CS electrification costs obtained using GWO and PSO are displayed in Table 4.7.

Table 4. 7. Investment cost and CS electrification cost of each CS installed in South Delhi areas

Charging Station Location	Investment cost ($)		CS electrification cost ($)	
	GWO	PSO	GWO	PSO
Saket	284200	298200	227.36	241.5
Shivalik	481600	509600	220.864	232.218
Greater Kailash	373800	387800	266	278.572
Lajpat Nagar	361200	389200	221.424	232.246
New Friends Colony	928200	1083600	181.44	208.026
Kalkaji	207200	221200	204.064	213.696
Hauz Khas	267400	281400	164.752	176.092
Safdarjung	589400	617400	526.288	545.398
Vasant Vihar	637000	651000	462.896	485.8
Green Park	267400	281400	46.704	50.05
Panchsheel	373800	376600	242.032	278.558
Defence Colony	373800	387800	134.4	136.556
Nehru Place	637000	651000	134.064	135.492
Chanakyapuri	637000	665000	618.24	654.92
Chirag Delhi	267400	273000	54.656	57.988
Vasant Kunj	361200	375200	696.416	720.398
Chhatarpur	267400	281400	118.832	120.568
RK puram	267400	281400	375.872	391.384
Golf Links	637000	651000	241.136	262.43
Malviya Nagar	438200	480200	281.792	300.412
Total	8657600	9143400	5419.232	5722.304

The performance of the GWO technique is proven by comparing the attained results with those of PSO. Application of GWO results in a noticeable improvement in CS electrification cost by 5.2% less than that of PSO. Fig. 4.10. shows the comparison of CS electrification cost obtained using GWO and PSO. The greater the distance between the CS and the electric substation, the higher the cost of CS electrification, and vice versa. Table 4.8. shows that charging stations in Safdarjung, Chanakyapuri, and Vasant Kunj have high CS electrification costs due to their remote location from the electric substation whereas because of the proximity to the substation, the Chirag Delhi and Green Park charging station sites have low costs. As a result, to meet lower CS electrification costs, the CS operator must choose the location wisely. Even, when the electric utility is obligated

to electrify the stations at no cost to the station owners, the cost of CS electrification can be reduced.

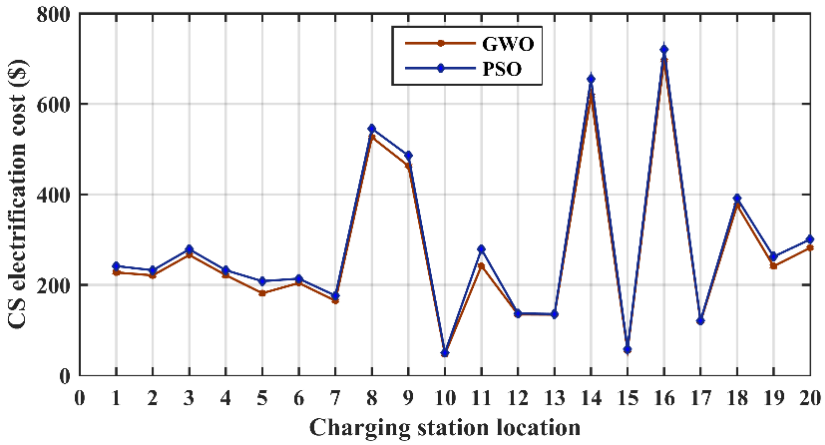

Fig. 4. 10. CS electrification cost for different CS in South Delhi area

Furthermore, EV energy loss cost or cost of energy consumption of EVs relies on the distance between the EV position and CS. The charging station in the neighborhood of the electric substation may be at a far distance from the EV position. Hence, it increases energy loss costs. Distance between each EV (i.e., 500 EVs in this work) and CS is calculated based on geographic information. EVs are assigned to the nearest charging station based on the minimum distance criterion. In this way, the energy loss cost of 500 EVs has been calculated by optimizing the distance to nearby charge stations. The proposed GWO leads to a considerable reduction in energy loss cost i.e., 15.5% less as compared to that of PSO. The obtained results using GWO prove its superiority over other algorithms. The varying behavior of EV energy loss cost obtained using algorithms considered in this work are shown in Fig. 4.11. It has been reported that the smaller the distance between the EV location and the CS site, the lower the EV's energy consumption, and vice versa. If the needs of EV owners are neglected, the cost of EV energy loss may be reduced.

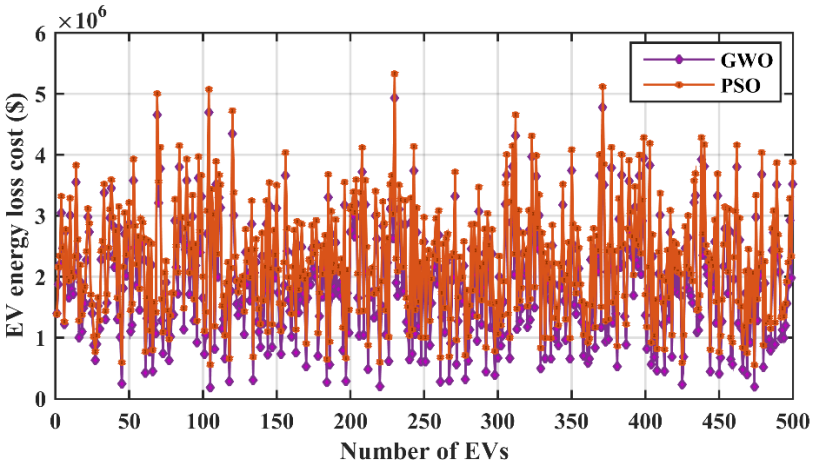

Fig. 4. 11. EV energy loss cost for 500 EVs

Travel time cost depends on the distance between the charging station and the location where the need of charging EV arises, as well as the cost of traveling of EV per km. The lesser the distance between the EV and CS, the smaller will be the travel time cost paid by the EV owner. Hence, the travel time cost of all 500 EVs to reach the nearby charging station has been calculated using the proposed GWO and compared with PSO to prove its dominance. It is observed that GWO results in a significant reduction in travel time cost as compared to the results attained via PSO. GWO provides the optimized value of travel time cost i.e., $ 280.43 which is 9.1% less than that of PSO ($ 308.72). This proves the supremacy of proposed GWO algorithms over PSO. The travel time cost of each EV (i.e., 500 EVs) determined using GWO and its comparison with PSO is portrayed in Fig. 4.12. The cost of travel time can be further decreased by placing more charging stations along EV routes, as this reduces the distance that EVs would travel for charging.

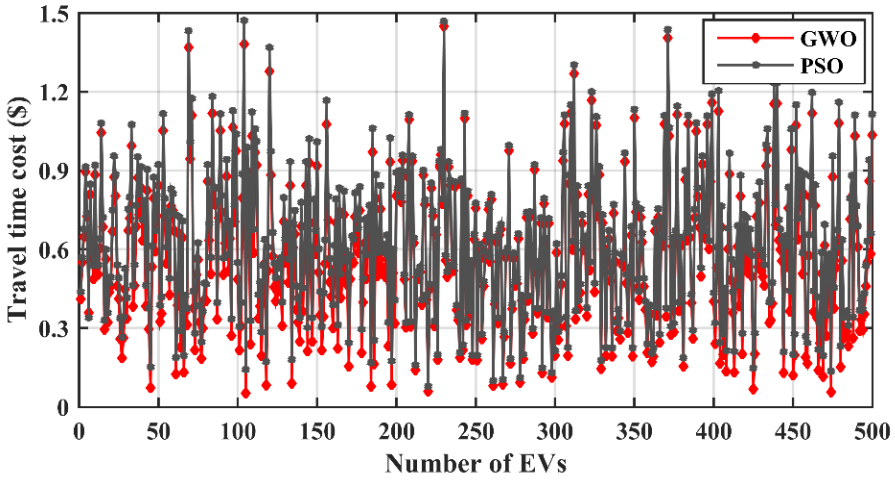

Fig. 4. 12. Travel time cost for 500 EVs

In addition to this, the impact on the reliability of the grid is investigated in terms of charging cost loss. The availability of electric components in the electric substation is calculated using Eqns. (4.21) – (4.24). CS capacity, effective operating hours, and electric supply availability at each CS site are presented in Table 4.8.

CCL differs for each charging station as it depends on CS capacity, effective operating hours, and electric supply availability. The optimized values of CCL for each CS site were obtained by applying GWO and its comparison with PSO is shown in Fig. 4.13.

Eq. (4.21) – (4.24) introduces the impact on the reliability of the grid in the optimal planning of EVCS. Basic parameters required for the evaluation of reliability are listed in Table 4.4. A comparison of the value of CCL for each CS site obtained using GWO and PSO considering the impact on the reliability of the grid network is shown in Table 4.9. Also, values of CCL are much dependent on the availability of electric supply at a particular CS as shown in Table 4.9. CCL value is high for those CS where the percentage of unavailability of electric supply is high and vice versa. It can be realized in Table 4.4. that ICC is considered as 10 times the electricity price to reveal the loss due to the power outage.

Table 4. 8. Average working hours, unavailability of electricity, and capacity of each CS

Charging Station Capacity (kW)	Effective Operating Hours of each CS, $\boldsymbol{\rho(i)}$ in hr	Unavailability of electric supply ($\boldsymbol{\xi_i}$) ($\times \mathbf{10^{-3}}$)
288	3.66	0.2750
384	4	0.1060
288	5	0.1523
384	4.25	0.4343
288	4.33	0.0967
192	3	0.1050
192	5	0.0640
480	4.2	0.2131
192	3.5	0.1347
192	5	0.1267
288	5	0.1004
288	4.66	0.0828
192	4.5	0.0820
192	3.5	0.0929
192	4	0.2333
384	4	0.1015
288	5	0.3271
288	3.66	0.1006
192	3.5	0.3752
480	4.4	0.1024

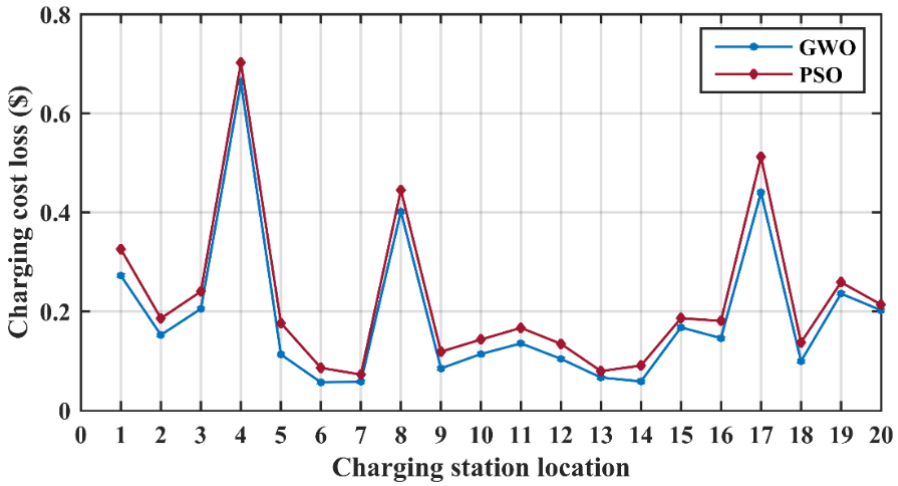

Fig. 4. 13. Charging cost loss for CS installed in south Delhi areas

Table 4. 9. Charging cost loss (CCL) of each charging station

Charging Station Location	Charging Cost Loss ($)	
	GWO	PSO
Saket	0.272104	0.3255
Shivalik	0.152124	0.18564
Greater Kailash	0.204904	0.23996
Lajpat Nagar	0.662242	0.7021
New Friends Colony	0.112672	0.17612
Kalkaji	0.056504	0.08568
Hauz Khas	0.057484	0.0721
Safdarjung	0.401408	0.44492
Vasant Vihar	0.084574	0.1183
Green Park	0.113638	0.14294
Panchsheel	0.135086	0.16646
Defence Colony	0.103824	0.13412
Nehru Place	0.066192	0.0791
Chanakyapuri	0.058324	0.0903
Chirag Delhi	0.167412	0.18592
Vasant Kunj	0.14567	0.18046
Chhatarpur	0.440104	0.51184
RK puram	0.099078	0.13692
Golf Links	0.235578	0.25858
Malviya Nagar	0.202062	0.2135
Total	3.770984	4.45046

The objective functions are represented by Eqns. (4.1) – (4.7) and set of technical constraints i.e., Eqns. (4.9) – (4.13) have been solved using grey wolf optimization. The optimized value of all the objective functions considered for the optimal planning of EVCS and their impact on the reliability of the grid is summarized in Table 4.10. It can be seen in Table 4.10; CCL is smaller as compared to the other cost functions. Though, CCL can be of significant value when EV loss is ignored in the optimization problem

Table 4. 10. Optimized values of objective functions

Objective Functions	Cost ($)	
	GWO	PSO
Investment cost	8657600	9143400
CS electrification cost	5419.232	5722.304
EV energy loss cost	9.51×10^{8}	11.26×10^{8}
Travel Time Cost	280.4305	308.7251
Charging cost loss	3.770984	4.45046

4.6 SUMMARY

In this chapter, a new approach for solving the multi-objective optimization problems for optimal siting and sizing of EVCS in different areas in South Delhi, New Delhi, India is proposed. Grey wolf optimization has been utilized to solve the multi-objective cost functions and the obtained results are compared with particle swarm optimization for validation purposes. The cost function includes investment cost, CS electrification cost, EV energy loss cost, and travel time cost. Investment cost and CS electrification cost of all CSs have been calculated and found that the investment cost strongly depends on the land cost and the number of connectors used in each CS. While CS electrification cost depends on the distance between the CS and electric substation. On the other hand, EV energy loss cost and travel time cost have been evaluated for all EVs. It is revealed that travel time cost and EV energy loss cost depends on the distance between the CS and EV location. After comparing the results obtained using GWO and PSO, it is revealed that GWO is more effective than PSO for the considered case study. Furthermore, reliability indices i.e., CCL is an important index that gives an idea about the reliability of a system. CCL is a function of CS capacity, effective working hours of CS, and unavailability of electric supply at each CS. CCL has been determined for each CS and results reveal that CCL will be high for CS having less availability of electric supply and vice versa.

CHAPTER 5

SINGLE-OBJECTIVE FORMULATION OF CHARGING STATION AND CAPACITOR PLACEMENT PROBLEM

5.1 INTRODUCTION

The simultaneous allocation of EVCS and capacitors in radial distribution system is discussed in this chapter. This allocation is focused on optimizing the power loss along with maximizing the net profit. The use of capacitors in the presence of an EVCS increases the system's stability by lowering losses and improving the voltage profile. Moreover, the operating and installation cost of EVCS has also been taken into consideration for maximizing the net profit. Also, the effect of EVs taking part in V2G mode is analyzed in this article by considering the reliability improvement benefit. Furthermore, a new hybrid intelligent optimization method is used to solve the objective functions. The performance of the chosen hybridized technique is validated by the comparison of the attained results with other intelligent algorithms such as GWO and PSO.

5.2 MATHEMATICAL MODELING OF RADIAL DISTRIBUTION SYSTEM

The two-bus model for the analysis of the distribution system is discussed in this section. The single line diagram of the two-bus radial distribution system is shown in Fig. 5.1.

From Fig. 5.1

$$V_n = V_m - I_j Z_j \tag{5.1}$$

$$|V_n|\,\delta_n = |V_m|\,\delta_m - |I_j| - \theta_j * |Z_j|\emptyset_m \tag{5.2}$$

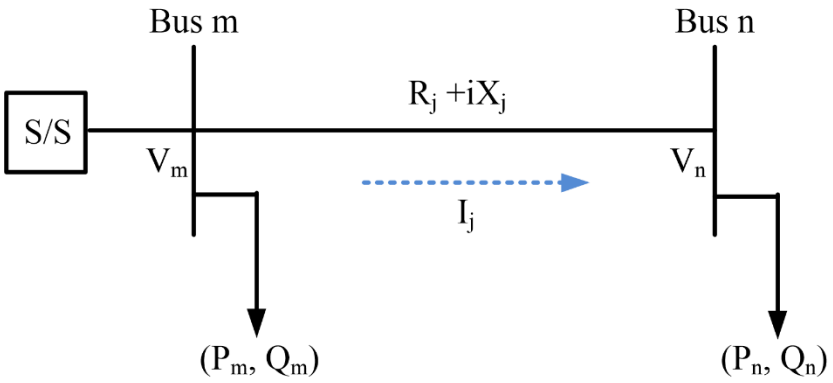

Fig. 5. 1. Representation of two nodes and one branch of the distribution system

$$|V_n|\cos\delta_n + |V_n|\sin\delta_n = |V_m|\cos\delta_m + |V_m|\sin\delta_m - |I_j|(\cos\theta_m - j\sin\theta_m)(R_j^2 + X_j^2) \tag{5.3}$$

By separating real and imaginary terms

$$|V_n|\cos\delta_n = |V_m|\cos\delta_m - |I_j|(R_j\cos\theta_m + X_j\sin\theta_m) \tag{5.4}$$

$$|V_n|\sin\delta_n = |V_m|\sin\delta_m - |I_j|(X_j\cos\theta_m - R_j\sin\theta_m) \tag{5.5}$$

Squaring and adding Eqns. (5.4) and (5.5)

$$|V_n|^2 = |V_m|^2 - 2 * |V_m| * |I_m| * \cos\delta_m\{(R_j\cos\theta_m + X_j\sin\theta_m)\} + |I_j|^2\{(R_j^2 + X_j^2)\} - 2 * |V_m| * |I_m| * \sin\delta_m\{(X_j\cos\theta_m - R_j\sin\theta_m)\} \tag{5.6}$$

After mathematical rearrangement Eq. (5.6) can be written as

$$|V_n|^2 = |V_m|^2 - 2 * |V_m| * |I_m|\{(R\cos(\delta_m - \theta_m)) + X\sin(\delta_m - \theta_m)\} + |I_j|^2\{(R_j^2 + X_j^2)\} \tag{5.7}$$

$$|V_n|^2 = |V_m|^2 - 2 * |V_m| * |I_m| * |Z_j|\cos(\delta_m - \theta_m - \emptyset_m) + |I_j|^2\{(R_j^2 + X_j^2)\} \tag{5.8}$$

Since $\delta_m - \theta_m - \emptyset_m$ is negligible hence, $\cos(\delta_m - \theta_m - \emptyset_m) = 1$

Because variation in voltage angle from source bus to end bus is very small.

Therefore, Eq. (5.8) can be written as

$$|V_n|^2 = |V_m|^2 - 2 * |V_m| * |I_m| * |Z_j| + |I_j|^2 \{(R_j^2 + X_j^2)\} \tag{5.9}$$

$$|V_n|^2 = [|V_m| - |I_m| * |Z_j|]^2 \tag{5.10}$$

$$|V_n| = |V_m| - |I_j||Z_j| \tag{5.11}$$

$$\text{where, } |I_m| = \frac{(P_m^2 + Q_m^2)^{1/2}}{|V_m|} \tag{5.12}$$

It can also be written as Eq. (5.13)

$$|I_n| = \frac{(P_n^2 + Q_n^2)^{1/2}}{|V_n|} \tag{5.13}$$

$$|V_n| = |V_m| - \frac{(P_n^2 + Q_n^2)^{1/2}}{|V_n|} * |Z_j| \tag{5.14}$$

$$|V_n|^2 = |V_m| * |V_n| - (P_n^2 + Q_n^2)^{1/2} * (R_j^2 + X_j^2) \tag{5.15}$$

$$|V_n|^2 - |V_m| * |V_n| - (P_n^2 + Q_n^2)^{1/2} * (R_j^2 + X_j^2) = 0 \tag{5.16}$$

The positive root of Eq. (5.16) is given as

$$|V_n| = \frac{|V_m| \pm (|V_m|^2 - 4((P_n^2 + Q_n^2)^{1/2})(R_j^2 + X_j^2))^{1/2}}{2} \tag{5.17}$$

The voltage at the receiving end can be calculated using Eq. (5.17).

The active power loss in the line connected between m and n bus can be calculated as

$$P_{loss}(m, n) = |I_j|^2 * R_j \tag{5.18}$$

Hence, the active and reactive power loss in the line connecting m and n bus can be calculated as

$$P_{loss}(m, n) = \frac{(P_n^2 + Q_n^2)}{|V_n|^2} * R_j \tag{5.19}$$

$$Q_{loss}(m,n) = \frac{(P_n^2+Q_n^2)}{|V_n|^2} * X_j \quad (5.20)$$

The total active power loss i.e., $P_{T,loss}$ can be evaluated by adding the individual power loss of all branches which can be expressed as

$$P_{T,loss} = \sum_{j=1}^{N_{br}} P_{loss,j}\,(m,n) \quad (5.21)$$

5.3 PROBLEM FORMULATION

For EV users and electric utilities, EVCS deployment at the proper position plays a major role. Due to the limitation of the all-electric range, the EV must be recharged several times during a ride. EVCS often serves as a heavy load which, when put in the distribution network incorrectly, induces increases in power loss. Therefore, for a minimal increase in power loss, the optimum location of EVCS is necessary. Installing capacitors overcomes the effect of incorporating EVCS into the distribution network as it lowers the power loss and strengthens the voltage profile. The proposed methodology is depicted in Fig. 5.2.

5.3.1 Modeling of EVCS Load

EVCSs act as an extra load for the distribution network. The total load in the distribution system after integrating EVCS can be evaluated using Eq. (5.22).

$$T_{load} = \sum_{bs=1}^{N_{bus}} P_{avail,bs} + P_{EVCS}^{bs} \quad (5.22)$$

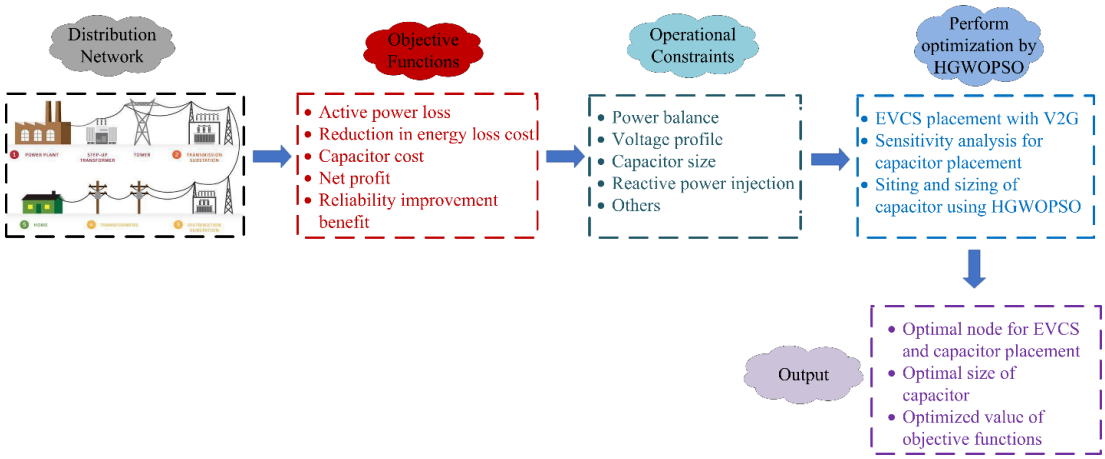

Fig. 5. 2. The layout of the proposed methodology

The size of EVCS depends on several factors which include the number of vehicles operating in the grid to vehicle (G2V) mode, vehicle to grid (V2G) mode, charging rate (C_R), discharging rate (DC_R), number of charging ports and their rated power.

Thus, the capacity of EVCS can be expressed as:

$$P_{EVCS}^{bs} = [N_{EV}(G2V) * C_R - N_{EV}(V2G) * DC_R] \quad (5.23)$$

Simply, the additional load of EVCS will be applied only on that bus where the CS is expected to be placed. That bus number i.e., CS location is the decision variable for which the optimization is performed. Fig. 5.3. shows the addition of EVCS into the distribution system.

5.3.2 Modeling of the Integrated Capacitor into the Distribution Network

The installation of capacitor units at suitable locations in the distribution system has many advantages which include line loss reduction, voltage profile enhancement, power factor correction, etc. The governing equations for integrating capacitors into the distribution network are shown below.

The net reactive power after injecting capacitor at bus n can be defined as

$$Q_N^{inj} = Q_n - Q_{cap} \tag{5.24}$$

The active power loss after connecting the capacitor at bus n is shown in Fig. 5.3 is expressed as

$$P_{loss(m.n)}^{cap} = \frac{P_n^2 + Q_N^{inj^2}}{|V_n|^2} * R_j \tag{5.25}$$

$$P_{loss(m.n)}^{cap} = \frac{(P_n^2 + (Q_n - Q_{cap})^2)}{|V_n|^2} * R_j \tag{5.26}$$

$$P_{loss(m.n)}^{cap} = R_j * \frac{(P_n^2 + Q_n^2)}{|V_n|^2} + \frac{Q_{cap}^2 - 2 * Q_n * Q_{cap}}{|V_n|^2} * R_j \tag{5.27}$$

The reduction in power loss i.e., $\Delta P_{loss(m.n)}^{cap}$ is the difference between the power loss before and after capacitor placement and can be given as

$$\Delta P_{loss(m.n)}^{cap} = \frac{Q_{cap}^2 - 2 * Q_n * Q_{cap}}{|V_n|^2} * R_j \tag{5.28}$$

Increasing the number of capacitors is effective in decreasing the power losses of the distribution network.

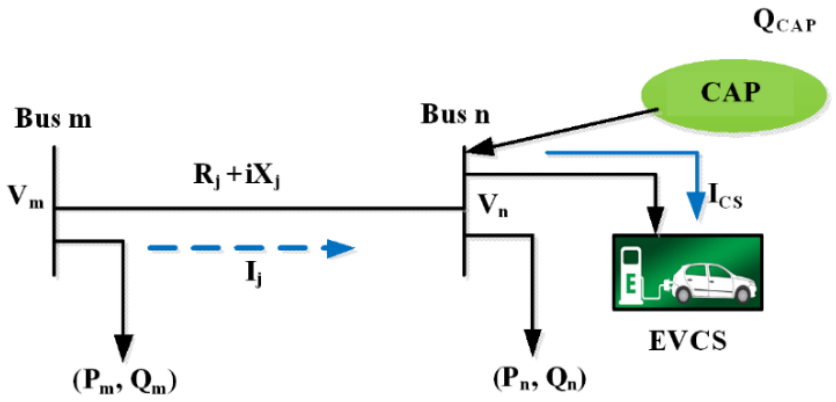

Fig. 5. 3. Representation of integrated EVCS and capacitor in the distribution system

5.3.3 Assumptions

Following points have been presumed for the research to be carried out:

- The electric distribution network is balanced in nature.
- No EVCS load and capacitor are located on the substation bus.
- Installed EVCS and capacitors are assumed to supply active and reactive power respectively.
- The voltage angle difference is believed to be constant as there is a change of a few degrees in the voltage angle from the source to the tail end.

5.3.4 Explanation of the Objective Functions

The primary objective of carrying out this research work is to optimally place the EVCS and capacitor in the distribution network. The incorporation of EVCS in the power network increases the power loss and deteriorates the voltage profile. Capacitors are located at optimum nodes in the distribution to mitigate increased losses. The capacitor allocation process preserves the voltage at each bus within desired limits. Therefore, the objective function is designed to minimize the loss of power, which eventually leads to a decrease in overall annual energy loss costs, maximizes net profit, and improves the reliability of the distribution system without violating the subject constraints. The objective functions of the proposed problem can be written as below.

$$\text{Total active power loss,} \qquad P_{T,loss} = \sum_{j=1}^{N_{br}} P_{loss,j}\,(m,n) \tag{5.29}$$

Maximize net profit (5.30)

$$= \text{energy loss reduction benefit}$$

$$- \text{installation cost of system components}$$

$$- \text{operating cost of system components}$$

$$\text{Energy loss reduction benefit} = K_{ep} * \left(P_{T,loss} - P_{T,loss}^{cap} \right) * T \quad (5.31)$$

The installation cost of system components (5.32)

$$= \beta \left[C_i^{cap} * N_{cap} + C_i^{EVCS} * N_{EVCS} + K_{cp} * \sum_{i=1}^{N_{cap}} Q_{cap}(i) \right]$$

$$\text{Operating cost of system components} = C_O^{cap} * N_{cap} + C_o^{EVCS} * N_{EVCS} \quad (5.33)$$

Reliability analysis is essential for upgrading electrical distribution networks under various operating conditions, allowing them to meet modern and ever-increasing loads. Therefore, energy not supplied (ENS) is an indicator of the reliability of the system and is taken into account for evaluating the reliability. The yearly cost of energy not supplied can be determined as follows:

$$C_{ENS} = \sum_{j=1}^{N_{br}} \left(\sum_{t=1}^{T=365} \left(\sum_{h} \left(\frac{E^d(h)}{T} F_h R_h \right) PC_t \right) \right) \quad (5.34)$$

Thus, the reliability improvement benefit may be defined as the difference between the cost of energy not supplied before and after installing EVs and can be written as follows:

$$C_{RE} = C_{ENS} - C_{ENS,V2G} \quad (5.35)$$

5.3.5 Explanation of Operational Constraints

The modeled objective functions are optimized taking into consideration the following constraints.

1) Load flow constraints

The constraints related to load flow in the distribution network can be stated as follows

$$P^{substation} = \sum_{j=1}^{N_{br}} P_{loss}^{j}(m,n) + \sum_{bs=1}^{N_{bus}} P_{avail,bs} + P_{EVCS}^{bs} \tag{5.36}$$

$$Q^{substation} + \sum_{bs=1}^{N_{bus}} Q^{cap}(bs) = \sum_{j=1}^{N_{br}} Q_{loss}^{j}(m,n) + \sum_{bs=1}^{N_{bus}} Q_{avail,bs} \tag{5.37}$$

2) Bus voltage tolerance

The voltage at each bus i.e., V (bs) must lie within the minimum $V_{bs}^{min}$and maximum V_{bs}^{max} limits.

$$V_{bs}^{min} \leq V\,(bs) \leq V_{bs}^{max} \qquad bs = 1, 2, 3 \ldots N_{bus} \tag{5.38}$$

3) Transmission line tolerance

The power flow in each line PF(j) should not exceed the maximum specified limit of PF_{j}^{max}.

$$PF(j) < PF_{j}^{max} \tag{5.39}$$

4) Limit on number of capacitors

This restriction is proposed to decrease the number of the capacitor element. Hence, the number of capacitors installed N_{cap} should be either less than or equal to the

maximum number of capacitors N_{cap}^{max}.

$$N_{cap} \leq N_{cap}^{max} \tag{5.40}$$

5) Limit on capacitor sizing

The reactive power to be injected Q_{cap} should be within the allowable minimum Q_{cap}^{min} and maximum Q_{cap}^{max}limits.

$$Q_{cap}^{min} \leq Q_{cap} \leq Q_{cap}^{max} \tag{5.41}$$

6) Limit on maximum compensation provided by capacitor

The total reactive power injected by the capacitor Q_{cap}^{total}must be either less than or equal to total reactive power load $Q_{avail,bs}^{total}$.

$$\sum_{p=1}^{N_{cap}} Q_{cap}(p) \leq \sum_{bs=1}^{N_{bus}} Q_{avail,bs} \tag{5.42}$$

5.4 PROPOSED APPROACH FOR EVCS AND CAPACITOR PLACEMENT

In this chapter, the hybrid approach of GWO and PSO is employed to solve the objective functions. The methodology adopted for dealing with the optimization problem under consideration is described with the flowchart shown in Fig. 5.4. The whole process can be grouped into four stages: the initialization stage, evaluation stage, updating stage, and termination stage. Initially, the constant parameters required to compute active power loss and net profit, etc., are given as input, and the initialization of HGWOPSO parameters, which includes several iterations, number of runs, number of search agents in GWO,

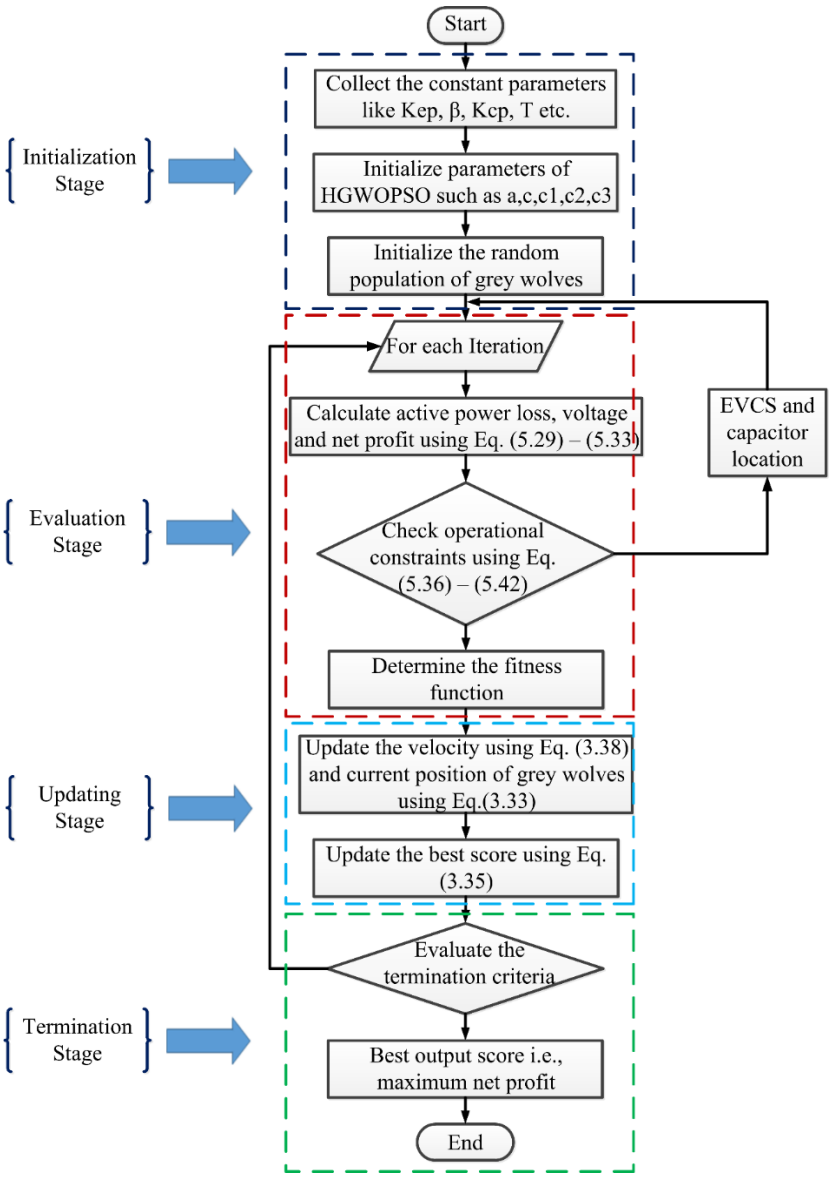

Fig. 5. 4. Flow chart of the proposed approach

number of particles in PSO, etc. Then load flow analysis is performed to calculate the active power losses and hence, the net profit calculation. In the first run, the most feasible solutions regarding the location and sizing of EVCS and capacitor are chosen from the random population and installed in the grid network. The load flow analysis is carried out after installing EVCS and capacitor and then determining the objective functions. The steps displayed in the flowchart are executed with taking care of operational constraints. In each iteration, the sizes and location of EVCS and capacitors are sent to the evaluation stage of

the flowchart to reduce the active power loss and increase the net profit. The procedure is repeated until the final criteria are achieved.

5.5 TEST SYSTEM

5.5.1 Input Parameter Related to the Study Area

In this work, the IEEE 33-bus system and 34-bus radial distribution network have been taken into account for testing the efficiency of the proposed approach. The line parameters and existing load demand of the respective network are mentioned in [141] and [142].

5.5.2 Input Data Related to EVs, EVCS, and Capacitors

This research work involves 100 EVs, 2 EVCS with multiple charging points, and a maximum of four capacitors to be optimally positioned. The EVCS load is determined by the number of EVs involved in the G2V, V2G mode, charge, and discharge rates. In this research analysis, the charging rate of 19 kW for the grid to vehicle mode and discharge rate of 8 kW for the vehicle to grid mode are taken into consideration [143]. Moreover, charging and discharge efficiencies vary from around 80 percent to 95 percent. This research assumes that G2V mode efficiency is 95 percent while V2G mode efficiency is 80 percent. Also, the battery of EVs is charged with a power of 15 kW and a battery capacity of 50 kWh is used in this work. The overall number of potential positions for the capacitor placement is presumed to be 4 for both the 33-bus and 34-bus networks. The voltage restriction on each bus is considered between 0.95 and 1.05 p.u. The maximum active power flow limit is taken to be 5000 kW for both test networks [79]. EVCS and capacitor are not expected to be located on bus 1, since it is a substation bus for all test

networks with a constant voltage of 1 p.u. Furthermore, the reactive power to be injected for compensation purposes is set within the range of 150 and 1200 kVAr.

5.6 SIMULATION RESULTS, DISCUSSIONS, AND MAIN ACHIEVEMENTS

The performance and efficiency of the proposed hybrid algorithm have been certified on 33-bus and 34-bus radial distribution systems to minimize the active power loss, maximizing the net profit and improving the reliability of the distribution network with different penetration levels of EVs in V2G mode. The suggested approach focuses on the optimum positioning of EVCS, assuming that EVs are 100 percent penetrated, and then capacitors are optimally installed to compensate for the increased losses incurred by the integration of EVCS and thus, increase the resilience of the electric network. For both test systems, the constants considered for net profit calculation are given in Table 5.1.

Table 5. 1. Constant parameters required for the computation of net profit and reliability [144] [145]

Parameter	Value	Unit
Cost of energy paid per kWh ($\mathbf{K_{ep}}$)	0.06	\$/kWh
Depreciation factor (β)	20%	-
Hours per year (T)	8760	Hours
Cost of purchase of capacitor per kVAr ($\mathbf{K_{cp}}$)	25	\$/kVAr
Installation cost of capacitor ($\boldsymbol{C_i^{cap}}$)	1400	\$/location
Installation cost of charging station ($\boldsymbol{C_i^{CS}}$)	6070	\$/location
Operating cost of capacitor($\boldsymbol{C_o^{cap}}$)	300	\$/year/location
Operating cost of charging station ($\boldsymbol{C_o^{CS}}$)	8400	\$/year/location
Rate of failure ($\boldsymbol{F_h}$)	2	Fail/year
Outage time ($\boldsymbol{R_h}$)	194.66	hour
Penalty cost for unsupplied energy ($\boldsymbol{PC_t}$)	0.1	\$/kWh

To assess the active power losses, a direct approach-based load flow analysis of the distribution network is performed [146]. All loads are considered as constant power loads

and the inclusion of tap-changing transformers is not considered to prevent complexity. Several trials have been carried out on the considered test network to verify the efficacy of the proposed algorithm. The tuned parameters of HGWOPSO are mentioned in Table 5.2.

Table 5. 2. Tuned parameters of the proposed algorithm

Algorithm	Parameter	Description	Value
GWO	maxitr	Maximum number of iterations	100
	NSA	Number of search agents	30
PSO	Npop	Swarm size	50
	w_{min}	Minimum value of inertia weight	0.4
	w_{max}	Maximum value of inertia weight	0.9
	c_1	Cognitive acceleration coefficients	2.01
	c_2	Social acceleration coefficients	2.02
	Nruns	Number of runs	50

5.6.1 Implemented Simulation Results and Discussion for 33-bus, 12.66 kV System

The 33-bus radial distribution network comprises 33 nodes and 32 branches as depicted in Fig. 5.5. The line data and bus data of such a system are taken from [147]. The total active power and reactive power demand of the network are 3715 kW and 2300 kVAr respectively. The distribution network operates at a rated voltage of 12.66 kV.

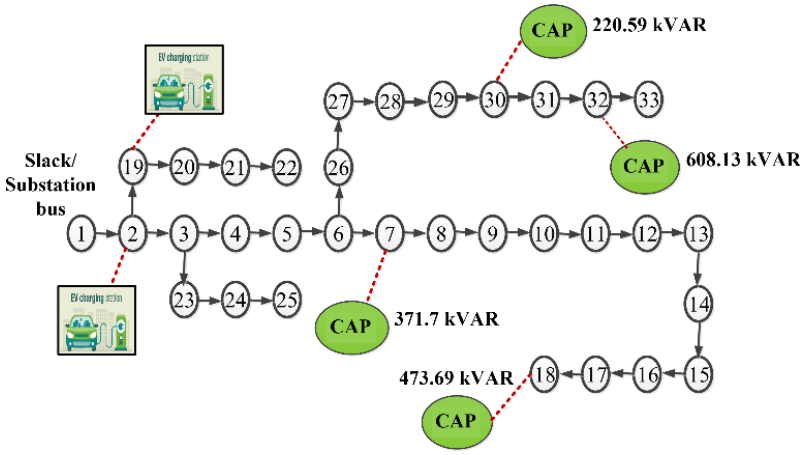

Fig. 5. 5. Typical configuration of the IEEE 33-bus system with two EVCS and four capacitors

Initially, the direct approach method for load flow analysis is implemented to investigate the active power losses which come out to be 201.87 kW. In this case, the

minimum voltage is 0.9132 p.u and the maximum voltage is 0.9972 p.u. The annual energy loss cost incurred for 201.87 kW is $106102.87. To certify the effectiveness of the proposed hybrid algorithm, results attained using HGWOPSO are compared with that of GWO and PSO. Using the proposed algorithm, the optimal nodes for EVCS placement comes out to be node 2 and 19 which results in a minimum power loss of 213.06 kW and 221.49 kW, respectively. The results indicate that the optimum EVCS placement strategy increases the loss of power and disturbs the voltage profile in electrical power networks, though EVCS is positioned near the substation bus. To improve the voltage profile and loss, capacitors are placed closer to EVCS and the end of feeders by delivering some reactive power. In this respect, the optimal location and capacities of EVCS and capacitors utilizing the proposed approach and its comparison with GWO and PSO are displayed in Table 5.3. When the capacitors of rating 371.7, 473.79, 220.59, and 608.13 kVAr are placed at optimal nodes 7, 18, 30, and 32 respectively lead to a significant drop in an active power loss of 139.94 kW from the base case active power loss of 201.87 kW, thus obtaining 30.6 % loss reduction benefit in annual energy loss cost. The minimum voltage of 0.9515 p.u. is registered at 15^{th} bus which is satisfying the voltage restriction limit. In this chapter, the percentage of loss reduction in annual energy loss cost is 30.67% using the proposed HGWOPSO which is better than that of GWO and PSO i.e., 29.74% and 29.42% respectively.

The proposed technique achieves a reliability improvement benefit of $ 169451.4 which is better than those of individual applications of GWO and PSO as shown in Table 5. 4.

Table 5. 3. The optimal results obtained via HGWOPSO in comparison with GWO and PSO for IEEE 33-bus system

Parameter	Base Case	EVCS and capacitor placement		
		HGWOPSO	GWO	PSO
Active power losses (kW)	201.87	139.94	141.82	142.47
Optimal nodes for EVCS	–	2, 19	2, 19	2, 19
Total number of EVs	–	100	100	100
Optimal nodes for capacitor	–	7, 18, 30, 32	7, 18, 30, 32	9, 16, 27, 32
Capacitor sizes (kVAr)	–	371.7, 473.7, 220.59, 608.13	425.18, 494.5, 353.8, 710.2	450.12, 519.45, 425.32, 740.56
Total kVAr	–	1674.12	1983.68	2135.45
Energy loss cost ($)	106102.87	73552.46	74540.59	74882.23
% Loss reduction in energy loss cost	–	30.67	29.74	29.42
Total capacitor cost ($)	–	41853	49592	53386.25
Net profit ($)	–	13358.55	12215.64	11798.11
Reliability improvement benefit ($)		169451.4	168176.94	168054.75
Convergence time in seconds	–	378.9	594.2	659.4
Computational time in seconds	–	2054.7	2391.3	2578.4
Efficiency	–	81.5	75.1	74.5

Also, the amount spent on the installation of capacitors using HGWOPSO is comparatively small when compared with GWO and PSO as shown in Table 5.3. In addition to this, the net profit obtained after integrating EVCS and capacitors to the 33-bus distribution system utilizing HGWOPSO is $ 13358.55 whereas GWO and PSO provide less net profit of $ 12215.11 and $ 11798.11 respectively.

The above analysis proves the supremacy of the HGWOPSO algorithm over GWO and PSO. The comparison of the attained results using the proposed algorithm against GWO and PSO for the 33-bus system is presented in Table 5.3.

Also, the computational time and convergence time for the HGWOPSO, GWO, and PSO are determined and mentioned in Table 5.3. The computational time refers to the time

needed to perform the total number of runs, while the time required by the specific algorithm to reach the termination criterion is the convergence time. The computational time for the proposed HGWOPSO is 2054.7 sec while it attains the optimum solution after 378.9 sec. The other approach is GWO which takes 2391.3 sec for computation and converges in 594.2 sec. The next approach is PSO which gives a convergence time of 659.4 sec and a computational time of 2578.4 sec. The efficiency of the proposed approach can be investigated by the ratio of the difference between the computational time and convergence time to the computational time. The efficiency of the proposed approach is 81.5 % while for GWO and PSO it is 75.1 % and 74.5% respectively. Fig. 5.6. shows the voltage profile of the 33-bus system after the optimal placement of EVCS and capacitor. It is shown that the voltage profile is enhanced by the installation of the capacitor. Thus, the proposed HGWOPSO technique is successful in maintaining the healthy voltage profile of the 33-bus distribution system.

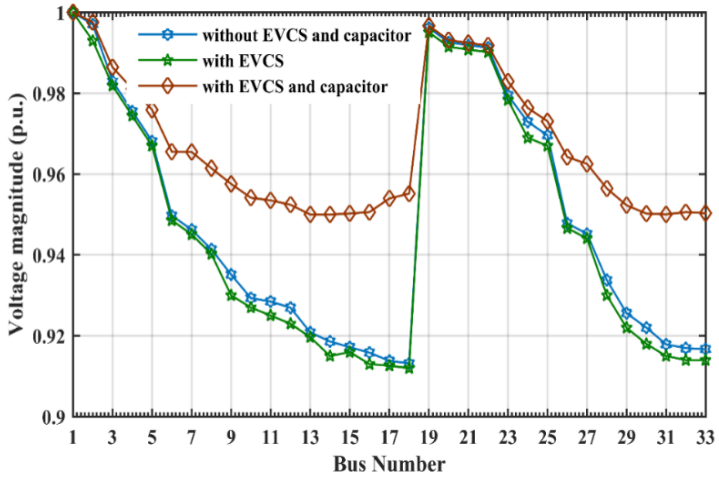

Fig. 5. 6. Improvement in voltage profile based on capacitor placement

Fig. 5.7. depicts the flow of active power in all branches of the distribution system after incorporating EVCS as well as the capacitor. The active power flow jumps to a higher

value due to increased loading of EVCS but it is managed by capacitor placement at optimal nodes and bringing it to the allowable limits.

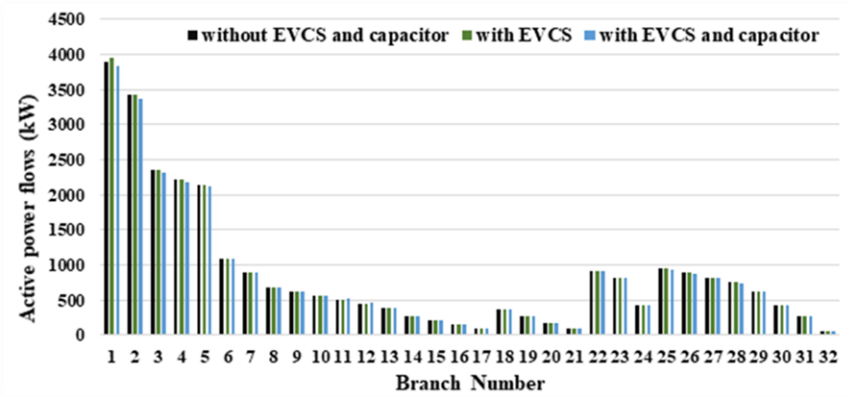

Fig. 5. 7. Improvement in the flow of active power based on capacitor placement

When EVs are having surplus energy, the extra energy is fed to the grid for maintaining the reliability of the system. Hence, EVs participation in the vehicle to grid mode assist the grid operator in keeping the acceptable voltage profile and also decreases the power losses of the system. In this regard, Fig. 5.8. shows the improvement in voltage profile when the different percentage of EVs participates in V2G mode. In this chapter, three different cases have been considered which comprise 10%, 20%, and 30% of the vehicles that take part in inverting mode i.e., V2G. Moreover, the V2G facility not only improves the voltage profile but reduces the active power losses as well. The effect on the reliability of the system with different levels of EVs participating in V2G can be understood with the help of Table 5.4. and Fig. 5.9.

Table 5. 4. Effect of EVs participation in V2G mode on the reliability improvement benefit for IEEE 33-bus system

Algorithm utilized	Reliability Improvement Benefit ($)			
	Without V2G	10% V2G	20% V2G	30% V2G
HGWOPSO	169451.4	175578.5467	178154.13	180231.25
GWO	168176.94	175234.5231	177597.54	180119.12
PSO	168054.75	174181.1591	177194.3	178547.54

Increasing the EVs participation in V2G leads to enhancement of the reliability improvement benefit. The results attained using HGWOPSO are superior to the other discussed techniques. In a 33-bus network, the active power losses for optimal EVCS nodes i.e., 2 and 19 are calculated to be 213.06 kW and 221.49 kW respectively when the V2G facility is not incorporated. As the EVs participation in V2G mode increases, active power losses come down. Fig. 5.10. portrays the active power losses of 33-bus systems for different percentages of EVs operation in V2G mode. Furthermore, Fig. 5.11. reflects the variation of power losses on integrating the EVCS and capacitor. It can be realized that power losses reduce as the quantity of capacitors increases. But the reduction in power loss is marginal on further increasing the capacitors and also it creates economic issues.

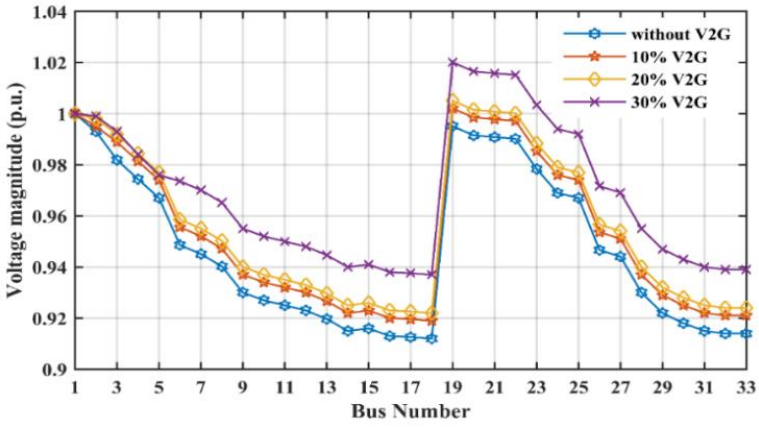

Fig. 5. 8. Voltage profile improvement due to the participation of EVs in V2G

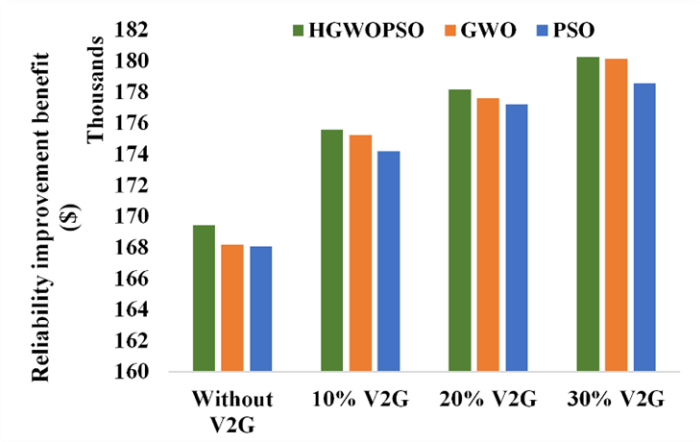

Fig. 5. 9. Variation of reliability improvement benefit for the IEEE 33-bus system with an increase in EVs participation in V2G

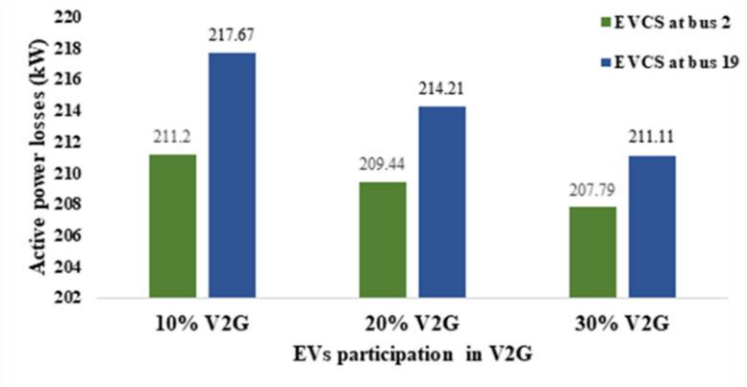

Fig. 5. 10. Reduction in active power losses with the increase in EVs participation in V2G for IEEE 33-bus system

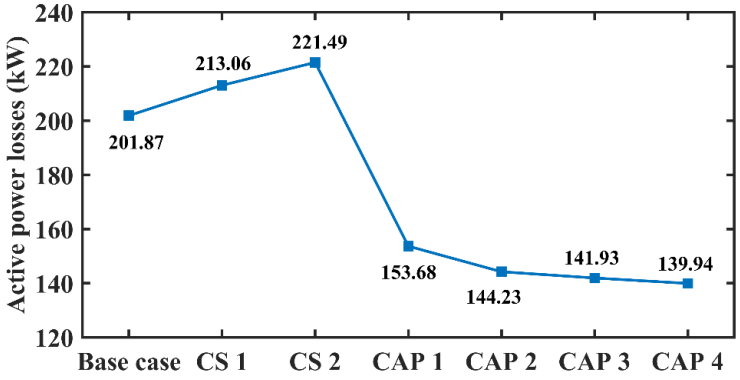

Fig. 5. 11. Variation of active power losses on integrating EVCS and capacitor for IEEE 33-bus system

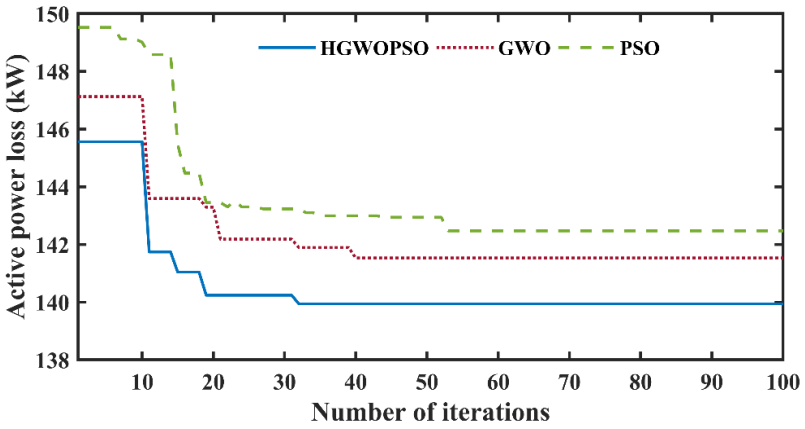

Fig. 5. 12. Response of HGWOPSO, GWO, and PSO for IEEE 33-bus distribution system

The efficacy of HGWOPSO can be verified by comparing the results with standalone GWO and PSO. The convergence characteristics of the proposed algorithm, GWO and PSO are shown in Fig. 5. 12., and found that the proposed algorithm has faster convergence towards the optimal solution as compared with GWO and PSO.

5.6.2 Simulation Results and Discussion for IEEE 34-bus, 12.66 kV System

The 34-bus system comprises 33 branches and 34 nodes as represented in Fig. 5.13. The line and bus data of such a system has been taken from [148]. The overall active power is 4636.5 kW and the reactive power demand of the network is 2873.5 kVAR. The distribution network operates at a rated voltage of 12.66 kV. The active power losses come out to be 163.45 kW using the direct approach method of load low. In this case, the minimum voltage is 0.9561 p.u and the maximum voltage is 0.9952 p.u. The annual energy loss cost incurred for 163.45 kW is $ 85909.32.

To validate the performance of HGWOPSO, obtained findings are compared with those obtained via GWO and PSO. The optimal nodes for EVCS placement for the 34-bus system are nodes 2 and 13 using the proposed algorithm, resulting in the lowest power loss

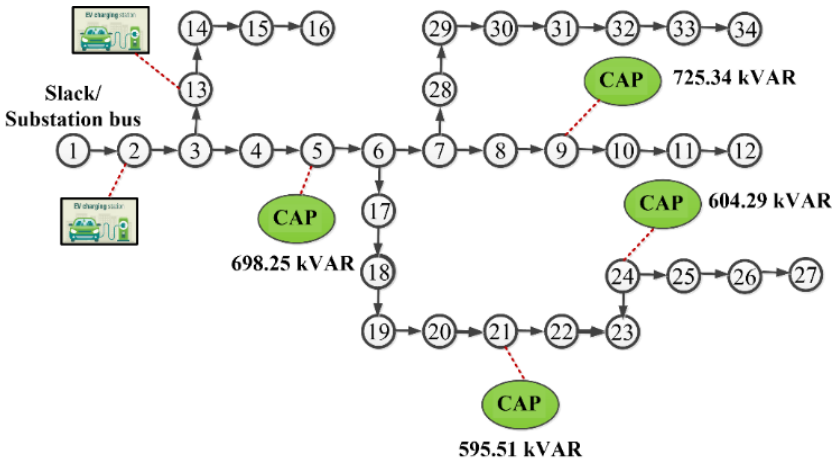

Fig. 5. 13. Typical configuration of the IEEE 34-bus system with two EVCS and four capacitors

of 180.01 kW and 199.42 kW, respectively. Concerning this, the optimal location and capacities of EVCS and capacitors using the proposed approach and its comparison with GWO and PSO are displayed in Table 5.5.

In the 34-bus system, when the capacitor of sizes displayed in Table 5. are placed at optimal nodes 5,9,21, and 24 results in the least power loss of 118.21 kW from the base value of 163.45 kW thus, achieving a 27.6 % reduction in active power loss. The minimum voltage of 0.9627 p.u. is registered at 27th bus which is satisfying the voltage restriction limit. The percentage of loss reduction in annual energy loss cost is 27.67% using the proposed HGWOPSO which is better than that of GWO and PSO i.e., 25.74% and 24.2% respectively. In the 34-bus system, the proposed technique achieves a reliability improvement cost of $ 484871.25 which is better than those of individual applications of GWO ($ 481584.15) and PSO ($ 481093.57) as shown in Table 5.6. Also, the amount spent on the installation of capacitors using HGWOPSO is comparatively small when compared with GWO and PSO as shown in Table 5.5. In addition to this, the net profit gained in the

Table 5. 5. The optimal results obtained via HGWOPSO in comparison with GWO and PSO for IEEE 34-bus system

Parameter	Base Case	EVCS and capacitor placement		
		HGWOPSO	GWO	PSO
Active power losses (kW)	163.45	118.21	121.56	123.97
Optimal nodes for EVCS	–	2, 13	2, 13	2, 13
Total number of EVs	–	100	100	100
Optimal nodes for capacitor	–	5, 9, 21, 24	5, 9, 21, 24	7, 12, 25, 32
Capacitor sizes (kVAr)	–	698.2, 725.3, 595.5, 604.2	713.5, 797.6, 628.1, 656.9	725.4, 821.5, 642.5, 678.8
Total kVAr	–	2623.2	2796.1	2868.2
Annual energy loss cost ($)	85909.32	62131.17	63891.93	65158.63
% Loss reduction in energy loss cost	–	27.6	25.7	24.2
Total capacitor cost ($)	–	65580	69902.5	71705
Net profit ($)	–	4111.74	2384.78	961.78
Convergence time in seconds	–	422.5	685.1	789.4
Reliability improvement benefit ($)	–	484871.25	481584.15	481093.57
Computational time in seconds	–	2246.9	2578.3	2798.4
Efficiency	–	81.1	73.4	71.8

34-bus distribution system utilizing HGWOPSO is $ 4111.74 whereas GWO and PSO provide less net profit of $ 2384.78 and $ 961.78 respectively.

Compared to GWO and PSO, the proposed technique possesses improved performance. The comparison results using the proposed algorithm with GWO and PSO for the 34-bus system have been tabulated in Table 5.5. The computational time for the proposed HGWOPSO is 2246.9 sec while it attains the optimal solution after 422.5 sec. The other approach is GWO which takes 2578.3 sec for computation and converges in 685.1 sec. Moreover, the convergence and computational time obtained using PSO are

789.4 sec and 2798.4 sec. The efficiency of the proposed approach is 81.1 % while for GWO and PSO it is 73.4 % and 71.8% respectively. Fig. 5.14. shows the voltage level of the 34-bus system after the optimal placement of EVCS and capacitor. Fig. 5.15. depicts the flow of active power in all branches of the distribution system for the 34-bus system after incorporating EVCS as well as the capacitor.

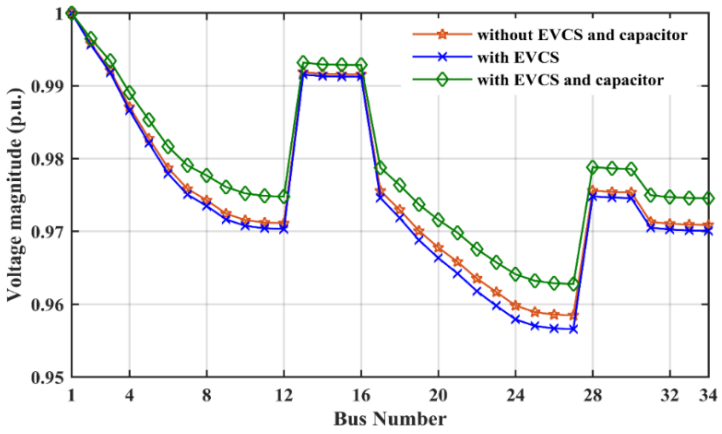

Fig. 5. 14. Improvement in voltage profile based on capacitor placement for IEEE 34-bus system

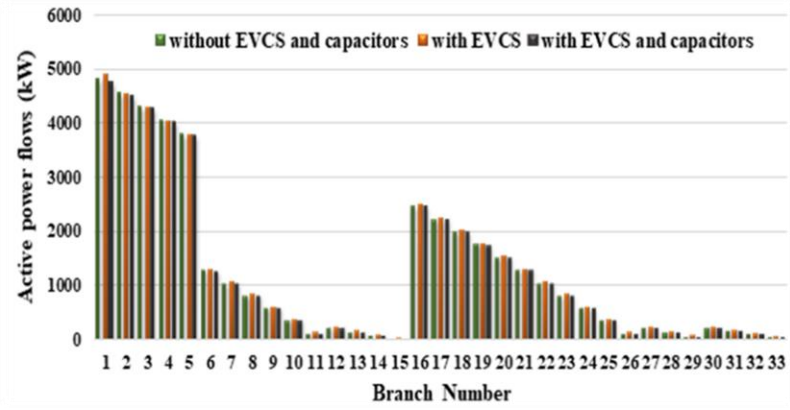

Fig. 5. 15. Improvement in the flow of active power based on capacitor placement

Fig. 5.16. shows the enhancement in voltage profile for the 34-bus system when the different percentage of EVs participates in V2G mode. Fig. 5.17. and Table 5.6 provides the variation of reliability improvement benefit with increasing penetration of EVs in V2G mode for the 34-bus system.

In the 34-bus network, the active power losses for optimal EVCS nodes i.e., 2 and 13 are calculated as 180.01 kW and 199.42 kW respectively when a V2G facility is not provided. Active power losses decrease as EVs operation in V2G mode increases. Fig. 5.18. displays the variation of power losses on integrating the EVCS and capacitor in the 34-bus system. It can be seen that power losses reduce with an increasing number of capacitors. Fig. 5.19. shows the active power losses of the 34-bus system for different percentages of EVs operation in V2G mode.

Table 5. 6 Effect of EVs participation in V2G mode on the reliability improvement benefit for IEEE 34-bus system

Algorithm utilized	Reliability Improvement Benefit ($)			
	Without V2G	10% V2G	20% V2G	30% V2G
HGWOPSO	484871.25	518794.45	522458.5	524547.5
GWO	481584.15	517549.41	521451.89	524193.4
PSO	481093.57	517149.84	519589.14	523589.5

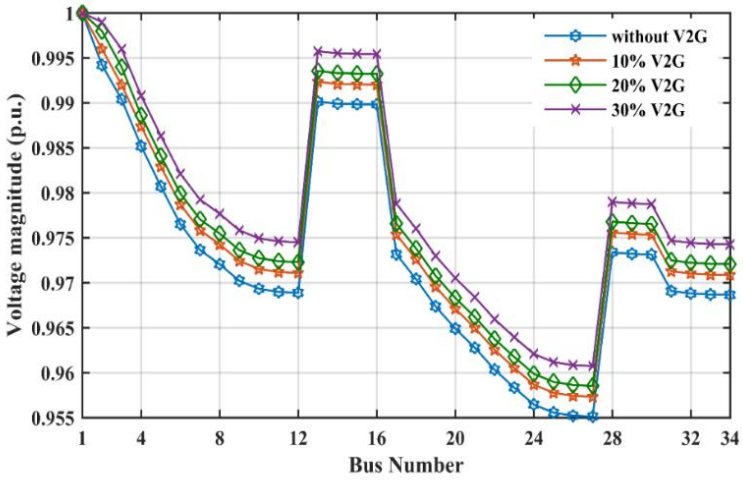

Fig. 5. 16. Voltage profile improvement due to the participation of EVs in V2G

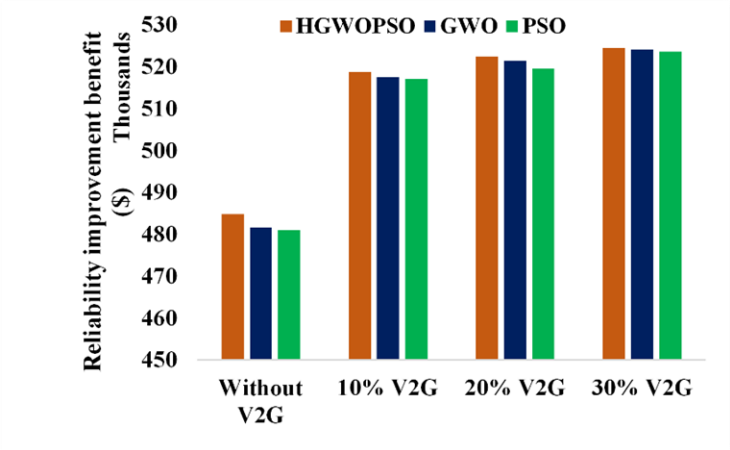

Fig. 5. 17. Variation of reliability improvement benefit for the IEEE 34-bus system with an increase in EVs participation in V2G

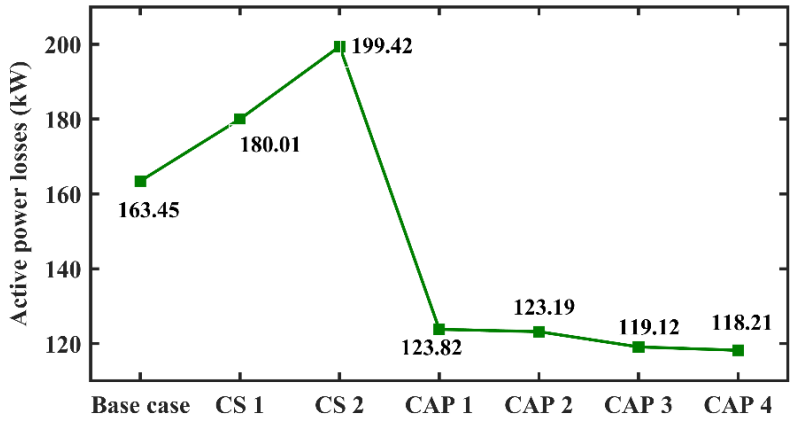

Fig. 5. 18. Variation of active power losses on integrating EVCS and capacitor for IEEE 34-bus system

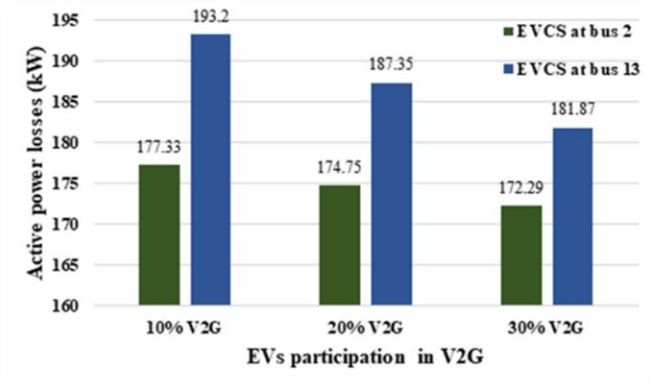

Fig. 5. 19. Reduction in active power losses with an increase in EVs participation in V2G

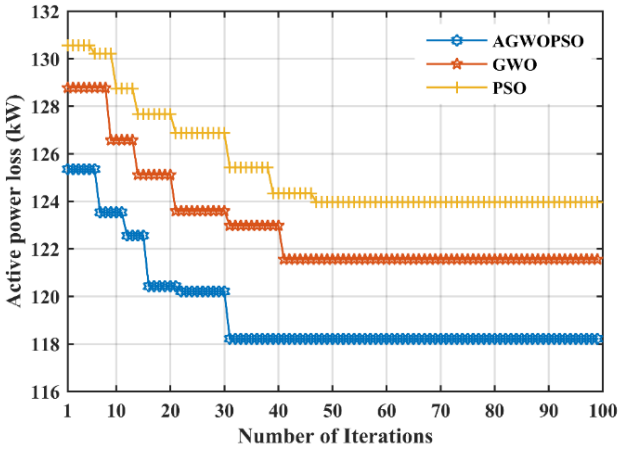

Fig. 5. 20. Response of HGWOPSO, GWO, and PSO for IEEE 34-bus distribution system

Furthermore, the efficacy of the proposed algorithm i.e., HGWOPSO is validated by comparing it with GWO and PSO. The convergence plot of the HGWOPSO, GWO, and PSO is displayed in Fig. 5.20. and found that, compared to GWO and PSO, the proposed algorithm converges more quickly towards the optimal solution.

5.7 SUMMARY

In this chapter, the HGWOPSO algorithm is developed to lessen the active power losses, maximizing the net profit and improving the reliability of the system with a different penetration level of EVs in V2G. The results have revealed that the optimum planning of EVCS elevates power loss and lowers the voltage in electrical power networks. The results have demonstrated that the optimum planning of capacitors after incorporating CS in the network minimizes power loss and also improves voltage profile. Capacitors are employed closer to EVCS and end of feeders for the enhancement of voltage profile and loss by contributing some reactive power. It is also shown that different percentages of EVs participating in V2G mode improved the active power flows, voltage profile and reduces the active power loss of the network. The proposed algorithm is applied on IEEE

33-bus and IEEE 34-bus systems. The hybrid method showed superiority against discrete PSO and GWO, by lessening the power losses, enhancing voltage profile, maximizing the net profit, and improving the reliability benefit. The hybrid method has reduced power losses by almost 31% as compared to GWO (29.74%) and PSO (29.42%) for the 33-bus system. The proposed hybrid approach achieves a reliability improvement benefit of $ 169451.4 which is $ 1274 and $ 1396 more than that of GWO and PSO respectively. Similarly, for the 34-bus system, the proposed technique results in a loss reduction of 27.6% while GWO and PSO reduce the power losses by 25.7% and 24.2% respectively. Furthermore, HGWOPSO results in more improvement in reliability benefit i.e., ($ 484871.2) as compared with other techniques i.e., GWO ($ 481584.15) and PSO ($ 481093.57). The attained results using the opted algorithm reveal the preeminence of the algorithm over other techniques discussed in the literature.

CHAPTER 6

SINGLE-OBJECTIVE FORMULATION OF CHARGING STATION AND DISTRIBUTED GENERATION PLACEMENT PROBLEM

6.1 INTRODUCTION

This chapter presents a hybrid optimization strategy for the optimal planning of EVCS. DGs units are utilized to reduce the charging impact of EVs. DGs are used in the suggested technique to preserve voltage profile, reduce active power loss and improve reliability. The integration of EVCS and DGs to the system adds extra demand to the system, affecting the power loss. The joint impact of EVs and DG integration is considered for two standard test systems. The efficacy of the suggested method is tested in MATLAB, and the results are equated with present techniques. The fundamental system reliability indicators, such as the system average interruption frequency index (SAIFI), system average interruption duration index (SAIDI), Customer Average Interruption Duration Index (CAIDI), and expected energy not supplied (EENS) and average energy not supplied (AENS), etc., are used to examine the impact on system reliability.

6.2 MATHEMATICAL FORMULATION OF PROBLEM

In general, load fluctuates with time at the distribution side in the electrical power network; however, the best site and size of EVCS and DG allocation with fluctuating load is not acceptable. Hence, the following assumptions are applied to the problem of optimal DG and EVCS allocation planning [149].

1) Radial distributions systems are balanced in nature.

2) Constant capacities EVCS are employed.

3) DGs having power factor unity are used in radial DS.

4) The DGs output is not time-varying.

5) The load has constant active and reactive power.

DGs are represented as negative loads in this work because they do not modulate the bus voltage. The best location and capacity of DG should be attained without violating the system constraint, which must be validated at every iteration using load flow analysis. Active power losses, voltage profile improvement, and voltage stability enhancement are basic objective functions that are investigated.

6.2.1 Multi-Objective Functions

The principal target of this research work is to find out the optimum nodes for EVCS and DGs placement in the radial distribution system for lessening the active power losses of the network, monitoring the voltage profile within required limits, and enhancing voltage stability index (VSI), keeping in view that, all the subjected constraints must not be violated. EVCS supplies current for charging EVs. The EV battery capacity is defined in kilowatt-hour (kWh) and ampere-hour (Ah). The EVCS is modeled in such a way that it delivers only real current for EV charging [88]. When EVCS is placed at any bus of the distribution network causes an increment in real power only. Hence, it necessitates the placement of EVCS at that node (bus) where the minimum branch current flows. Regarding this, Fig. 6.1 shows a portion of the distribution network in which EVCS is

located at $(k+1)^{th}$ bus and available connected load at the same bus takes power from the grid.

$$\min\left(F_1(x), F_2(x), F_3(x)\right) \quad x\epsilon\copyright \tag{6.1}$$

$$\text{subjected to} \quad g_u(x) = 0 \;\; u = 1, 2, 3 \ldots, t \tag{6.2}$$

$$h_v(x) = 0 \;\; v = 1, 2, 3 \ldots, s \quad x_L \leq x \leq x_U \tag{6.3}$$

where, $g_u(x)$ are the equality constraint, $h_v(x)$ are the inequality constraint, t and s are the numbers of equality and inequality constraints, $x_L$and x_U are the lower bound and upper bound of variables, © is the variable space.

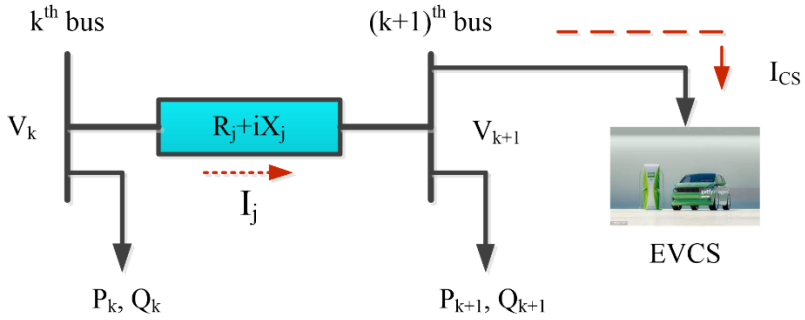

Fig. 6. 1. EVCS located at the bus of the radial distribution system

1) Active power loss (APL)

The largest power loss in an electric network typically occurs over the distribution system, which impacts annual sales. Consequently, APL minimization is the major concern while allocating EVCS and DGs in radial distribution networks. The load flow analysis of the distribution network is conducted to determine the APL, i.e., base case power loss. The direct approach-based load flow analysis is performed in this article [146]. The active power loss after the load flow is determined using Eq. (6.4), and it depends on the amount of current drawn/injected into the bus [150].

$$\mathrm{APL} = \sum_{i=1}^{N_{br}} |P_i|^2 * R_i = \mathrm{TPS(R)} * |\mathrm{BIBC} * I|^2 \tag{6.4}$$

where, P_i is the current flowing in i^{th} branch, R_i is the resistance of i^{th} branch, R is the branch resistance matrix, which contains all of the branches' resistances.

Because EVCS functions as a high load, it increases APL when it is deployed at any node in the distribution system. Therefore, the goal is to choose the bus that increases APL to the minimum. The additional losses of the distribution system can be offset by arranging the DGs optimally. The primary function of DG is to inject real and reactive power into the network, compensating for the losses caused by EVCS deployment.

When current I is disintegrated into its real and imaginary parts, Eqn. (6.4) becomes as given below:

$$\mathrm{APL} = \mathrm{TPS(R)} * \left[\left(\mathrm{BIBC} * \mathrm{Real(I)}\right)^2 + \left(\mathrm{BIBC} * \mathrm{Imag(I)}\right)^2\right] \tag{6.5}$$

By putting the real and imaginary parts of current to Eq. (6.5), the overall real power loss can be given as:

$$\min F_1 = \mathrm{TPS(R)} * \left(\mathrm{BIBC} * \frac{P\sin\theta + Q\cos\theta}{|V|}\right)^2 + \mathrm{TPS(R)} * \left(\mathrm{BIBC} * \frac{P\cos\theta + Q\sin\theta}{|V|}\right)^2 \tag{6.6}$$

2) Voltage Deviation Index (VDI)

The voltage quality of the bus is measured in terms of the voltage deviation index. As a result, bus VDI must be minimized to produce a more controlled bus voltage profile

over the radial distribution network. Bus VDI is used as an objective function in the proposed optimal EVCS and DG allocation and is expressed as [151]:

$$\min F_2 = \sum_{k=1}^{N_{bus}} (V_k - V_{ref})^2 \tag{6.7}$$

Each bus's voltage magnitude must lie between the minimum value (0.95 p.u) and the maximum value (1.05 p.u).

3) Voltage Stability Index (VSI)

In light of the voltage deviation alone, the distribution system's security level is insufficient. As a result, VSI is suggested as one of the main functions in this effort for enhanced voltage profiles. The distribution system's maximum VSI indicates that the bus can maintain its voltage profile within acceptable limits under varying loading conditions. The utility strives to keep the VSI of the distribution system near-unity of all buses for the safe operation of the system. VSI of distribution system can be formulated as follows:

$$VSI_{k+1} = |V_k|^4 - 4 * \left[P_{k+1}X_j - Q_{k+1}R_j\right]^2 - 4 * \left[P_{k+1}R_j - Q_{k+1}X_j\right]|V_k|^2 \tag{6.8}$$

where, VSI_{k+1} represents the VSI of $(k+1)^{th}$ bus, R_j and X_j represents the resistance and reactance of j^{th} branch connecting the k^{th} and $(k+1)^{th}$ bus, P_{k+1} denotes the active power at $(k+1)^{th}$ bus and Q_{k+1} indicates the reactive power at $(k+1)^{th}$ bus.

During the operation, the voltage level of the entire network must be increased by maximizing the bus with the lowest VSI value. As a result, the objective function for maximization of VSI is given as [152]:

$$\max F_3 = \frac{1}{\min(VSI_{k+1})} \tag{6.9}$$

6.2.2 Operational Constraints

The constraints subjected to the EVCS and DGs allocation in the radial distribution network are presented below.

1) Equality Constraints

a) Active and reactive power balance

The active and reactive power delivered by electric substation and DG must be equal to the summation of APL, active and reactive power demand, and additional CS load capacity.

$$P^{substation} + \sum_{k=1}^{N_{bus}} P^{DG}(k) = \sum_{j=1}^{N_{br}} P_{loss}^{j}(k, k+1) + \sum_{k=1}^{N_{bus}} P_{D,k} + P_{EVCS}^{k} \tag{6.10}$$

$$Q^{substation} + \sum_{k=1}^{N_{bus}} Q^{DG}(k) = \sum_{j=1}^{N_{br}} Q_{loss}^{j}(k, k+1) + \sum_{k=1}^{N_{bus}} Q_{D,k} \tag{6.11}$$

where, $P^{substation}$ and $Q^{substation}$ are the real and reactive power supplied by electric substation respectively, $P_{D,k}$ and $Q_{D,k}$ are the active and reactive power demand at k^{th} bus, $P^{DG}(k)$ and $Q^{DG}(k)$ are the total real and reactive power injected by DGs at k^{th} bus, P_{loss}^{j} and Q_{loss}^{j} represents the real and reactive power loss in the j^{th} branch, P_{EVCS}^{k} is the charging station load at k^{th} bus and N_{br} and N_{bus} denotes the number of branches and buses in the distribution network, respectively.

2) Inequality Constraints

a) Voltage limit constraint

Each bus's voltage magnitude ranges between 0.95 to 1.05 p.u.

$$V_{min} \leq V_k \leq V_{max} \;\; k = 1, 2, 3 \ldots . N_{bus} \tag{6.12}$$

b) Line current constraint

The actual current flows in each line should not exceed the maximum limit of line current.

$$I_j \leq I_j^{max} \; j = 1, 2, 3 \ldots . N_{br} \tag{6.13}$$

where, I_j represents the actual current flows in j^{th} line and I_j^{max} is the maximum limit of line current.

c) Active and reactive power injected by DG

The active and reactive power injected by DGs should lie within some specified limits.

$$P_{DG_k}^{min} \leq P_{DG_k} \leq P_{DG_k}^{max} \tag{6.14}$$

$$Q_{DG_k}^{min} \leq Q_{DG_k} \leq Q_{DG_k}^{max} \tag{6.15}$$

$P_{DG_k}^{min}$ and $P_{DG_k}^{max}$ are the minimum and maximum active power limits of k^{th} DG respectively and $Q_{DG_k}^{min}$ and $Q_{DG_k}^{max}$ are the minimum and maximum active power limits of k^{th} DG.

d) DG unit's penetration

$$\sum_{k=1}^{N_{DG}} P_{DG_k} \leq \%\, J \times \sum_{k=1}^{N_{bus}} P_{L_k} \tag{6.16}$$

where J represents maximum DG unit penetration in the distribution system, N_{DG} is the number of DGs installed in the system.

6.3 IMPACT OF EVCS AND DGs ON RELIABILITY OF DISTRIBUTION SYSTEM

The reliability study of the electrical distribution system has emerged as a demanding area of research. The possibility that a system will perform satisfactorily for a particular period under a specific set of operating constraints is referred to as reliability [153]. The reliability of generation, transmission, and distribution is prioritized in electrical network reliability studies. The amount of consumer satisfaction is strongly correlated to the distribution network's reliability. Quantitative data for the failure rate, repair rate, average outage duration, and the number of customers on load points of the distribution network is needed to evaluate the distribution network's reliability indices [154]. Some of the reliability indices which are predominantly used to evaluate the system's reliability are SAIFI, SAIDI, CAIDI, EENS, AENS, ASAI, and ASUI. They are also employed in this research work to judge the reliability of the distribution system. An appropriate set of indices must be determined based on the application to attain the reliability evaluation.

6.3.1 Statistical Parameters for Reliability at Different Load Points

The reliability indices strongly depend on various statistical parameters such as failure rate, repair rate, average outage duration. The reliability parameters can be calculated at different load points i.e., q^{th} load point as follows.

$$\text{Average failure rate } (\rho_q) = \sum_{k \epsilon z} num_k \times FR_k \quad \text{failure/year}$$

$$\text{Annual outage duration } (U_q) = \sum_{k=z} FR_k D_{qk} \quad \text{hour/year}$$

$$\text{Average outage duration } (D_q) = \frac{U_q}{\rho_q} \quad \text{hour}$$

where FR_k is the average failure rate of the k^{th} element, z is the number of elements in the distribution system, num_k denotes the number of k^{th} elements in the distribution system, D_{qk} represents the period of failure at q^{th} load point due to failure of k^{th} element, ρ_q is the average failure rate at q^{th} load point and U_q denotes the annual outage duration at q^{th} load point.

6.3.2 Reliability Indices of Distribution System

The reliability indices are characterized into load-oriented and customer-oriented indices. The complete categorization of reliability analysis of distribution system is depicted in Fig. 6.2.

A broad overview and mathematical formulae of different load and customer-oriented reliability indices are as follows [154].

1) Customer Oriented Reliability Indices

These indices have increased the reliability of power systems in terms of improving consumer or load facilities. An extensive outline and mathematical formulae of different customer-oriented reliability indices are as follows.

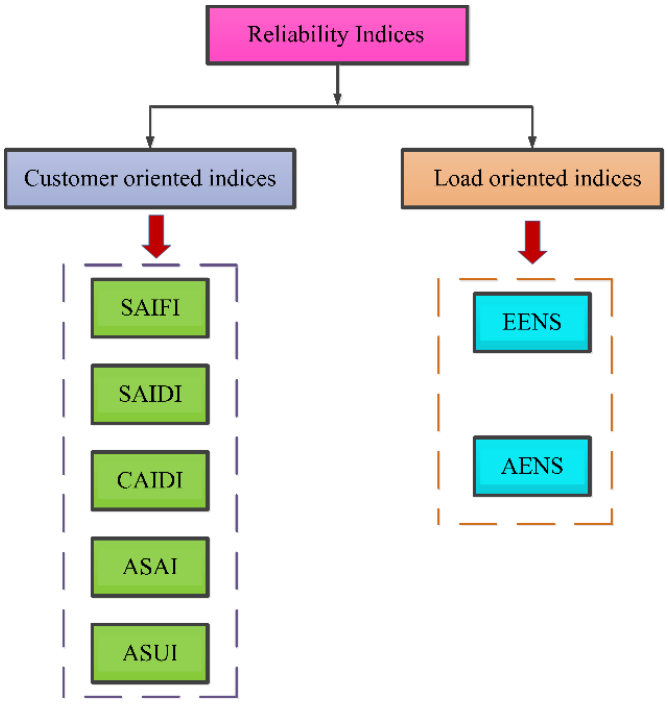

Fig. 6. 2. Categorization of reliability indices of distribution network

The System Average Interruption Frequency Index (SAIFI) is calculated as the ratio of the total number of interruptions to the total number of customers served each year, as given in Eq. (6.17). SAIFI depicts the state of the system in terms of interruption. It is measured in failures/customers. year.

$$\text{SAIFI} = \frac{\sum_{q=1}^{z_q} \rho_q N_q}{\sum_{q=1}^{z_q} N_q} \text{ failures/customer. year} \tag{6.17}$$

The System Average Interruption Duration Index (SAIDI) is a fraction of total continuous interruptions divided by the number of customers served per year, as provided in Eq. (6.18). SAIDI depicts the state of the system in terms of interruption time. It is measured in hour per customer year.

$$\text{SAIDI} = \frac{\sum_{q=1}^{z_q} U_q N_q}{\sum_{q=1}^{z_q} N_q} \text{ hour per customer. year} \tag{6.18}$$

The Customer Average Interruption Duration Index (CAIDI) is the ratio of the overall time of continuous interruptions to the total number of interruptions served by customers in a year, as shown in Eq. (6.20). CAIDI calculates the average outage time for any individual customer. It is measured in hour/customer. interruption.

$$\text{CAIDI} = \frac{\text{SAIDI}}{\text{SAIFI}} \tag{6.19}$$

$$\text{CAIDI} = \frac{\sum_{q=1}^{z_q} U_q N_q}{\sum_{q=1}^{z_q} \rho_q N_q} \text{ hour/customer. interruption} \tag{6.20}$$

The Average Service Availability Index (ASAI) is expressed in per unit (p.u.). It is defined as the ratio of total available hours in a year to total desired hours, as specified in Eq. (6.21).

$$\text{ASAI} = \frac{\sum N_q \times 8760 - \sum_{q=1}^{z_q} U_q N_q}{\sum N_q \times 8760} \text{ (p. u)} \tag{6.21}$$

The Average Service Unavailability Index (ASUI) is expressed in per unit (p.u.) and is defined as the ratio of total unavailable hours in a year to total desired hours, as specified in Eq. (6.22)

$$\text{ASUI} = 1 - \text{ASAI (p.u)} \tag{6.22}$$

2) Energy or Load Oriented reliability indices

Load-oriented reliability indices are determined at different load points as follows.

The network's Expected Energy Not Supplied (EENS) is measured in MWh/year and equals the sum of all consumers' EENS as shown in Eq. (6.24). The EENS is an indication of energy insufficiency.

$$\text{EENS}_q = \sum \begin{bmatrix} (\text{Demand at } q^{th} \text{load point}) * \\ \text{annual outage duration at } q^{th} \text{load point} \end{bmatrix} \tag{6.23}$$

$$\text{EENS}_q = L_q U_q \text{ MWh per year} \tag{6.24}$$

The Average Energy Not Supplied (AENS) index indicates how much energy isn't served within a given period, as shown in Eq. (6.26). It is expressed in MWh per customer per year.

$$\text{AENS} = \frac{\sum(\text{EENS at } q^{th} \text{ load point})}{\text{Total number of customers at all load points}} \tag{6.25}$$

$$\text{AENS} = \frac{\sum_{q=1}^{z_q} L_q U_q}{\sum_{q=1}^{z_q} N_q} \text{ MWh per customer per year} \tag{6.26}$$

where L_q is average demand/load at q^{th} load point, EENS_q denotes the expected ENS at q^{th} load point, z_q is the total number of load points, N_q represents the total number of customers at q^{th} load point. The steps employed for the calculation of reliability indices are indicated in Fig. 6.3.

The interruption in the power system network occurs due to the following causes.

1) outages resulting in the disturbance.

2) Failure of power system equipment leads to interruption.

3) Load shedding occurs due to an abrupt rise in demand.

4) Planned preservation of equipment necessitating an interruption.

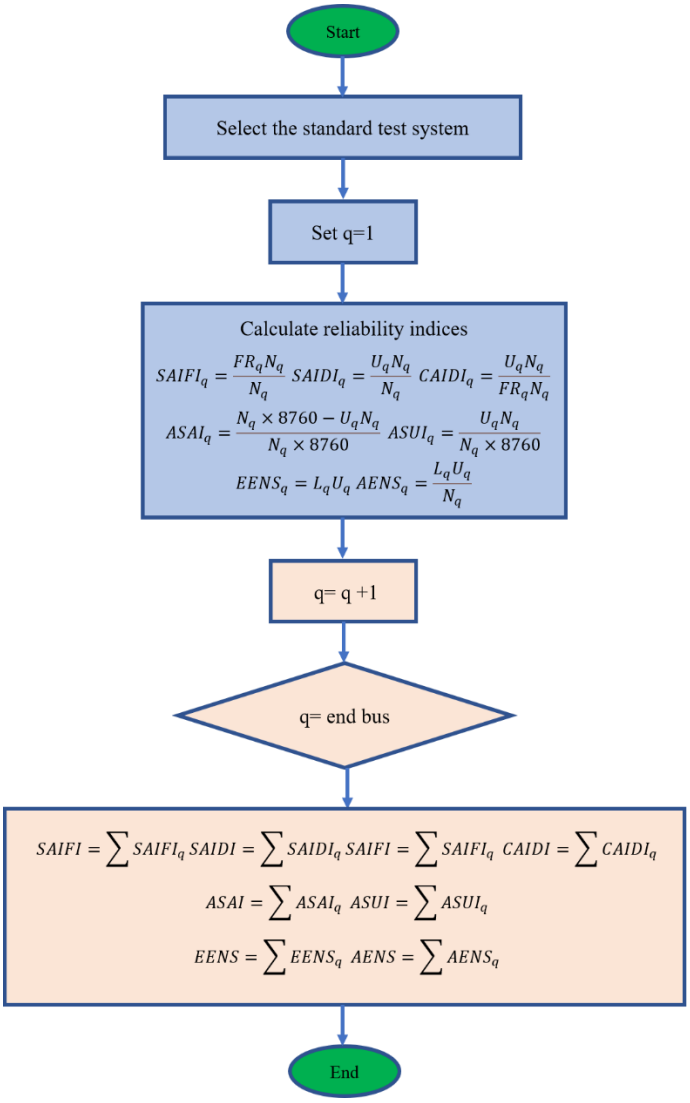

Fig. 6. 3. Flow chart for the computation of reliability indices

6.4 THE HGWOPSO ALGORITHM IMPLEMENTATION FOR EVCS AND DG ALLOCATION

The EVCS and DG allocation problem is associated with discrete bus numbers, whereas the capacity of the DG unit is decided by operational constraints. GWO and PSO would not yield the same results after every iteration due to the stochastic behavior of the problem, exclusively in sophisticated systems. Therefore, it is a challenging task to investigate the optimum solution. On the other hand, the proposed hybrid approach HGWOPSO solves this issue. With the combination of GWO and PSO, a hybrid strategy is proposed. PSO's flaw is that it can't access the best answer across a large search area and is trapped in local optima. While GWO has the shortcoming of inefficient exploitation. Therefore, a combination of GWO and PSO is used to overcome the shortcomings of each method. The key ability is to combine the PSO's exploitation skills with the GWO's exploration capabilities to keep a proper exploration and exploitation to avoid local optima and arrive at an optimal solution with ease. HGWOPSO is presented in this work, in which GWO updates the initial population and then PSO updates the updated solutions [132]. Furthermore, the proposed hybrid approach is selected to efficiently tackle the optimization problem because it provides high-speed convergence and the capability of handling discrete as well as integer variable problems involving a smaller number of control parameters.

Optimum allocation of DG units and the EVCS decreases system losses due to the addition of EVCS in the radial distribution system. It also improves voltage profile and stability. In this research analysis, EVCS and DG's allocation problems are addressed

using the proposed HGWOPSO technique. Fig. 6.4 displays the flow chart of the suggested hybrid algorithm.

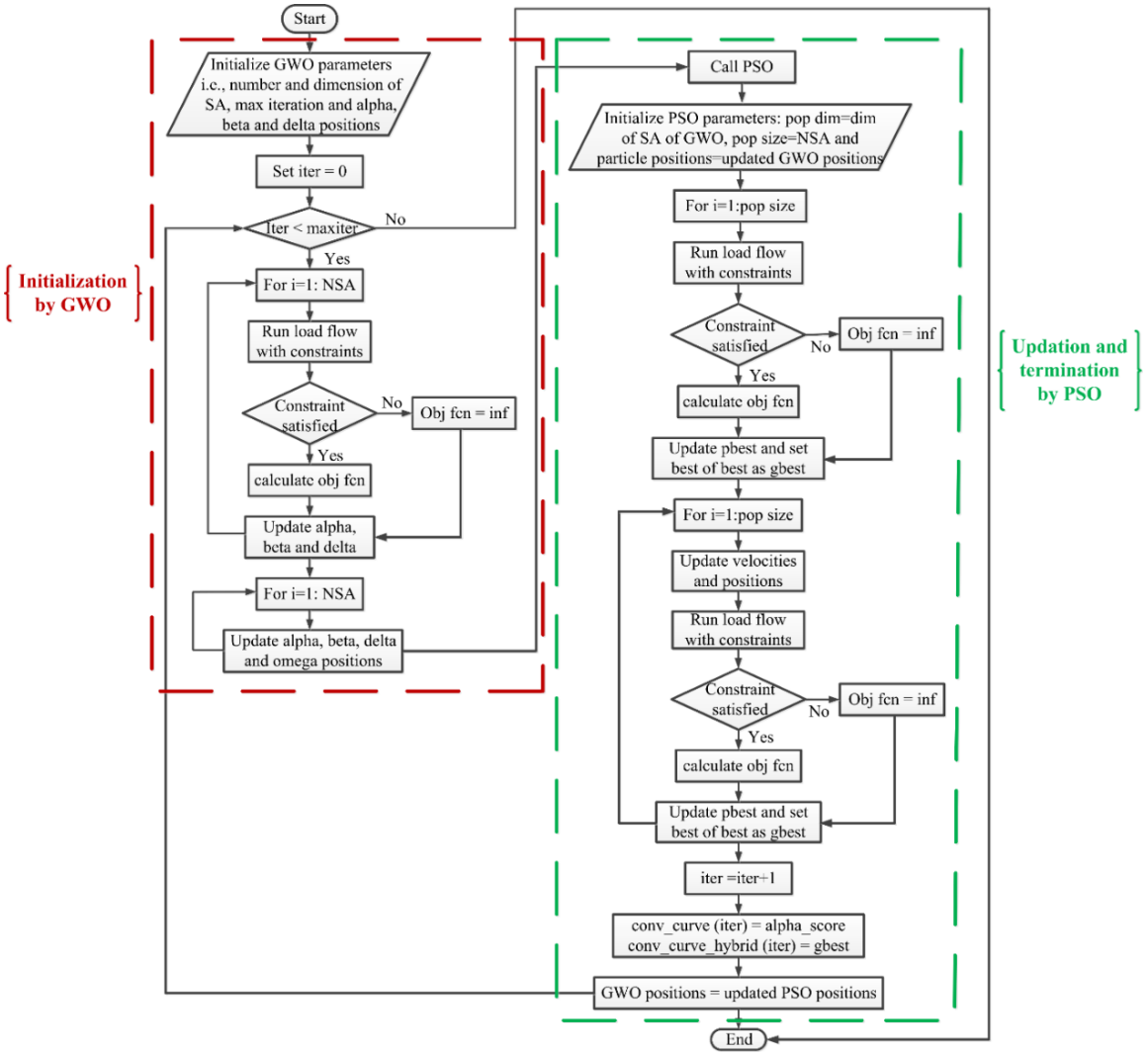

Fig. 6. 4. Flow chart of HGWOPSO for EVCS and DG allocation

The steps mentioned below explain the working of the HGWOPSO algorithm.

Step 1: Initializing the maximum iterations.

Step 2: Initializing the number of search agents (NSA).

Step 3: Running GWO algorithm.

Step 4: The points minimized by GWO are passed through PSO as initial points.

Step 5: Running PSO algorithm.

Step 6: Updated points are passed back to the GWO algorithm.

Step 7: Increasing the iteration one by one.

Step 8: If the termination conditions are fulfilled, go to step 9; otherwise, go to step 3.

Step 9: The gbest solution is the desired solution of HGWOPSO technique.

The tuned parameters of the proposed HGWOPSO algorithm are NSA=30, swarm size=50, maximum iterations=100, inertia weight=0.4 to 0.9, and values of cognitive and social acceleration coefficients are 2.01 and 2.02, respectively.

6.5 RESULTS AND DISCUSSION

This section describes the implementation of the proposed hybrid algorithm first on the 33 and 69 bus systems. The hybrid algorithm has been validated by applying benchmark functions in chapter 3. Also, the impact of EVCS and DG integration on the two considered standard systems in terms of reliability indices, i.e., SAIFI, SAIDI, CAIDI, etc., has been evaluated and explained in detail.

The suggested HGWOPSO is employed in the IEEE 33-bus and IEEE 69-bus radial distribution systems for the location and sizing of EVCS and DG units. The results are compared with GWO and PSO for the single objective function corresponding to (1) minimizing the active power loss (2) minimization of voltage deviation (3) maximizing the voltage stability index. The proposed HGWOPSO algorithm is executed in MATLAB R2016a on an Intel i7, 3.2 GHz, 4 GB RAM, desktop PC.

6.5.1 IEEE-33 Bus Balanced Radial Distribution System

The detailed diagram of the IEEE 33 bus radial distribution system along with two DG and two EVCS is shown in Fig. 6.5. The IEEE-33 bus distribution network has 33 nodes and 32 branches. The system is allowed to operate at 100 MVA and 12.66 kV. It has total real power loads of 3715 kW and total reactive power loads of 2300 kVAr.

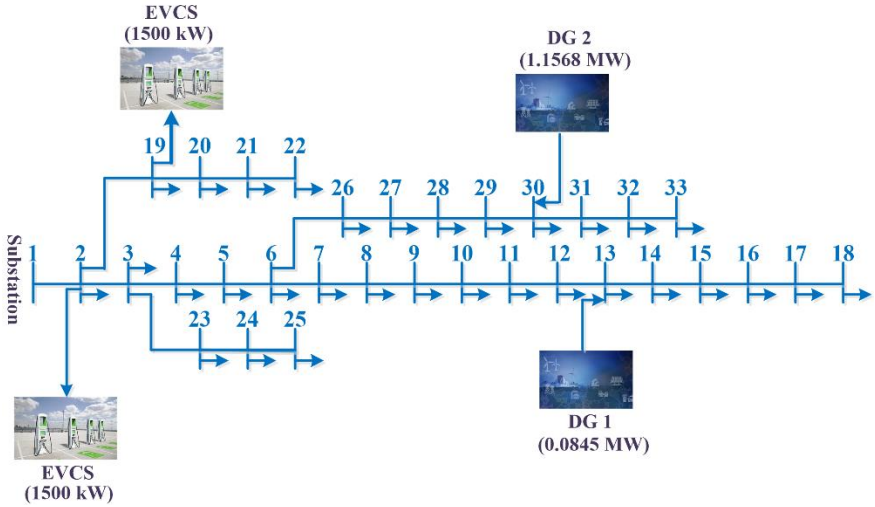

Fig. 6. 5. Effect of EVCS and DG integration on system loss in IEEE 33-bus system

Charging stations are assumed to have 30 charging points, and each charger consumes 50 kW. So, CS can charge 30 EVs at the same time. The optimal number of CS needs to be placed at the optimal bus in the distribution network. Since CS installation increases the active power loss of the network. Hence, DGs are optimally placed to compensate for the losses due to installed EVCS. The power loss is optimized using the suggested HGWOPSO method. Before installing EVCS and DG, a direct approach-based load flow study is carried out to determine the base case losses. The active and reactive power values before installing EVCS and DGs are observed to be 201.9 kW and 134.7 kVAr, respectively. Also, the minimum voltage appears at bus 18 of magnitude 0.9131 p.u. Whereas the minimum value of VSI comes out to be 0.6953 p.u.

1) Effect of EVCS and DG Integration on System Loss in IEEE 33-bus System

The addition of EVCS to the distribution network raises the APL while lowering the voltage profile due to the increased loading of EVs. Therefore, there is a requirement to allocate the EVCS in the most efficient way possible, resulting in the lowest possible rise in APL. It's worth noting that installing a fixed capacity EVCS on bus 2 results in a power loss of only 211.7 kW. To meet customer demand and ensure the availability of EVCS for EV users, an increasing number of EVCS must be installed to address the power loss issues. The best placement of the second EVCS at bus 19 results in a total active power loss of 214.8 kW.

Five different scenarios are addressed in this work for validating the methodology. The scenarios are given below:

Scenario 1: Balanced IEEE 33-bus radial distribution network with existing loads only

Scenario 2: Addition of one EVCS in the radial distribution network

Scenario 3: Addition of one more EVCS in the distribution network

Scenario 4: Addition of one DG in the radial distribution network

Scenario 5: Simultaneous allocation of two DGs

The placement of DG in an optimal location with an optimal size result in minimization of APL, improvement in voltage profile, and enhancement in VSI. A large number of research articles has focused on minimizing APL due to the domination of I^2R losses in the power system. The APL, VDI, and VSI are calculated before the reliability

evaluation. This is done to evaluate the reliability of the system by determining the best DG size, DG location, power loss, VDI, and VSI.

Two DGs are installed in the 33-bus network to reduce the charging impact of EVs. When one 2.56 MW DG is optimally located at bus 6, it results in a 103.6 kW active power loss. The power loss is reduced to 85.5 kW when two DGs with capacities of 0.0845 MW and 1.1568 MW are situated optimally at bus numbers 13 and 30 in the distribution network. Table 6.1. illustrates the APL values when EVCS and DGs are installed sequentially in 33 bus distribution networks.

Table 6. 1. APL values after the placement of EVCS and DGs using HGWOPSO in IEEE 33-bus system

Scenarios	Bus number and size	APL (kW)
Base case	–	201.9
1 EVCS	1500 kW at bus 2	211.7
2 EVCS	1500 kW at bus 2 and 19	214.8
1 DG	2.56 MW at bus 6	103.6
2 DGs	0.0845 MW and 1.1568 MW at bus 13 and 30	85.5

Also, the varying power loss values after placing EVCS and DGs are depicted in Fig. 6.6. The comparison analysis of the size and location of EVCS and DG and their impact on power loss is portrayed in Table 6.2. Also, it is realized from Table 6.2. that results obtained by implementing HGWOPSO are superior to GWO and PSO for the same parameter consideration.

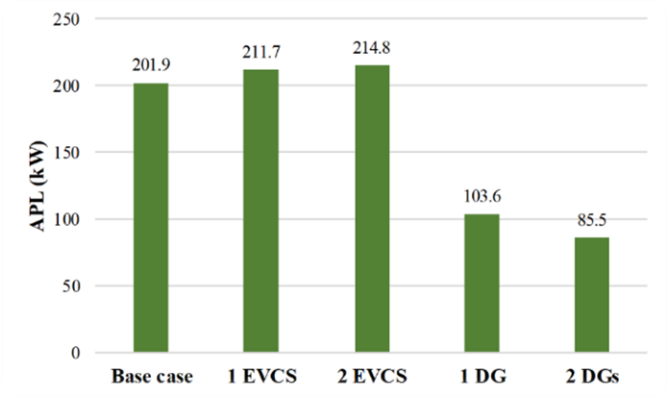

Fig. 6. 6. Effect of EVCS and DG integration on active power loss in the IEEE 33-bus system

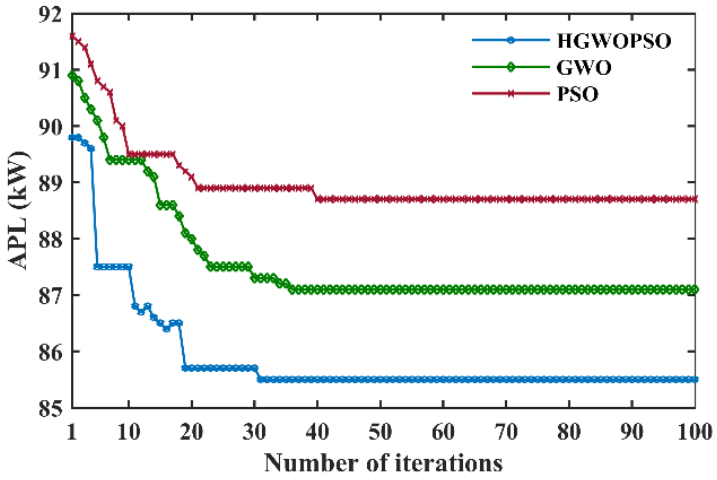

Fig. 6. 7. Convergence plot for active power loss using HGWOPSO, GWO, and PSO in 33-bus network

Likewise, the efficacy of the proposed hybrid technique, i.e., HGWOPSO, is confirmed by comparing the obtained results with those of other existing techniques such as GWO and PSO.

The proposed technique results in an active power loss of 85.5 kW which is lesser than those of GWO (87.1 kW) and PSO (88.7 kW). Fig. 6.7 shows the converging nature of the active power loss throughout iteration using proposed HGWOPSO, GWO, and PSO. Also, it is evident from the convergence characteristics that HGWOPSO has a faster rate of achieving optimal solutions as compared to standalone GWO and PSO.

Table 6. 2. Comparison of optimal size, location and APL of EVCS and DG obtained using HGWOPSO and GWO, for 33-bus system

Scenarios	HGWOPSO				GWO			
	EVCS Location	Optimal DG		APL (kW)	EVCS Location	Optimal DG		APL (kW)
		Location	Size (MW)			Location	Size (MW)	
Base case	-	-	-	201.9	-	-	-	202.2
1 EVCS	2	-	-	211.7	2	-	-	213.9
2 EVCS	2, 19	-	-	214.8	2, 19	-	-	215.6
1 DG	2, 19	6	2.56	103.6	2, 19	8	2.71	105.7
2 DGs	2, 19	13 30	0.0845 1.1568	85.5	2, 19	17 29	0.0978 1.2193	87.1

2) Effect of EVCS and DG Integration on Voltage Profile and Voltage Stability Index in 33-bus System

As similar to system loss, integration of EVCS imposes a detrimental effect on the voltage profile and VSI. Due to the increased loading of EVs, the system's voltage profile and voltage stability index deteriorates. These disturbances are compensated by the suitable incorporation of DG units at the appropriate node in the distribution system. The voltage profile of the 33- bus system when multiple EVCS and DGs are sited in the system is depicted in Fig. 6.8.

The voltage at each bus continues to decrease as the charging load grows, as seen in Fig. 6.8. When one 1500 kW EVCS is optimally placed on bus 2, the voltage profile of the entire system falls. Furthermore, as the number of EVCS grows, the voltage profile degrades.

DGs are integrated into the distribution system along with EVCS to ensure that the system runs smoothly. Integration of DG units creates positive impacts on the voltage profile of the system. Improvement in voltage profile after incorporating DG units is

shown in Fig. 6.9. The voltages on all the buses fluctuate depending on the distribution system's actual and reactive power losses. As a result, real power support is required for real power loss reduction, which enhances voltage levels by mitigating I^2R losses. Also, it is observed that the improvement in bus voltages takes place when many DGs are located. Also, it is noted that the size of a single DG is greater than the combined size of two DG units. In the case of one DG, the minimum magnitude of voltage is 0.9511 p.u at bus number 18; for simultaneous allocation of two DG units, the minimum voltage is improved to 0.9685 p.u at bus 33. So, it is deduced that minimum voltage improves with the employment of multiple DGs.

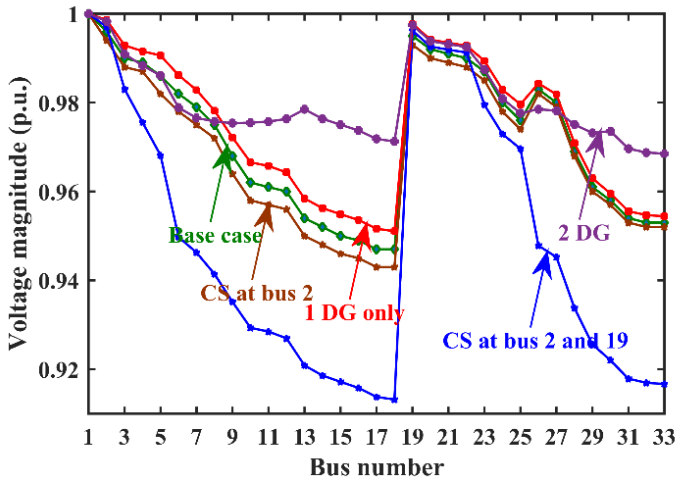

Fig. 6. 8. Voltage profile of IEEE 33 bus system after integrating EVCS and DG units

The addition of EVCS and DG units to the distribution network impacts the voltage stability index as it does on the voltage profile. The base case (before installing EVs and DGs) value of VSI is 0.6953 p.u. It drops to 0.6924 p.u when one EVCS of capacity 1500 kW is optimally installed at bus number 2. DGs implementation in distribution networks enhances the VSI. It can be noticed from Fig. 6.9. that VSI enhances when a greater number of DGs are situated optimally in the distribution system.

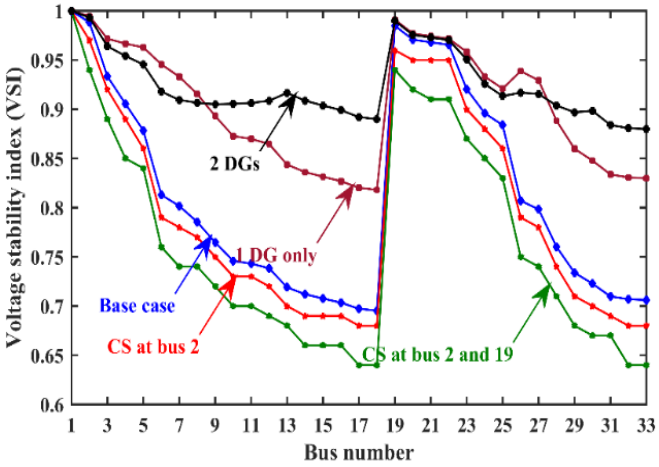

Fig. 6. 9. VSI for 33 bus systems for different scenarios

Table 6. 3. Comparison of VSI values for different scenarios in the IEEE 33-bus system

Scenarios	HGWOPSO		GWO		PSO	
	VSI (p.u.)	Inverse VSI	VSI (p.u.)	Inverse VSI	VSI (p.u.)	Inverse VSI
Base case	0.695	1.438	0.691	1.447	0.6893	1.451
1 EVCS	0.692	1.444	0.689	1.451	0.6857	1.458
2 EVCS	0.681	1.467	0.679	1.472	0.6723	1.487
1 DG	0.818	1.222	0.807	1.239	0.7981	1.252
2 DGs	0.879	1.136	0.853	1.172	0.8343	1.198

When one DG is placed causes the VSI to be increased to the value of 0.8181 p.u. Similarly, VSI becomes 0.8798 p.u. on the implementation of two DGs. Also, VSI is investigated for different scenarios using the suggested hybrid technique and compared to other techniques to demonstrate its superiority. The VSI results obtained using the two techniques for the IEEE 33-bus system are tabulated in Table 6.3.

6.5.2 IEEE-69 Bus Balanced Radial Distribution System

The proposed algorithm HGWOPSO is now implemented on IEEE 69-bus radial distribution system for the optimal allocation of EVCS and DG. The detailed diagram of the IEEE 69-bus distribution system is shown in Fig. 6.10.

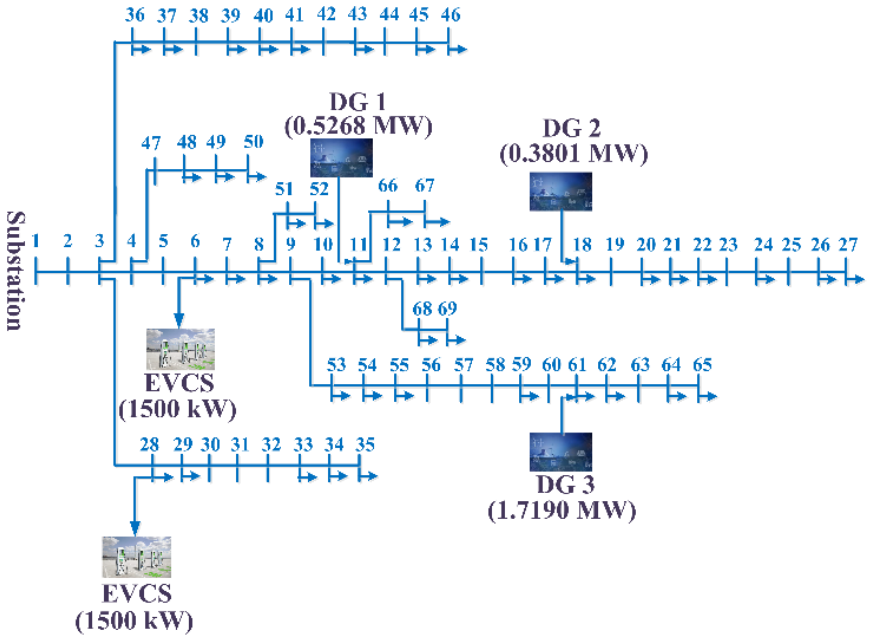

Fig. 6. 10. Connection diagram of IEEE 69-bus system with two EVCS and three DGs

Two fixed capacity EVCS and three type 1 DG have been considered. The details of the IEEE 69-bus DS are as follows: The IEEE-69 bus DS has 69 nodes and 68 branches. The system is allowed to operate at 100 MVA and 12.66 kV. It has total real power loads of 3801.4 kW and total reactive power loads of 2693.6 kVAr. As that of IEEE 33-bus radial distribution system, the objective functions, i.e., power loss minimization, improvement in voltage profile, and maximizing VSI, are optimized using HGWOPSO and compared with those of GWO and PSO.

To validate the methodology for the proposed work, the following scenarios are considered.

Scenario 1: Balanced IEEE 69-bus radial DS with existing loads only

Scenario 2: Addition of one EVCS in the radial distribution network

Scenario 3: Addition of one more EVCS in the distribution network

Scenario 4: Addition of one DG in the radial distribution network

Scenario 5: Simultaneous allocation of two DGs

Scenario 6: Simultaneous allocation of three DGs

1) Effect of EVCS and DG integration on system loss in IEEE 69-bus system

The base case active and reactive power loss in the 69-bus system is calculated to be 224.9 kW and 102.1 kVAr respectively. Similar to the 33-bus system, the addition of EVCS creates power loss issues in the 69-bus system. When one EVCS is optimally installed at bus 28 results in an active power loss of 225.31 kW. It is recommended to install a large number of charging infrastructures on the way of EV users to increase the wide adoption of EVs. To this end, one more EVCS is placed at bus 6, which leads to a further increment in a power loss of 254.45 kW. It is realized that the addition of charging infrastructures is essential for the survival of EVs but at the same time causes detrimental effects on the health of the power system. Thus, compromise has to be made between the power system health and charging infrastructure. DGs are added to reduce the charging impact of EVs. However, the implementation of DGs on optimal nodes compensates for the power loss issues. In this context, when one DG of 1.8726 MW capacity is optimally placed at bus 61 results in an active power loss of 83.2 kW. When two DGs are located at buses 17 and 61, their sizes are 0.5312 MW and 1.7815 MW, respectively, providing a reduced APL of 71.7 kW. Also, APL is reduced to the value of 69.4 kW when three DGs with sizes 0.5268 MW, 0.3801 MW, and 1.7190 MW are installed at bus numbers 11, 18, and 61, respectively. When EVCS and DGs are placed successively in a 69-bus distribution network, the APL values are shown in Table 6.4.

Table 6. 4. APL values after the placement of EVCS and DGs using HGWOPSO in IEEE 69-bus system

Scenarios	Bus number and size	APL (kW)
Base case	–	224.9
1 EVCS	1500 kW at bus 28	225.31
2 EVCS	1500 kW at bus 6 and 28	254.45
1 DG	1.8726 MW at bus 61	83.2
2 DGs	0.5312 MW and 1.7815 MW at bus 17 and 61	71.7
3 DGs	0.5268 MW, 0.3801 MW and 1.7190 at bus 11, 18 and 61	69.4

Table 6.5. shows a comparison of the size and placement of EVCS and DG, as well as their impact on power loss. In addition to this, Fig. 6.11. shows the varied power loss values after installing EVCS and DGs.

The efficacy of the suggested hybrid technique, HGWOPSO, is also proven by comparing the acquired findings to those of other existing techniques like GWO and PSO.

Table 6. 5. Comparison of optimal size, location and APL of EVCS and DG obtained using HGWOPSO and GWO for IEEE 69-bus system

Scenarios	HGWOPSO				GWO			
	EVCS Location	Optimal DG		APL (kW)	EVCS Location	Optimal DG		APL (kW)
		Location	Size (MW)			Location	Size (MW)	
Base case	-	-	-	224.9	-	-	-	225.7
1 EVCS	28	-	-	225.31	28	-	-	227.67
2 EVCS	6, 28	-	-	254.45	6, 28	-	-	257.89
1 DG	6, 28	61	1.8726	83.2	6, 28	61	1.9536	85.9
2 DGs	6, 28	17	0.5312		6, 28	17	0.7134	
		61	1.7815	71.7		61	1.9235	72.5
3 DGs	6, 28	11	0.5268	69.4	6, 28	13	0.5312	70.5
		18	0.3801			21	0.3876	
		61	1.7190			67	1.8138	

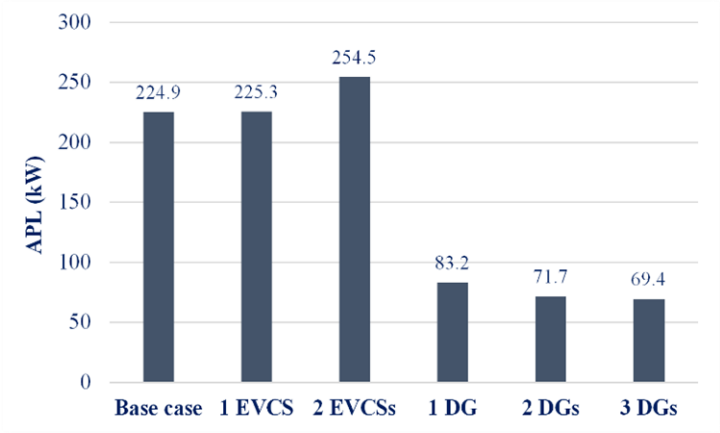

Fig. 6. 11. Effect of EVCS and DG integration on active power loss in the IEEE 69-bus system

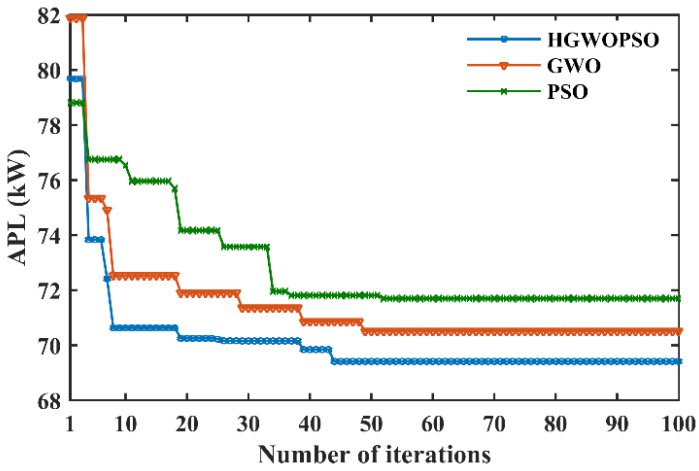

Fig. 6. 12. Convergence plot for active power loss using HGWOPSO, GWO, and PSO in IEEE 69-bus network

The proposed technique results in an active power loss of 69.4 kW, which is lower than the 70.5 kW and 71.7 kW incurred by GWO and PSO respectively. Fig. 6.12. depicts the converging nature of active power loss throughout iteration using proposed HGWOPSO, GWO, and PSO. In addition, the convergence curve clearly shows that HGWOPSO achieves optimal solutions faster than isolated GWO and PSO.

2) Effect of EVCS and DG Integration on Voltage Profile and Voltage Stability Index in IEEE 69-bus system

The addition of EVCS disrupts the voltage profile of this system, which is similar to that of a 33-bus network. The minimal voltage of magnitude 0.9091 p.u. exists at bus 65 in the base case. When EVCS is installed at bus 28, the minimum voltage value is dropped to 0.9015, which occurs at bus 65. When one more EVCS is added to node 6, the minimum voltage drops even lower to 0.8997 p.u. As a result, EVCS installation degrades the voltage profile of the system. DG units are integrated along with EVCS to maintain a healthy voltage profile. The voltage profile improves with the incorporation of DG units. In the case of one DG only, the minimum voltage is improved to 0.9683 p.u. at bus 27. When two DGs are optimally placed, the minimum voltage value comes out to be 0.9789 p.u. at bus 65. Moreover, simultaneous allocation of DG units further improves the bus voltage, i.e., the minimum voltage of 0.9790 p.u. at bus 65. Fig. 6.13. shows the voltage profile of the 69-bus system when EVCS and DGs are integrated.

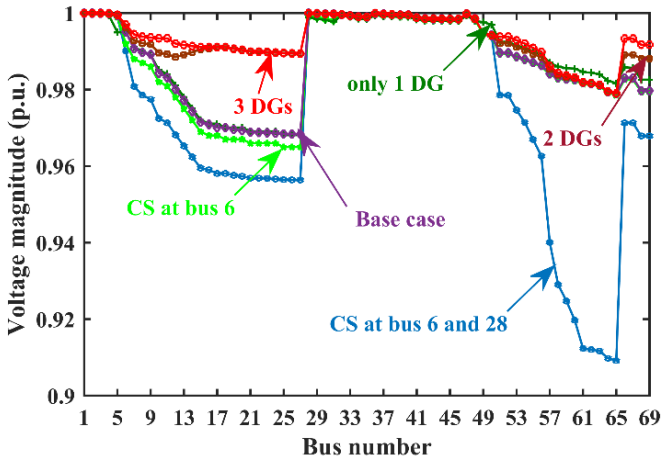

Fig. 6. 13. Voltage profile of IEEE 69 bus system after integrating EVCS and DG units

VSI is influenced in the same way as voltage profile with the gradual increase of charging loads. The value of VSI before integrating EVCS is observed to be 0.6833 p.u. but it is decreased to 0.6709 p.u when charging load is added on bus 28. In the same way, VSI further drops to 0.6615 p.u with the addition of another EVCS at bus 6. Thus, the incorporation of charging infrastructures badly affects the system in terms of VSI. This problem is compensated by the integration of DGs into the distribution network. VSI improves to 0.8792 p.u. in the presence of one DG only. Further improvement in VSI takes place with the incorporation of more DG units. Integration of two DGs improves the VSI to 0.9083 p.u. While in the case of three DGs, it becomes 0.9185 p.u. Regarding this, improvement in VSI is seen in Fig. 6.14 by incorporating DGs.

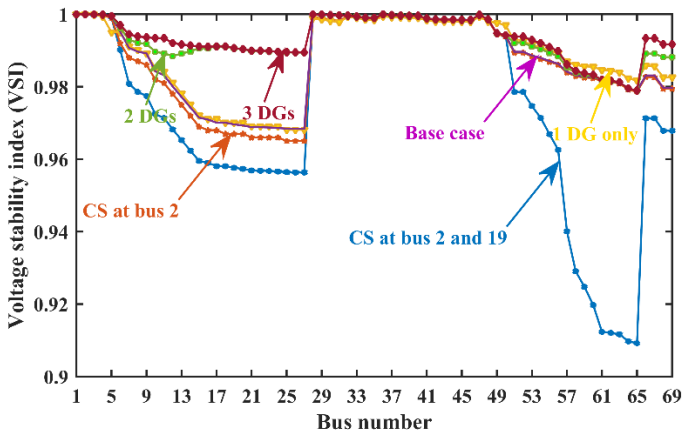

Fig. 6. 14. VSI for IEEE 69 bus systems for different scenarios

In addition, VSI is explored for various scenarios using the recommended technique and compared to other techniques to establish its superiority. The VSI findings for the 69-bus system obtained using the two techniques are shown in Table 6.6.

Table 6. 6. Comparison of VSI values for different scenarios in the IEEE 69-bus system

Scenarios	HGWOPSO		GWO		PSO	
	VSI (p.u.)	Inverse VSI	VSI (p.u.)	Inverse VSI	VSI (p.u.)	Inverse VSI
Base case	0.683	1.463	0.672	1.488	0.6793	1.472
1 EVCS	0.670	1.491	0.664	1.506	0.6546	1.527
2 EVCS	0.661	1.511	0.648	1.543	0.6358	1.572
1 DG	0.879	1.137	0.871	1.148	0.8647	1.156
2 DGs	0.908	1.101	0.892	1.121	0.8957	1.116
3 DGs	0.918	1.089	0.911	1.097	0.9089	1.100

6.5.3 Effect of Integrated EVCS and DGs on Reliability of IEEE 33 bus and IEEE 69 bus Distribution Networks

The reliability indices are obtained to demonstrate the consequence of integrating EVCS and DG units on the system reliability. The reliability indices for the electrical network are calculated considering quantitative information about failure and repair rate, average outage time, and the number of customers at each load point. The reliability indices considered in this article are SAIFI, SAIDI, CAIDI, EENS, AENS, ASAI, and ASUI.

1) Reliability analysis for IEEE 33-bus system

The major goal of this section is to offer a detailed examination of the impact of the EV charging station and DG placement on the IEEE 33-bus system's reliability. Reliability indices are estimated for all the above-mentioned scenarios, i.e., after the placement of EVCS and DGs. Customer information and other statistical parameters such as failure rate, repair rate, and average outage time for the IEEE 33-bus system are stated in A.4 and A.5, respectively.

Both consumer and load (energy) oriented indices deteriorate after the installation of EVCS. On the other hand, DGs integration into the distribution system enhances both types of reliability indices. This is because DGs enable immediate and efficient bus voltage management, which improves power transfer capability and reduces power loss by regulating supplied power to the system. They also directly alter the power flow by controlling injected power. It is realized from Table 6.7 that the value of reliability indices worsens after the allocation of EVCS. The value of SAIFI before installing EVCS and DG, i.e., the base case is 0.0982 failures/customer. year. After installing a fast-charging station with 30 charging points on bus 2, the SAIFI increased to 0.1195 failures/customer. year. The value of SAIDI and CAIDI also increased to 0.6321 hours per customer. year and 5.2915 hour/customer. interruption when one EVCS is allocated at bus 2. Likewise, deprivation of EENS and AENS is also observed in the case of one CS placement. The base value of AENS is 1.9369 MWh per customer per year. Its value increased to 10.2612 MWh per customer per year after the integration of one EVCS. As the EVCS is integrated into the distribution network, the energy is supplied to meet the load requirement, and thus, the indices associated with the energy not supplied are increased. The increment in reliability indices is not desirable from the perspective of the distribution system. Also, the value of ASAI decreases with the incorporation of charging loads. It refers to the condition that the availability of electricity decreases with increasing charging loads. Further, all reliability indices are evaluated when two EV charging loads are placed at buses 2 and 19. When two charging station loads are shared between two nodes, the reliability is higher than when the two charging stations are concentrated on a single node. In some circumstances, when strong nodes of the electrical power network and high-traffic-density

nodes of the transportation network merge, the paths connecting to that node become too crowded. As a result, distributing the charging stations has the added benefit of making the charging capability available to a broader number of EVs traveling in diverse routes, minimizing overcrowding of traffic on the particular paths leading to the bus where charging loads are concentrated.

Thus, it is desirable to inject some amount of energy into the distribution system to improve its reliability. One of the alternatives is to make use of DGs, which injects active and reactive power into the system depending on the requirement. Multiple DGs are optimally integrated into the network, which enhances the system's reliability. All reliability indices are investigated after integrating DGs. The impact of DGs integration on reliability indices is shown in Table 6.7. After the placement of one DG at bus 6, the value of SAIFI decreased to 0.1217 failures/customer. year. Similarly, the values of SAIDI and CAIDI also decreased to 0.5238 hours per customer. year and 4.304 hour/customer. interruption respectively. Hence, these reliability indices continue to reduce with the increasing integration of DGs. As more DGs are introduced into the network, the period of the disturbance and the number of interruptions that occur in the system decrease. Therefore, the SAIDI and SAIFI have been decreased. Furthermore, a reduction in SAIDI and SAIFI values is desired for improving the reliability of the distribution system.

Table 6. 7 Effect of EVCS and DG integration on reliability indices in IEEE 33-bus system

Scenarios	SAIFI	SAIDI	CAIDI	EENS	AENS	ASAI	ASUI
Base case	0.0982	0.5048	5.1385	1780	1.9369	0.9999	0.0001
1 EVCS	0.1195	0.6321	5.2915	9430.04	10.2612	0.9997	0.0003
2 EVCS	0.1361	0.7155	5.2558	15029.9	16.3547	0.9994	0.0007
1 DG	0.1217	0.5238	4.304	8765.46	9.5381	0.9997	0.0003
2 DGs	0.1147	0.4914	4.2842	6517.23	7.0946	0.9998	0.0002

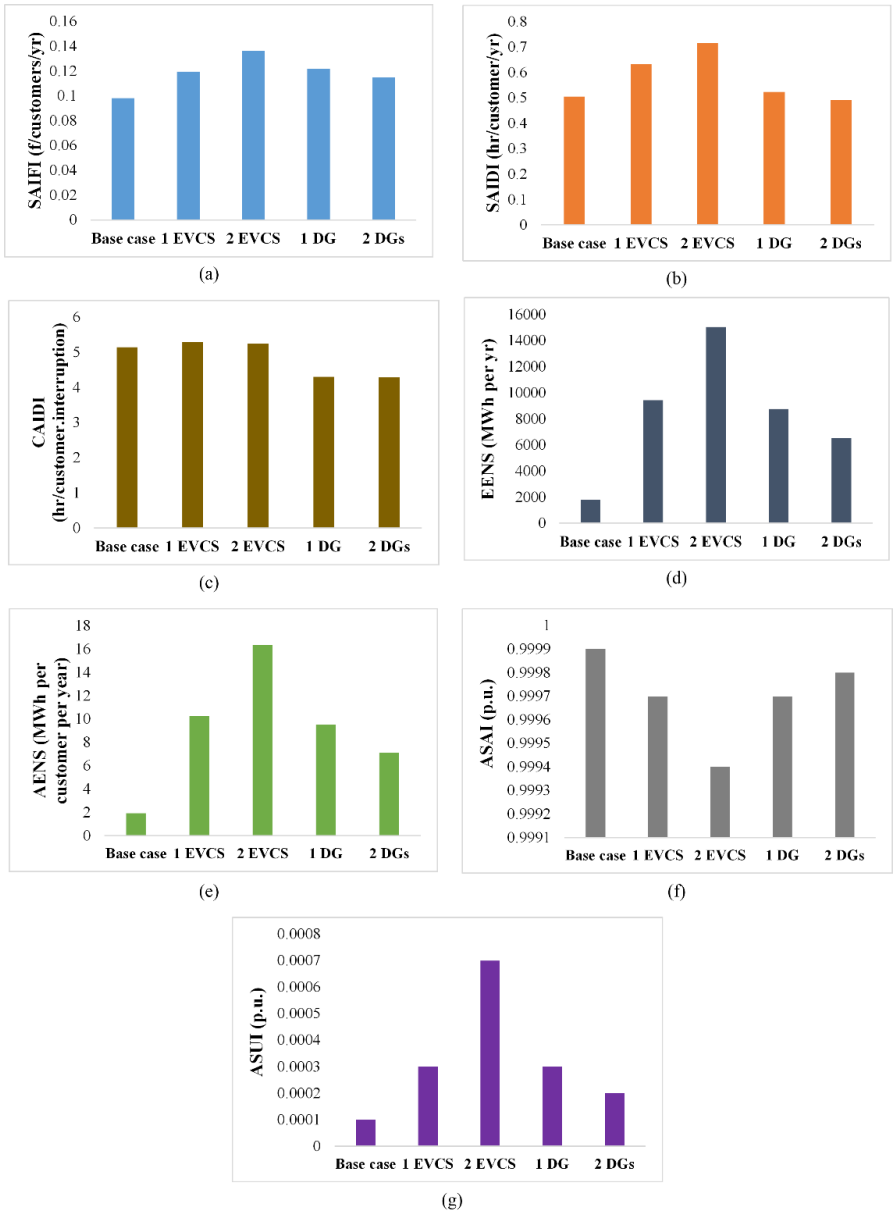

Fig. 6. 15. Variation in reliability indices with the integration of EVCS and DGs in IEEE 33-bus system

It's worth noting that the EENS and AENS reduce as the number of DGs increases. The value of AENS is 9.5381 MWh per customer per year with one DG only, whereas it is reduced to 7.0946 MWh per customer per year when one more DG is added into the system. As more DGs are incorporated into the network, the supplied energy to the system improves, and the indices for energy not supplied decrease. The reduction in EENS and

AENS values is desirable for a reliable power system. Hence, the reliability of the electrical system improves with the integration of DGs with adequate reliability data.

Also, DGs integration has positive impacts on electrical supply-based reliability indices, i.e., ASAI and ASUI. It is noted from Table 6.7, ASAI values increase with increasing DGs integration. The increase in ASAI results in a decrease in ASUI, which is beneficial for improving system reliability. Fig. 6.15. shows the impact of EV charging loads and DG units on various reliability indices in the 33-bus network.

2) Reliability Analysis for IEEE 69-bus System

This section of the article provides the impact on the reliability of the IEEE 69-bus distribution system after the optimal integration of EV charging loads followed by DG units. Here, 2 EVCS and 3 DGs are placed, which is different from the case of the 33-bus system where only two DGs were integrated. Table A.6 and Table A.7 report the statistical parameters such as failure rate, repair rate and average outage time, and customer information for the IEEE 69-bus system, respectively.

Similar to the IEEE 33-bus system, the addition of charging loads disturbs the customer as well as load-oriented reliability indices of the IEEE 69-bus system. DGs are integrated to maintain the reliability of the power system network by injecting energy into the system, thereby resulting in power loss reduction. The effect of integrating EV charging loads and DG units on various reliability indices in the IEEE 69-bus system is illustrated in Table 6.8.

Table 6. 8. Effect of EVCS and DG integration on reliability indices in IEEE 69-bus system

Scenarios	SAIFI	SAIDI	CAIDI	EENS	AENS	ASAI	ASUI
Base case	2.4795	77.6787	31.3283	27195.51	33.4921	0.9911	0.0089
1 EVCS	2.4919	79.8148	31.9796	37006.33	45.5743	0.9908	0.0092
2 EVCS	2.5159	82.4789	32.7845	46967.21	57.8414	0.9906	0.0094
1 DG	2.5043	81.4879	32.5391	41857.06	51.5481	0.991	0.009
2 DGs	2.4951	80.8794	32.4153	35688.78	43.9517	0.9916	0.0084
3 DGs	2.4847	78.4879	31.5884	32487.54	40.00929	0.9925	0.0075

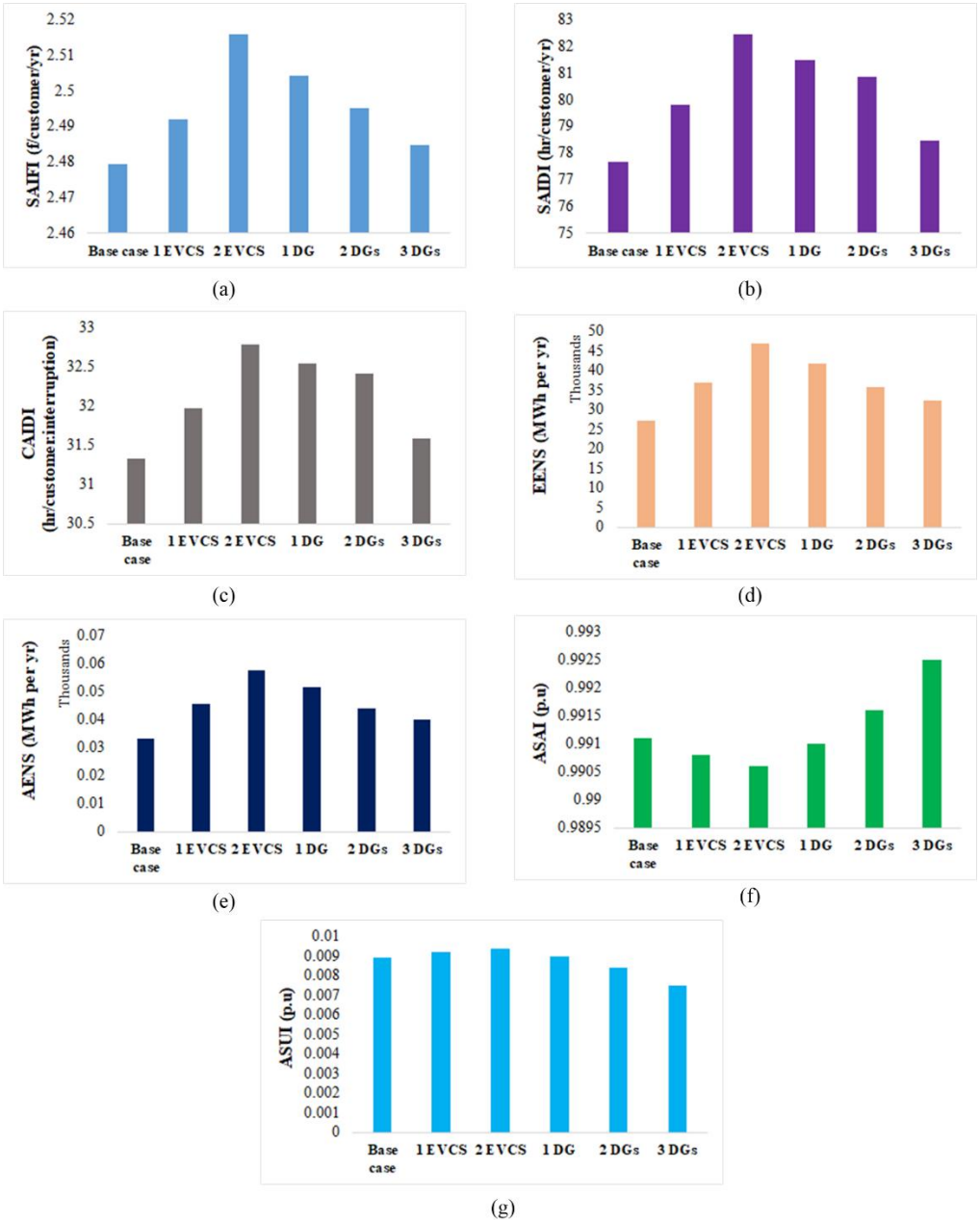

Fig. 6. 16. Variation in reliability indices with integration of EVCS and DGs in 69-bus system

As explained in the case of the IEEE 33-bus system, the value of all customer-oriented reliability indices, i.e., SAIFI, SAIDI, and CAIDI increases from the base value after the integration of EV charging loads which are not desirable for a reliable power system.

Similarly, load-oriented indices, i.e., EENS and AENS, also degrades due to the addition of EVCS. The value of all indices increases from their respective base value when charging loads are integrated. Hence, DGs are integrated as in the case of IEEE 33- bus network to bring the system to operate in reliable mode. With the increasing integration of DGs, all the reliability indices improve, i.e., SAIFI, SAIDI, CAIDI, EENS, and AENS reduce, which is required from the reliability point of view of the distribution system.

Additionally, ASAI decreases when EVCS is placed. On the other hand, it goes on the increase with the integration of DGs, which is desirable. Fig. 6.16 shows the impact of EV charging loads and DG units on various reliability indices in the IEEE 69-bus network.

6.6 SUMMARY

Electric vehicles are a viable option for reducing transportation-related pollution. The rising reputation of EVs has resulted in the setting up of EVCSs; though, the negative influence of EV charging station loads on the electrical system cannot be overlooked. This paper presents the EVCS impact on the IEEE standard system based on a direct approach-based load flow analysis. The process of charging electric vehicles necessitates additional power from the grid, resulting in greater power losses. As a result, DG should be employed to offset the power losses generated by EVCS. Type 2 DG is utilized in this work, which repays for the system's power loss. Furthermore, a hybrid algorithm called HGWOPSO

has been employed to reduce losses by determining the optimal node for EVCS and DG placement. The proposed hybrid algorithm is validated on the IEEE-33 and IEEE-69 bus systems. Additionally, the accuracy of the suggested method is validated by comparing the outcomes acquired using other methodological approaches such as GWO and PSO. It is observed that HGWOPSO shows a significant reduction in system losses when compared to GWO and PSO for 33-bus as well as 69-bus systems.

Apart from the voltage and current constraints, the number of EV charging loads is fixed, and DGs are added to the grid network to reduce the system's losses. It is easy for the power engineers to choose the number of DGs for compensating the influence of EVCS by analyzing the mismatch in the capacity of the additional EVCS load and total system load. In the IEEE-33 bus system, two DGs satisfactorily improve the performance of the system, whereas the quantity of DGs required in the IEEE-69 bus system is four. Although power losses are minimized, and the voltage profile gets enhanced on increasing the DGs, the impact of specific fourth DG is marginal.

In addition, reliability analysis is performed to determine the cumulative influence of EV loads and DGs on the distribution system's health. All reliability indices are investigated in different scenarios. It is noticed that the placement of EVCS degrades the reliability of the network in 33-bus and 69-bus systems. However, results show that the DGs incorporation along with EVCS improves the reliability indices.

However, the current research work has several limitations, such as the use of a stochastic approach to construct the EV load at charging stations to estimate the impact of increased EV demand on the distribution system. Furthermore, rather than conventional

DGs, renewable-based DGs, such as solar/wind, may be included. Additionally, coupled transportation and distribution networks can be taken as a test system.

Following are the research problems that can be addressed in the future:

- By taking into account larger standard IEEE systems like the 118-bus.
- Subsystem reliability data can also be added, providing a precise picture of the total system's reliability.
- The number of branches in a power system can also be changed to improve reliability, which is referred to as system reconfiguration. Furthermore, the dependency on CO_2 emissions, as well as the protection and security of power system components, can also be addressed when assessing the system's reliability.
- A more systematic approach to charging station location issues could be investigated, taking into account EV consumers' activity-based behavior.
- Variations in daytime load, fluctuations in environmental variables such as temperature, irradiance, and the wind, which might affect DGs such as solar photovoltaic and wind turbines, should be considered appropriately.

.

CHAPTER 7

TECHNO-ECONOMIC AND ENVIRONMENTAL ANALYSIS OF GRID-CONNECTED ELECTRIC VEHICLE CHARGING STATION

7.1 INRODUCTION

The control and power management of EVs in grid-connected systems are the primary focus of researchers. However, one of the important aspects that must be addressed is an economic analysis that takes into account the power exchange with the grid. The fast adoption of EVs poses both constraints and opportunities for the current electricity system. A small grid-connected SPV and diesel generator (DG)-based hybrid system with EVs are presented in this chapter for a charging station in the northwest region of Delhi, India. The main objective is to formulate a statistical model of a SPV and DG-based hybrid system with EVs and a backup grid. Furthermore, the purpose of this research is to reduce power interchange with the grid. This chapter discusses the implementation of HGWOPSO technique for satisfying the EV load requirement using hybrid SPV and DG with utility grid as a backup. Hence, the assessment described in this chapter will be a useful guide for researchers looking to select a technique for their sizing concern.

7.2 MODELING OF HYBRID SYSTEM COMPONENTS

The mathematical modeling of the hybrid energy system to meet the charging demand of EVs is described in this section. An SPV panel, DG, battery, inverter, and backup grid are all part of the hybrid energy system under consideration. To enhance load

supply reliability, the battery is utilized to control the variation of renewable energy (RE) generation. A graphical representation of the proposed SPV/DG/battery storage system is shown in Fig. 7.1.

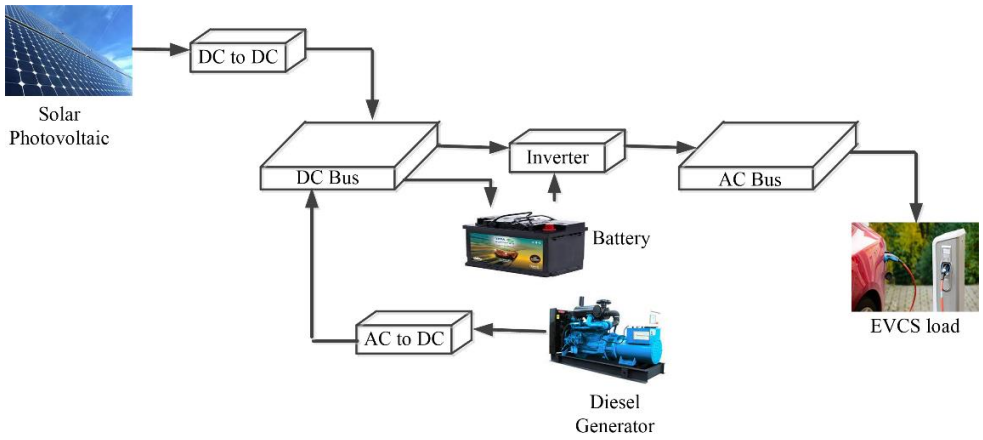

Fig. 7. 1. Schematic representation of the proposed hybrid energy system

7.2.1 SPV Array Output

Solar radiation is the most prevalent component on the planet, as well as being the most robust RE source. It is comparatively simple to execute and can be made affordable in all remote areas of the country. Concerning the maximum output pattern of SPV, modules are widely used to estimate the quality of an SPV generation system to its peak power. SPV panels are used to generate electricity by collecting solar energy. Only a small portion of the solar radiation that penetrates the SPV panels is transformed to electricity, with the remainder being converted to heat. Several factors can influence the quality of the SPV power output. The power output obtained from SPV is dependent on the area of the panel, solar irradiance incident on the surface of the panel, temperature of the SPV cells, and geographical parameters, i.e., latitude and longitude of the panel location, using Eqn. (7.1):

$$P_{SPV-out}(t) = \eta_{SPV} A_{SPV} G_h(t)\{1 - 0.005(T_{cell} - 25)\} \quad (7.1)$$

where η_{SPV} is the efficiency of solar panels, A_{SPV} represents the surface area of the solar panel, $G_h(t)$ denotes the hourly solar irradiance falling on the surface of the solar panel, and T_{cell} is the temperature of the cell. The parameters taken for the selected PV panel are tabulated in Table 7.1. The temperature of the cell and the fluctuation of power as a function of temperature are given by

$$\mathrm{T_{cell}} = \mathrm{T_a} + \frac{\mathrm{NOCT-20}}{0.8}\mathrm{G_h(t)} \tag{7.2}$$

where T_a is the ambient temperature.

The rated maximum power output of solar panel can be expressed as

$$\mathrm{P_{max}} = \mathrm{V_{max}I_{max}} \tag{7.3}$$

where V_{max} denotes the maximum value of voltage, and I_{max} represents the maximum current, respectively.

The overall power generated using SPV modules can be estimated by

$$\mathrm{P^{total}_{SPV-out}(t)} = \mathrm{N_{SPV}P_{SPV-out}(t)} \tag{7.4}$$

where N_{SPV} is the number of the installed solar PV panels.

7.2.2 Diesel Generator (DG)

The quantity of energy storage necessary for isolated villages and rural enterprises can be lowered by using DGs, resulting in a profitable and reliable solution. In the event of battery degradation during peak loads, diesel can be used as a backup source of energy.

The DG's efficiency and hourly fuel usage should be accounted for when planning a hybrid system and may be represented using the equation below [155]:

$$u(t) = a \times P_{DG}(t) + b \times P_{rated-DG} \quad (7.5)$$

where u(t) is the fuel consumption in liters per hour, $P_{DG}(t)$ is produced power in kW, $P_{rated-DG}$ is the rated power, a (0.246) and b (0.08415) are constant parameters in liter per kW, which characterize the coefficients of fuel consumption.

The efficiency of DG can be computed by

$$\eta_{overall} = \eta_{brake\ thermal} \times \eta_{DG} \quad (7.6)$$

where $\eta_{overall}$ is the overall efficiency of DG, whereas $\eta_{brake\ thermal}$ represents the brake thermal efficiency of DG.

7.2.3 Modeling of Battery Energy Storage System (BESS)

Due to the erratic nature of SPV output, optimum battery sizing is essential to meet the load demand. The existing state of charge (SOC) is the most important decision variable for monitoring the charging/discharging states of the battery. Overcharging of the battery takes place when the hybrid model generates too much power or when the load demand is too low. When the battery's SOC reaches its maximum value, i.e., SOC (max), the control system gets involved and stops the charging mechanism, whereas when it acquires its minimum value, i.e., SOC (min), the control system disables the load to avoid the battery from being drained [156].

There are instances when the state of the battery varies depending on the power output and load demand. The battery performs an important role in the system's energy management by adjusting power demands and power supply. The battery is said to be charging when the generated power is higher than the required energy, and the charging state of the battery at time t is given by [156].

$$SOC_{bat}(t+1) = SOC_{bat}(t)(1-\sigma) + \left[\left(P_{SPV-out}(t) + \frac{P_{DG}(t)}{\eta_{bdinv}}\right) - P_{EVCS-dem}(t)\right] \times \eta_{bat} \quad (7.7)$$

On the other hand, when RE sources are unable to create enough power to meet demand, the battery is employed as a backup to feed the load system and operate in discharging state. The discharging state of the battery at time t is given by

$$SOC_{bat}(t+1) = SOC_{bat}(t)(1-\sigma) - \frac{\left[P_{EVCS-dem}(t) - \left(P_{SPV-out}(t) + \frac{P_{DG}(t)}{\eta_{bdinv}}\right)\right]}{\eta_{bat}} \quad (7.8)$$

where $SOC_{bat}(t+1)$ and $SOC_{bat}(t)$ are the SOC of battery at an instant $(t+1)$ and (t), respectively, σ is the self-discharge rate of the battery, η_{bdinv} is the efficiency of bi-directional inverter used, $P_{SPV-out}(t)$ and $P_{DG}(t)$ are the power output of SPV and DG, respectively, and η_{bat} is the round trip efficiency of the battery. The round-trip efficiency of the battery can be expressed using Eqn. (7.9):

$$\eta_{bat} = \eta_{bat}^{charge} \times \eta_{bat}^{discharge} \quad (7.9)$$

where η_{bat}^{charge} represents the charging efficiency of the battery, whereas $\eta_{bat}^{discharge}$ denotes the discharging efficiency of the battery. The round-trip efficiency of the battery bank is reported to be 92.2 percent. Furthermore, charging/discharging efficiencies are assumed to be 85/100 percent, respectively. SOC_{max} round-trip efficiency of the battery is the maximum value of SOC and is equivalent to the total energy of the battery bank C_{total}(Ampere hour), as follows:

$$C_{total}(\text{Ampere hour}) = \frac{N_{bat}}{N_{bat}^{series}} C_{sbat}(\text{Ampere hour}) \tag{7.10}$$

where C_{sbat} is the energy of a single battery, N_{bat} represents the total number of batteries, and N_{bat}^{series} represents the number of batteries connected in series. The battery bank is only allowed to discharge to a certain minimal level, known as SOC_{min}. This restriction can be used as a system constraint depending on how the battery bank is utilized. Batteries are arranged in series to get the desired bus voltage. The number of batteries in a series can be computed using the formula:

$$N_{bat}^{series} = \frac{V_{bus}}{V_{bat}} \tag{7.11}$$

where V_{bat} is the voltage level of a single battery.

The maximum charge/discharge power at any given time is another important consideration in battery modeling. It is determined by the maximum charging current and may be computed using the equation below:

$$P_{bat}^{max} = \frac{N_{bat} \times V_{bat} \times I_{max}}{1000} \tag{7.12}$$

where I_{max} is the maximum charging current drawn by the battery in amperes, and P_{bat}^{max} is the maximum input/output power of the battery.

7.2.4 Bi-Directional Inverter Modeling

The bi-directional inverter performs the function of conversion of DC to AC power and vice versa. Solar panels provide DC electricity to EVs at the charging station. Hence, the bi-directional inverter is required to transform the DC power of SPV. The output of the bi-directional inverter can be computed as follows:

$$P_{AC} = \eta_{bdinv} \times P_{DC} \tag{7.13}$$

The proposed system takes into account a bi-directional inverter efficiency of 97 percent.

7.2.5 Utility grid

In the first phase, when the demand exceeds the generated power from the different energy sources and BESS capacity, the energy shortage can be fulfilled by borrowing the energy from the grid network and may be represented using Eqn. (7.14):

$$P_P^{grid}(t) = P_D^{EV}(t) - \left[P_{SPV-out}^{total}(t) + P_{DG}(t) + \left[\left(P_{SPV-out}^{total}(t) + \left(SOC_{bat}(t) - SOC_{bat}^{min}(t)\right)\right) \times \eta_{bdinv}\right]\right] \tag{7.14}$$

where $P_P^{grid}(t)$ represents the energy to be borrowed from the grid in kWh, and $SOC_{bat}^{min}(t)$ denotes the minimum SOC of battery.

In the second phase, when the demand is less than the generated power from the different energy sources, and the battery is wholly charged, the extra energy is sold to the utility grid and may be represented using Eqn. (7.15):

$$P_S^{grid}(t) = \left[P_{SPV-out}^{total}(t) + P_{DG}(t) + \left[\left(P_{SPV-out}^{total}(t) - \left(SOC_{bat}^{max}(t) - SOC_{bat}(t)\right)\right) \times \eta_{bdinv}\right]\right] - P_D^{EV}(t) \tag{7.15}$$

where $P_S^{grid}(t)$ represents the extra energy to be sold to the grid in kWh, and $SOC_{bat}^{max}(t)$ denotes the maximum SOC of the battery.

7.2.6 Modeling of EVCS Load

The main components of EVCS are dual converter, charging ports, and EVs. The charging station is coupled to a regulator, which facilitates controlling the direction of the power

Table 7. 1 Technical and economic parameters of different hybrid system components

Components	Characteristics	Values
Solar PV panel (Canadian Solar Max Power CS6X-325P) [157]	Rated power	325 W
	Normal operating cell temperature	45 ± 2 °C
	Open circuit voltage (V_{OC})	45.5 Volts
	Short circuit current (I_{SC})	9.34 Amps
	Module efficiency:	16.94%
	Dimensions	76.90 × 38.70 × 1.57 inches
	Power tolerance	0/+5 W
	Initial cost	$ 950/kW
	Replacement cost	$ 900/kW
	Operation and maintenance cost	$ 10/kW
	Life span	25 years
	Derating factor	80%
Diesel generator (Generic 10 kW fixed capacity genset) [155]	Minimum load ratio	50%
	Heat recovery ratio	10%
	Operating time	15,000 h
	Fuel price	$ 1.21/litre
	Density	820 Kg/m^3
	Initial capital cost	$ 500/kW
	Replacement cost	$ 500/kW
	Operation and maintenance cost	$ 10
Battery (Generic 1 kWh lead acid) [132]	Battery material	Lead acid
	Nominal voltage	12 V
	Nominal capacity	81–100 Ampere hour
	Lifetime	5–8 years
	Initial capital cost	$ 235/kW
	Replacement cost	$ 190/kW
	Operation and maintenance cost	$ 2/kW/year
Bi-directional converter [132]	Rated power	100 kW
	Initial capital cost	$ 171/kW
	Replacement cost	$ 171/kW
	Operation and maintenance cost	$ 4/kW/year
Utility grid [158]	Grid purchase price	$ 0.12/kWh
	Grid sell back price	$ 0.08/kWh
Others [132]	Nominal interest rate	3.75%
	Inflation rate	1.75%
	Lifetime of project	25 years
	SOC_{max}	0.95
	SOC_{min}	0.35
	Inverter efficiency (%)	0.95
	Rectifier efficiency (%)	0.95

flow at a specific time. The charging of EV takes place based on its current SOC. It is defined as the ratio of available charging state to the maximum charging state, i.e., when the battery is fully charged. Hence, it describes how much battery needs to be charged.

The amount of power consumed by an EV is determined by the distance traveled, battery capacity, and driving mode. An EV uses power, which may be estimated using the Eqn. (7.16).

$$P_D^{EV} = \frac{D_{km} \times E_{req/km}}{T} \tag{7.16}$$

where D_{km} is the number of kilometers traveled, the power needed per kilometer is $E_{req/km}$, and T is the time to recharge the battery. T is the difference between the time of arrival and departure. T is determined by the SOC of the vehicle's battery. The power requirement of an EV can be illustrated using the capacity of battery, SOC, and time of charging:

$$P_D^{EV} = \frac{Q_{bat}^{EV} \times \left(SOC_{max}^{EV} - SOC_{min}^{EV}\right)}{T} \tag{7.17}$$

where Q_{bat}^{EV} represents the capacity of the EV battery, SOC_{max}^{EV} and SOC_{min}^{EV} are the maximum and minimum limit of SOC, and T denotes the duration of charging.

Therefore, the total power required for charging the N number of EVs is given as follows:

$$P_{total}^{EV} = \sum_{i=1}^{N_{EV}} P_D^i \tag{7.18}$$

The technical features of different components of a hybrid energy system are summarized in Table 7.1.

7.3 PROBLEM FORMULATION

In this paper, the problem formulation deals with the optimization of different configurations of energy system for satisfying the load demand of EVCS installed in the northwest region of Delhi, India, with real annual data of solar irradiance, temperature, and EV load. These configurations are stated as follows: (a) SPV/DG/battery-based EVCS, (b) SPV/ battery-based EVCS, and (c) grid-and-SPV-based EVCS. The hybrid energy system is constructed with a maximum load of 25.45 kW, and the yearly average energy requirement is 257 kWh/day. The goal of optimization is to minimize the total net present cost (TNPC), keeping the reliability constraint in terms of loss of power supply probability within specified limits. Moreover, another parameter for analyzing the performance of the hybrid energy system is the levelized cost of energy (LCOE). In this work, the energy management of the hybrid system is based on load following strategy (LFS). The numbers of SPV panels and batteries are chosen as the optimization variables, which are determined optimally using the HGWOPSO. The primary goal of this research work is to perform a cost-effective analysis for all select-ed configurations with lowest TNPC, LCOE, and best reliability. The GWO performance in the optimization of hybrid energy system is compared to conventional GWO and PSO. The objective functions, i.e., TNPC and LCOE and constraints, are coded in MATLAB environment considering the energy management strategy reported in Figs. 7.2. and 7.3. for SPV/DG/battery-based EVCS and grid-and-SPV-based EVCS, respectively.

7.3.1 Assumptions

- Charging stations operate for the whole day.
- Different number of EVs arrive at charging station on a daily basis.

- Only one charging station is considered.
- Limited output power of battery is taken into account.
- Load following strategy (LFS) is considered.
- Diesel generator is allowed to operate only when no power output from SPV is available.
- Cost of EV charger is around USD 50.

7.3.2 Objective Functions

The optimal number of solar panels, i.e., N_{SPV} and batteries, i.e., N_{bat}, must be determined to ensure that the system formulated in different configurations meets the charging demand of EVs. The objective function is formulated using the total net present cost (TNPC), levelized cost of energy (LCOE), and reliability in terms of loss of power supply probability (LPSP).

1) Total Net Present Cost (TNPC)

The total cost of a hybrid energy system is represented by the total net present cost (TNPC). It includes all costs and revenues incurred during the life cycle of the system, including system component capital costs, replacement costs incurred during the system's operation, and maintenance expenses. The numbers of SPV panels and batteries are chosen as the two primary decision variables for the optimum configuration. Hence, one of the objectives of this research work is to minimize the TNPC of the system, which is described as follows:

$$\mathrm{TNPC(USD)} = \mathrm{NPC_{SPV}} + \mathrm{NPC_{DG}} + \mathrm{NPC_{bat}} + \mathrm{NPC_{bdinv}} + C_P^{grid} - C_S^{grid} \qquad (7.19)$$

2) Levelized Cost of Energy (LCOE)

Levelized cost of energy may be defined as the average cost incurred per kW of energy production by the system. LCOE is computed by dividing the annualized cost of energy generation by the total energy production per year. It can be computed with the help of capital recovery factor (CRF), using the following Eqn. (7.20) [159]:

$$\mathrm{LCOE} = \frac{\mathrm{TNPC} \times \mathrm{CRF}}{\sum_{t=1}^{T} P_{gen}(t)} \ \mathrm{USD/kW} \tag{7.20}$$

CRF can be evaluated using Eqn. (7.21), as follows:

$$\mathrm{CRF} = \frac{R(1+R)^{\Omega}}{((1+R)^{\Omega}-1)} \tag{7.21}$$

LCOE depends on numerous features, such as capital cost, solar radiation, lifetime, operation and maintenance cost, CRF and degradation of the SPV panels used, etc.

3) Renewable Fraction

The renewable fraction (RF) is an important criterion to consider when designing an energy system. The total energy produced via RE sources is divided by the total power drawn by the load to calculate the RF. It can be calculated using Eqn. (7.22):

$$\mathrm{RF} = \left(1 - \frac{\sum P_{DG}}{P_{SPV}}\right) \times 100\ \% \tag{7.22}$$

7.3.3 Decision Variables and Constraints

To optimize the hybrid system, a compromise must be made between the cost-based objectives and various technical constraints. However, the proposed optimization approach should be used to obtain the optimal decision variables. The decision variable of the

suggested optimization procedure is subject to specific limits: the minimum limit put on the number of SPVs and battery, and the N_{SPV}^{max} = 1000, N_{bat}^{max} = 600.

- The following are the limits associated with the maximum and minimum sizes of decision variables:

$$N_{SPV}^{min} \leq N_{SPV} \leq N_{SPV}^{max} \tag{7.23}$$

$$N_{bat}^{min} \leq N_{bat} \leq N_{bat}^{max} \tag{7.24}$$

$$E_{bat}^{min} \leq N_{bat} \leq E_{bat}^{max} \tag{7.25}$$

- The charging state of the battery should be preserved using Eqn. (7.26). At any given time, the amount of energy stored in the battery $SOC_{bat}(t)$ is limited by the maximum and minimum quantities SOC_{bat}^{min} and SOC_{bat}^{max} as follows:

$$SOC_{bat}^{min} \leq SOC_{bat} \leq SOC_{bat}^{max} \tag{7.26}$$

SOC_{bat}^{max} takes the value of the theoretical capacity of the battery $C_{bus} \times V_{bus}$. The maximum depth of discharge, i.e., DOD and theoretical capacity $C_{bus} \times V_{bus}$ is used to calculate SOC_{bat}^{min}, as expressed in Eqn. (7.27):

$$SOC_{bat}^{min} = (1 - DOD) \times C_{bus} \times V_{bus} \tag{7.27}$$

DOD is assumed to be 50%.

- The maximum permissible lack of power supply should be considered for a reliable system:

$$LPSP \leq LPSP_{max} \tag{7.28}$$

where $LPSP_{max}$ represents the maximum allowable lack of power supply probability.

7.3.4 Operational Strategy

1) Solar PV and Diesel Generator-Based EVCS

To attain the reliability of the system in any hybrid energy system, optimal energy management is required. In this system, the DG is kept at the bottom of that list, which means it only needs to operate when the solar and battery systems are unable to supply the load requirement. The steps for the simplest implementation strategy for SPV/DG/battery system are as follows:

- If the total power generated by SPV panels is sufficient, demand can be met solely by solar power. After the load has been satisfied, excess electricity can be supplied to the BESS and is provided as follows:

$$P_{bat}(t) = P_{SPV-out}(t) - P_{EVCS-dem}(t) \quad (7.29)$$

- In the preceding case, if $P_{bat}(t)$ is greater than the maximum permissible capacity of the BESS, i.e., P_{bat}^{max}, then additional energy can be dumped or directed to deferrable loads. Excess or dump energy $(P_{dp}(t))$ can be given as

$$P_{dp}(t) = P_{bat}(t) - P_{bat}^{max}(t) \quad (7.30)$$

- If the SPV panels do not generate sufficient power, the battery can provide the remaining power, which can be calculated as

$$P_{bat}(t) = P_{EVCS-dem}(t) - P_{SPV-out}(t) \quad (7.31)$$

- If solar power is insufficient and batteries are unable to generate the required power to meet the power requirements, DG is used to energize the load. There are two ways to use DG.

(a) First, it employs a load-following strategy, which means that whenever it performs, it produces only the power necessary to satisfy the primary load requirements. The diesel generator's power output is calculated as

$$P_{DG}(t) = \frac{P_{EVCS-dem}(t) - P_{SPV-out}(t)}{\eta_{bdinv}} \quad (7.32)$$

(b) In the second strategy, it runs at maximum capacity or minimum load ratio. When the DG is fully operational, the surplus energy is used to charge batteries and is expressed as follows:

$$P_{bat}(t) = \left(P_{DG}(t) * \eta_{bdinv} - P_{EVCS-dem}(t)\right) + P_{SPV-out}(t) \quad (7.33)$$

The operational strategy of the SPV/DG/battery system can be understood with the help of the flow chart depicted in Fig 7.2.

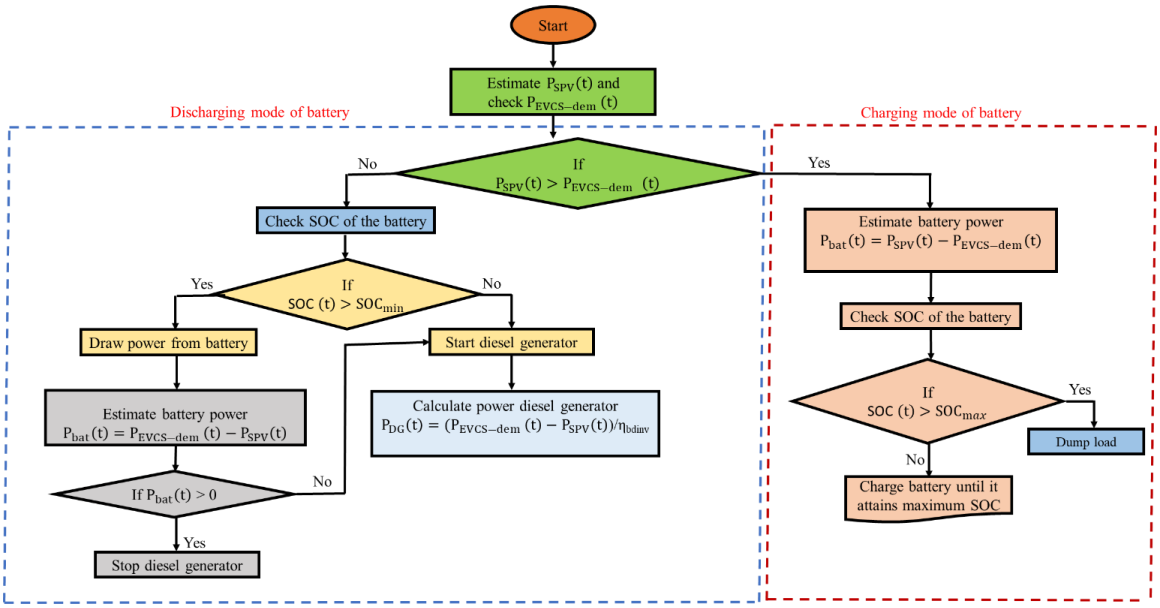

Fig. 7. 2. Flow chart of the energy management strategy of the SPV/DG/battery system

2) Grid-and-Solar PV-Based EVCS

In this scenario, it is assumed that SPV is the only source to satisfy the load demand of EVs. The difference between power obtained by SPV and power demand by EVs can be determined as

$$\Delta P(t) = P_{SPV}(t) - P_{EVCS-dem}(t) \tag{7.34}$$

- If solar panels are unable to fulfill the power requirements of EV load, the extra power is purchased from the grid network ($P_P^{grid}(t)$) to meet the requirements.

Furthermore, if more power is available from the SPV after meeting the requirements, it is sold to the grid ($P_S^{grid}(t)$). Nevertheless, there are some limitations on selling and purchasing power to and from the grid, which are defined as maximum purchase capacity of grid ($P_{P,max}^{grid}$) and maximum selling capacity of grid ($P_{S,max}^{grid}$). Beyond these limits, power cannot be purchased from or sold to the grid. The following cases are formed depending on the $\Delta P(t)$.

- When SPVs alone fulfill the power requirement of EV load, i.e., $\Delta P(t) > 0$, the extra power is sold to the grid network, which can be determined as

$$P_S^{grid}(t) = (P_{SPV}(t) - P_{EVCS-dem}(t))/\eta_{bdinv} \tag{7.35}$$

- When SPV power output is high enough, which fulfills the power requirement of EV load, as well as exceeds the maximum selling capacity of grid ($P_{S,max}^{grid}$), i.e., $\Delta P(t) > 0$ and $\Delta P(t) > P_{S,max}^{grid}$, the extra power is fed to the dump load, which can be determined as

$$P_{dp}(t) = (P_{SPV}(t) - P_{EVCS-dem}(t) - P_S^{grid}(t)/\eta_{bdinv}) \quad (7.36)$$

- When SPV power is unable to satisfy the charging demand of EVs, i.e., $\Delta P(t) < 0$, power is purchased from the grid which can be computed as

$$P_P^{grid}(t) = (P_{EVCS-dem}(t) - P_{SPV}(t)/\eta_{bdinv} \quad (7.37)$$

- If $\Delta P(t) = 0$, there is no exchange of power from grid, and SPV power fulfills the load requirement.
- When both SPV and grid are unable to satisfy the load demand, deficiency of power takes place, which can be given as

$$P_{def}(t) = P_P^{grid}(t) - P_{P,max}^{grid} \quad (7.38)$$

$P_{def}(t)$ must be zero to make sure the total power requirement of EV load demand is served in a reliable manner when minimizing the LPSP.

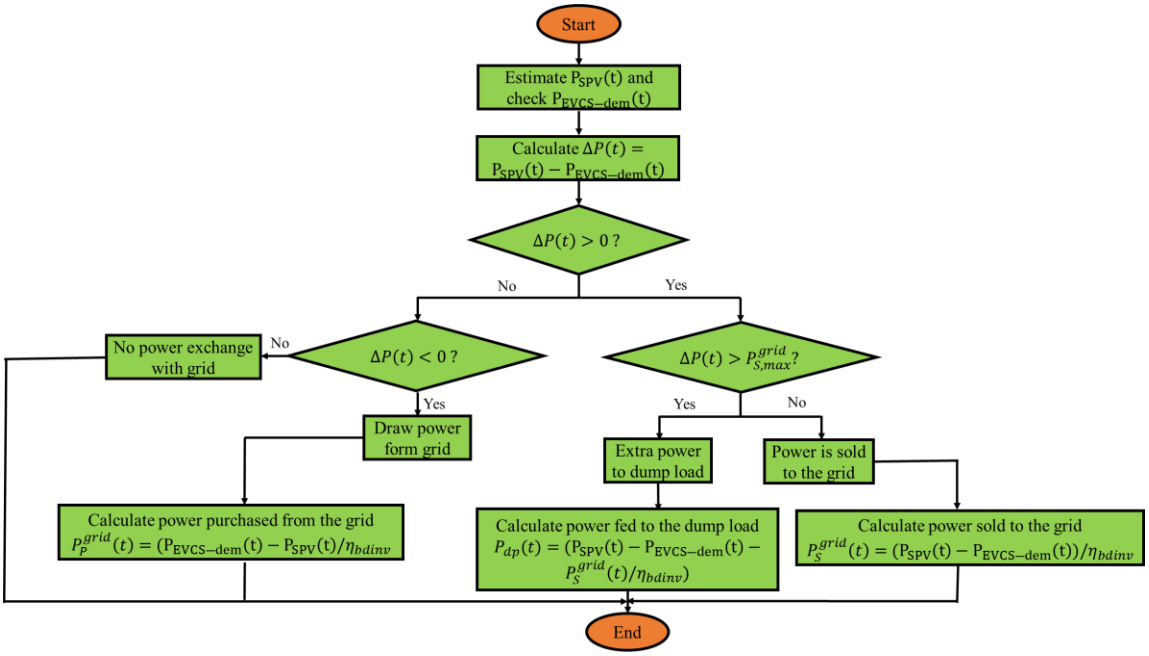

Fig. 7. 3. Flow chart of the energy management strategy in grid-and-solar PV-based EVCS

The LPSP can be kept within a specific tolerance band to solve the optimization problem. In this paper, the maximum limit of LPSP, i.e., $LPSP_{max}$ is assumed to be 1%. The energy management strategy for grid-and-solar PV-based EVCS can be demonstrated with the help of the flow chart shown in Fig. 7.3.

7.4 RESULTS AND DISCUSSION

7.4.1 Components and Methods

This section contains the important components, such as the place of the study area, resources available, and the load demand of the developed framework.

1) Area under Study

The proposed study is conducted in the northwest region of Delhi, India. The geographical coordinates of the studied area are 28.7408° N (latitude), 77.1126° E (longitude). Fig. 7.4. depicts the study area from a geographical standpoint.

Fig. 7. 4. The geographical view of the study area

The population of Rohini sector-17 is 21,460 individuals. Because the majority of citizens in this area are cultured and working, EVs are employed as a mode of transportation to get to their destinations on a day-to-day basis. This area has nearly 120–150 EVs, and there are 15 facilities in which these vehicles are kept and provided with electricity. As per the owner of different facilities, the amount required to charge the EVs is significantly high because these vehicles are charged using the grid.

2) Assessment of the Available Energy Sources

Solar radiation in Delhi is at its highest from March to October. It is available during the wintertime, but not at its high point. Additionally, it is regarded as an outstanding source of energy due to its practical features. Fig. 7.5. shows the annual variation of irradiance at the chosen area. Fig. 7.5. also depicts the clearness index, which is the percentage of solar radiation that is reflected by the atmosphere. It can also be defined as the ratio of surface irradiance and extraterrestrial irradiance. Fig. 7.6 portrays the annual fluctuation of temperature for the study site. The DG is also incorporated as one of the energy providers in the proposed research work. Energy generation from DG is comparatively easy and cost effective as well. Thus, DG is used for charging EVs, especially during peak hours.

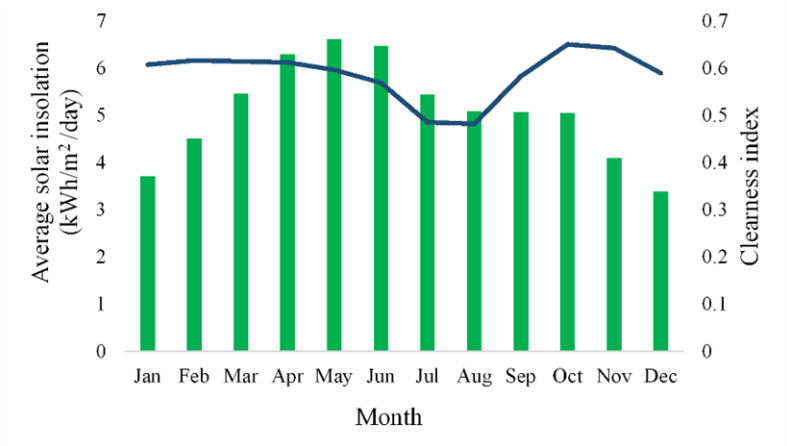

Fig. 7. 5. Annual variation of solar insolation and clearness index of the selected area

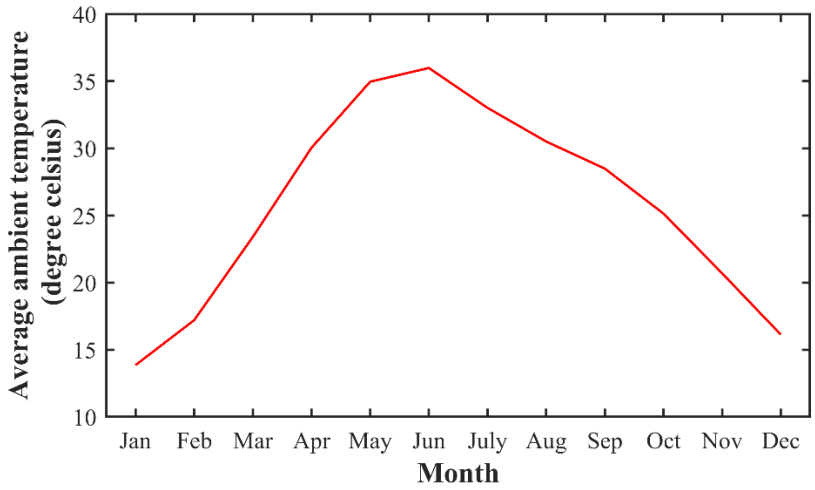

Fig. 7. 6. Annual variation of the mean temperature of the selected area

3) Assessment of the EVCS Load in the Selected Area

The research study considers three-wheeler EVs, i.e., e-rickshaw, to be the system's load. Four 12-Volt lead-acid batteries with capacities of 160 to 180 Ampere hour are used in a three-wheeler. The theoretical battery energy is 2.2 kWh when the 12 V and 180 Ampere hour battery is considered. Generally, a 12 V battery is recharged to 90% of its design capacity. As a result, the battery's energy would be 1.94 kWh. The total energy consumption for four 12 V battery vehicles, such as e-rickshaws, would be 7.8 kWh. Taking the system's 15% system losses into account, the energy consumed is determined to be 9 kWh. Thus, the energy consumed by every e-rickshaw per day is 9 kWh. According to the re-search findings, the yearly average energy is 257 kWh/day, the average power is 10.71 kW, and the maximum load is 25.45 kW. A graphical representation of the EVCS load on an hourly and daily basis is shown in Figs 7.7 and 7.8, respectively.

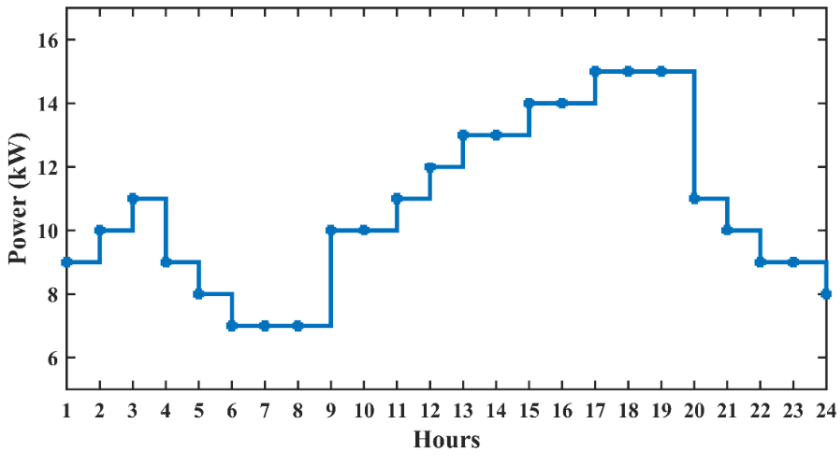

Fig. 7. 7. EVCS load profile on a daily basis

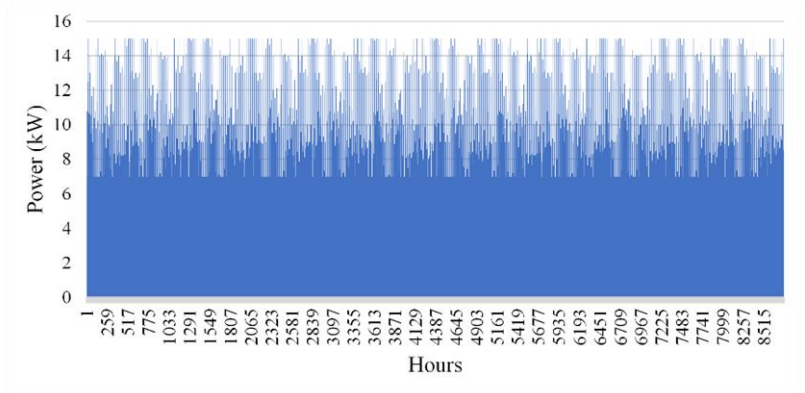

Fig. 7. 8. EVCS load profile on an hourly basis

7.4.2 Simulation Outcomes and Main Findings

This section evaluates the technical and economic parameters for three different scenarios using HOMER software and the proposed HGWOPSO technique. These scenarios are SPV and DG-based EVCS, only SPV-based EVCS, and grid-and-SPV-based EVCS. The objective is to achieve the best EVCS design by reducing the total net present cost, levelized cost of energy while keeping the lack of power supply probability within limits, accounting for environmental emissions, and different energy supply options. The outcomes are estimated in terms of TNPC, LCOE, SPV energy, the contribution of DG, battery and converter capacity, additional electricity generation, and the proportion of renewables utilized. The study then compares a hybrid energy system with a grid

connection to a standalone system. The analysis of the obtained results for different scenarios is summarized in the latter part of this section. Furthermore, to demonstrate the efficacy of meta-heuristic techniques, different algorithms are used to analyze the results and are compared and contrasted with HOMER results. The three different scenarios considered are as follows:

Scenario 1: Solar PV and diesel generator–based EVCS

This scenario addresses "range anxiety," a prevalent consideration among EV users about the vehicle's range. EV users can schedule long trips with greater certainty if an EVCS is as easily accessible as a petrol pump. Hence, the layout of an EVCS on roadways with SPV, DG, and a BESS with the different electricity providers is investigated and considered as Scenario 1. The goal is to reduce the capital, operation and maintenance, replacement, and fuel cost of every component associated with the system. The size and number of the SPV, DG, battery, and converter are considered to be the decision variable of the optimization problem.

Scenario 2: Only Solar PV–based EVCS

In some countries, such as Saudi Arabia, the DG acts as a primary source of energy. In such cases, the diesel option is a good example. On the other hand, DG units are prohibitively expensive due to the high costs of maintenance, fuel supply, and fuel transport. Furthermore, DGs emit a lot of pollution. Hence, SPV- and battery-based EVCS are also being investigated and considered as Scenario 2. In this scenario, the size and number of solar PVs and batteries are the only decision variables.

Scenario 3: Grid-and-solar PV–based EVCS

In this scenario, the EVCS is supposed to be grid-connected, and solar PV, battery, and grid are the various energy supply sources. Because EVCS is grid connected, it can purchase/sell power from/to the grid network, and the design is improved to account for the EVCS's net costs. The price of electricity provided in the Feed-in Tariff program of New Delhi, India, is taken into account for drawing/selling power from/to the utility grid. Feed-in Tariffs are the rates charged to RE providers for the energy provided by their power plants. The evaluating model is distinguished by project length and technology method and offers a profitable return on investment. The Feed-in-Tariff is a standard rate for the buying and selling of power from and to the grid network throughout the agreement, whereas the Time-of-Use Tariff is only pertinent to buyers, in contrast to Feed-in Tariffs, and varies throughout the day over time. In this work, Feed-in Tariffs are considered.

1) Techno–Economic Analysis of Different Scenarios Using HOMER Software

HOMER is used to model the hybrid energy system to meet the load demand. HOMER defines weather information, different parametric values of components used, and EVCS load profile. Many different assumptions are made to attain the optimal plan that decreases the TNPC, LCOE, while maintaining restrictions, such as supply continuity. It is worth noting that the information related to cost is indicated in USD.

Table 7.2 shows the results obtained for Scenario 1, i.e., SPV/DG/battery system. SPV makes a significant contribution of 1,22,864 kWh per year and operates for 4,369 h per year, while the DG constitutes 2767 kWh per year and functions for 364 h per year. To operate optimally, this system makes use of 590 batteries and a 12.1 kW bi-directional

converter. The obtained system has a TNPC of USD 6,38,917.29, an initial capital cost of USD 3,75,855, and an operating cost of USD 16,144.69. The LCOE for this configuration is calculated to be USD 0.6328/kWh. Furthermore, the NPC of SPV and diesel generator is 42.8 percent and 11.1 percent of TNPC, respectively, whereas the NPC of the bi-directional converter is only 0.58 percent of TNPC.

Table 7. 2 Results attained using HOMER software for Scenario 1

Parameter	Value
SPV (kWh/Year)	122,864
DG (kWh/Year)	2767
Batteries Used	590
Converter (kW)	12.1
Initial Capital Cost (USD)	375,855
Operating Cost (USD)	16,144.69
TNPC (USD)	638,917.29
LCOE (USD/kWh)	0.6328
% Of Renewable Utilized	96.5

Similarly, Tables 7.3 and 7.4 display the outcomes of Scenarios 2 and 3, respectively. When the only energy-producing source is an SPV and a battery, the LCOE is USD 0.7318/kWh, the TNPC is USD 8,75,481.24. In Scenario 3, when the grid is used to meet load demand, the LCOE is USD 0.587/kWh, and the TNPC is USD 2,75,349. In this scenario, the energy produced by SPV is 126811 kWh per year, accounting for 71.3 percent of total energy production, while energy purchased from the grid is 51155 kWh per year, accounting for 28.7 percent of total energy generation.

Table 7. 3. Results attained using HOMER software for Scenario 2

Parameter	Value
SPV (kWh/Year)	298,911
Batteries Used	590
Converter (kW)	–
Initial Capital Cost (USD)	647,261
Operating Cost (USD)	14,079.41
TNPC (USD)	875,481.24
LCOE (USD/kWh)	0.7318
% Of Renewable Utilized	100

Table 7. 4. Results attained using HOMER software for Scenario 3

Parameter	Value
SPV (kWh/Year)	126,811
Batteries Used	590
Grid Purchase (kWh/Year)	51,155
Converter (kW)	49.4
Initial Capital Cost (USD)	228,402
Operating Cost (USD)	2705
TNPC (USD)	275,349
LCOE (USD/kWh)	0.587
% Of Renewable Utilized	70.1

2) Techno-Economic Analysis of Different Scenarios Using Meta-Heuristic Algorithms

This section contains a summary of the optimization results obtained using various meta-heuristic techniques, as well as a comparison of those results for the various scenarios. The HGWOPSO, GWO, and PSO are used in 30 separate runs with a population size of 50 and a maximum iteration of 100, with the best results cropped.

- **Techno–economic analysis for Scenario 1 (SPV and DG–based EVCS)**

Table 7.5 shows a comparison of results for Scenario 1 using HGWOPSO, GWO, and PSO in terms of LCOE, TNPC, and computational time. According to Table 7.5, HGWOPSO has the lowest TNPC, LCOE, and computational time with USD 584,566.44,

USD 0.4822/kWh, and 27,615.716 sec, respectively, due to its lower capital, replacement, and operation and maintenance costs. HGWOPSO takes less time than other compared techniques and gives minimum TNPC and LCOE as well. GWO comes in the second place, with high TNPC, LCOE, and taking more time to compute the results as compared to HGWOPSO, whereas PSO gives a high value of TNPC, LCOE, and is slowest in comparison to the previous two meta-heuristic techniques. This system necessitates 232 SPV panels with 325 W energy, 3284 kWh of energy production per year from a diesel generator rated at 10 kW, 650 battery units, and 9 bi-directional converters rated at 100 kW. The maximum energy flow from the DC bus to the AC bus or vice versa determines the energy of a bi-directional converter.

Table 7. 5. Comparative study of achieved outcomes using meta-heuristic techniques for Scenario 1

Parameter	Value		
	HGWOPSO	GWO	PSO
Solar PV (325 W)	232	220	190
DG Power Production (kWh/Year)	3284	3056	2859
Batteries	650	580	610
Converter (100 kW)	9	9	9
TNPC (USD)	5,84,566.44	6,04,482.82	6,77,615.38
LCOE (USD/kWh)	0.4822	0.5381	0.6328
Computational Time (Sec)	27,615.716	29,834.165	37,656.673

Fig. 7.9. depicts hourly information about power generation for a three-day sample (1–3 October). It is observed that maximum EVs are charged during night hours, and there is no solar output available during that time. Hence, the energy requirement is fulfilled by DG and BESS using energy flow through the converter, as indicated in Fig. 7.9. When PV power generates more than the load demand during the day, surplus electricity is used to charge the battery (Fig. 7.9). Despite having a higher SPV energy, the converter energy is

much lower in this context of system sizing. The amount of excess electricity produced in this scenario is 25,053 kWh per year, which is 19.2 % of total generated energy. It is worth noting that, despite the fact that the maximum energy shortage was set to zero, there was only a 23.7 kWh unmet load throughout the simulation model, accounting for 0.02 percent of the total load.

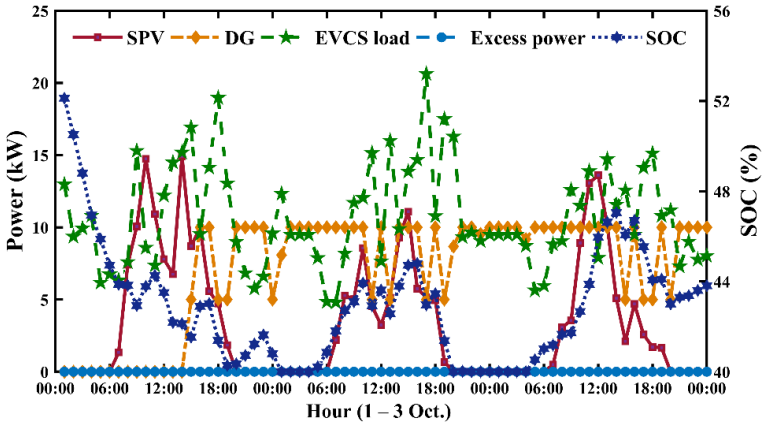

Fig. 7. 9. Power analysis on an hourly basis of SPV/DG/battery system

Fig. 7.10. depicts a cost description of various system components for the SPV/DG/battery system. The SPV module and battery entail the most capital investment. Despite the fact that the BESS has a high cost of replacement over the project's lifespan, the resource cost is significantly more than the investment. As a result, this hybrid energy system needs constant economic infusion to keep the system running properly.

As shown in Fig. 7.11., the DG contributes significantly when the load demand is high. The monthly average power production from the SPV module is lesser in summer weather in comparison to winter because of continuous rain and clouds in the summertime. Further, the effectiveness of the proposed algorithm, i.e., HGWOPSO, can be proved using Fig. 7.12. It has better convergence than other algorithms and results in a lower LCOE value.

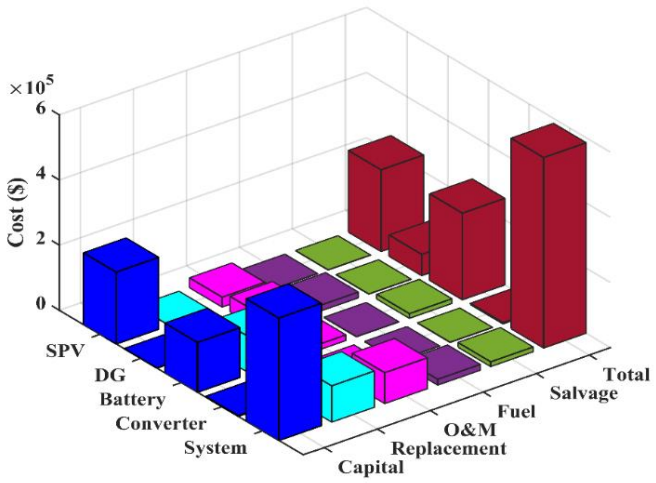

Fig. 7. 10. Cost description of the various system components for the SPV/DG/battery system

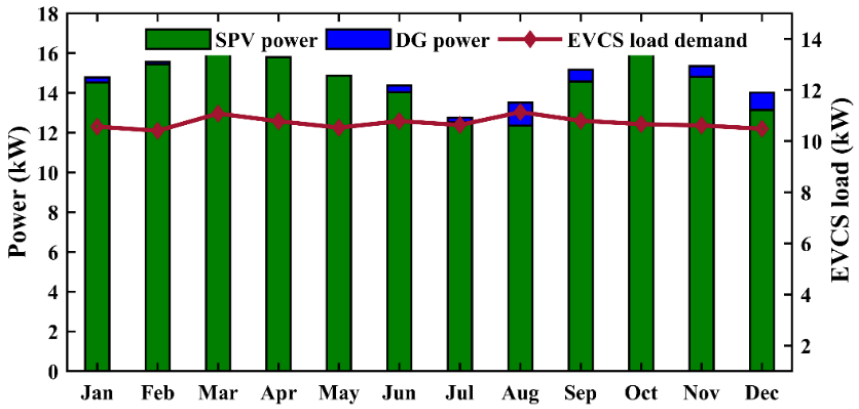

Fig. 7. 11. Monthly average power share for satisfying EVCS load demand in SPV/DG/battery system

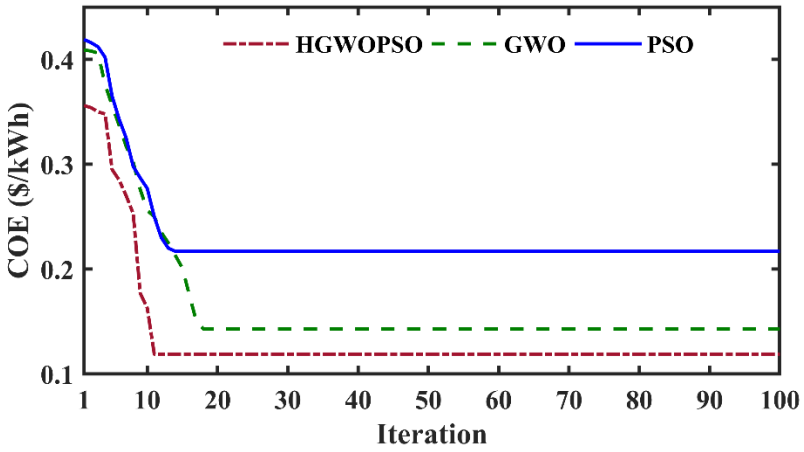

Fig. 7. 12. Convergence curves of different optimizers

- **Techno–economic analysis for Scenario 2 (only solar PV/battery-based EVCS)**

In Scenario 2, diesel generator is not available, and solar PV is the only energy source available to meet the EVCS load requirement. This PV/battery system has the greatest LCOE and TNPC because it uses a larger PV module and battery storage to meet power demands, which increases the cost and produces more surplus power (194,140 kWh per year). Table 7.6 provides the different technical and economic parameters optimized by various algorithms for SPV/battery system.

Table 7. 6. Comparative study of achieved outcomes using meta-heuristic techniques for Scenario 2

Parameter	Methods Used		
	HGWOPSO	GWO	PSO
Solar PV (325 W)	545	490	415
Batteries	548	518	476
Converter (100 kW)	12	12	12
TNPC (USD)	843,461.28	902,761.37	981,736.38
LCOE (USD/kWh)	0.6844	0.7045	0.7167
Computational Time (Sec)	25,284.342	29,451.984	35,324.673

As in Scenario 1, computation time taken by HGWOPSO is less as compared to other techniques. This system requires 545 solar PV panels with 325 W energy, 548 battery units, and 12 bi-directional converters rated at 100 kW. HGWOPSO gives better results when equated with other techniques and, hence, proved its efficacy to solve various optimization problems. The hourly information about power generation for a three-day sample for SPV/battery system is depicted in Fig. 7.13. The cost description of the various system components for the SPV/battery system is shown in Fig.7.14.

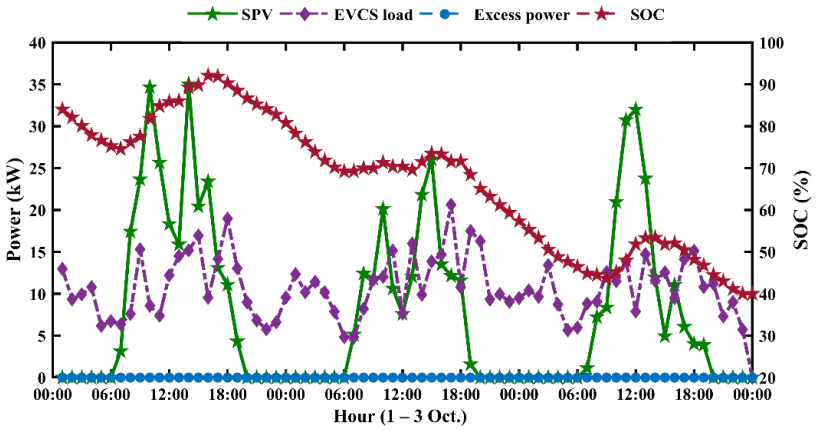

Fig. 7. 13. Power analysis on an hourly basis of SPV/battery system

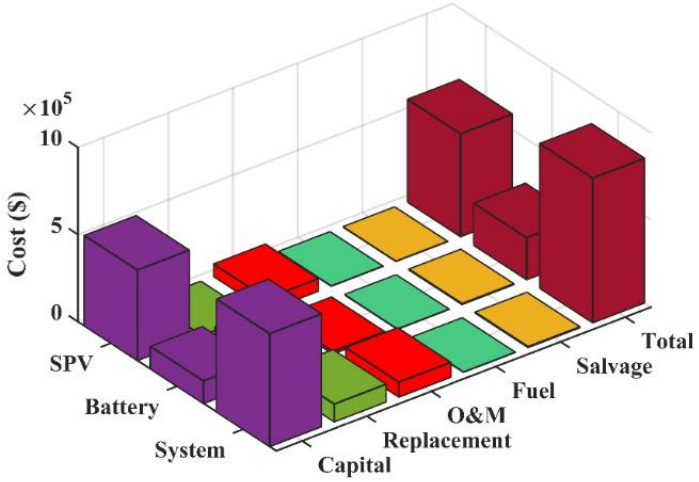

Fig. 7. 14. Cost description of the various system components for the SPV/battery system

- **Techno–economic analysis for Scenario 3 (grid-and-solar PV-based EVCS)**

This scenario looks at the technological, economic, and environmental concerns of hybrid energy systems connected to the grid. In this strategy, electricity is purchased from the grid to meet power requirements when solar PV is unable to fulfill them. Excess power is sold back to the grid, requiring a small storage capacity while leveraging the monumental amount of additional energy dumped in hybrid energy options. In this respect, a fixed grid power price is chosen to be $ 0.12/kWh and a fixed grid sell back price is selected to be USD 0.08/kWh. According to the results in Table 7.7, the grid-connected solar PV-based

EVCS has a significantly lower LCOE (0.119/kWh) than the solar PV and diesel generator-based EVCS ($ 0.482/kWh) and solar PV/battery-based EVCS ($ 0.684/kWh). The hybrid energy system in Scenarios 1 and 2 requires more resources and battery storage than the grid-connected system. whereas in the grid-connected system, net grid purchase is zero, i.e., the amount of energy purchased from the grid is equal to the amount of energy sold to the grid, and no battery storage is required. Despite having a 232 PV module of 325 W energy and a 49.4 kW bi-directional converter, the grid-connected hybrid system needs no battery storage and has insubstantial energy costs due to a significantly lower LCOE ($ 0.119/kWh) compared to a solar PV and diesel generator-based EVCS ($ 0.482/kWh) and solar PV/battery-based EVCS ($ 0.684/kWh). It is also worth noting that HGWOPSO has a lower TNPC ($ 263377) and LCOE ($ 0.119/kWh) than GWO and PSO. More prominently, the extra electricity in the grid-connected system (408 kWh/year) is considerably lower than in the solar PV and diesel generator-based EVCS (25,053 kWh/year) and solar PV/battery-based EVCS (1,94,140 kWh/year). This is because a large portion of excess energy is sold back to the grid, and only a few storage devices are needed to meet the requirement when solar power is not available.

When solar power is not accessible, grid power meets the load requirements. According to Fig. 7.15, the spring season necessitates a high amount of energy to be purchased from the grid due to higher power requirements. India, as a tropical country, has nearly equal solar exposure all year. Even though the summer season is supposed to generate more electricity from solar PV, rainy days lead to decreasing SPV production than the rest of the regular time of year.

Solar energy accounts for approximately 71.3 percent of total energy demand, with grid power accounting for the remaining 28.7 percent. Fig. 7.16. depicts the time series data for various components used to satisfy the load demand. The cost description of the various system component for the grid-and-solar PV-based EVCS is shown in Fig. 7.17. The monthly average energy purchased/sold from/to the grid is portrayed in Fig. 7.18.

Table 7. 7. Comparative study of achieved outcomes using meta-heuristic techniques for Scenario 3

Parameter	Methods Used		
	HGWOPSO	GWO	PSO
Solar PV (325 W)	232	218	196
Grid Purchase (kWh/Year)	51,155	52,671	54,367
Grid Sales (kWh/Year)	77,135	76,432	76,197
Converter (100 kW)	2	2	2
TNPC (USD)	263,377	276,543	298,654
LCOE (USD/kWh)	0.119	0.143	0.217
Computational Time (Sec)	29,812.873	30,341.457	32,349.952

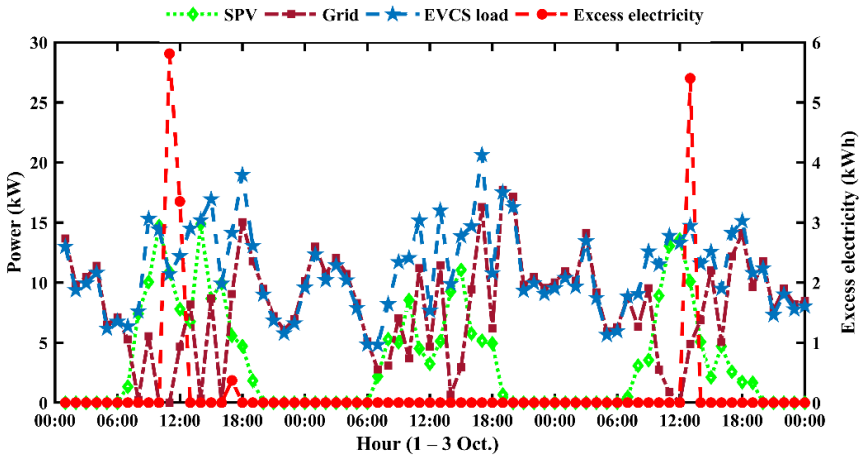

Fig. 7. 15. Power analysis on an hourly basis for grid-and-solar PV-based EVCS

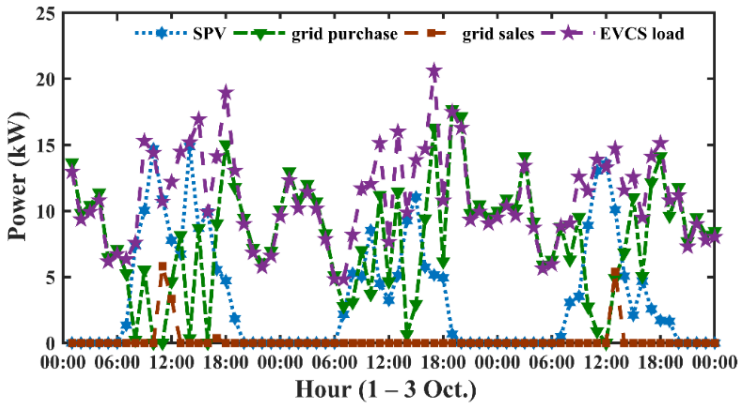

Fig. 7. 16. Time series data for various components used to satisfy the load demand

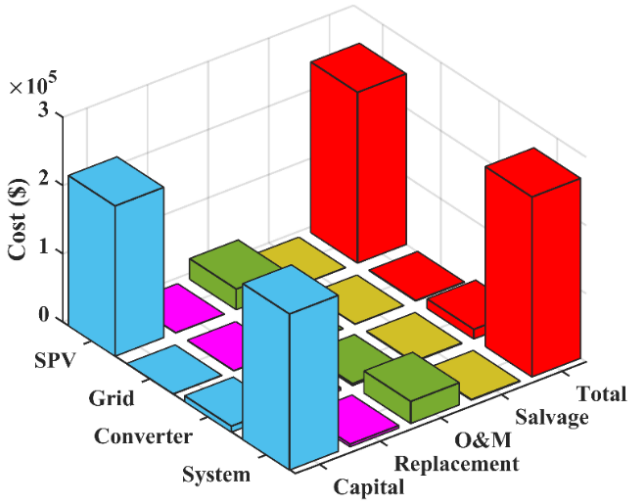

Fig. 7. 17. The cost-wise breakup of different components in grid-and-solar PV-based EVCS

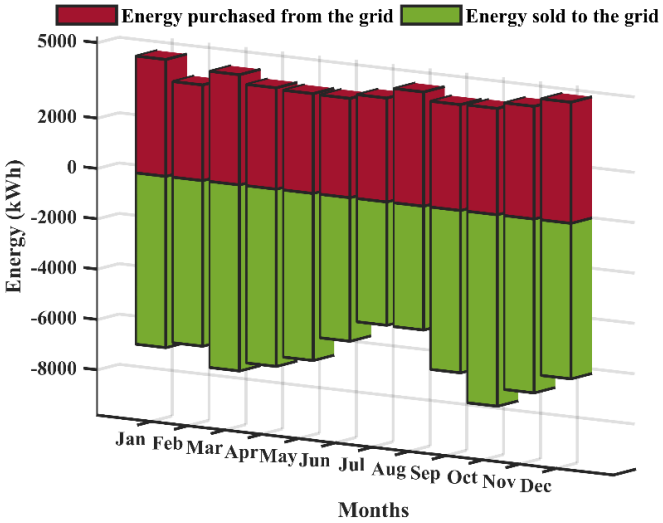

Fig. 7. 18. Monthly average energy purchased from the grid and sold to the grid

- **Impact of grid purchase and grid sales on LCOE**

The implications of energy buying from grid infrastructure and the quantity of energy being sold to the grid on the LCOE are outlined and discussed in this section. A net grid procurement of 0% indicates that the quantity of energy buying from and sold back to the grid is the same. The value of LCOE increases more with increasing purchases from the grid than with increasing grid sell-back, as shown in Fig. 7.19.

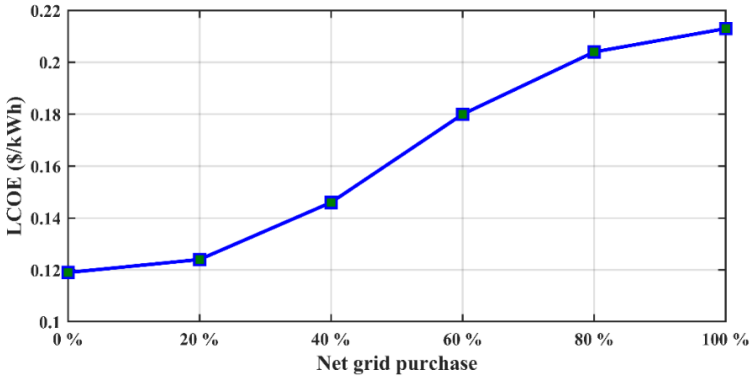

Fig. 7. 19. Impact of net grid purchase on LCOE

According to Fig. 7.19, an increase in grid energy to fulfill load demand leads to an increase in LCOE. For example, a 50% increase in grid energy purchase versus selling back to the grid results in a 36% increase in LCOE.

- **Analysis of the Environmental Emissions in Different Scenarios**

As previously stated, one of the primary goals of this work is to lower emissions by utilizing renewable technologies. The results displayed in Table 7.8. show that SPV/battery-based EVCS (Scenario 2) reduces the overall emissions by a significant amount when equated to all other cases. However, while the SPV/DG/battery-based EVCS (Scenario 1) produces higher emissions than SPV/battery-based EVCS, it will be far more ecologically friendly than the grid-and-SPV-based EVCS.

Table 7. 8. Scenario-wise comparison of environmental emissions

Pollutants	Scenario 1	Scenario 2	Scenario 3
Carbon dioxide (CO_2) (kg/year)	2910	2417	32330
Carbon monoxide (CO) (kg /year)	22	0	0
Unburned hydrocarbons (UHC) (kg /year)	0.802	0	0
Particulate matter (PM) (kg/year)	1.33	0	0
Sulphur dioxide (SO_2) (kg/year)	7.14	4.94	140
Nitrogen dioxide (NO_x) (kg/year)	25	0	68.5

7.5 SUMMARY

Hybrid energy systems can deliver energy to the grid and off-grid sites cost effectively and reliably. The efficiency of the system improves when RE components are implemented with the grid. In this chapter, the complete mathematical modeling is presented for the diverse configurations of the hybrid energy system to meet the load requirements of EVCS situated in the northwest region of Delhi, India. The financial, technological, and ecologic implications of different configurations are also carefully investigated. The use of meta-heuristic methods, which include HGWOPSO, GWO, and PSO, is carried out to optimize the objective functions. The obtained results using HGWOPSO are compared with HOMER software and other techniques. According to comparisons, HGWOPSO gives a more efficient solution than HOMER. Furthermore, the HGWOPSO offers a robust framework, which aids model development. In all three configurations, the HGWOPSO results in reduced LCOE values of $ 0.482/kWh, $ 0.684/kWh, and $ 0.119/kWh, respectively. According to the analysis, the grid-connected solar PV-based EVCS offers significant cost savings over the other two configurations. In addition, a hybrid energy system with equal grid purchase and sell-back can be a profitable choice. More significantly, the LCOE associated with the grid selling back schemes is

lower than the grid purchase price. The results show that a 60% increase in grid sell-back price leads to a 46% decrease in LCOE.

The feasibility analysis discussed in this work can be used to guide the development and operation of hybrid energy system applications in distant regions where grid utility is not accessible, as well as hybrid grid-connected systems in India. Future research is needed to investigate the impacts of charging/discharging cycles of a battery on its lifespan and cost of energy.

.

CHAPTER 8

CONCLUSION AND FUTURE SCOPE OF WORK

8.1 CONCLUSION

In this thesis, various meta-heuristic techniques have been developed and implemented on number of problems such as allocation of EVCS, DG and capacitors. These techniques involve PSO, GWO and hybrid of PSO and GWO i.e., HGWOPSO. PSO has low convergence, implying exploitation in large search spaces, whereas GWO has low solving precision, implying exploration. As a result, these swarm intelligence techniques, namely PSO and GWO, require modifications to improve their ability to find the best solution. For the sizing problem, a HGWOPSO has been developed. A performance-based comparison of the GWO with the HGWOSPO is presented using various benchmark functions. When the nonlinearity and stochastic nature of renewable energy sources and EV load are mathematically modelled, the computational speed and convergence of the HGWOPSO technique is found to be better.

A new approach for solving the multi-objective optimization problems for optimal siting and sizing of EVCS in different areas in South Delhi, New Delhi, India is presented. GWO has been utilized to solve the multi-objective cost functions and the obtained results are compared with PSO for validation purposes. The cost function includes investment cost, CS electrification cost, EV energy loss cost, and travel time cost. Investment cost and CS electrification cost of all CSs have been calculated and found that the investment cost strongly depends on the land cost and the number of connectors used in each CS. While

CS electrification cost depends on the distance between the CS and electric substation. On the other hand, EV energy loss cost and travel time cost have been evaluated for all EVs. It is revealed that travel time cost and EV energy loss cost depends on the distance between the CS and EV location. After comparing the results obtained using GWO and PSO, it is revealed that GWO is more effective than PSO for the considered case study.

Further, HGWOPSO algorithm is suggested to lessen the active power losses, maximizing the net profit and improving the reliability of system with different penetration level of EVs in V2G. The results have revealed that the optimum planning of EVCS elevates power loss and lowers the voltage in electrical power networks. The results have demonstrated that the optimum planning of capacitor after incorporating CS in the network minimizes power loss and also improves voltage profile. Capacitors are employed closer to EVCS and end of feeders for the enhancement of voltage profile and loss by contributing some reactive power. It is also shown that, different percentage of EVs participated in V2G mode improved the active power flows, voltage profile and reduces the active power loss of the network. The proposed algorithm is applied on 33-bus and 34-bus system. The hybrid method showed superiority against discrete PSO and GWO, by lessening the power losses, enhancing voltage profile, maximizing the net profit and improving the reliability benefit. The hybrid method has reduced power losses for almost 31% as compared to GWO (29.74%) and PSO (29.42%) for 33-bus system. The proposed hybrid approach achieves reliability improvement benefit of $ 169451.4 which is $ 1274 and $ 1396 more than that of GWO and PSO respectively. Similarly, for 34 bus system, the proposed technique results in loss reduction of 27.6% while GWO and PSO reduces the power losses by 25.7% and 24.2% respectively. Furthermore, HGWOPSO results in more improvement in reliability

benefit i.e., ($ 484871.25) as compared with other techniques i.e., GWO ($ 481584.15) and PSO ($ 481093.57).

Moreover, this chapter presents the EVCS impact on the IEEE standard system based on a direct approach-based load flow analysis. The process of charging electric vehicles necessitates additional power from the grid, resulting in greater power losses. As a result, DG should be employed to offset the power losses generated by EVCS. Type 2 DG is utilized in this work, which repays for the system's power loss. Furthermore, a hybrid algorithm called HGWOPSO has been employed to reduce losses by determining the optimal node for EVCS and DG placement. The proposed hybrid algorithm is validated on the IEEE-33 and IEEE-69 bus systems. Additionally, the accuracy of the suggested method is validated by comparing the outcomes acquired using other methodological approaches such as GWO and PSO. It is observed that HGWOPSO shows a significant reduction in system losses when compared to GWO and PSO for 33-bus as well as 69-bus systems. In addition, reliability analysis is performed to determine the cumulative influence of EV loads and DGs on the distribution system's health. All reliability indices are investigated in different scenarios. It is noticed that the placement of EVCS degrades the reliability of the network in 33-bus and 69-bus systems. However, results show that the DGs incorporation along with EVCS improves the reliability indices.

The complete mathematical modeling is presented for the diverse configurations of the hybrid energy system to meet the load requirements of EVCS situated in the northwest region of Delhi, India. The financial, technological, and ecologic implications of different configurations are also carefully investigated. The use of meta-heuristic methods, which include HGWOPSO, GWO, and PSO, is carried out to optimize the objective functions.

The obtained results using HGWOPSO are compared with HOMER software and other techniques. According to comparisons, HGWOPSO gives a more efficient solution than HOMER. Furthermore, the HGWOPSO offers a robust framework, which aids model development. In all three configurations, the HGWOPSO results in reduced LCOE values of $ 0.482/kWh, $ 0.684/kWh, and $ 0.119/kWh, respectively. According to the analysis, the grid-connected solar PV-based EVCS offers significant cost savings over the other two configurations. In addition, a hybrid energy system with equal grid purchase and sell-back can be a profitable choice. More significantly, the LCOE associated with the grid selling back schemes is lower than the grid purchase price. The results show that a 60% increase in grid sell-back price leads to a 46% decrease in LCOE.

8.2 FUTURE SCOPE

- The proposed work may be advanced by the reconfiguration of radial distribution system after introducing EVCS and capacitor for further reduction in system's losses. Valley filling and peak clipping of load curves are two demand side management strategies that can be used by proper management of EVCS to flatten the load curve of the system.
- The use of a stochastic approach can be developed to construct the EV load at charging stations in order to estimate the impact of increased EV demand on the distribution system. Furthermore, rather than conventional DGs, renewable-based DGs, such as solar/wind, may be included. Additionally, coupled transportation and distribution networks can be taken as a test system.

- A more systematic approach to charging station location issues could be investigated, taking into account EV consumers' activity-based behavior.
- To investigate the impacts of charging/discharging cycles of a battery on its lifespan and cost of energy which can be used to guide the development and operation of hybrid energy system applications in distant regions where grid utility is not accessible.

LIST OF PUBLICATIONS

- **List of papers (s) published in Peer Reviewed Referred International Journals**

1. M. Bilal and M. Rizwan, "Integration of electric vehicle charging stations and capacitors in distribution systems with vehicle-to-grid facility," *Energy Sources, Part A Recover. Util. Environ. Eff.*, pp. 1–30, May 2021, doi: 10.1080/15567036.2021.1923870. (Published)
   [Impact Factor: 3.447 (SCI Indexed)]

2. M. Bilal and M. Rizwan, "Intelligent Algorithm based Efficient Planning of Electric Vehicle Charging Station: A Case Study of Metropolitan City of India," *Sci. Iran.*, Aug.2021, doi: 10.24200/sci.2021.57433.5238. (Accepted)
   [Impact Factor: 1.435 (SCIE Indexed)]

3. M. Bilal and M. Rizwan, "Electric vehicles in a smart grid: a comprehensive survey onoptimal location of charging station," *IET Smart Grid*, vol. 3, no. 3, pp. 267–279, Jun.2020, doi: 10.1049/iet-stg.2019.0220. (Published)
   Scopus Indexed

- **List of Paper(s) Published in Peer Reviewed International Conference**

1. M. Bilal and M. Rizwan, "Opportunities and Challenges in Solar Photovoltaic-Based Electric Vehicles Charging Stations: A Step Toward Smart Cities Development," *Advances in Energy Technology*, vol 766, pp. 507-516, 2022. https://doi.org/10.1007/978-981-16-1476-7_46. **[Scopus Indexed]**
2. M. Bilal and M. Rizwan, "Improved Grey Wolf Optimization Approach for Electric Vehicles Charging Infrastructure," *in 2021 International Electrical & Electronics Engineering Conference (IEEEC)*, pp. 1-6, 2021.

List of other publications

Journals:

1. M. Bilal, M. Rizwan, I. Alsaidan, and F. M. Almasoudi, "AI-Based Approach for Optimal Placement of EVCS and DG With Reliability Analysis," *IEEE Access*, vol. 9,pp.154204–154224, 2021, doi: 10.1109/ACCESS.2021.3125135. **[Impact Factor: 3.367 (SCI Indexed)]**
2. M. Bilal, I. Alsaidan, M. Alaraj, F. M. Almasoudi, and M. Rizwan, "Techno-Economic and Environmental Analysis of Grid-Connected Electric Vehicle Charging Station Using AI-Based Algorithm," *Mathematics*, vol. 10, no. 6, p. 924, Mar. 2022, doi: 10.3390/math10060924. **[Impact Factor: 2.258 (SCIE Indexed)]**

Conferences:

1. M. Bilal, A. Kumar, and M. Rizwan, "Coordinated Allocation of Electric Vehicle Charging Stations and Capacitors in Distribution Network," in *2021 IEEE 2nd International Conference on Electrical Power and Energy Systems (ICEPES)*, Dec. 2021, pp. 1–6, doi: 10.1109/ICEPES52894.2021.9699775. **[Scopus Indexed]**
2. A. Kumar, M. Bilal, M. Rizwan, and U. Nangia, "Grey Wolf Optimization Inspired Maximum Power Extraction from SPV System for Water Pumping Application," in *2022 International Conference for Advancement in Technology (ICONAT)*, Jan. 2022, pp. 1–6, doi: 10.1109/ICONAT53423.2022.9726028. **[Scopus Indexed]**

REFERENCES

[1] A. Cooper and K. Schefter, "Electric vehicle sales forecast and the charging infrastructure required through 2030," *Inst. Electr. Innov.*, pp. 1–16, 2018.

[2] "World Research Institute (Climate Analysis Indicators Tool (CAIT))".

[3] "WHO Global Ambient Air Quality Database".

[4] S. Deb, K. Tammi, K. Kalita, and P. Mahanta, "Review of recent trends in charging infrastructure planning for electric vehicles," *WIREs Energy Environ.*, vol. 7, no. 6, Nov. 2018, doi: 10.1002/wene.306.

[5] "Statista Research Department."

[6] Z. A. S. Martin Geske, Przemyslaw Komarnicki, Martin Stötzer, "Modeling and simulation of electric car penetration in the distribution power system — Case study," *Mod. Electr. Power Syst.*, pp. 1–6, 2010.

[7] P. Juanuwattanakul and M. A. S. Masoum, "Identification of the weakest buses in unbalanced multiphase smart grids with Plug-in Electric Vehicle charging stations," in *2011 IEEE PES Innovative Smart Grid Technologies*, Nov. 2011, pp. 1–5, doi: 10.1109/ISGT-Asia.2011.6167155.

[8] R. Shi, X. P. Zhang, D. C. Kong, N. Deng, and P. Y. Wang, "Dynamic impacts of fast-charging stations for electric vehicles on active distribution networks," in *IEEE PES Innovative Smart Grid Technologies*, May 2012, pp. 1–6, doi: 10.1109/ISGT-Asia.2012.6303270.

[9] M. M. Rahman, S. Barua, S. T. Zohora, K. Hasan, and T. Aziz, "Voltage sensitivity based site selection for PHEV charging station in commercial distribution system," in *2013 IEEE PES Asia-Pacific Power and Energy Engineering Conference (APPEEC)*, Dec. 2013, pp. 1–6, doi: 10.1109/APPEEC.2013.6837191.

[10] Y. Zhang, X. Song, F. Gao, and J. Li, "Research of voltage stability analysis method in distribution power system with plug-in electric vehicle," in *2016 IEEE PES Asia-Pacific Power and Energy Engineering Conference (APPEEC)*, Oct. 2016, pp. 1501–1507, doi: 10.1109/APPEEC.2016.7779740.

[11] G. Ma, L. Jiang, Y. Chen, C. Dai, and R. Ju, "Study on the impact of electric vehicle charging load on nodal voltage deviation," *Arch. Electr. Eng.*, vol. 66, no. 3, pp. 495–505, Sep. 2017, doi: 10.1515/aee-2017-0037.

[12] S. Suganya, S. C. Raja, and P. Venkatesh, "Simultaneous coordination of distinct plug-in Hybrid Electric Vehicle charging stations: A modified Particle Swarm Optimization approach," *Energy*, vol. 138, pp. 92–102, Nov. 2017, doi: 10.1016/j.energy.2017.07.036.

[13] J. de Hoog *et al.*, “The importance of spatial distribution when analysing the impact of electric vehicles on voltage stability in distribution networks,” *Energy Syst.*, vol. 6, no. 1, pp. 63–84, Mar. 2015, doi: 10.1007/s12667-014-0122-8.

[14] P. W. Dean McCarthy, “The HV System Impacts of Large Scale Electric Vehicle Deployments in a Metropolitan Area,” *20th Australas. Univ. Power Eng. Conf. Christchurch*, pp. 1–6, 2010, doi: The HV system impacts of large scale electric vehicle deployments in a metropolitan area.

[15] Y. Fan, C. Guo, P. Hou, and Z. Tang, “Impact of Electric Vehicle Charging on Power Load Based on TOU Price,” *Energy Power Eng.*, vol. 05, no. 04, pp. 1347–1351, 2013, doi: 10.4236/epe.2013.54B255.

[16] T. Gnann, A.-L. Klingler, and M. Kühnbach, “The load shift potential of plug-in electric vehicles with different amounts of charging infrastructure,” *J. Power Sources*, vol. 390, pp. 20–29, Jun. 2018, doi: 10.1016/j.jpowsour.2018.04.029.

[17] F. Li, H. Guo, Z. Jing, Z. Wang, and X. Wang, “Peak and valley regulation of distribution network with electric vehicles,” *J. Eng.*, vol. 2019, no. 16, pp. 2488–2492, Mar. 2019, doi: 10.1049/joe.2018.8540.

[18] M. H. Bollen, “Understanding power quality problems,” *Piscataway, USA*, pp. 1–35, 2000.

[19] X. Z. and Y. M. Z. Gao, H. Zhao, “Summary of power system harmonics,” *29th Chinese Control Decis. Conf. (CCDC), Chongqing, China*, pp. 2287–2291, 2017.

[20] J. Lamoree, D. Mueller, P. Vinett, W. Jones, and M. Samotyj, “Voltage sag analysis case studies,” *IEEE Trans. Ind. Appl.*, vol. 30, no. 4, pp. 1083–1089, 1994, doi: 10.1109/28.297926.

[21] M. F. McGranaghan, D. R. Mueller, and M. J. Samotyj, “Voltage sags in industrial systems,” *IEEE Trans. Ind. Appl.*, vol. 29, no. 2, pp. 397–403, 1993, doi: 10.1109/28.216550.

[22] F. De la Rosa, “Harmonics and power systems,” *Boca Rat. CRC Press*, 2006.

[23] D. Shmilovitz, “On the definition of total harmonic distortion and its effect on measurement interpretation,” *IEEE Trans. Power Deliv.*, vol. 20, no. 1, pp. 526–528, 2005.

[24] P. T. Staats, W. M. Grady, A. Arapostathis, and R. S. Thallam, “A statistical analysis of the effect of electric vehicle battery charging on distribution system harmonic voltages,” *IEEE Trans. Power Deliv.*, vol. 13, no. 2, pp. 640–646, Apr. 1998, doi: 10.1109/61.660951.

[25] J. Niitsoo, P. Taklaja, I. Palu, and I. Kiitam, “Modelling EVs in residential distribution grid with other nonlinear loads,” in *2015 IEEE 15th International Conference on Environment and Electrical Engineering (EEEIC)*, Jun. 2015, pp. 1543–1548, doi: 10.1109/EEEIC.2015.7165401.

[26] A. Ul-Haq, C. Cecati, A. Ehsan, and K. Strunz, “Impact of electric vehicles on voltage profile and harmonics in a distribution network,” in *2015 First Workshop on Smart Grid and Renewable Energy (SGRE)*, Mar. 2015, pp. 1–6, doi: 10.1109/SGRE.2015.7208724.

[27] A. Lucas, F. Bonavitacola, E. Kotsakis, and G. Fulli, “Grid harmonic impact of multiple electric vehicle fast charging,” *Electr. Power Syst. Res.*, vol. 127, pp. 13–21, Oct. 2015, doi: 10.1016/j.epsr.2015.05.012.

[28] R. Godina, E. Rodrigues, J. Matias, and J. Catalão, “Effect of Loads and Other Key Factors on Oil-Transformer Ageing: Sustainability Benefits and Challenges,” *Energies*, vol. 8, no. 10, pp. 12147–12186, Oct. 2015, doi: 10.3390/en81012147.

[29] P. Grahn, J. Rosenlind, P. Hilber, K. Alvehag, and L. Soder, “A method for evaluating the impact of electric vehicle charging on transformer hotspot temperature,” in *2011 2nd IEEE PES International Conference and Exhibition on Innovative Smart Grid Technologies*, Dec. 2011, pp. 1–8, doi: 10.1109/ISGTEurope.2011.6162755.

[30] Q. Gong, S. Midlam-Mohler, V. Marano, and G. Rizzoni, “Study of PEV Charging on Residential Distribution Transformer Life,” *IEEE Trans. Smart Grid*, vol. 3, no. 1, pp. 404–412, Mar. 2012, doi: 10.1109/TSG.2011.2163650.

[31] S. Ge, L. Feng, and H. Liu, “The planning of electric vehicle charging station based on Grid partition method,” in *2011 International Conference on Electrical and Control Engineering*, Sep. 2011, pp. 2726–2730, doi: 10.1109/ICECENG.2011.6057636.

[32] L. Jia, Z. Hu, Y. Song, and Z. Luo, “Optimal siting and sizing of electric vehicle charging stations,” in *2012 IEEE International Electric Vehicle Conference*, Mar. 2012, pp. 1–6, doi: 10.1109/IEVC.2012.6183283.

[33] Z. Hu and Y. Song, “Distribution network expansion planning with optimal siting and sizing of electric vehicle charging stations,” in *2012 47th International Universities Power Engineering Conference (UPEC)*, Sep. 2012, pp. 1–6, doi: 10.1109/UPEC.2012.6398568.

[34] Y. Ahn and H. Yeo, “An Analytical Planning Model to Estimate the Optimal Density of Charging Stations for Electric Vehicles,” *PLoS One*, vol. 10, no. 11, p. e0141307, Nov. 2015, doi: 10.1371/journal.pone.0141307.

[35] Z. Liu, F. Wen, and G. Ledwich, “Optimal Planning of Electric-Vehicle Charging Stations in Distribution Systems,” *IEEE Trans. Power Deliv.*, vol. 28, no. 1, pp. 102–110, Jan. 2013, doi: 10.1109/TPWRD.2012.2223489.

[36] G. Liu, L. Kang, Z. Luan, J. Qiu, and F. Zheng, “Charging Station and Power Network Planning for Integrated Electric Vehicles (EVs),” *Energies*, vol. 12, no. 13, p. 2595, Jul. 2019, doi: 10.3390/en12132595.

[37] Z. Liu, W. Zhang, X. Ji, and K. Li, “Optimal Planning of charging station for electric vehicle based on particle swarm optimization,” in *IEEE PES Innovative Smart Grid Technologies*, May 2012, pp. 1–5, doi: 10.1109/ISGT-Asia.2012.6303112.

[38] M. C. S. Martins and F. C. L. Trindade, “Time series studies for optimal allocation of electric charging stations in urban area,” in *2015 IEEE PES Innovative Smart Grid Technologies Latin America (ISGT LATAM)*, Oct. 2015, pp. 142–147, doi: 10.1109/ISGT-LA.2015.7381143.

[39] Y.-W. Wang and C.-R. Wang, “Locating passenger vehicle refueling stations,” *Transp. Res. Part E Logist. Transp. Rev.*, vol. 46, no. 5, pp. 791–801, Sep. 2010, doi: 10.1016/j.tre.2009.12.001.

[40] F. Baouche, R. Billot, R. Trigui, and N.-E. El Faouzi, “Efficient Allocation of Electric Vehicles Charging Stations: Optimization Model and Application to a Dense Urban Network,” *IEEE Intell. Transp. Syst. Mag.*, vol. 6, no. 3, pp. 33–43, 2014, doi: 10.1109/MITS.2014.2324023.

[41] M. Hosseini and S. A. MirHassani, “Selecting optimal location for electric recharging stations with queue,” *KSCE J. Civ. Eng.*, vol. 19, no. 7, pp. 2271–2280, Nov. 2015, doi: 10.1007/s12205-015-0153-2.

[42] Z.-H. Zhu, Z.-Y. Gao, J.-F. Zheng, and H.-M. Du, “Charging station location problem of plug-in electric vehicles,” *J. Transp. Geogr.*, vol. 52, pp. 11–22, Apr. 2016, doi: 10.1016/j.jtrangeo.2016.02.002.

[43] X. Yan, C. Duan, X. Chen, and Z. Duan, “Planning of Electric Vehicle charging station based on hierarchic genetic algorithm,” in *2014 IEEE Conference and Expo Transportation Electrification Asia-Pacific (ITEC Asia-Pacific)*, Aug. 2014, pp. 1–5, doi: 10.1109/ITEC-AP.2014.6941087.

[44] C. Zhang and Y. Cheng, “Research on joint planning model for EVs charging/swapping facilities,” in *2016 China International Conference on Electricity Distribution (CICED)*, Aug. 2016, pp. 1–8, doi: 10.1109/CICED.2016.7576245.

[45] X. Tang, J. Liu, X. Wang, and J. Xiong, “Electric vehicle charging station planning based on weighted Voronoi diagram,” in *Proceedings 2011 International Conference on Transportation, Mechanical, and Electrical Engineering (TMEE)*, Dec. 2011, pp. 1297–1300, doi: 10.1109/TMEE.2011.6199443.

[46] X. Fan, Y. Guo-Qin, Lin-Feng, G., “Tentative analysis of layout of electrical vehicle charging stations,” *East China Electr. Power*, vol. 37, no. 10, pp. 1677–1682, 2009.

[47] J. Prasomthong, J. Ongsakul, W. Meyer, “Optimal placement of vehicle-to-grid charging station in distribution system using particle swarm optimization with time varying acceleration coefficient,” *Int. Conf. Green Energy Sustain. Dev. (ICUE), Pattaya, Thail.*, pp. 1–8, 2014.

[48] S. Chen, Y. Shi, X. Chen, and F. Qi, “Optimal location of electric vehicle charging stations using genetic algorithm,” in *2015 17th Asia-Pacific Network Operations and Management Symposium (APNOMS)*, Aug. 2015, pp. 372–375, doi: 10.1109/APNOMS.2015.7275344.

[49] L. Phonrattanasak, P., Nopbhorn, “Optimal location of fast charging station on residential distribution grid,” *Int. J. Innov. Manag. Technol.*, vol. 3, no. 6, pp. 675–681, 2012.

[50] M. Mavrovouniotis, G. Ellinas, and M. Polycarpou, “Ant Colony optimization for the Electric Vehicle Routing Problem,” in *2018 IEEE Symposium Series on Computational Intelligence (SSCI)*, Nov. 2018, pp. 1234–1241, doi: 10.1109/SSCI.2018.8628831.

[51] S. Deb, K. Tammi, K. Kalita, and P. Mahanta, “Charging Station Placement for Electric Vehicles: A Case Study of Guwahati City, India,” *IEEE Access*, vol. 7, pp. 100270–100282, 2019, doi: 10.1109/ACCESS.2019.2931055.

[52] H. W. J. Lenstra, “Integer programming with a fixed number of variables,” *Math. Oper. Res.*, vol. 8, no. 4, pp. 538–548, 1983.

[53] R. E. Bixby, “A brief history of linear and mixed-integer programming computation,” *Doc. Math*, pp. 107–121, 2012.

[54] O. Worley, D. Klabjan, and T. M. Sweda, “Simultaneous vehicle routing and charging station siting for commercial Electric Vehicles,” in *2012 IEEE International Electric Vehicle Conference*, Mar. 2012, pp. 1–3, doi: 10.1109/IEVC.2012.6183279.

[55] W. Meng and L. Kai, “Optimization of electric vehicle charging station location based on game theory,” in *Proceedings 2011 International Conference on Transportation, Mechanical, and Electrical Engineering (TMEE)*, Dec. 2011, pp. 809–812, doi: 10.1109/TMEE.2011.6199325.

[56] H. Zhang, S. J. Moura, Z. Hu, and Y. Song, “PEV Fast-Charging Station Siting and Sizing on Coupled Transportation and Power Networks,” *IEEE Trans. Smart Grid*, vol. 9, no. 4, pp. 2595–2605, Jul. 2018, doi: 10.1109/TSG.2016.2614939.

[57] N. Rastegarfar, B. Kashanizadeh, M. Vakilian, and S. A. Barband, “Optimal placement of fast charging station in a typical microgrid in Iran,” in *2013 10th International Conference on the European Energy Market (EEM)*, May 2013, pp. 1–7, doi: 10.1109/EEM.2013.6607284.

[58] M. M. Islam, H. Shareef, and A. Mohamed, “Optimal location and sizing of fast charging stations for electric vehicles by incorporating traffic and power networks,” *IET Intell. Transp. Syst.*, vol. 12, no. 8, pp. 947–957, Oct. 2018, doi: 10.1049/iet-its.2018.5136.

[59] A. S. Masoum, S. Deilami, P. S. Moses, M. A. S. Masoum, and A. Abu-Siada, "Smart load management of plug-in electric vehicles in distribution and residential networks with charging stations for peak shaving and loss minimisation considering voltage regulation," *IET Gener. Transm. Distrib.*, vol. 5, no. 8, p. 877, 2011, doi: 10.1049/iet-gtd.2010.0574.

[60] M. M. Islam, H. Shareef, and A. Mohamed, "Improved approach for electric vehicle rapid charging station placement and sizing using Google maps and binary lightning search algorithm," *PLoS One*, vol. 12, no. 12, p. e0189170, Dec. 2017, doi: 10.1371/journal.pone.0189170.

[61] H. Zhang, S. J. Moura, Z. Hu, W. Qi, and Y. Song, "A Second-Order Cone Programming Model for Planning PEV Fast-Charging Stations," *IEEE Trans. Power Syst.*, vol. 33, no. 3, pp. 2763–2777, May 2018, doi: 10.1109/TPWRS.2017.2754940.

[62] Y. Xiang, J. Liu, R. Li, F. Li, C. Gu, and S. Tang, "Economic planning of electric vehicle charging stations considering traffic constraints and load profile templates," *Appl. Energy*, vol. 178, pp. 647–659, Sep. 2016, doi: 10.1016/j.apenergy.2016.06.021.

[63] M. M. Vazifeh, H. Zhang, P. Santi, and C. Ratti, "Optimizing the deployment of electric vehicle charging stations using pervasive mobility data," *Transp. Res. Part A Policy Pract.*, vol. 121, pp. 75–91, Mar. 2019, doi: 10.1016/j.tra.2019.01.002.

[64] X. Dong, Y. Mu, H. Jia, J. Wu, and X. Yu, "Planning of Fast EV Charging Stations on a Round Freeway," *IEEE Trans. Sustain. Energy*, vol. 7, no. 4, pp. 1452–1461, Oct. 2016, doi: 10.1109/TSTE.2016.2547891.

[65] C. Luo, Y.-F. Huang, and V. Gupta, "Placement of EV Charging Stations--Balancing Benefits Among Multiple Entities," *IEEE Trans. Smart Grid*, pp. 1–10, 2015, doi: 10.1109/TSG.2015.2508740.

[66] J. He, H. Yang, T.-Q. Tang, and H.-J. Huang, "An optimal charging station location model with the consideration of electric vehicle's driving range," *Transp. Res. Part C Emerg. Technol.*, vol. 86, pp. 641–654, Jan. 2018, doi: 10.1016/j.trc.2017.11.026.

[67] H. Simorgh, H. Doagou-Mojarrad, H. Razmi, and G. B. Gharehpetian, "Cost-based optimal siting and sizing of electric vehicle charging stations considering demand response programmes," *IET Gener. Transm. Distrib.*, vol. 12, no. 8, pp. 1712–1720, Apr. 2018, doi: 10.1049/iet-gtd.2017.1663.

[68] S. Pazouki, A. Mohsenzadeh, S. Ardalan, and M.-R. Haghifam, "Simultaneous Planning of PEV Charging Stations and DGs Considering Financial, Technical,and Environmental Effects," *Can. J. Electr. Comput. Eng.*, vol. 38, no. 3, pp. 238–245, 2015, doi: 10.1109/CJECE.2015.2436811.

[69] B. Deng and Z. Wang, "Research on Electric-Vehicle Charging Station Technologies Based on Smart Grid," in *2011 Asia-Pacific Power and Energy Engineering Conference*, Mar. 2011, vol. 25, no. 6, pp. 1–4, doi: 10.1109/APPEEC.2011.5748759.

[70] S. Han, S. Han, and K. Sezaki, “Development of an Optimal Vehicle-to-Grid Aggregator for Frequency Regulation,” *IEEE Trans. Smart Grid*, vol. 1, no. 1, pp. 65–72, Jun. 2010, doi: 10.1109/TSG.2010.2045163.

[71] M. Singh, P. Kumar, and I. Kar, “A Multi Charging Station for Electric Vehicles and Its Utilization for Load Management and the Grid Support,” *IEEE Trans. Smart Grid*, vol. 4, no. 2, pp. 1026–1037, Jun. 2013, doi: 10.1109/TSG.2013.2238562.

[72] C. H. Dharmakeerthi, N. Mithulananthan, and T. K. Saha, “A comprehensive planning framework for electric vehicle charging infrastructure deployment in the power grid with enhanced voltage stability,” *Int. Trans. Electr. Energy Syst.*, vol. 25, no. 6, pp. 1022–1040, Jun. 2015, doi: 10.1002/etep.1886.

[73] L. Liu, Y. Zhang, C. Da, Z. Huang, and M. Wang, “Optimal allocation of distributed generation and electric vehicle charging stations based on intelligent algorithm and bi-level programming,” *Int. Trans. Electr. Energy Syst.*, vol. 30, no. 6, Jun. 2020, doi: 10.1002/2050-7038.12366.

[74] A. Awasthi, K. Venkitusamy, S. Padmanaban, R. Selvamuthukumaran, F. Blaabjerg, and A. K. Singh, “Optimal planning of electric vehicle charging station at the distribution system using hybrid optimization algorithm,” *Energy*, vol. 133, pp. 70–78, Aug. 2017, doi: 10.1016/j.energy.2017.05.094.

[75] S. Davidov and M. Pantoš, “Optimization model for charging infrastructure planning with electric power system reliability check,” *Energy*, vol. 166, pp. 886–894, Jan. 2019, doi: 10.1016/j.energy.2018.10.150.

[76] A. Pal, A. Bhattacharya, and A. K. Chakraborty, “Allocation of electric vehicle charging station considering uncertainties,” *Sustain. Energy, Grids Networks*, vol. 25, p. 100422, Mar. 2021, doi: 10.1016/j.segan.2020.100422.

[77] A. Fathy and A. Y. Abdelaziz, “Competition over resource optimization algorithm for optimal allocating and sizing parking lots in radial distribution network,” *J. Clean. Prod.*, vol. 264, no. 6, p. 121397, Aug. 2020, doi: 10.1016/j.jclepro.2020.121397.

[78] S. R. Salkuti, “Optimal Location and Sizing of Shunt Capacitors with Distributed Generation in Distribution Systems,” *ECTI Trans. Electr. Eng. Electron. Commun.*, vol. 19, no. 1, pp. 34–42, Feb. 2021, doi: 10.37936/ecti-eec.2021191.222295.

[79] A. A. Abou El-Ela, R. A. El-Sehiemy, A. Kinawy, and M. T. Mouwafi, “Optimal capacitor placement in distribution systems for power loss reduction and voltage profile improvement,” *IET Gener. Transm. Distrib.*, vol. 10, no. 5, pp. 1209–1221, Apr. 2016, doi: 10.1049/iet-gtd.2015.0799.

[80] S. S. Reddy, “Optimal power flow using hybrid differential evolution and harmony search algorithm,” *Int. J. Mach. Learn. Cybern.*, vol. 10, no. 5, pp. 1077–1091, May 2019, doi: 10.1007/s13042-018-0786-9.

[81] S. Sachan and M. H. Amini, “Optimal allocation of EV charging spots along with capacitors in smart distribution network for congestion management,” *Int. Trans. Electr. Energy Syst.*, vol. 30, no. 9, pp. 1–14, Sep. 2020, doi: 10.1002/2050-7038.12507.

[82] S. R. Gampa, K. Jasthi, P. Goli, D. Das, and R. C. Bansal, “Grasshopper optimization algorithm based two stage fuzzy multiobjective approach for optimum sizing and placement of distributed generations, shunt capacitors and electric vehicle charging stations,” *J. Energy Storage*, vol. 27, no. 6, p. 101117, Feb. 2020, doi: 10.1016/j.est.2019.101117.

[83] P. Rajesh and F. H. Shajin, “Optimal allocation of EV charging spots and capacitors in distribution network improving voltage and power loss by Quantum-Behaved and Gaussian Mutational Dragonfly Algorithm (QGDA),” *Electr. Power Syst. Res.*, vol. 194, no. 6, p. 107049, May 2021, doi: 10.1016/j.epsr.2021.107049.

[84] S. Deilami, A. S. Masoum, P. S. Moses, and M. A. S. Masoum, “Real-Time Coordination of Plug-In Electric Vehicle Charging in Smart Grids to Minimize Power Losses and Improve Voltage Profile,” *IEEE Trans. Smart Grid*, vol. 2, no. 3, pp. 456–467, Sep. 2011, doi: 10.1109/TSG.2011.2159816.

[85] J. Y. Yong, V. K. Ramachandaramurthy, K. M. Tan, and N. Mithulananthan, “Bi-directional electric vehicle fast charging station with novel reactive power compensation for voltage regulation,” *Int. J. Electr. Power Energy Syst.*, vol. 64, pp. 300–310, Jan. 2015, doi: 10.1016/j.ijepes.2014.07.025.

[86] M. Dixit, P. Kundu, and H. R. Jariwala, “Incorporation of distributed generation and shunt capacitor in radial distribution system for techno-economic benefits,” *Eng. Sci. Technol. an Int. J.*, vol. 20, no. 2, pp. 482–493, Apr. 2017, doi: 10.1016/j.jestch.2017.01.003.

[87] Shaaban, Y. M. Atwa, and E. F. El-Saadany, “PEVs modeling and impacts mitigation in distribution networks,” *IEEE Trans. Power Syst.*, vol. 28, no. 2, pp. 1122–1131, May 2013, doi: 10.1109/TPWRS.2012.2212467.

[88] M. S. K. Reddy and K. Selvajyothi, “Optimal placement of electric vehicle charging station for unbalanced radial distribution systems,” *Energy Sources, Part A Recover. Util. Environ. Eff.*, pp. 1–15, Feb. 2020, doi: 10.1080/15567036.2020.1731017.

[89] R. Sanjay, T. Jayabarathi, T. Raghunathan, V. Ramesh, and N. Mithulananthan, “Optimal Allocation of Distributed Generation Using Hybrid Grey Wolf Optimizer,” *IEEE Access*, vol. 5, pp. 14807–14818, 2017, doi: 10.1109/ACCESS.2017.2726586.

[90] O. Erdinc, A. Tascikaraoglu, N. G. Paterakis, I. Dursun, M. C. Sinim, and J. P. S. Catalao, “Comprehensive Optimization Model for Sizing and Siting of DG Units, EV Charging Stations, and Energy Storage Systems,” *IEEE Trans. Smart Grid*, vol. 9, no. 4, pp. 3871–3882, Jul. 2018, doi: 10.1109/TSG.2017.2777738.

[91] A. Selim, S. Kamel, A. S. Alghamdi, and F. Jurado, "Optimal Placement of DGs in Distribution System Using an Improved Harris Hawks Optimizer Based on Single- and Multi-Objective Approaches," *IEEE Access*, vol. 8, pp. 52815–52829, 2020, doi: 10.1109/ACCESS.2020.2980245.

[92] K. B. B. and S. Maheswarapu, "A solution to multi-objective optimal accommodation of distributed generation problem of power distribution networks: An analytical approach," *Int. Trans. Electr. Energy Syst.*, vol. 29, no. 10, Oct. 2019, doi: 10.1002/2050-7038.12093.

[93] K. Hesaroor and D. Das, "Annual energy loss reduction of distribution network through reconfiguration and renewable energy sources," *Int. Trans. Electr. Energy Syst.*, vol. 29, no. 11, Nov. 2019, doi: 10.1002/2050-7038.12099.

[94] M. BiazarGhadikolaei, M. Shahabi, and T. Barforoushi, "Expansion planning of energy storages in microgrid under uncertainties and demand response," *Int. Trans. Electr. Energy Syst.*, vol. 29, no. 11, Nov. 2019, doi: 10.1002/2050-7038.12110.

[95] M. Bilal and M. Rizwan, "Integration of electric vehicle charging stations and capacitors in distribution systems with vehicle-to-grid facility," *Energy Sources, Part A Recover. Util. Environ. Eff.*, pp. 1–30, May 2021, doi: 10.1080/15567036.2021.1923870.

[96] E. Akhavan-Rezai, M. F. Shaaban, E. F. El-Saadany, and F. Karray, "Managing Demand for Plug-in Electric Vehicles in Unbalanced LV Systems With Photovoltaics," *IEEE Trans. Ind. Informatics*, vol. 13, no. 3, pp. 1057–1067, Jun. 2017, doi: 10.1109/TII.2017.2675481.

[97] B. Zeng, J. Feng, J. Zhang, and Z. Liu, "An optimal integrated planning method for supporting growing penetration of electric vehicles in distribution systems," *Energy*, vol. 126, pp. 273–284, May 2017, doi: 10.1016/j.energy.2017.03.014.

[98] S. J. Gunter, K. K. Afridi, and D. J. Perreault, "Optimal Design of Grid-Connected PEV Charging Systems With Integrated Distributed Resources," *IEEE Trans. Smart Grid*, vol. 4, no. 2, pp. 956–967, Jun. 2013, doi: 10.1109/TSG.2012.2227514.

[99] S. F. Abdelsamad, W. G. Morsi, and T. S. Sidhu, "Impact of Wind-Based Distributed Generation on Electric Energy in Distribution Systems Embedded With Electric Vehicles," *IEEE Trans. Sustain. Energy*, vol. 6, no. 1, pp. 79–87, Jan. 2015, doi: 10.1109/TSTE.2014.2356551.

[100] M. Bilal and M. Rizwan, "Electric vehicles in a smart grid: a comprehensive survey on optimal location of charging station," *IET Smart Grid*, vol. 3, no. 3, pp. 267–279, Jun. 2020, doi: 10.1049/iet-stg.2019.0220.

[101] C. Kelman, "Supporting increasing renewable energy penetration in Australia the poten_tial contribution of electric vehicles," *Proc. 20th Australas. Univ. power Eng. Conf.*, pp. 1–6, 2010.

[102] B. J. Barker PP, “Advances in solar photovoltaic technology: an applications perspective,” *Proc Power Eng Soc Gen Meet 2*, pp. 1955–1960.

[103] V. A. Kadar P, “Photovoltaic EV charge station,” *Proc. IEEE 11th Int. Symp. Appl. Mach. Intell. informatics*, pp. 57–60, 2013.

[104] K. Branker, M. J. M. Pathak, and J. M. Pearce, “A review of solar photovoltaic levelized cost of electricity,” *Renew. Sustain. Energy Rev.*, vol. 15, no. 9, pp. 4470–4482, Dec. 2011, doi: 10.1016/j.rser.2011.07.104.

[105] J. Van Roy, N. Leemput, F. Geth, R. Salenbien, J. Buscher, and J. Driesen, “Apartment Building Electricity System Impact of Operational Electric Vehicle Charging Strategies,” *IEEE Trans. Sustain. Energy*, vol. 5, no. 1, pp. 264–272, Jan. 2014, doi: 10.1109/TSTE.2013.2281463.

[106] G. Gamboa *et al.*, “Control strategy of a multi-port, grid connected, direct-DC PV charging station for plug-in electric vehicles,” in *2010 IEEE Energy Conversion Congress and Exposition*, Sep. 2010, pp. 1173–1177, doi: 10.1109/ECCE.2010.5617838.

[107] S. J. Chiang, H. Shieh, and M. Chen, “Modeling and Control of PV Charger System With SEPIC Converter,” *IEEE Trans. Ind. Electron.*, vol. 56, no. 11, pp. 4344–4353, Nov. 2009, doi: 10.1109/TIE.2008.2005144.

[108] M. D. Galus and G. Andersson, “Demand Management of Grid Connected Plug-In Hybrid Electric Vehicles (PHEV),” in *2008 IEEE Energy 2030 Conference*, Nov. 2008, pp. 1–8, doi: 10.1109/ENERGY.2008.4781014.

[109] Hawaii, “Natural energy institute school of ocean and earth science and technology univer_sity of Hawaii, Organization UoHiER. Statewide and electricity-sector models for economic assessments of Hawaii clean energy policies. Hawaii distributed energy resource tech,” 2012.

[110] G. Preetham and W. Shireen, “Photovoltaic charging station for Plug-In Hybrid Electric Vehicles in a smart grid environment,” in *2012 IEEE PES Innovative Smart Grid Technologies (ISGT)*, Jan. 2012, pp. 1–8, doi: 10.1109/ISGT.2012.6175589.

[111] S. J. Tong, A. Same, M. A. Kootstra, and J. W. Park, “Off-grid photovoltaic vehicle charge using second life lithium batteries: An experimental and numerical investigation,” *Appl. Energy*, vol. 104, pp. 740–750, Apr. 2013, doi: 10.1016/j.apenergy.2012.11.046.

[112] H. Ibrahim, A. Ilinca, and J. Perron, “Energy storage systems—Characteristics and comparisons,” *Renew. Sustain. Energy Rev.*, vol. 12, no. 5, pp. 1221–1250, Jun. 2008, doi: 10.1016/j.rser.2007.01.023.

[113] J. Traube, F. Lu, and D. Maksimovic, “Electric vehicle DC charger integrated within a photovoltaic power system,” in *2012 Twenty-Seventh Annual IEEE Applied Power Electronics Conference and Exposition (APEC)*, Feb. 2012, pp. 352–358, doi: 10.1109/APEC.2012.6165843.

[114] J. Traube *et al.*, "Mitigation of Solar Irradiance Intermittency in Photovoltaic Power Systems With Integrated Electric-Vehicle Charging Functionality," *IEEE Trans. Power Electron.*, vol. 28, no. 6, pp. 3058–3067, Jun. 2013, doi: 10.1109/TPEL.2012.2217354.

[115] Z. Salam, J. Ahmed, and B. S. Merugu, "The application of soft computing methods for MPPT of PV system: A technological and status review," *Appl. Energy*, vol. 107, pp. 135–148, Jul. 2013, doi: 10.1016/j.apenergy.2013.02.008.

[116] T.-F. Wu and H.-C. Hsieh, "Digital control for a three-phase transformerless bi-directional photovoltaic inverter with wide inductance variation," in *2013 1st International Future Energy Electronics Conference (IFEEC)*, Nov. 2013, pp. 658–662, doi: 10.1109/IFEEC.2013.6687586.

[117] P. Goli and W. Shireen, "PV powered smart charging station for PHEVs," *Renew. Energy*, vol. 66, pp. 280–287, Jun. 2014, doi: 10.1016/j.renene.2013.11.066.

[118] T. Ma and O. A. Mohammed, "Optimal Charging of Plug-in Electric Vehicles for a Car-Park Infrastructure," *IEEE Trans. Ind. Appl.*, vol. 50, no. 4, pp. 2323–2330, Jul. 2014, doi: 10.1109/TIA.2013.2296620.

[119] AA. Abu-jasser, "Stand-alone photovoltaic system, case study: a residence in Gaza," *J Appl Sci Env. Sanit*, vol. 5, no. 1, pp. 81–91, 2014.

[120] A. M. Sharaf and M. E. Sahin, "A novel photovoltaic PV-powered battery charging scheme for electric vehicles," in *2011 International Conference on Energy, Automation and Signal*, Dec. 2011, pp. 1–5, doi: 10.1109/ICEAS.2011.6147212.

[121] J. Mossoba *et al.*, "Analysis of solar irradiance intermittency mitigation using constant DC voltage PV and EV battery storage," in *2012 IEEE Transportation Electrification Conference and Expo (ITEC)*, Jun. 2012, pp. 1–6, doi: 10.1109/ITEC.2012.6243473.

[122] W. D. Stevenson, "Elements of Power System Analysis, India," *McGraw-Hill*, 1982.

[123] W. Tinney and C. Hart, "Power Flow Solution by Newton's Method," *IEEE Trans. Power Appar. Syst.*, vol. PAS-86, no. 11, pp. 1449–1460, Nov. 1967, doi: 10.1109/TPAS.1967.291823.

[124] B. Stott and O. Alsac, "Fast Decoupled Load Flow," *IEEE Trans. Power Appar. Syst.*, vol. PAS-93, no. 3, pp. 859–869, May 1974, doi: 10.1109/TPAS.1974.293985.

[125] T.-H. Chen, M.-S. Chen, K.-J. Hwang, P. Kotas, and E. A. Chebli, "Distribution system power flow analysis-a rigid approach," *IEEE Trans. Power Deliv.*, vol. 6, no. 3, pp. 1146–1152, Jul. 1991, doi: 10.1109/61.85860.

[126] D. Shirmohammadi, H. W. Hong, A. Semlyen, and G. X. Luo, "A compensation-based power flow method for weakly meshed distribution and transmission networks," *IEEE Trans. Power Syst.*, vol. 3, no. 2, pp. 753–762, May 1988, doi: 10.1109/59.192932.

[127] R. D. Zimmerman and H. Chiang, "Fast decoupled power flow for unbalanced radial distribution systems," *IEEE Trans. Power Syst.*, vol. 10, no. 4, pp. 2045–2052, Nov. 1995, doi: 10.1109/59.476074.

[128] A. Garces, "A Linear Three-Phase Load Flow for Power Distribution Systems," *IEEE Trans. Power Syst.*, vol. 31, no. 1, pp. 827–828, Jan. 2016, doi: 10.1109/TPWRS.2015.2394296.

[129] S. M. Chopra, Nitish, Gourav Kumar, "Hybrid GWO-PSO algorithm for solving convex economic load dispatch problem," *Int J Res Adv Technol*, vol. 4, no. 6, pp. 37–41, 2016.

[130] S. Mirjalili, S. M. Mirjalili, and A. Lewis, "Grey Wolf Optimizer," *Adv. Eng. Softw.*, vol. 69, pp. 46–61, Mar. 2014, doi: 10.1016/j.advengsoft.2013.12.007.

[131] A. A. El-Fergany and H. M. Hasanien, "Single and Multi-objective Optimal Power Flow Using Grey Wolf Optimizer and Differential Evolution Algorithms," *Electr. Power Components Syst.*, vol. 43, no. 13, pp. 1548–1559, Aug. 2015, doi: 10.1080/15325008.2015.1041625.

[132] A. Kumar, M. Rizwan and U. Nangia, "A new approach to design and optimize sizing of hybrid microgrid in deregulated electricity environment," *CSEE J. Power Energy Syst.*, pp. 1–11, 2020, doi: 10.17775/CSEEJPES.2020.03200.

[133] P. Sadeghi-Barzani, A. Rajabi-Ghahnavieh, and H. Kazemi-Karegar, "Optimal fast charging station placing and sizing," *Appl. Energy*, vol. 125, pp. 289–299, Jul. 2014, doi: 10.1016/j.apenergy.2014.03.077.

[134] M. M. Islam, H. Shareef, and A. Mohamed, "Optimal siting and sizing of rapid charging station for electric vehicles considering Bangi city road network in Malaysia," *Turkish J. Electr. Eng. Comput. Sci.*, vol. 24, pp. 3933–3948, 2016, doi: 10.3906/elk-1412-136.

[135] M. Sanchari, D. Karuna, K. Xiao-Zhi, G. Kari, T. and Pinakshwar, "Optimal placement of charging station using CSO-TLBO algorithm," *2017 Int. Conf. Res. Comput. Intell. Commun. Networks*, pp. 84–89, 2017.

[136] "https://www.google.com/search?q=latitudes+and+longitudes+of+areas+of+south+delhi&oq=latitudes+and+longitudes+of+areas+of+south+delhi&aqs=chrome..69i57j33i22i29i30.13439j0j7&sourceid=chrome&ie=UTF-8."

[137] "https://www.google.com/maps/d/u/0/edit?mid=1MYBWdZhX_Ay0IWXwRHNjbXcigF88."

[138] D. Mayfield, "Site design for electric vehicle charging stations. Sustainable transportation strategies," 2012.

[139] R. N. B. Allan, "Reliability evaluation of power systems," *Springer*, 1996.

[140] “https://www.myloancare.in/delhi-circle-rate-revised/(as cited on 19th June 2018).”

[141] I. A. Quadri, S. Bhowmick, and D. Joshi, “A hybrid teaching–learning-based optimization technique for optimal DG sizing and placement in radial distribution systems,” *Soft Comput.*, vol. 23, no. 20, pp. 9899–9917, Oct. 2019, doi: 10.1007/s00500-018-3544-8.

[142] J. S. Chis M, Salama MMA, “Capacitor placement in distribution system using metaheuristic search strategies,” *IET Gener. Transm. Distrib.*, vol. 144, no. 3, pp. 225–230, 1997.

[143] A. Pal, A. Bhattacharya, and A. K. Chakraborty, “Allocation of electric vehicle charging station considering uncertainties,” *Sustain. Energy, Grids Networks*, vol. 25, no. 6, p. 100422, Mar. 2021, doi: 10.1016/j.segan.2020.100422.

[144] S. K. Injeti, V. K. Thunuguntla, and M. Shareef, “Optimal allocation of capacitor banks in radial distribution systems for minimization of real power loss and maximization of network savings using bio-inspired optimization algorithms,” *Int. J. Electr. Power Energy Syst.*, vol. 69, pp. 441–455, Jul. 2015, doi: 10.1016/j.ijepes.2015.01.040.

[145] H. Saboori, R. Hemmati, and M. A. Jirdehi, “Reliability improvement in radial electrical distribution network by optimal planning of energy storage systems,” *Energy*, vol. 93, pp. 2299–2312, Dec. 2015, doi: 10.1016/j.energy.2015.10.125.

[146] J. Teng, “A direct approach for distribution system load flow solutions,” *IEEE Trans. Power Deliv.*, vol. 18, no. 3, pp. 882–887, Jul. 2003, doi: 10.1109/TPWRD.2003.813818.

[147] S. S. Reddy, “Determination of Optimal Location and Size of Static VAR Compensator in a Hybrid Wind and Solar Power System,” *Int. J. Appl. Eng. Res.*, vol. 11, no. 23, 2016.

[148] A. A. El-Fergany and A. Y. Abdelaziz, “Capacitor placement for net saving maximization and system stability enhancement in distribution networks using artificial bee colony-based approach,” *Int. J. Electr. Power Energy Syst.*, vol. 54, no. 6, pp. 235–243, Jan. 2014, doi: 10.1016/j.ijepes.2013.07.015.

[149] K. Nekooei, M. M. Farsangi, H. Nezamabadi-Pour, and K. Y. Lee, “An Improved Multi-Objective Harmony Search for Optimal Placement of DGs in Distribution Systems,” *IEEE Trans. Smart Grid*, vol. 4, no. 1, pp. 557–567, Mar. 2013, doi: 10.1109/TSG.2012.2237420.

[150] D. P. Kothari, “Power system optimization,” in *2012 2nd National Conference on Computational Intelligence and Signal Processing (CISP)*, Mar. 2012, pp. 18–21, doi: 10.1109/NCCISP.2012.6189669.

[151] S. Sultana and P. K. Roy, “Multi-objective quasi-oppositional teaching learning based optimization for optimal location of distributed generator in radial distribution systems,” *Int. J. Electr. Power Energy Syst.*, vol. 63, pp. 534–545, Dec. 2014, doi: 10.1016/j.ijepes.2014.06.031.

[152] I. A. Quadri, S. Bhowmick, and D. Joshi, “A comprehensive technique for optimal allocation of distributed energy resources in radial distribution systems,” *Appl. Energy*, vol. 211, pp. 1245–1260, Feb. 2018, doi: 10.1016/j.apenergy.2017.11.108.

[153] S. Deb, K. Tammi, K. Kalita, and P. Mahanta, “Impact of Electric Vehicle Charging Station Load on Distribution Network,” *Energies*, vol. 11, no. 1, p. 178, Jan. 2018, doi: 10.3390/en11010178.

[154] S. Kumar, K. Sarita, A. S. S. Vardhan, R. M. Elavarasan, R. K. Saket, and N. Das, “Reliability Assessment of Wind-Solar PV Integrated Distribution System Using Electrical Loss Minimization Technique,” *Energies*, vol. 13, no. 21, p. 5631, Oct. 2020, doi: 10.3390/en13215631.

[155] H. Borhanazad, S. Mekhilef, V. Gounder Ganapathy, M. Modiri-Delshad, and A. Mirtaheri, “Optimization of micro-grid system using MOPSO,” *Renew. Energy*, vol. 71, pp. 295–306, Nov. 2014, doi: 10.1016/j.renene.2014.05.006.

[156] D. K. Geleta, M. S. Manshahia, P. Vasant, and A. Banik, “Grey wolf optimizer for optimal sizing of hybrid wind and solar renewable energy system,” *Comput. Intell.*, p. coin.12349, Jun. 2020, doi: 10.1111/coin.12349.

[157] A. K. Podder *et al.*, “Feasibility Assessment of Hybrid Solar Photovoltaic-Biogas Generator Based Charging Station: A Case of Easy Bike and Auto Rickshaw Scenario in a Developing Nation,” *Sustainability*, vol. 14, no. 1, p. 166, Dec. 2021, doi: 10.3390/su14010166.

[158] T. Aldhanhani, A. Al-Durra, and E. F. El-Saadany, “Optimal design of electric vehicle charging stations integrated with renewable DG,” in *2017 IEEE Innovative Smart Grid Technologies - Asia (ISGT-Asia)*, Dec. 2017, pp. 1–6, doi: 10.1109/ISGT-Asia.2017.8378428.

[159] D. Fares, M. Fathi, and S. Mekhilef, “Performance evaluation of metaheuristic techniques for optimal sizing of a stand-alone hybrid PV/wind/battery system,” *Appl. Energy*, vol. 305, p. 117823, Jan. 2022, doi: 10.1016/j.apenergy.2021.117823.

[160] D. Kumar, S. R. Samantaray, I. Kamwa, and N. C. Sahoo, “Reliability-constrained Based Optimal Placement and Sizing of Multiple Distributed Generators in Power Distribution Network Using Cat Swarm Optimization,” *Electr. Power Components Syst.*, vol. 42, no. 2, pp. 149–164, Jan. 2014, doi: 10.1080/15325008.2013.853215.

APPENDICES

Table A.1: System data of 33-bus test distribution system

Branch	Bus number		Resistance	Reactance	Load at receiving end	
	Sending	Receiving	(Ω)	(Ω)	P (MW)	Q (MVAr)
1	1	2	0.0922	0.047	0	0
2	2	3	0.493	0.2511	0.1	0.06
3	3	4	0.366	0.1864	0.09	0.04
4	4	5	0.3811	0.1941	0.12	0.08
5	5	6	0.819	0.707	0.06	0.03
6	6	7	0.1872	0.6188	0.06	0.02
7	7	8	0.7114	0.2351	0.2	0.1
8	8	9	1.03	0.74	0.2	0.1
9	9	10	1.044	0.74	0.06	0.02
10	10	11	0.1966	0.065	0.06	0.02
11	11	12	0.3744	0.1238	0.045	0.03
12	12	13	1.468	1.155	0.06	0.035
13	13	14	0.5416	0.7129	0.06	0.035
14	14	15	0.591	0.526	0.12	0.08
15	15	16	0.7463	0.545	0.06	0.01
16	16	17	1.289	1.721	0.06	0.02
17	17	18	0.732	0.574	0.06	0.02
18	2	19	0.264	0.2565	0.09	0.04
19	19	20	1.5042	1.3554	1.59	0.04
20	20	21	0.4095	0.4784	9.00E-02	4.00E-02
21	21	22	0.7089	0.9373	0.09	0.04
22	3	23	0.4512	0.3083	0.09	0.04
23	23	24	0.898	0.7091	0.09	0.05
24	24	25	0.896	0.7011	0.4	0.2
25	6	26	0.203	0.1034	0.42	0.2
26	26	27	0.2842	0.1447	0.06	0.025
27	27	28	1.059	0.9337	0.06	0.025
28	28	29	0.8042	0.7006	0.06	0.02
29	29	30	0.5075	0.2585	0.12	0.07
30	30	31	0.9744	0.963	0.2	0.6
31	31	32	0.3105	0.3619	0.15	0.07
32	32	33	0.341	0.5302	0.21	0.1

Table A.2: System data of 34-bus test distribution system

Branch	Bus number		Resistance	Reactance	Load at receiving end	
	Sending	Receiving	(Ω)	(Ω)	P (kW)	Q (kVAr)
1	1	2	0.195	0.080	0	0
2	2	3	0.195	0.080	230	142.5
3	3	4	0.299	0.083	0	0
4	4	5	0.299	0.083	230	142.5
5	5	6	0.299	0.083	230	142.5
6	6	7	0.524	0.090	0	0
7	7	8	0.524	0.090	0	0
8	8	9	0.524	0.090	230	142.5
9	9	10	0.524	0.090	230	142.5
10	10	11	0.524	0.090	0	0
11	11	12	0.524	0.090	230	142.5
12	3	13	0.524	0.090	137	84
13	13	14	0.524	0.090	72	45
14	14	15	0.524	0.090	72	45
15	15	16	0.524	0.090	72	45
16	6	17	0.299	0.083	13.5	7.5
17	17	18	0.299	0.083	230	142.5
18	2	19	0.387	0.086	230	142.5
19	19	20	0.387	0.086	230	142.5
20	20	21	0.387	0.086	230	142.5
21	21	22	0.524	0.090	230	142.5
22	3	23	0.524	0.090	230	142.5
23	23	24	0.524	0.090	230	142.5
24	24	25	0.524	0.090	230	142.5
25	6	26	0.524	0.090	230	142.5
26	26	27	0.524	0.090	230	142.5
27	7	28	0.524	0.090	137	85
28	28	29	0.524	0.090	75	48
29	29	30	0.524	0.090	75	48
30	10	31	0.524	0.090	57	48
31	31	32	0.524	0.090	57	34.5
32	32	33	0.524	0.090	57	34.5
33	33	34	0.524	0.090	57	34.5
					57	34.5

Table A.3: System data of 69-bus test distribution system

Branch	Bus number		Resistance	Reactance	Load at receiving end	
	Sending	Receiving	(Ω)	(Ω)	P (MW)	Q (MVAr)
1	1	2	0.0005	0.0012	0	0
2	2	3	0.0005	0.0012	0	0
3	3	4	0.0015	0.0036	0	0
4	4	5	0.0251	0.0294	0	0
5	5	6	0.366	0.1864	0	0
6	6	7	0.381	0.1941	0.0026	0.0022
7	7	8	0.0922	0.047	0.0404	0.03
8	8	9	0.0493	0.0251	0.075	0.054
9	9	10	0.819	0.2707	0.03	0.022
10	10	11	0.1872	0.0619	0.028	0.019
11	11	12	0.7114	0.2351	0.145	0.104
12	12	13	1.03	0.34	0.145	0.104
13	13	14	1.044	0.34	0.008	0.005
14	14	15	1.058	0.3496	0.008	0.0055
15	15	16	0.1966	0.065	0	0
16	16	17	0.3744	0.1238	0.0455	0.03
17	17	18	0.0047	0.0016	0.06	0.035
18	18	19	0.3276	0.1083	0.06	0.035
19	19	20	0.2106	0.0696	0	0
20	20	21	0.3416	0.1129	0.001	0.0006
21	21	22	0.014	0.0046	0.114	0.081
22	22	23	0.1591	0.0526	0.005	0.0035
23	23	24	0.3463	0.1145	0	0
24	24	25	0.7488	0.2475	0.028	0.02
25	25	26	0.3089	0.1021	0	0
26	26	27	0.1732	0.0572	0.014	0.01
27	3	28	0.0044	0.0108	0.014	0.01
28	28	29	0.064	0.1565	0.026	0.0186
29	29	30	0.3978	0.1315	0.026	0.0186
30	30	31	0.0702	0.0232	0	0
31	31	32	0.351	0.116	0	0
32	32	33	0.839	0.2816	0	0
33	33	34	1.708	0.5646	0.014	0.01
34	34	35	1.474	0.4873	0.0195	0.014
35	3	36	0.0044	0.0108	0.006	0.004
36	36	37	0.064	0.1565	0.026	0.01855
37	37	38	0.1053	0.123	0.026	0.01855
38	38	39	0.0304	0.0355	0	0
39	39	40	0.0018	0.0021	0.024	0.017
40	40	41	0.7283	0.8509	0.024	0.017
41	41	42	0.31	0.3623	0.0012	0.001
42	42	43	0.041	0.0478	0	0

43	43	44	0.0092	0.0116	0.006	0.0043
44	44	45	0.1089	0.1373	0	0
45	45	46	0.0009	0.0012	0.03922	0.0263
46	4	47	0.0034	0.0084	0.03922	0.0263
47	47	48	0.0851	0.2083	0	0
48	48	49	0.2898	0.7091	0.079	0.0564
49	49	50	0.0822	0.2011	0.3847	0.2745
50	8	51	0.0928	0.0473	0.3847	0.2745
51	51	52	0.3319	0.114	0.0405	0.0283
52	9	53	0.174	0.0886	0.0036	0.0027
53	53	54	0.203	0.1034	0.00435	0.0035
54	54	55	0.2842	0.1447	0.0264	0.019
55	55	56	0.2813	0.1433	0.024	0.0172
56	56	57	1.59	0.5337	0	0
57	57	58	0.7837	0.263	0	0
58	58	59	0.3042	0.1006	0	0
59	59	60	0.3861	0.1172	0.1	0.072
60	60	61	0.5075	0.2585	0	0
61	61	62	0.0974	0.0496	1.244	0.888
62	62	63	0.145	0.0738	0.032	0.023
63	63	64	0.7105	0.3619	0	0
64	64	65	1.041	0.5302	0.227	0.162
65	11	66	0.2012	0.0611	0.059	0.042
66	66	67	0.0047	0.0014	0.018	0.013
67	12	68	0.7394	0.2444	0.018	0.013
68	68	69	0.0047	0.0016	0.028	0.02

Table A.4: Consumer information at different load points for 33-bus system [153]

Number of load points	Load points	Number of customers
1	2	26
7	3, 18, 19, 20, 21, 22, 23	23
3	4, 14, 29	31
11	5, 6, 12, 13, 15, 16, 17, 26, 27, 28, 33	16
2	7, 8	52
2	9, 10	15
2	24, 25	109
1	11	12
1	30	25
1	31	39
1	32	35

Table A.5: Statistical input parameters at different load points for 33-bus system [153]

Load point	Failure rate (Failure per year)	Outage duration (Hour per year)
2	0.05	0.03
3	0.04	0.03
4	0.06	0.03
5	0.03	0.02
6	0.03	0.02
7	0.09	0.6
8	0.03	0.6
9	0.03	0.2
10	0.02	0.2
11	0.03	0.1
12	0.03	0.2
13	0.06	0.2
14	0.03	0.3
15	0.03	0.2
16	0.03	0.2
17	0.03	0.2
18	0.04	0.2
19	0.04	0.2
20	0.04	0.2
21	0.04	0.2
22	0.04	0.2
23	0.04	0.2
24	0.19	1.1
25	0.19	1.1
26	0.03	0.2
27	0.03	0.2
28	0.03	0.2
29	0.54	0.3
30	0.09	0.5
31	0.07	0.4
32	0.1	0.6
33	0.03	0.2

Table A.6: Statistical input parameters at different load points for 69-bus system [160]

Load Point	Failure rate (Failure per year)	Outage duration (Hour per year)
2, 52, 53, 54, 55, 56, 68, 69	0.221	1.94
3, 4, 35, 36, 37, 38, 39, 40, 41, 42, 43, 44, 45, 46, 47, 48	0.321	11.04
5, 8, 9, 11, 12, 29, 30, 14, 16, 18, 19, 20, 21, 22, 25, 27, 28	0.301	11.44
13, 15, 49, 50, 51, 62, 63, 64, 65	0.314	11.17
17, 23, 24, 57, 58, 59, 60, 61	0.208	1.75
31, 32, 33, 34, 66, 67	0.327	10.96

Table A.7: Consumer information at different load points for 69-bus system [160]

Number of load points	Load Points	Number of customers
8	2, 3, 4, 5, 52, 53, 54, 55, 56	148
6	8, 9, 57, 58, 59, 60	10
9	11, 12, 62, 63, 64, 65, 66, 67, 68	132
4	13, 14, 15, 69	110
2	16, 61	2
5	17, 18, 19, 20, 50	118
20	21, 22, 23, 24, 25, 26, 35, 36, 37, 38, 39, 40, 41, 42, 43, 44, 45, 46, 47, 48	126
6	27, 28, 29, 30, 31, 49	108
4	32, 33, 34, 51	58